Two-dimensional spectroscopy of γ-aminobutyric acid on a clinical MRI scanner

Katherine Lymer

PhD

The University of Edinburgh

2004

I declare that this thesis has been written by myself, and that the work contained in it is my own. Where work has been published that has been done by other people associated with the research group, acknowledgement is made.

Katherine Lymer

September 2004

For Jonathan

"Now I will believe that there are unicorns..."

--William Shakespeare--

(The Tempest)

Acknowledgements

I am indebted to Dr. Ian Marshall for his supervision and for his tireless proof-reading of this thesis. I am also grateful to both my second supervisor, Prof. Joanna Wardlaw, and the fourth member of "team GABA", Dr. Kristin Haga, for their suggestions and comments throughout the three years. I'd like to thank Dr Peter Hoskins, my official mentor, for his advice, and to my "un-official" mentors, Drs Paul Armitage and Mark Bastin, for many useful discussions and their proof-reading of this and other documents.

In terms of the practical implementation of this work, a big thank you is due to all the radiographers, past and present, for their assistance in learning to use the MRI scanner. I am privileged to have enjoyed extensive use of the scanner, and I appreciate their help in negotiating some of this time around clinical work, and for their assistance in scanning the volunteers. Many thanks to all those volunteers who have given-up many hours to help in the search for GABA! Thanks also to staff in the Medical Physics servicing workshop for the regular loan of the scales, essential for phantom preparation, and to Prof. Peter Sadler and Dr. Viv Munk, School of Chemistry, for their help in solving the GABA/glutamate/pH problem.

I am grateful to Dr. Jon Turner and colleagues for the organisation of the University's Transferable Skills Programme from which I believe I have benefited tremendously. Thanks also to the University librarians at the Western General Hospital, Claire Leach and June Morrison, for their help in accessing reference material from all the university libraries without ever having to leave the hospital! I am grateful to Caroline Ness and Irene Craig, Medical Physics secretaries, and Ann Deary, Clinical Neurosciences, for all their much-appreciated assistance. My thanks also to Martin Connell for the UNIX support and the DCN IT support team, led by David Perry, for all their help with PCs, printers and requests for more and more memory! Thanks to all other members of the SHECF Brain Imaging Centre for Scotland for their support throughout this PhD.

This work was funded by a Postgraduate Research Scholarship from the College of Medicine and Veterinary Medicine. I am grateful to Mr. Paul McGuire for his assistance in securing and managing this source of financial support.

I am grateful for the all the advice and assistance I have received from individuals outside the university. In particular, I'd like to thank Dr. Pom Sailasuta, GE Healthcare, for providing the 2D J-resolved and editing sequences, for sharing some of her 3T data and for patiently answering all my questions! In addition, my thanks go to Dr. M. Albert Thomas, University of California, for supplying us with his 2D L-COSY sequence and providing helpful on-line support. Many thanks also to Dr. John Higginbotham for the generous donation of his collection of Journal of Magnetic Resonance.

On a personal note, I'd like to thank my office mates Carly and Susana for their unfailing sense of humour and for the generous way they shared their time and PCs! Thank you to my fellow Medical Physics postgraduate students, especially Jude, Mairéad, Michael and Andrew: It's been a tough time for us all but you've been a constant source of strength and inspiration. Heartfelt thanks to the other members of my much valued support network, including Carolyn for her honest analysis of the PhD process and appearing when she was most needed, and Cesca, for coffee, chocolate and a shoulder to cry on.

Finally, my thanks to my family, for asking questions and sending cakes. And to Jonathan, for making me smile.

Abstract

Measurement of the cerebral metabolite γ-aminobutyric acid (GABA) has been performed on clinical MRI scanners using a variety of magnetic resonance spectroscopy (MRS) techniques. MRS studies of GABA are difficult, especially at 1.5T due to low *in-vivo* concentrations and overlapping of higher concentration metabolites. Unlike spectral editing methods, two-dimensional (2D) MRS allows the simultaneous measurement of GABA and other, more traditional metabolites. This work evaluates three implementations of 2D MRS for both *in-vitro* and *in-vivo* GABA measurement on a clinical MRI scanner.

Existing spectroscopy sequences were used to develop a protocol for performing 2D J-resolved MRS *without* a dedicated sequence. GABA was measured *in-vitro* at concentrations approaching normal physiological levels and volunteer results allowed assignment of the 3.01ppm GABA resonance at its J-coupling frequency (7.4Hz). However, the prolonged scan time of over two hours prevented practical application of this approach.

A far more efficient method of acquiring 2D J-resolved spectra is achieved with a dedicated 2D J-resolved sequence. An optimised set of acquisition parameters was produced to allow GABA measurement with maximum SNR, and without macromolecule contamination, in 35 minutes. Since the reproducibility of the sequence must be sufficient to detect physiological changes, a formal reproducibility study was performed acquiring three measures of reproducibility at six concentrations of GABA, using a standard volume head coil, 3"- and 5"- surface coils. To our knowledge, this is the first such reproducibility study dedicated to 2D J-resolved GABA measurement, and as such, could have significant implications on the interpretation of *in-vivo* results. *In-vivo* 2D J-resolved spectra were acquired and compared well to the published results, allowing assignment of the 3.01ppm GABA (plus macromolecule) peak (J = 7.4Hz). In the first reported 2D J-resolved spectra specifically designed to reduce the macromolecule contribution by optimising the echo time range, assignment of the *in-vivo* 3.01ppm GABA peak was less convincing.

As an alternative to 2D J-resolved spectroscopy, preliminary testing of 2D correlation spectroscopy (COSY) showed that it was not as sensitive or robust for either *in-vitro* or *in-vivo* GABA measurement. Although provisional assignment of the 3.01ppm GABA peak was made, in their current form, neither technique is suitable for pure GABA measurement at 1.5T.

Contents

List of Figures

List of Tables

Abbreviations

B_0	Main magnetic field
CHESS	*Che*mical *s*hift *s*elective excitation
COSY	*C*orrelated *s*pectroscop*y*
CSF	*C*erebral *s*pinal *f*luid
CSI	*C*hemical *s*hift *i*maging
CV	*C*oefficient of *v*ariation
DRESS	*D*epth-*re*solved *s*urface-coil *s*pectroscopy
DQC	*D*ouble *q*uantum *c*oherence
DQF	*D*ouble *q*uantum *f*ilter
FID	*F*ree *i*nduction *d*ecay
FOV	*F*ield *o*f *v*iew
FT	*F*ourier *t*ransform
GABA	γ-aminobutyric acid
IR	*I*nversion *r*ecovery
L-COSY	*L*ocalised *c*orrelated *s*pectroscop*y*
MQC	*M*ultiple *q*uantum *c*oherence
MQF	*M*ultiple *q*uantum *f*ilter
NAA	*N*-*a*cetyl *a*spartate
MRI	*M*agnetic *r*esonance *i*maging
MRS	*M*agnetic *r*esonance *s*pectroscopy
NMR	*N*uclear *m*agnetic *r*esonance
PET	*P*ositron *e*mission *t*omography
PRESS	*P*oint *r*esolved *e*cho *s*elective *s*pectroscopy
ROI	*R*egion *o*f *i*nterest
RF	*R*adio-*f*requency
SNR	*S*ignal-to-*n*oise *r*atio
SPECT	*S*ingle *p*hoton *e*mission *c*omputed *t*omography
STEAM	*St*imulated *e*cho *a*cquisition *m*ode
SV	*S*ingle *v*oxel
TE	*E*cho *t*ime
TI	*I*nversion *t*ime
TR	*R*epetition *t*ime
VOI	*V*olume *o*f *i*nterest
ZQC	*Z*ero *q*uantum *c*oherence
ZQF	*Z*ero *q*uantum *f*ilter

1 Introduction

1.1 Background

GABA (γ-aminobutyric acid) is the major inhibitory transmitter in the mammalian brain (1) and changes in concentration of this metabolite have been associated with several neuropsychiatric disorders (2-5). Normal physiological cerebral concentrations of GABA are low and reported to be in the range of 0.8mM – 1.9mM (6,7). In a study of depressed patients, Sanacora *et al* found a 52% reduction in the GABA levels of depressed patients compared to a group of non-depressed controls using a spectral editing method on a 2.1T system (8). Abnormal GABA concentrations have also been observed in women with pre-menstrual dysphoric disorder (a severe form of pre-menstrual syndrome) compared to a group of healthy controls (9).

With such results from *in-vivo* GABA measurements being increasingly reported, the incentive behind the work presented in this thesis was the study of GABA levels in a population of post-stroke patients. In a review by R. Robinson, the author stated that *"depression is probably the most common and most severe emotional disorder*

associated with stroke" (10). It has been estimated that between 25% and 63% of people will develop depression following a stroke, figures that are significantly larger when compared to the incidence of depression in a general, elderly population. Patients suffering from post-stroke depression will experience impaired physical and cognitive recovery, and their chances of surviving the first two years post stroke will be dramatically reduced when compared to a similar population of non-depressed stroke patients. Ultimately, it is hoped that results from magnetic resonance spectroscopy (MRS) could aid the management of such patients, with decreases in cortical GABA levels providing a predictive marker for depression.

Recent advances in MR methods have made it possible to measure GABA non-invasively, *in-vivo* (8,9,11,12). However, the application of such methods at 1.5T is very difficult: The low normal physiological concentrations of GABA means that it is on the threshold of detection using clinical MRI scanners. At clinical field strengths, GABA is strongly J-coupled, giving rise to complex resonance patterns.

To further complicate the matter, GABA is extensively overlapped by higher concentration metabolites, which means that conventional 1D spectroscopy techniques are unable to resolve multiplets at any of its chemical shift frequencies, at 1.5T. Despite this, GABA measurements at 1.5T using a variety of techniques have been published, including spectral editing (13-16), double quantum filters (17-19), 2D correlated spectroscopy (COSY) (20,21) and 2D J-resolved MRS (22-27). Unlike the spectral editing methods, 2D spectroscopy is not as susceptible to complications caused by patient motion and allows for the simultaneous measurement of GABA and other metabolites.

1.2 Aims

The main aim of this work is to evaluate two methods of two-dimensional spectroscopy and to assess their suitability for *in-vivo* GABA measurement at 1.5T. This will include extensive *in-vitro* experimental work to validate the techniques,

optimise acquisition protocols and establish the reproducibility of the methods before evaluating their performance in healthy volunteers.

1.3 Outline of chapters

The background to the work in this thesis is provided in two theoretical chapters. It is assumed that the readers of this thesis will have a basic understanding of magnetic resonance, and so a detailed description of the physical basis of the technique is not included. However, it is acknowledged that this experience may not extend to magnetic resonance *spectroscopy*. For this reason, Chapter 2 introduces MRS as it is currently applied on clinical MRI scanners. This includes a brief history of MRS, an outline of the background theory and a description of the cerebral metabolites studied using this non-invasive technique.

Since the focus of this work is on GABA measurement using MRS, chapter 3 provides a review of the MRS methods currently applied for GABA detection at 1.5T. These techniques are critically assessed in terms of the quality and type of metabolite information acquired and ease of application on a clinical MRI scanner. Two-dimensional MRS has the advantage of providing information on *all* of the metabolites within the sample, and from the encouraging GABA-related results identified in this review, was chosen as the most efficient method of evaluating the complete biochemical status of the individual.

Each of the experimental chapters lists the materials and methods employed, and then presents and discusses the results from each series of experiments. In the first of these chapters, chapter 4 presents the work performed investigating the application of the standard PRESS sequence to perform 2D J-resolved MRS. The results from the preliminary *in-vitro* experiments are presented, including the general reproducibility of the scanning and post-processing protocol, and the sensitivity of this method to GABA measurement. The chapter concludes with the results from the application of this technique *in-vivo*.

Practical work using 2D J-resolved MRS continued with the evaluation of a *dedicated* 2D J-resolved MRS sequence. This sequence provides an automated method of acquiring the same data as obtained using a protocol of 64 individual PRESS sequences. However, a difference in the data acquired during prescan necessitated a change to the post-processing, the results of which are presented in chapter 5. This chapter also contains the results from the initial *in-vitro* practical work to re-evaluate 2D J-resolved MRS using automated acquisition of the raw data. By performing a similar series of experiments to those presented in chapter 4, the results from the two scanning protocols can be directly compared.

To address the specific application of GABA measurement using 2D J-resolved MRS, practical work was performed to optimise the scanning protocol. These results are presented in chapter 6 and include investigation of different coil arrangements, spectroscopy voxel sizes and acquisition parameters. The results from testing the optimised protocol on a phantom containing physiological concentrations of all the common cerebral metabolites are also shown.

The final stage before acquiring *in-vivo* data was to establish the reproducibility of the scanning and post-processing protocol. Despite the increasing interest in GABA measurement using a variety of MRS methods, as described in chapter 3, there have been few studies specifically addressing the reliability of these measurements, and none using 2D J-resolved MRS. Therefore, chapter 7 presents the results from formal investigation into the reproducibility of 2D J-resolved GABA measurement, as recorded in phantoms and using different coil arrangements.

Completion of evaluation of 2D J-resolved MRS *in-vitro* allowed application of the technique *in-vivo*. The 2D J-resolved spectra acquired from healthy volunteers, using the optimised protocol, are presented in chapter 8.

As an alternative method for *in-vivo* GABA measurement, chapter 9 presents the initial practical work performed to evaluate a dedicated 2D L-COSY sequence. To allow comparison between these results and those using 2D J-resolved MRS, a

similar series of *in-vitro* experiments were performed as those described in chapters 4 and 5, to establish the reliability of the technique in both general terms and specifically for GABA measurement. The chapter concludes by presenting the results from the acquisition of 2D L-COSY spectra *in-vivo*.

Finally, chapter 10 presents the conclusions drawn from this work, and offers suggestions for future work.

2 Introduction to Magnetic Resonance Spectroscopy

2.1 Introduction

Since its introduction into the clinical environment in 1981 (28), MRS has been an extremely useful tool for studying the biochemistry of different living tissues non-invasively (29). In doing so, MRS has been able to provide insight into different disease courses and their response to treatment (30). Although it is somewhat restricted by a limited chemical shift range and overwhelming water peak (31), ^{1}H MRS has been applied extensively to evaluate brain metabolism in different disease states including stroke (32), tumours (33), Alzheimer's disease (34) and head injury (35).

The aim of this chapter is to quickly bring the reader up to speed with the current state of clinical MRS, and use this as a foundation on which to build-up to the non-standard, research MRS techniques described in later chapters. To help achieve this, a brief history of MRS is provided in §2.2 to illustrate the significant developments accomplished in this field over such a short time.

For a complete understanding of the technique, an appreciation of the physical basis of magnetic resonance (MR) is required. This is not a new discipline and so it is beyond the scope of this thesis to provide a thorough description of MR from first principles – there are many texts with excellent descriptions of the physics behind magnetic resonance imaging (MRI) and MRS. However, a quick overview of MR is included in §2.3, with appropriate references to guide the reader in obtaining a more comprehensive understanding of the subject.

The focus of this thesis is the application of MRS to identify and quantify GABA *in-vivo*, and so GABA and some of the other cerebral metabolites studied *in-vivo* using MRS are introduced in this chapter. This is also an appropriate place to mention alternative techniques for GABA measurement, and at the same time, stress the advantages of using MRS. §2.4 not only describes these metabolites, but also includes any effect their presence may have on GABA measurement.

Building on the physical basis of MR, §2.6 describes clinical MRS as currently applied at 1.5T. It is important to appreciate the role and limits of conventional, one-dimensional (1D) spectroscopy before introducing two-dimensional (2D) MRS in §2.7. It should be noted that where 1D MRS is still establishing its role in clinical practice, 2D MRS remains very much in the research domain.

2.2 History of Magnetic Resonance Spectroscopy

In 1946, two independent scientists published their results regarding the " Nuclear Magnetic Resonance (NMR) phenomenon". Bloch led one group at Stanford University and received acclaim for their work into "Nuclear Induction" (36). This pioneering work involved superimposing a small gradient over a main static magnetic field to produce tiny variations in the Larmor frequency of the protons in the water sample. By placing a coil with its axis in the same direction as the applied gradient, Bloch *et al* were able to record a signal from the sample. This technique was to form the basis of spatial encoding.

At the same time, Purcell and his group, at the Massachusetts Institute of Technology (37), employed similar methods to determine the Larmor frequency of paraffin. At a time where the concept of "spin-lattice relaxation" was known and accepted, results from this group revealed relaxation times far shorter than those expected from consideration of only longitudinal relaxation. It was such observations that led to the definition of spin-spin (T_2) relaxation time.

Both Bloch and Purcell were awarded the Nobel Prize in 1952 for their achievements, and their work formed the platform on which the technique of magnetic resonance has evolved into the spectrum of applications that exists today.

In one of the first practical applications of MRS, Shaw and Elsken used the so called "Nuclear absorption phenomenon" to investigate the peak intensity of the water signal in a selection of organic samples, including apples, potatoes and maple wood (38). Measurements taken during controlled dehydration of the samples showed a linear relationship between the peak intensity of the absorption signal and the amount of water in the tissue. Thus, it was proposed that by recording the absorption signal from resonating hydrogen nuclei, the water content of hygroscopic materials could be evaluated. However, the large linewidth of the signal prevented observation of "splitting" of the absorption curve due to the structural and chemical properties of the samples.

A similar low-resolution technique was applied to a cohort of biological samples including human red blood cells and rat muscle (39). Odebald and Lindström found a linear relationship between the received signals and measured water content in most of their samples. However, exceptions to this rule were found in adipose, cartilage and fibrous tissue where the recorded signals were greater than expected from consideration of their water content alone. It was hypothesised that this anomaly was due to the presence of bound protons within a structured lattice or, in the case of adipose tissue, protons bound to the carbon chains forming the fat molecule, unable to contribute to the observed signal. In addition, it was speculated that the binding of protons to proteins and other macromolecules caused the

broadening of the signals. More recent work has confirmed this hypothesis, with broad resonances from macromolecules shown to contribute to ^{1}H MRS of the human brain in both normal (40,41) and diseased states (42-44).

Spectral resolution was to remain an issue until the introduction of super-conducting magnets and the application of Fourier Transform (FT) to NMR in the 1960's (31). The first truly high resolution NMR spectra were reported by Moon and Richards, and allowed the identification of phosphorous containing compounds in red blood cells (45).

From the early 1970's, work focussed on the use of NMR spectroscopy to study the major phosphorous containing compounds. In 1974, Hoult *et al* obtained the first reported spectrum of this type on intact muscle taken from the hind leg of a dead rat (46). Their measurements allowed the identification of a number of phosphate compounds and these were related to tissue metabolism immediately prior to death. A few years later, Dawson *et al* acquired spectra from frog skeletal muscle in different metabolic states: rest, contraction and recovery (47). Of particular importance, the MRS results in this work were confirmed by similar results obtained using the more traditional chemical analysis techniques on extracted and frozen samples, and consequently furthered the understanding of metabolic changes in muscle.

An increase in the available bore size of the NMR spectrometer facilitated the study of larger organs, and one of the first to exploit this technology were Garlick *et al* (48). Using specially designed apparatus, ^{31}P MRS was used to measure pH and obtain indications of tissue metabolism from the concentrations of phosphorous containing compounds, from isolated rat hearts under normal and ischaemic conditions.

The introduction of surface coils to provide basic spatial localisation permitted the study of tissue *in-situ*. Ackerman *et al* used surface coils to acquire ^{31}P MR spectra from the brain and muscle of an anaesthetised rat (49). Consequently, ^{31}P NMR was

able to provide information about phosphorous containing compounds *non-invasively* for the first time. In addition to providing localisation of the MRS signal from within a volume, this technique had the added advantage of improving the signal to noise ratio (SNR) by eliminating the acquisition of noise from outside the volume of interest (VOI).

Construction of high field, horizontal, homogenous magnets, large enough for human study, prompted the first non-invasive, biochemical studies of human disease. The very first application of MRS to confirm a clinical diagnosis was in a patient with McArdle's syndrome (28). Results from ^{31}P MRS of the forearm of the patient showed differences in muscle metabolism and a consistently higher intracellular pH when compared to normal control subjects.

The first *in-vivo* studies of the human brain were performed on newborn babies (50,51). ^{31}P MRS showed abnormal changes in phosphorous containing compounds when, at the same time as MRS was performed, both neurological and ultrasound examinations were normal. Consequently, it was suggested that MRS had predictive value in detecting metabolic changes *before* the observation of structural abnormalities, and as such, could influence treatment management. The predictive value of MRS was later confirmed in the follow up of severely hypoxic newborn babies in a ^{31}P / ^{1}H MRS study (51). In three of the infants studied, their PCr/Pi ratio improved with their clinical condition and in another, the abnormal ^{31}P MR spectrum in one hemisphere was related to tissue loss as later shown on ultrasound.

With developments of large bore magnets and improvements in image quality, MRI became established as a clinical tool in the 1980's with the acquisition of whole body images based on the mapping of water protons (52). However, up to this point, MR imaging and MR spectroscopy had effectively been considered as two different modalities using different nuclei: ^{31}P (or ^{13}C) for spectroscopy and ^{1}H for imaging. ^{1}H MRS was complicated by the need to suppress the much higher concentration water signal to detect the lower concentration metabolites, and by the comparatively small chemical shift range of the metabolites of interest: 10ppm in ^{1}H MRS and

40ppm in ^{31}P MRS. Despite these limitations, Behar *et al* were able to obtain high resolution ^{1}H MRS spectra from a rat brain *in-vivo* (53). The cerebral metabolites N-acetyl aspartate (NAA), phosphocreatine and creatine were identified, in addition to lactate under hypoxic conditions.

The advent of strong magnetic field gradients allowed MRS (^{31}P and ^{13}C) to be performed using the *same* instrumentation as ^{1}H MRI, to obtain both anatomical and biochemical information of the human head in the same examination (54,55). Using hardware that would not seem out of place in a modern clinical setting, a 1.5T superconducting magnet with 1m bore, Bottomley *et al* acquired 4mm thick transverse whole brain images, as well as ^{31}P and ^{13}C spectra from a volume using surface coil localisation. In addition to performing imaging and spectroscopy on the same MR system, this work was the first to acquire high resolution ^{1}H MR images of the human brain, and in doing so, set the course for clinical MR imaging as applied today.

To overcome contamination of spectra by signals from the tissue surface due to the use of surface coils, localisation techniques using radiofrequency (RF) pulses and magnetic field gradients were developed. Bottomley was among the first with this approach and he developed a simple, single pulse sequence known as Depth-REsolved Surface coil Spectroscopy (DRESS) to excite the sample *away* from the high sensitivity region at the tissue surface (56). Using DRESS, it was possible to excite only the nuclei in a rectangular plane parallel to the surface coil, and by varying the frequency of the excitation pulse, the depth of the region of interest (ROI) with respect to the surface coil could be altered.

Localisation pulse sequences quickly advanced to provide 3D localisation without the need of a surface coil. Point RESolved Spectroscopy (PRESS), for example, uses three RF pulses and three magnetic field gradients to excite the volume at the intersection of the three orthogonal gradients (57). So in addition to being able to use a standard imaging coil for spectroscopy, PRESS also allows finer control of the shape and location of the excited volume.

Methods for biochemical imaging evolved from the multidimensional techniques used in high resolution, organic chemistry NMR (58) to obtain a matrix of spatially localised spectra (59). Selective post-processing of the data allows the spectra to be quantified at a specific chemical shift frequency, to produce an image displaying the distribution of chemicals, within the localised volume, resonating at that frequency. Images of the different chemicals within the sample are obtained by varying the selection frequency, and this technique of processing MRS data to indicate the spatial distribution of a specific chemical eventually led to the technique "metabolite mapping" or "chemical shift imaging" (CSI).

By the mid-1990's, both single-voxel (SV) and CSI techniques were being applied to an increasing variety of clinical conditions, particularly in the human brain (30,31,60-63). With the increased use of ^{1}H MRI in clinical imaging, ^{1}H MRS became the MRS method of choice for gaining measures of brain metabolism with the detection of the cerebral metabolites NAA, choline and total creatine (63). Recent advances in MRS research have concentrated on identifying strongly overlapping resonances such as glutamate, glutamine and GABA, and it is to this problem that the attention of this thesis is focused.

2.3 Physical basis of ^{1}H MRS

To any reader familiar with MR imaging and / or spectroscopy, the physics underlying both techniques will be well understood, and any further discussion in this thesis quite unnecessary. However, it is appreciated that scientists new to this field may require a basic grounding in the physical principles under-pinning magnetic resonance. For a complete and thorough description of the physics relating to MR, it is highly recommended that the reader study one of the many available texts or publications, for example (52,64-67). As a very brief introduction to ^{1}H magnetic resonance spectroscopy and its clinical relevance, the remainder of this section will provide a quick overview of the topic. It is emphasised that the following paragraphs offer only a short summary and far more comprehensive descriptions can be found in the published literature.

By mass, the human body is made up of about 60% water (68). Every molecule of water, as its chemical name H_2O implies, contains one oxygen atom and two hydrogen atoms, thus making hydrogen one of the most abundant elements in the human body (69).

The magnetic properties of any atom are defined by the spin and charge distributions of the neutrons and protons within the atom's nucleus. The positively charged proton gives rise to a magnetic field, and when combined with the inherent spin of the nucleus, produces a magnetic dipole. Since the resulting dipole has both magnitude and direction, it is often presented in vector form, with the strength and orientation defining its magnetic moment.

The hydrogen nucleus, containing a single proton surrounded by a single orbiting electron, has the largest magnetic moment of any biologically occurring element (65). This makes the proton the most MR sensitive stable nucleus, and combined with its natural abundance, has made ^{1}H MRS a clinically useful tool (61).

Hydrogen, like most biologically relevant nuclei, possesses a quantum spin number of ½, which means that it can exist in two different orientations relative to an arbitrary axis (31). When a hydrogen nucleus is placed into a static magnetic field, its magnetic moment is forced to align itself either with or against the direction of the field. Both classical and quantum models exist to describe this interaction and the reader is directed to the literature for a full description of these models (e.g. (64,65,67,70)). In a sample containing many millions of protons, such as the human body, then a proportion of the protons will align themselves *with* the field (in the lower energy state) and the remainder *against* (in the higher energy state) according to the Boltzman law. The difference in spin population between the two states is known as the "net magnetisation" and it has two components: A component aligned parallel with the field, known as longitudinal magnetisation, and a second aligned at 90° from the external field known as transverse magnetisation. In the presence of a static magnetic field, the number of protons aligning themselves with the field is

slightly greater than those against, leading to an excess of spins in the lower energy state.

For a proton with only two possible energy levels, the ratio of the number of protons in the higher energy level (n_h) compared to the lower energy level (n_l) is given by Equation 2.1. At room temperatures and clinical magnetic field strengths, the excess population in the lower energy state is less than 1 in 10^5 (67). Since an MR signal is only detected from this excess of lower energy nuclei, it makes MRS a low sensitivity technique when compared to other spectroscopic methods, e.g. optical spectroscopy.

$$\frac{n_l}{n_h} = \exp\left(\frac{\gamma\hbar B_0}{2\pi\kappa T}\right) \approx 1 + \frac{\gamma\hbar B_0}{2\pi\kappa T}$$

Equation 2.1 Boltzman distribution where (n_h) = number of nuclei in the higher energy level, (n_l) = number of nuclei in the lower energy level, γ = gyromagnetic ratio, h = Plank's constant, B_0 = applied magnetic field, k = Boltzman constant and T = temperature (Kelvin) (71).

The static magnetic field has a second effect on the spinning protons. Interactions between the magnetic fields of individual protons and the much larger external field, generate a force on the protons causing them to rotate, or precess, about their own axis. The frequency at which the protons precess is proportional to the strength of the applied magnetic field in a relationship described by the Larmor equation, Equation 2.2.

$$\omega_L = \gamma B_0$$

Equation 2.2: The Larmor equation stating that the applied frequency, ω_L is proportional to the static external field B_0; the constant of proportionality is γ, the gyromagnetic ratio (65).

MR experiments are composed of a series of RF pulses applied with specific local variations in the magnetic field, known as magnetic field gradients. Without application of RF pulses or changes in the local magnetic field, the sample will remain in equilibrium. In this position, the longitudinal magnetisation is maximal and there is zero magnetisation in the transverse direction, resulting in no signal. The sample leaves its equilibrium position when it is excited by RF radiation. The frequency of the radiation must be exactly matched to the difference between the

energy levels and if this condition is met, resonance occurs. The amplitude and duration of the RF pulse determines the number of nuclei that make the transition between the lower to higher energy state (70). Resonance can also be described using both quantum physical or classical models and again, the reader is directed to suitable texts to study both approaches, e.g. (64,65).

Once the spins have been excited and the RF pulse switched off, a signal can be detected as the spins return to equilibrium. This is a sinusoidally varying signal, whose envelope decays due to the spin-spin and spin-lattice interactions, and is known as a Free Induction Decay (FID). The length of the recorded FID depends on the relaxation parameters of the spins within the sample and its amplitude on the spin density, and so exactly reflects the tissue structure and composition of the sample. A signal will only be recorded from a coil in the transverse plane while the precessing spins are also in the transverse plane and maintain their phase coherence.

In order for the spins to return to their equilibrium position, they must give up the energy acquired to obtain resonance, and this is achieved through two relaxation mechanisms. Immediately after the RF pulse is removed and as the spins continue to precess, they start to interact with one another, causing tiny changes in the magnetic fields surrounding each of the protons, causing them to precess at slightly different frequencies. This is known as spin-spin interaction, or spin-spin relaxation (T_2), and is responsible for the loss of phase coherence in the sample, leading to the exponential loss of the MR signal. T_2^* relaxation takes into account the intrinsic inhomogeneities of the applied magnetic field and is therefore much faster than T_2.

In order for the spins to return to the equilibrium position, the individual protons must give up their energy to the surrounding tissue (historically known as the "lattice"). This again is an exponential process and the efficiency of the spins in giving up their energy is determined by the nature of the interaction of the nuclei with the surrounding environment. This interaction is known as spin-lattice (T_1) relaxation.

However, in a uniform magnetic field, all protons within the sample in that field are excited by the *same* frequency RF pulse, and since they are all precessing at the same rate, they all contribute to the recorded signal. In most clinical applications, where often the whole body is in the magnet, this would not be particularly useful.

Localisation of the signal is achieved using magnetic field gradients (61). These are applied in conjunction with the RF pulses to influence the spins in a pre-determined manner. The gradients have both positive and negative maxima, and the combination of these gradients with the main magnetic field produces a linear variation in the magnetic field experienced by the protons across a set field of view (FOV). Thus, according to the Larmor equation, Equation 2.2, the frequency of precession of the protons will vary in a uniform and predicable manner across the FOV. Consequently, the frequency and bandwidth of the RF pulses can be selected to excite a specific volume of protons in a particular location within the sample.

Three orthogonal gradients exist in the main body of the magnet to allow localisation in any direction. The order and duration of the gradients in the MR pulse sequence defines its exact mechanism of localisation and the reader is referred to §2.6.2 or published text, e.g. (56,72,73), for further details on VOI definition.

MR imaging provides high-resolution, anatomical images. Using the local gradients, frequency information is used to determine the spatial location of the MRI signal. In MR spectroscopy, the frequencies obtained are determined by the exact chemical environment of the sample, thus allowing identification of the molecules by their unique Larmor frequencies. The electrons surrounding each nucleus shield it from the external magnetic field, causing very local and very specific differences in the resulting field experienced by the nucleus. These minute changes in magnetic field produce proportional variations in the Larmor frequency of the nuclei, and since the variations are due to the chemical environment of the nuclei, a chemical shift (frequency) scale is adopted. Therefore, the end result of an MRS experiment is a series of peaks at different chemical shift locations and intensities (60). These peaks

can be exactly related to the concentration, couplings and relaxation properties of the molecules in the sample, thus making MRS an extremely useful tool.

2.4 Reading a ^{1}H MR spectrum

2.4.1 Introduction

Clinical MRS has focussed on using ^{31}P and ^{1}H although MRS using nuclei such as ^{19}F, ^{13}C and ^{15}N is available (30). However, in most clinical MR systems where, by convention, the resulting images are maps of the protons arising from water and fat, the associated RF hardware is all tuned to protons. Therefore, ^{1}H MRS is the most readily available MRS technique (74). The practical work in this thesis is based entirely on ^{1}H MRS and so the discussion of MRS using any other nuclei is not included.

As shown in Figure 2.1, an MR spectrum comprises a series of peaks whose positions are defined in terms of the chemical shifts and couplings of the molecules in the sample. The intensity of these peaks is proportional to the number of nuclei resonating at that frequency, and so integration of the peak areas can allow a measure of the metabolite concentration to be derived (75). To understand the significance of the appearance of these spectral peaks, the remainder of this introductory section will discuss chemical shift and scalar coupling.

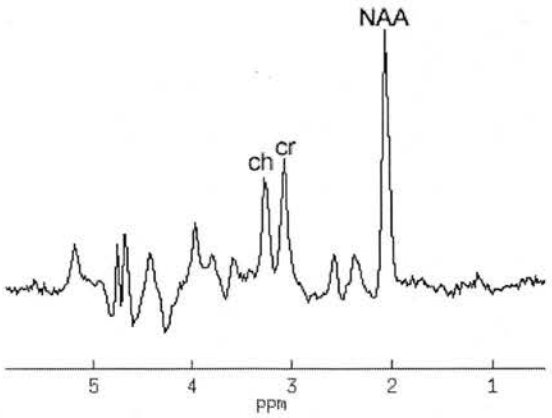

Figure 2.1 Long echo time (TE) (TE = 135ms) *in-vivo* 1D MR spectrum identifying the metabolites choline (ch), creatine (cr) and NAA.

2.4.2 Chemical Shift

In the discussion thus far, it has been assumed that every proton experiences the same magnetic field, from the applied field, B_0. If this were true, then the same MR signal would be recorded from every proton and, as stated very nicely by Derek Shaw in his book, "n.m.r. would be a very dull and not useful technique" (67)! The beauty of MRS is that the acquired signals differ according to the type of nucleus and its surrounding environment i.e. the other atoms forming the molecule in which it resides (70).

When a molecule is placed in a magnetic field, its magnetic moment precesses around the nucleus in the direction of the field, giving rise to a small magnetic field at the nucleus. This opposes the applied magnetic field (B_0), and effectively shields the nucleus from the main field, Equation 2.3. The extent to which the field is perturbed at the nucleus is dependent on the applied magnetic field strength, the specific nuclei under investigation and its chemical environment. This is known as the chemical shift phenomenon (δ) and is defined by Equation 2.4.

$$B_{eff} = B_0(1-\sigma)$$

Equation 2.3 Definition of the effective magnetic field (B_{eff}) at the nucleus, where B_0 = main magnetic field and σ is the screening constant, (67).

$$\delta = \frac{\nu_S - \upsilon_R}{\upsilon_R} \times 10^6$$

Equation 2.4 Basic definition of chemical shift (δ) in ppm, where υ_S is the resonant frequency of the nuclei of interest and υ_R is the resonant frequency of the chosen reference nuclei. (70).

According to the Larmor equation, Equation 2.2, the differences in magnetic field will be observed as changes in the resonant frequencies of the nuclei in different chemical environments. Thus, each line (or peak) in the spectrum corresponds to the resonant frequency of one nuclei within the molecule, hence the term "resonant line" is sometimes used. The exception to this general rule is when studying molecules with chemically equivalent protons, where each experiences the same chemical environment, or screening factor as described in Equation 2.4, and so has the same resonant frequency. Therefore, at clinical field strengths, such protons will occupy the same chemical shift position.

For example, the differences in nuclei shielding due to the changing number of electrons, will force the methine (CH), methylene (CH_2) and methyl (CH_3) chemical groups to resonate at slightly different frequencies, and so occupy different chemical shift positions on the MR spectrum. Since more electrons shield the methyl group, the effective field sensed by the protons will be less than that experienced by any of the other groups, and it will resonate at a lower frequency. However, when the protons in each of the methylene and methyl groups are chemically equivalent (e.g. ethanol), only one resonant line per chemical group is observed on the spectrum.

Since the resonant frequency of the metabolites is a function of the effective magnetic field, the spectrum of the same metabolite at different field strengths will vary with B_0. However, by expressing the chemical shift frequency of the metabolite of interest as a fraction of a reference compound frequency (e.g. tetramethylsilane (TMS) in ^1H MRS), the chemical shift will always have a constant value, independent of B_0 (64). This scale has units of parts per million (ppm) and is extremely useful in allowing metabolites to be identified at the *same* ppm position, regardless of the magnetic field strength. Thus, GABA will always have multiplets at 1.89ppm, 2.28ppm and 3.01ppm (7). It should be noted, however, that the resonant frequency of the water is temperature dependant and so a shift to the right of approximately 0.1ppm is observed in spectra from room temperature phantoms (52).

The chemical shift range of the common proton-containing compounds is 10ppm, resulting in a highly overlapped spectrum of peaks at clinical field strengths. The spectrum is further complicated by scalar coupling, a concept that is discussed in the next section.

2.4.3 Scalar (J) coupling

Scalar, or J-, coupling refers to the interaction of nuclei as transmitted through the electrons in the outer "shells" or orbits of the nuclei (67). At high fields, the effect of scalar coupling can be observed as the splitting of the resonant line into a multiplet of lines, occurring in a well-defined pattern, at different frequencies along the chemical

shift axis. This leads to an inherent loss in SNR since the proton signal is split into multiplets. An example of the complex coupling pattern of GABA is given in Figure 2.2. The J-coupling of GABA will be considered in detail in §3.3.2.

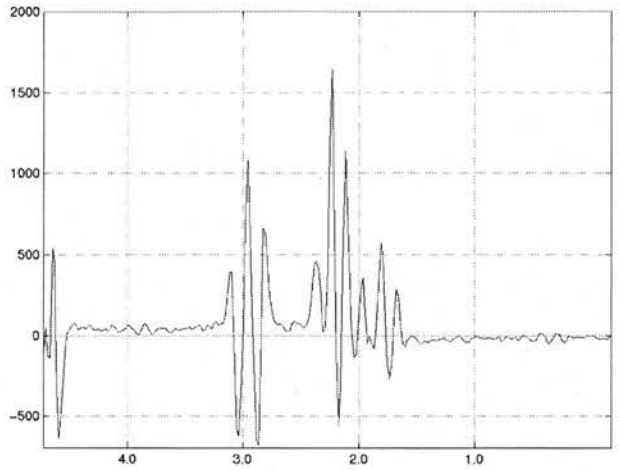

Figure 2.2 Modelled 1D spectrum of GABA (TE = 35ms, TR = 2000ms, B_0 = 1.5T) to demonstrate the complex splitting pattern of the metabolite resonances, (135).

J-coupling is a fixed property of the molecule, and so is independent of the applied magnetic field (76). The strength of the interaction is given by the scalar coupling constant J_{ab}, where a and b denote the two nuclei coupled by the bond, with its magnitude expressed in Hertz (77).

The effect of these interactions can most easily be explained using a two-spin, weakly coupled system. By convention, the spins are designated I and S where S is the spin to be studied. Spins are considered to be weakly coupled if the difference in their precessional frequencies is much greater than the coupling frequency (76). Assuming that in the presence of a magnetic field, each spin has two equilibrium states corresponding to the magnetic quantum number, $m = \pm \frac{1}{2}$, then the complete two-spin system can be described by four possible states, Table 2.1.

Table 2.1 Description of a two-spin system

I	S
+ ½	+ ½
- ½	+ ½
+ ½	- ½
- ½	- ½

In the absence of any scalar coupling, the energy for each of these states is the sum of the energies of each spin, Table 2.2.

Table 2.2 Description of the four possible energy levels of an uncoupled, two-spin system, where ν_I and ν_S are the Larmor frequencies of the two spins. By convention, the spin-state aligned parallel with the magnetic field (m = + ½) is designated α, and the spin-state aligned anti-parallel (m = - ½) β.

I	S	Energy level
β	β	$E_4 = + ½ \nu_I + ½ \nu_S$
β	α	$E_3 = + ½ \nu_I - ½ \nu_S$
α	β	$E_2 = - ½ \nu_I + ½ \nu_S$
α	α	$E_1 = - ½ \nu_I - ½ \nu_S$

In terms of transition between the energy levels, only those that obey the selection rule $\Delta m = \pm 1$ are allowed, leading to four possible transitions, Figure 2.3 and Table 2.3.

Table 2.3 Possible energy transitions of a two spin, uncoupled system

I	S	Energy	Total magnetic quantum number (m)	Allowable transition to state ($\Delta m = +1$):
β	β	$E_4 = + ½ \nu_I + ½ \nu_S$	+1	None (highest energy state)
β	α	$E_3 = + ½ \nu_I - ½ \nu_S$	0	4
α	β	$E_2 = - ½ \nu_I + ½ \nu_S$	0	4
α	α	$E_1 = - ½ \nu_I - ½ \nu_S$	-1	2 or 3

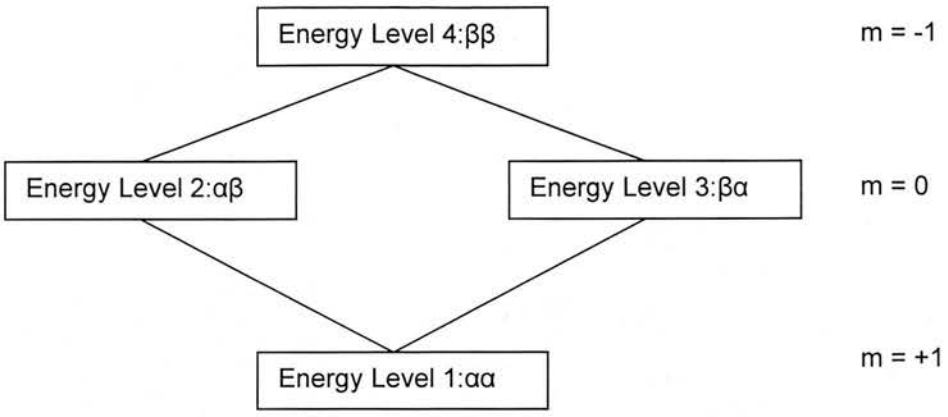

Figure 2.3 Energy level diagram for an uncoupled two-spin system

Since the transitions are due to changes in the I spin *or* the S spin, the resulting spectrum will consist of two lines, one at each of the chemical shift frequencies for I and S, Figure 2.4.

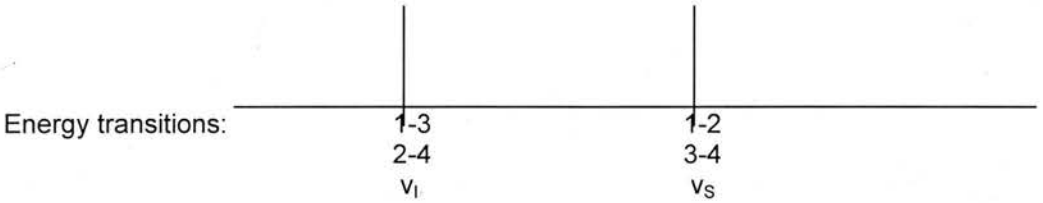

Figure 2.4 Resulting spectrum from a hypothetical, uncoupled two-spin system. Each resonance line represents the change in spin state of spin I at ν_I or spin S at ν_S.

The resulting MR spectrum is modified if the two spins I and S are coupled: The presence of spin I causes spin S to experience a tiny magnetic field at the site of S. This additional field will be positive or negative, depending on the orientation of I to the B_0 (parallel or anti-parallel), and on the sign of the coupling constant J_{IS}. Consequently, the resultant field at S will either be reinforced or diminished, Table 2.4.

Table 2.4 Description of a coupled, two-spin system.

I	S	Energy
β	β	$E_4 = +\frac{1}{2}\nu_I + \frac{1}{2}\nu_S + \frac{1}{2}J_{IS}$
β	α	$E_3 = +\frac{1}{2}\nu_I - \frac{1}{2}\nu_S - \frac{1}{2}J_{IS}$
α	β	$E_2 = -\frac{1}{2}\nu_I + \frac{1}{2}\nu_S - \frac{1}{2}J_{IS}$
α	α	$E_1 = -\frac{1}{2}\nu_I - \frac{1}{2}\nu_S + \frac{1}{2}J_{IS}$

Thus, the transitional changes are not only determined by changes in the I or S spin, but also on scalar coupling between the spins, J_{IS}. Therefore, the resulting spectrum consists of four lines, whereby the resonant frequency of S will be split into a doublet at the frequency J_{IS} Hz and likewise, spin S will have a similar effect on spin I, Figure 2.5. Consequently, the resulting spectrum will contain the resonances of I and S at their chemical shifts, each one split into doublets by J-coupling interactions. This description of a weakly coupled system is a valid approximation for the metabolite lactate, and will be given further consideration in §2.6.4.

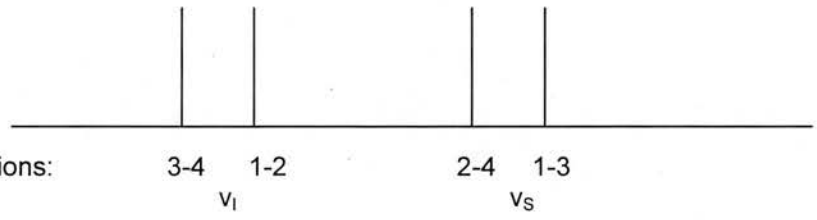

Figure 2.5 Resulting spectrum from a hypothetical, coupled two-spin system now consisting of four lines: Two centred around the transition frequency of Spin S , ω_S , and separated by $2\pi J_{IS}$; Two more centred around the transition frequency of Spin I , ω_I , also separated by $2\pi J_{IS}$.

In conventional 1D spectroscopy, the spectra are complicated by the splitting of molecules due to their J-couplings, causing further overlapping of the molecular resonances and, in some cases, preventing the identification and quantification of individual chemical shifts. Therefore, complex editing or 2D techniques are employed to aid detection of these chemicals.

2.5 Metabolites detected using ^{1}H MRS

2.5.1 Introduction

MR neuro-spectroscopy is not a new field (54), and throughout its history, the number of metabolites identified using this non-invasive technique has increased. Fundamental to reading any MR spectrum is knowing which metabolites are likely to be present, where they exist on the spectrum and the range of values constituting "normal physiological" concentrations. Consequently, this section will briefly

introduce some of the metabolites more commonly studied using ^{1}H MRS, as well as those of significant interest to the work in this thesis.

2.5.2 N-Acetyl Aspartate

The most prominent peak in any normal, 1D MR spectrum is that from the three protons in the N-Acetyl Aspartate (NAA) methyl group, Figure 2.6. NAA is believed to provide a marker for neuronal density with decreases in its concentration observed with degenerative diseases such as multiple sclerosis (7).

In an MR spectrum, the NAA singlet exists at 2.01ppm, and due to the broad base of this peak, plus the smaller contributions from N-Acetlyaspartylglutamate (NAAG), the peak overlaps GABA at its 1.89ppm resonance. Since NAA is normally present in much larger concentrations than GABA (~ x10 greater (7)), GABA is virtually invisible in both 1D and 2D spectra at this chemical shift frequency. Consequently, it is unusual to find methods devoted to quantifying this GABA resonance at clinical magnetic fields.

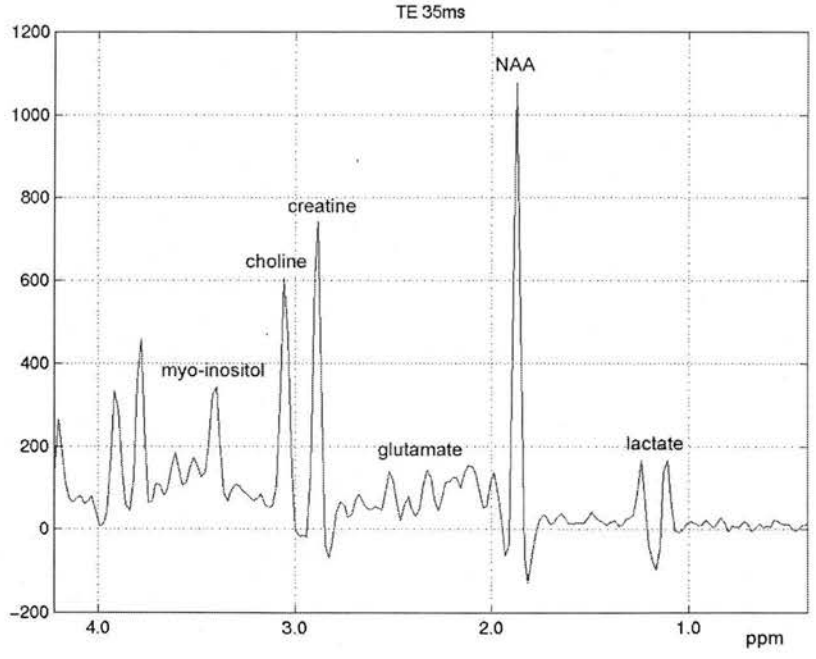

Figure 2.6 Short-echo time (TE = 35ms) ^{1}H spectrum acquired from a phantom containing N-Acetyl Aspartate (NAA), choline, creatine, glutamate, myo-inositol and lactate at 1.5T.

2.5.3 Choline

The most prominent signal from choline exists at 3.2ppm, Figure 2.7, and is due to the nine magnetically equivalent protons on the trimethylamine group. Normal physiological concentrations of choline are in the range 0.9mM – 2.5mM (7). *In-vivo*, this peak also contains contributions from glycerophosphorylcholine and phosphorylcholine, so it is more accurate to refer to the singlet as "total choline". Changes in the concentration of choline have been observed in cancer, Alzheimer's disease and stroke, which has led to its association with membrane integrity (7) and as an indicator of myelination (60).

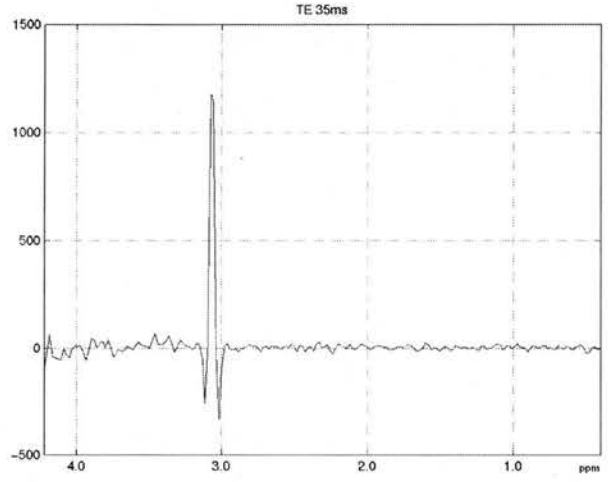

Figure 2.7 Short TE (35ms) spectrum from a phantom containing 2.5mM choline (with all peaks shifted by ~ 0.1ppm in the room temperature phantom).

In normal 1D MR spectra, the total choline singlet is sufficiently distant from all the GABA resonances to prevent overlap, although in white matter where it exists at higher concentrations, there may be some "bleed" from the choline obscuring the 3.01ppm GABA multiplet.

2.5.4 Creatine and phosphocreatine

The methyl protons of creatine and phosphocreatine are observed as a singlet at 3.03ppm. With normal physiological concentrations of creatine between 5.1mM – 10.6mM (7), this peak significantly overlaps the lower concentration 3.01ppm GABA resonance in 1D spectra. However, creatine exhibits no J-coupling, whereas

GABA shows complex J-coupling patterns between each of its methyl groups. Therefore, it is possible to separate the metabolites from one another on the basis of their J-coupling properties using a 2D J-resolved MRS technique.

Creatine is believed to be an indicator of brain metabolism (62) and decreased levels of Cr and PCr have been recorded in low-energy tumours with reduced glycolysis rates (63). Reduced total creatine levels have also been shown in cerebral ischaemia although the significance of this is unclear since some researchers use total creatine as a reference to compare against other metabolite changes (61).

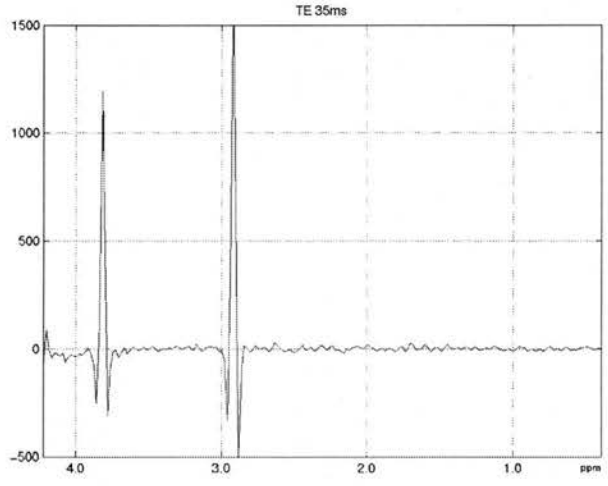

Figure 2.8 Short TE (35ms) spectrum from a phantom containing 9mM creatine (with all peaks shifted by ~ 0.1ppm in the room temperature phantom).

2.5.5 Glutamate and glutamine

The excitatory neurotransmitter glutamate is found in the human brain in concentrations of the range 6.0mM – 12.5mM (7). The strongly coupled methine and two methylene groups form a complex series of multiplets distributed over the 2.04ppm – 2.35ppm range, with an additional doublet-of-doublet centred at 3.74ppm arising from the proton on the methine group, Figure 2.9.

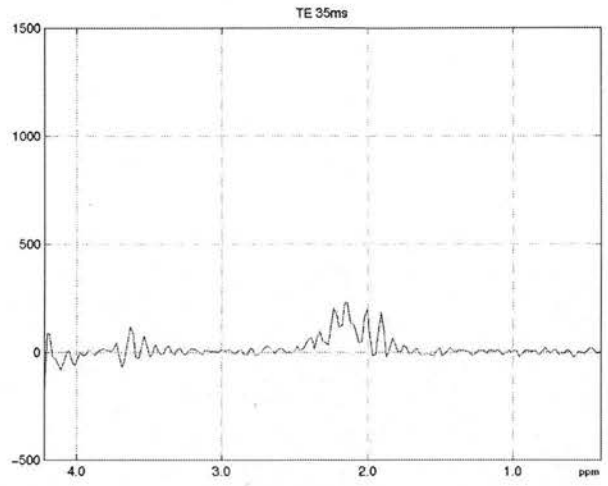

Figure 2.9 Short TE (35ms) spectrum from a phantom containing 12mM glutamate (with all peaks shifted by ~ 0.1ppm in the room temperature phantom).

As its precursor, glutamine is very similar to glutamate, both in terms of its structure and J-coupling. The four protons in the two glutamine methylene groups have resonances grouped across 2.12ppm – 2.46ppm, with an additional triplet centred at 3.75ppm due to the methine proton, Figure 2.10. With normal concentrations between 3.0mM – 5.8mM, glutamine exists at lower concentrations than glutamate.

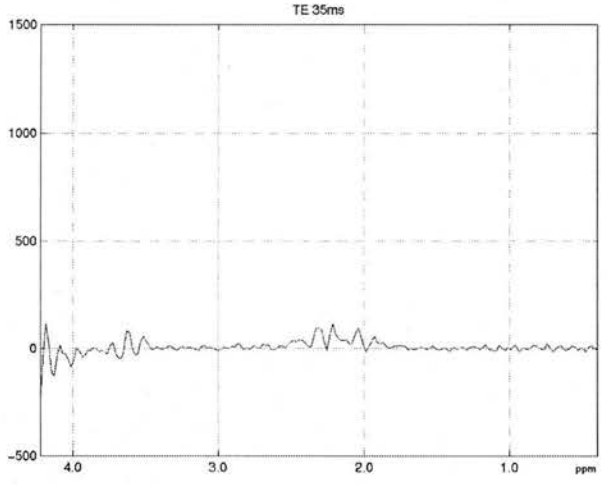

Figure 2.10 Short TE (35ms) spectrum from a phantom containing 2.5mM glutamine (with all peaks shifted by ~ 0.1ppm in the room temperature phantom).

Using clinical MR scanners, it is very difficult to resolve glutamate from glutamine using conventional 1D techniques, and so the complex multiplet arising from both in the 2.04ppm – 2.46ppm range is referred to as the "Glx" contribution. In patients

with severe liver damage causing chronic hepatic encephalopathy, elevated levels of Glx have been reported (61). Due to the enormous spread of these metabolite resonances in the MR spectrum, the Glx contribution overlaps the GABA resonances at both 1.89ppm and 2.28ppm. With similar J-coupling frequencies, it is also very difficult to separate the metabolites from each other using 2D J-resolved methods. Consequently, approaches have been adopted targeting the 3.01ppm GABA resonance, which is free from the complex overlapping of Glx.

2.5.6 *Myo*-inositol

Myo-inositol is a cyclic sugar alcohol, and has six protons giving rise to four multiplets centred at 3.27ppm, 3.52ppm, 3.61ppm and 4.05ppm, Figure 2.11. Normal physiological concentrations of this metabolite vary between 4mM – 8mM (7). In a conventional 1D MR spectrum, *myo*-inositol is not easily detected due to overlap of higher concentration metabolites, although contributions may be identified at very short TEs. In respect to GABA detection, the myo-inositol resonances are such that they do not overlap GABA at any of its resonances.

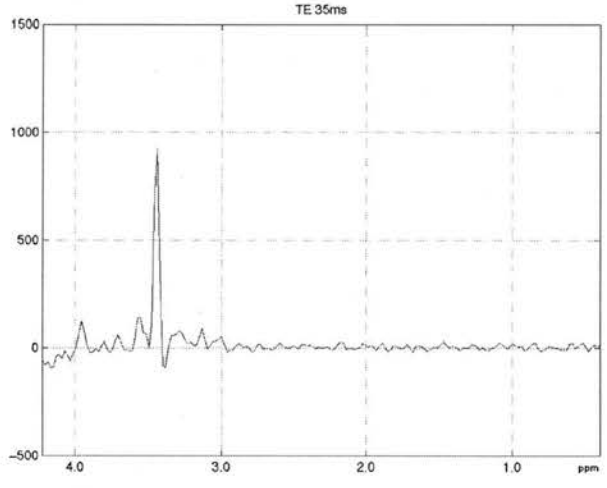

Figure 2.11 Short TE (35ms) spectrum from a phantom containing 8mM myo-inositol (with all peaks shifted by ~ 0.1ppm in the room temperature phantom).

Increases in the ratio of myo-inositol to creatine have been observed immediately following clinical diagnosis of ischaemic stroke, suggesting cell swelling due to an osmotic imbalance (32).

2.5.7 Lactate

As a product of anaerobic glycolysis, the presence of lactate is highly significant in conditions such as stroke (42). If present, the lactate methyl group is observed as a doublet centred at 1.31ppm, Figure 2.12, and so is distant enough from all the GABA resonances so as not to complicate GABA detection. Nevertheless, since the target population of this work is in patients following stroke, an awareness of this normally very low concentration metabolite (0.4mM (7)) is required.

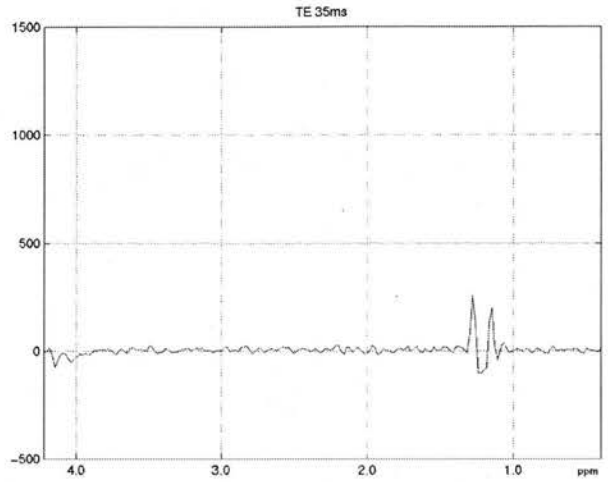

Figure 2.12 Short TE (35ms) spectrum from a phantom containing 5mM lactate (with all peaks shifted by ~ 0.1ppm in the room temperature phantom).

2.5.8 γ-Aminobutyric acid

Of primary interest to this thesis is the study of γ-aminobutyric acid (GABA), Figure 2.13. GABA is found extensively throughout the different brain regions, and it is the main inhibitory transmitter of the central nervous system (16). It acts by increasing the permeability of the postsynaptic membranes to chloride ions (78) or potassium ions (68), resulting in an increase in the threshold required for triggering an action potential. Consequently, the membrane remains stabilised in its hyperpolarised state. Early studies have shown that a deficit of GABA in the hypothalamus, which is partially responsible for the regulation of food intake, could lead to hyperphagia (excessive over-eating) or anorexia (79). In the same paper, it was reported that a defect in GABA functions in the retina might affect visual perception and integration. In addition, it was found that GABA-ergic dysregulation in layer IV

neurons of the motor cortex may result in an increased susceptibility to grand mal seizures. Through such mechanisms, GABAergic neurons are thought to play a significant role at all levels.

$$H_3N^+ - {}^4CH_2 - {}^3CH_2 - {}^2CH_2 - {}^1COO^-$$

Figure 2.13 Chemical structure of gamma aminobutyric acid, taken from (7)

The change of GABA levels in humans has been studied in numerous ways including peripheral measures of plasma and cerebral spinal fluid (CSF) concentrations, in addition to neuroimaging studies such as positron emission tomography (PET), single photon emission computed tomography (SPECT) and MRS. Decreases in the mean plasma GABA levels were observed in a group of patients with mood disorders when compared to another group of healthy controls (80), but the extent to which GABA brain activity is reflected by GABA plasma levels remains unclear. Reductions of CSF GABA levels have also been shown in depressed patients in a number of studies and have so far provided the most convincing evidence of the link between dysfunction of the GABAergic system and depression (3). In terms of routine assessment of GABA levels, these invasive, laboratory techniques are unlikely to obtain popularity, where other non-invasive methods can be reliably applied.

Nuclear medicine techniques such and PET and SPECT have been applied to neuropsychiatric disorders such as anxiety and panic attacks, to image the distribution of binding sites most frequency associated with $GABA_A$ receptors (3). (It is to this type of GABA receptor that anti-anxiety drugs bind to enhance the effect of GABA in the CNS.) In epileptic patients, PET has also been used to monitor the response of $GABA_A$ receptors to treatment with GABA-increasing medication (16). Specifically to post-stroke depression, results from PET imaging studies have been used to establish a relationship between serotonin receptor binding and the severity of symptoms of depression (81-83). However, to date, no work imaging GABA receptors in patients with post-stroke depression has been reported.

In a clinical environment however, one of the major advantages of using MRS over PET or SPECT is that MRS can be performed as part of the standard MR examination, without needing another piece of equipment, often necessitating return to the hospital at a different time (30). In addition, biochemical information is obtained using MRS without the need to inject radioactive tracers. In terms of the interpretation of the resulting data, MRS has another advantage over PET: In MRS the magnitude of the recorded peak is proportional to the concentration of the metabolite from which it arose, thus allowing it to be quantified (using either relative or absolute values). Although PET is able to quantify processes *related* to metabolites, such as metabolism and receptor binding, it is unable to quantify the *actual* concentration of the metabolite present. SPECT is able to produce colour maps displaying uptake of a specific tracer in respect to a reference region, but due to the inherent problems of the technique, such as scatter and attenuation, these results are not quantitative.

Recent MRS evidence has been acquired linking GABA dysfunction with major depression. Animal models have shown decreases in the levels of GABA with depression, a finding that has been replicated in human studies (3). In a study by Sanacora *et al,* SV MRS methods were used to quantify GABA concentrations in the occipital cortex of medication-free depressed patients and healthy volunteers (8). The findings demonstrated a 52% decrease in the measured levels of GABA in the depressed patients when compared to the normal healthy volunteers, and demonstrated the diffuse nature of the dysfunction.

However, the actual mechanisms underlying the reduction in GABA levels associated with mood disorders is not well understood and caution has been recommended in assuming that abnormally functioning GABAergic neurones have a causative role in depressive disorders (1). In cortical biopsies taken from patients undergoing surgery, reduction in GABA levels were correlated with severity of depressive mood disorders among the patients studied (84). This finding has not been replicated in post mortem results, but may be due to variation in biopsy material due to differences in the temperature of the brain at death, the cooling rate of the

brain after death, the time between death and biopsy as well as complications of death (e.g. cardiac, respiratory) and prescribed drugs (85).

Understanding the role of GABA dysfunction in mood disorders has been further complicated by the results of depression-related pharmacological animal studies. In the studies reviewed by Sanacora *et al*, treatment of depression using a variety of anti-depressants saw hugely variable results (including increases, decreases and no measured change in the GABA levels) suggesting no consistent pattern of response (3).

In MR spectra, GABA exhibits three resonances, due to the three methylene groups, Figure 2.13, with multiplets centred at 1.89ppm, 2.28ppm and 3.01ppm, Figure 2.14. Despite its prominent role in maintaining normal brain activity, GABA is only present in the brain in concentrations of 1.3mM – 1.9mM (7). At high field strengths, with larger chemical shift resolution, it is possible to observe GABA using a numerically optimised, "single-shot" pulse sequence (12). Using an editing sequence at 7T, Terpstra *et al* identified GABA in 14 normal volunteers, at concentrations in agreement with previously published ^{13}C MRS results (11). However, at 1.5T, GABA is extensively overlapped by other metabolites. Therefore, editing methods, or techniques exploiting differences other than chemical shift (such as J-coupling) have to be applied. These sequences are often more complicated than the standard clinical spectroscopy sequences and extensive post-processing is essential. Consequently, such sequences are not routinely applied. A review of the MR methods for detecting GABA is provided in §3.

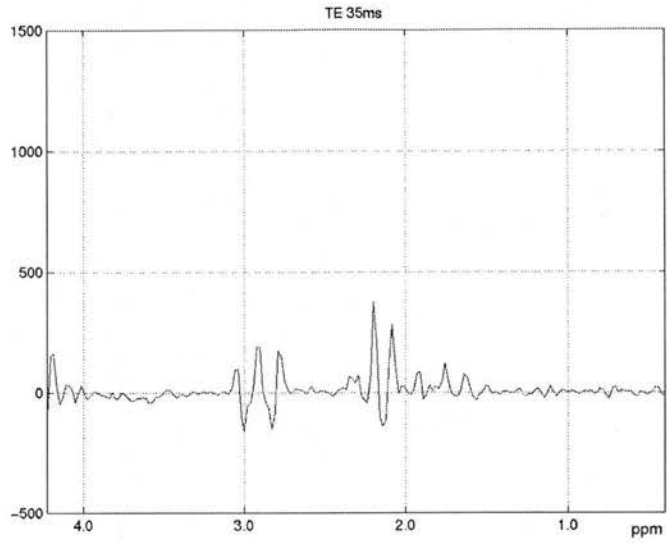

Figure 2.14 Short TE (35ms) spectrum from a phantom containing 10mM GABA (with all peaks shifted by ~ 0.1ppm in the room temperature phantom).

2.5.9 Macromolecules

Macromolecules are large organic molecules with a molecular weight greater than 3500 Dalton (42). They are detected in MRS as broad resonances appearing below metabolites of smaller molecular weight. At short echo times, macromolecule contributions exist across the entire frequency range (0.6ppm – 4.4ppm) complicating accurate quantification of all the metabolites of interest, including GABA (86). It is possible to separate macromolecules from the low molecular weight metabolites on the basis of their different T_1 relaxation times: Metabolites have longer T_1's than the macromolecules, which means that the macromolecules will recover their longitudinal magnetisation before the metabolites (44). Therefore, by using an inversion recovery (IR) pulse, with an inversion time (TI) equal to the time taken for the longitudinal magnetisation of the metabolites to reach zero, only the magnetisation from the macromolecules will be excited producing a metabolite-free spectrum. Such IR techniques have been used to eliminate macromolecules from the metabolite spectra (41,44,87). However, analysis of the macromolecule baseline is starting to provide clinical information, with differences in the observed baseline attributed to cerebral location and age (86), and pathologies such as stroke (42,43).

2.5.10 Other GABA contaminating resonances

It is clear from the discussion in the preceding sections how the overlapping of higher concentration metabolites complicates the detection of GABA at 1.5T. In addition to these commonly studied metabolites, contributions from glutathione (GSH) and homocarnosine can contaminate GABA resonances. GSH is normally present *in-vivo* at concentrations between 2mM and 3mM, with multiplets occurring across the spectrum in the range 2.15ppm to 4.56ppm (7). Of particular concern to this work, this tripeptide has two doublets of doublet centred at 2.93ppm and 2.98pm, very close to the 3.01ppm GABA multiplet. Homocarnosine exists at much smaller concentrations of between 0.3mM to 0.6mM, but also has a multiplet group close to that of 3.01ppm GABA at 2.96ppm (7). The constituents of this dipeptide include GABA, so it is no surprise that the protons in its three methylene groups are similar to those of GABA. Although normally at such low concentrations as to remain undetectable *in-vivo* at 1.5T, elevated levels have be reported in epileptic treatment using vigabatrin (88), ensuring that its presence in an MR spectrum cannot be entirely discounted.

2.6 Conventional, one-dimensional spectroscopy

2.6.1 Introduction

Although the focus of this thesis is the use of 2D spectroscopy techniques, a short section on conventional, 1D methods is included to demonstrate how MRS is currently applied on clinical MR scanners.

In theory, it is possible to acquire MR spectra from all body regions, but clinical use of the technique has concentrated on MRS of specific organs, such as the brain, and specific disorders within those organs (62). Since this work is concerned only with the application of MRS in the brain, discussion of its use in other organs will be omitted.

A common protocol for MR spectroscopy exists, independent of the exact technique adopted. This comprises of localisation and shimming of the VOI followed by

suppression of the water signal, and each of these processes will be discussed in turn. In addition, a description of the effects of changing some of the acquisition timing parameters will also be included.

2.6.2 Localisation

The aim of MRS is to obtain chemical information from a specific anatomical region and so accurate localisation of a VOI is essential. Ideally, perfect localisation would allow measurement of 100% of the available signal within the VOI while suppressing all other signals from outside the volume (89). In early MRS experiments, localisation was achieved using a surface coil (49). However, this type of localisation alone is not sufficient for *in-vivo* MRS of the brain due to contaminating resonances from the layer of fat within the scalp of the subject (61) and obtaining only poor definition of the VOIs (52).

Similar to conventional MRI, localisation in MRS is achieved using a specific series of RF pulses in the presence of slice selection gradients. However, unlike localisation in MRI, acquisition of the FID must occur in the absence of any gradient in order to maintain the chemical shift information. Using this combination of switched magnetic field and RF pulses, it is possible to acquire signals from a single voxel or simultaneously from a number of voxels to form low resolution, chemical shift images (61).

2.6.2.1 Single Voxel Spectroscopy

As the name implies, MR signals from a single volume of interest are acquired using single-voxel (SV) spectroscopy. Localisation is achieved using three slice–selective gradients, applied in orthogonal directions, and the MRS signal is recorded from the intersection of these three planes (57).

In clinical, single-voxel spectroscopy, the most commonly used localisation techniques are Point RESolved Spectroscopy (PRESS) and Stimulated Echo Acquisition Mode (STEAM) (61,89). Both sequences achieve accurate 3D

localisation using three RF pulses (90). PRESS consists of a 90° excitation pulse followed by two 180° refocusing pulses, all in the presence of mutually orthogonal gradients, after which a full spin-echo is acquired in the VOI (61). STEAM consists of three 90° excitation pulses resulting in a stimulated echo, which at maximum, is only half the signal of a full-echo. Since several 2D sequences have been based on PRESS (22-24), it is appropriate that this sequence is studied in more detail.

As mentioned above, PRESS consists of an excitation pulse followed by two refocusing pulses, Figure 2.15. When the 90° RF pulse is applied at the same time as the X magnet field gradient, the spins in the YZ plane are excited. By the same argument, it is clear that when the Y gradient is applied at the same time as the first re-focussing pulse, then the spins located in the XZ plane are refocused, Figure 2.15 (b). The resulting echo is then refocused by the second 180° pulse in the presence of the Z gradient, and a second spin echo formed at TE including the spins excited in the XY plane. Therefore, the recorded echo contains data from the spins in the intersection of all three planes (90). Spoiler gradients are also applied to prevent the detection of signals experiencing only one or two of the three RF pulses (52).

The actual size of the intersection of the three planes, or the VOI, can be changed by altering the strength of the applied gradients (61). Consequently, the dimensions of the VOI can be identical for all MRS experiments. The situation is more complicated when defining the actual spatial location of the VOI. Differences in chemical shift between the metabolites result in the generation of voxels – of the dimensions as defined by the gradients – for each of the resonances within the sample. The effective VOI for each metabolite peak will be displaced from the next according to the chemical shift separation of the resonances. The recorded spin-echo will only contain information from the overlapping voxels, which due to the chemical shift displacement, may not contain 100% of the metabolite signal (90). This chemical shift artefact is particularly important when applying PRESS to coupled systems, and will be discussed further in §3.

The timings between each of the pulses and before spin-echo acquisition are carefully controlled. Examination of the PRESS sequence software listing, e.g. on the 1.5T GE Signa Horizon scanner used for all experimental work in this thesis, allows definition of each of the time intervals as shown in Figure 2.15. These are listed in Table 2.5. It is important to note that the actual numerical value stated for TE is split equally across the last refocusing pulse – the relevance of which will become apparent in the examination of 2D J-resolved MRS in §3.

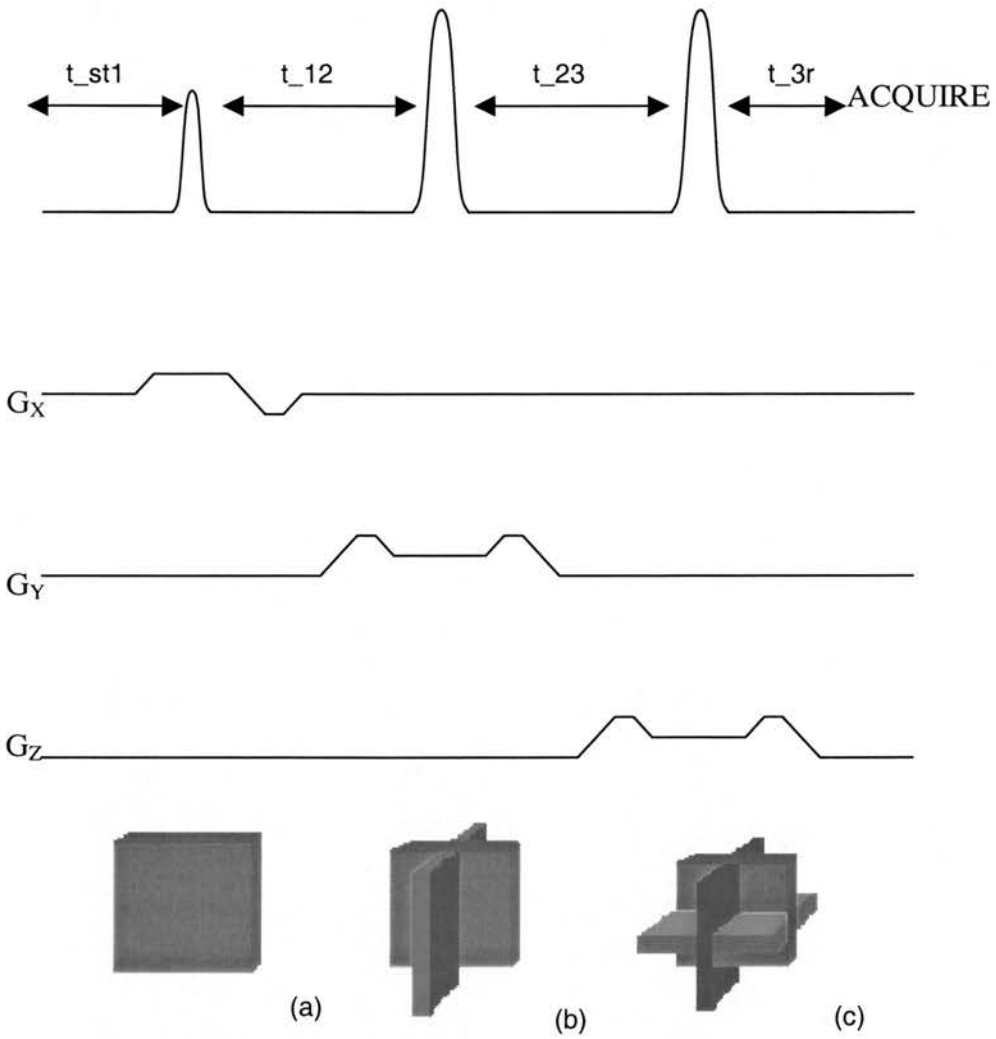

Figure 2.15 RF pulse and gradient sequence for PRESS localisation (spoiler gradients not shown). (a), (b) and (c) show the planes of excitation following application of an RF pulse in each of the three gradient directions, resulting in a signal recorded from the excited spins in the intersection of the planes.

Although the PRESS sequence is very successful in allowing a signal to be recorded from a well-defined voxel, the minimum echo time (TE_{min}) is larger than the TE_{min} permitted using STEAM localisation. In PRESS, the TE has to be long enough to allow all three RF pulses to be played out including the formation of two spin-echoes and allow sufficient time for application of the spoiler gradients. These are necessary to eliminate signals excited from outside the VOI so that only the second spin echo arising from all three RF pulses at the intersection of all three planes is recorded

Table 2.5. Description of the timing parameters used in the GE PRESS spectroscopy sequence

Time	Description	Value
t_{st1}	time from start to centre of pulse 1	Fixed at 2.548ms
t_{12}	time from centre of pulse 1 to centre of pulse 2	Fixed at 9.392 ms
t_{23}	time from centre of pulse 2 to centre of pulse 3	Varies according to $t_{23} = \frac{te}{2}$
t_{3r}	time from centre of pulse 3 to centre of the echo (when acquisition starts)	Varies according to $t_{3r} = \frac{te}{2} - t_{12}$

PRESS is less sensitive to motion than STEAM and so signals from diffusing metabolites are less attenuated using PRESS (61). However, better water suppression can be achieved with STEAM compared to PRESS localisation, due to the additional water suppression pulse between the last two RF pulses. Immediately after the second 90° pulse (in STEAM), the magnetisation is along the z-axis and so is unaffected by variations in the magnetic field gradients, thus allowing another water suppression pulse without compromising the recorded signal.

Despite these drawbacks, PRESS has become the localisation technique of choice for *in-vivo* MRS since it records the maximum available signal from uncoupled resonances (91). This is a considerable advantage when acquiring signals from low concentration metabolites.

2.6.2.2 Chemical shift imaging

As with conventional MR imaging, localisation in ^{1}H chemical shift imaging (CSI) is achieved after the 90° excitation pulse, using phase encoding gradients in three dimensions to spatially encode the metabolite information (61). A 180° refocusing pulse is then applied to produce a spin echo. By varying the gradient from a minimum (negative) value in a step-wise manner to the set maximum (positive) value, then a series of spin-echoes are recorded allowing reconstruction of the metabolite information across the whole CSI slice.

Although in theory, distinct FIDs are recorded from each voxel in an n x n spectroscopy matrix, the true spatial sensitivity of each is more akin to a point-spread function, with maximum sensitivity in the centre of the voxel and oscillating side-bands spreading outwards. This gives rise to the main disadvantage of CSI, so called "Fourier Bleed", where signals contribute to FIDs both within and outside the voxel from which they arose, due to the side-bands extending out of the voxel from which they were generated (61). In clinical applications, the CSI matrix size is small compared to that required for MR imaging purposes, and so signals arising from Fourier Bleed that contaminate adjoining voxels have a much larger influence over the spectroscopic image. Fourier bleed can be reduced with post-processing methods, e.g. by extrapolating the lipid k-space region to reduce the ringing artefacts, or using rapid acquisition sequences to prevent loss of SNR of the metabolites of interest (92). In addition, PRESS and STEAM localisation can be incorporated into CSI to improve localisation and prevent contamination from lipids present in the scalp, bone marrow or white matter myelin.

In diseases with extensive patterns of brain abnormality, such as stroke (63) or gliomas (93), CSI is able to provide information about both diseased and normally appearing brain matter across whole brain slices. This multi-voxel spectroscopy data can be compiled into chemical-specific colour maps overlaid onto anatomical images of the same slice, to allow immediate comparison between structural and functional information.

CSI lies outside the scope of this thesis, but is included here to complete the discussion on 1D MRS techniques. Readers particularly interested in 1D MRS methods are directed towards the published literature (for example (60,61,94,95)) for further details.

2.6.3 Shimming and water suppression

Precise localisation is essential in ^{1}H MRS to prevent contamination of the spectra from scalp lipids that may obscure the signals from the metabolites of interest. In addition, effective suppression of the water signal is required for the acquisition of well resolved spectra (90).

Shimming is the process by which the homogeneity of the static magnetic field is improved by manipulating the electrical currents in the gradient coils (64). Clinical MR scanners have an automated shimming procedure that adjusts the shim currents in the gradient coils until the FID of the water signal is optimised. Successful shimming produces a slowly decaying FID which, when Fourier Transformed, results in a high intensity water peak with a narrow linewidth. Without satisfactory shimming, the natural inhomogeneity in the magnetic field would prevent the detection of the very small chemical differences of the metabolites, thereby producing very low-resolution spectra. For clinical MRS at 1.5T, the homogeneity needs to be less than the desired resolution of measurement (0.1ppm) over the VOI, which practically is better than five parts in 10^{8} to achieve linewidths of 3Hz (52).

In terms of spectroscopy, and specifically spectroscopy of the brain, the chemicals of interest are contained within the intracellular water compartment. Since intracellular water accounts for 85% of brain water (60), water is the main signal in any ^{1}H MR spectrum, and without water suppression, would be the *only* visible signal.

Most spectroscopy sequences use a CHEmical Shift Selection (CHESS) pulse to suppress the water signal. A frequency-selective 90° pulse is applied to flip the water into the transverse plane where it is then immediately dephased by a spoiler

gradient. Typically three CHESS pulses are required for adequate water suppression. This allows only the magnetisation from the metabolites in the longitudinal plane available to contribute to the FID after the specific spectroscopy sequence has been played out (61).

2.6.4 Sequence timings

Although the number of metabolites detected using conventional, 1D MRS techniques is restricted by overlap from the highest concentration metabolites, the appearance of the spectra can be altered to aid metabolite identification by changing the timing parameters used at acquisition.

Spectra acquired with a short TE have a more complex appearance, Figure 2.16 (a). This is due to the presence of short T_2 metabolites such as glutamate and glutamine, as well as those from the longer T_2 metabolites such as NAA, choline and creatine. Another characteristic of such spectra is the underlying broad resonance due to macromolecules.

Using a longer TE to acquire MR spectra, typically TE = 125ms - 145ms, removes all contributions from macromolecules and signals from the very short T_2 metabolites. The resulting spectrum will only contain metabolites with longer T_2's, such as NAA, choline and creatine, and will therefore be much simpler to read, Figure 2.16 (b). However, it should be noted that the magnitude of the remaining metabolites will be reduced, also due to T_2 relaxation (42).

Short TE spectra are useful for providing a more complete spectrum with information from several cerebral metabolites. However, at longer TEs, quantification of the metabolites can occur without complications from the underlying macromolecules or associated very short T_2 metabolites. Therefore, in cases where the investigator / clinician is only interested in NAA, choline and creatine, it is often more useful to collect longer TE spectra.

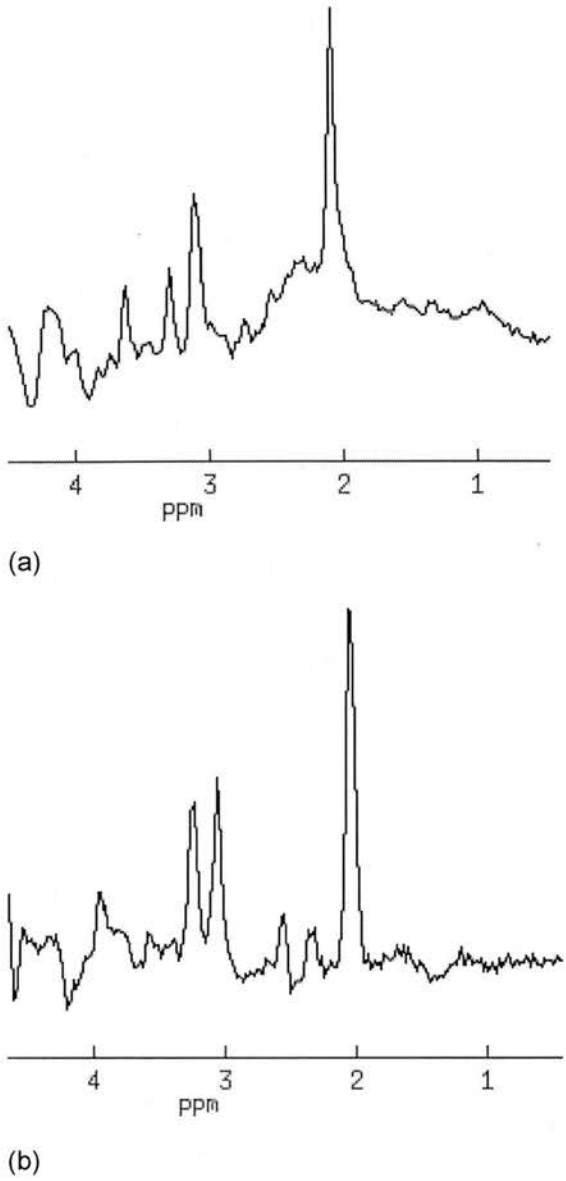

Figure 2.16 (a) Short TE (35ms) *in-vivo* MR spectrum acquired using a volume head coil. Note the broad macromolecule baseline underneath the metabolite spectra across the entire chemical shift range. (b) Long TE (145ms) *in-vivo* MR spectrum from the same volunteer.

The choice of echo time is also very important in the detection of J-coupled metabolites. For example, lactate, a J-coupled metabolite with the three methyl protons, gives rise to a doublet at 1.31ppm (90). In addition, lactate has a quartet at 4.11ppm, but this is not usually observed due to its close proximity to the water peak. However, the difference between the chemical shift frequencies of lactate (4.11ppm – 1.31ppm = 2.8ppm ≈ 180Hz) is much greater than the coupling between the resonances (6.9Hz (7)), and so at clinical field strengths, lactate is considered a weakly coupled spin system (76), Figure 2.17.

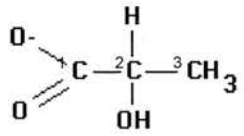

Figure 2.17 Chemical structure of lactate. Weak scalar coupling occurs between ^2CH and $^3CH_3$.

As discussed in §2.5.7, lactate is not detected in normal *in-vivo* spectra since it is an end product of anaerobic metabolism. However, when present in increased levels *in-vivo*, or simply *in-vitro*, lactate is very interesting as the effect of its J-coupling properties can be observed in routine, 1D MR spectra.

Lactate can be completely described by a A_3X spin system (90). (By convention, spin-systems described by letters that are well separated are weakly coupled, whereas those described by adjacent letters (AB) are strongly coupled.) During the evolution period after an excitation pulse, the individual resonances will have slightly different resonant frequencies due to the effects of chemical shift, scalar coupling and magnetic field inhomogeneities, and will therefore precess at a slightly different rate in the transverse plane. Consequently, immediately before the refocusing pulse, the resonances will have acquired slightly different phase shifts. The evolution of each of the resonances, and therefore the end phase shift, is governed by the applied echo time, and so the resulting spectra are characterised by pure in-phase or pure anti-phase magnetisation or a combination of both. Examples of the evolution of lactate, as measured *in-vitro*, are shown in Figure 2.18. As a result of J-coupling, the appearance of lactate spectra will change according to the TE used and this can be a useful tool in differentiating coupled from uncoupled metabolites. It is this principle that is applied to facilitate the identification of GABA using 2D J-resolved spectroscopy as described in §3.3.2.

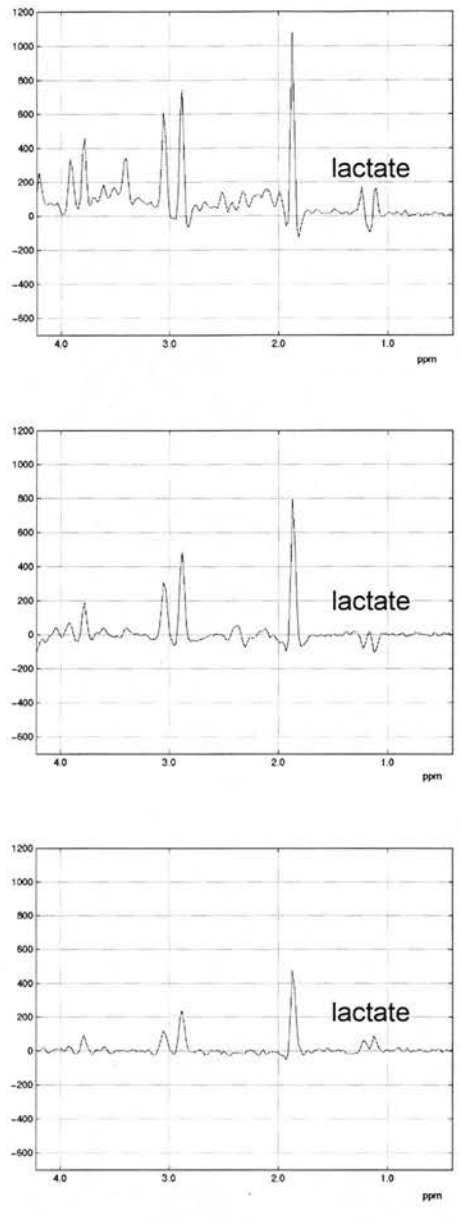

Figure 2.18 J-evolution of lactate. All experiments were performed *in-vitro*, using a GE spectro phantom containing 5mM lactate. Single-voxel spectroscopy was performed (TR = 2000ms, NEX = 8, VOI = 3 x 3 x 3 cm^3) with (a) TE = 35ms (~ J/4), (b) TE = 145ms (4J/4), (c) TE = 290ms (8J/4) where J ≡ 6.9Hz.

2.7 Two-dimensional spectroscopy

Two-dimensional (2D) MRS techniques refer to the two *frequency* dimensions. In conventional MR spectroscopy, there is only one frequency axis – the chemical shift axis – and so such methods are known as one-dimensional. The other variable –

signal amplitude – is not included in any discussion of the dimension of an experiment (71).

The actual information on the frequency axis depends on the type of experiment being performed, and on the interactions within (or between) the molecules of interest. These interactions fall into three categories of (1) "through-bond coupling", such as shift correlation (COSY) and J-resolved experiments; (2) "through-space coupling", utilising the nuclear Overhauser effect; (3) "chemical exchange", also utilising a technique based on the NOSEY experiment.

In general terms, the principles behind generating a second dimension follow a similar structure, independent of the precise technique, Figure 2.19. As with conventional, 1D spectroscopy, each 2D experiment has a preparation period, where the spins are initially excited, and a detection period during which the FIDs are acquired. Two additional periods are required for 2D MRS: An evolution and a mixing period. These are introduced between the preparation and detection periods, Figure 2.19. Crucial to all 2D experiments is a variable time delay (t_1), applied in the evolution period and uniformly increased to a set final value as the experiment proceeds (77). At each value of t_1, the same pulse sequence is repeated and an FID recorded. As the t_1 time interval increases, the spectra will decay exponentially due to T_2* relaxation effects, and so spectra collected with long t_1 will show considerably diminished intensities. Consequently, each signal recorded during the detection time (t_2) is modulated by the precessional time in t_1. Fourier transform of the recorded signal with respect to t_1 produces the frequency information appearing on the F1 dimension in the resulting 2D spectrum.

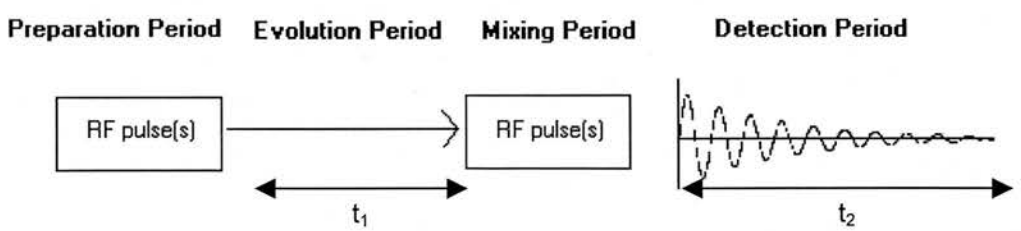

Figure 2.19 General requirements for a 2D experiment

The mixing period is particularly important in experiments containing coupled spins, as in any *in-vivo* MRS experiment of the brain. During this period, coupled spins are able to transfer polarisation (or coherence) between two nuclei (96), which means that magnetisation originating from one spin is transferred onto another spin. Therefore, the frequency of the spins during t_1 is no longer equal to the frequency during t_2, and this property can be exploited to provide coupling information about the spin systems. Depending on the exact nature of the 2D experiment, the mixing period may contain one or more RF pulses and so will determine the relationship between the two frequency dimensions. The frequency information in F2 always corresponds to the chemical shift frequencies of the peaks, but F1 is used to display information not normally acquired in a 1D experiment, Figure 2.20. Different types of 2D MRS will be discussed further in §3.

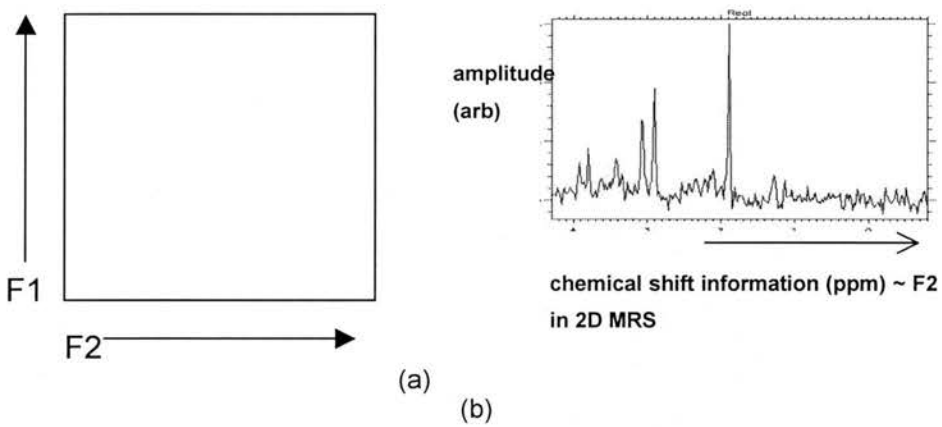

Figure 2.20 (a) General format of a 2D MR spectrum. F1 is used to display information not resolved in 1D experiments (such as J-coupling) whereas F2 shows the chemical shift information of the peaks, analogous to a 1D MRS experiment (b).

3 GABA detection using MRS at 1.5T

3.1 Introduction

It has been established in the preceding chapter that *in-vivo* MR spectroscopy can provide considerable metabolic information, particularly for the higher concentration cerebral metabolites such as NAA, choline and creatine. However, due to its low concentration, its complex spectrum and the overlapping of higher concentration metabolites, GABA is not as easy to detect using conventional, 1D-spectroscopy methods. At very high fields, such as 11.7T, the improvement in spectral resolution associated with the increase in B_0 means that single shot sequences can be used to identify GABA (2). However, at lower field strengths of 1.5T, simplification of the spectrum is required to allow identification of overlapped, lower concentration metabolites such as GABA. This can be achieved in a variety of ways, including spectral editing and two-dimensional techniques. In this chapter, the principles behind each of these approaches will be discussed and the application of these methods to GABA detection at 1.5T will be examined.

3.2 Spectral editing techniques

3.2.1 Introduction

Spectral editing exploits the J-coupling of coupled metabolites to differentiate them from the spins in uncoupled metabolites. There are different types of spectral editing techniques, which can simplify spectra by using differences in chemical shift, couplings within nuclei or relaxation times (15). Methods using differences in chemical shift are routinely used in both MRI and MRS to suppress the signal from fat and water (75). However, for the small chemical shift range of the metabolites of interest, this approach is not sensitive enough to discriminate adequately between the resonances. Methods utilising changes in relaxation time are equally insensitive. Consequently, approaches making use of differences in J-coupling have been investigated, and this section will explore the success of two examples of such schemes for GABA measurement: Multiple quantum filters and difference editing.

3.2.2 Difference method

3.2.2.1 Background theory

As the name suggests, spectral editing using a spectrum difference method relies on the acquisition of two spectra, with the difference between the two providing the edited spectrum. In its simplest form, selective 180° pulses can be used to eliminate uncoupled resonances from the difference spectrum, Figure 3.1. The first MRS experiment, acquired without the 180° RF pulse, results in a complete spectrum of all the metabolite resonances. The second sequence includes the refocusing pulse. This selective pulse affects only the coupled spins, and so the uncoupled spins remain positive in the resulting spectrum. After subtraction of the two spectra, the difference spectrum will only contain resonances from the targeted coupled spins.

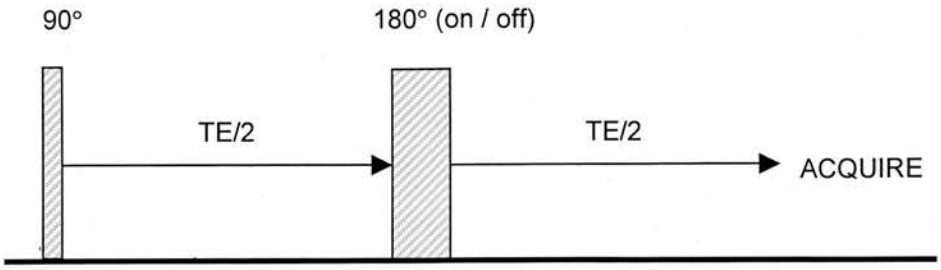

Figure 3.1 Basic pulse sequence for spectral editing based on differences in J coupling (97). The 180° pulse is designed to select one frequency component of the coupled system. A first spectrum is acquired without the pulse and a second spectrum with the refocusing pulse on, so that subtraction of the two spectra yields a difference with the targeted resonances.

3.2.2.2 Clinical application

To date, very little work has been published using difference editing techniques to measure GABA at 1.5T (13,14,16). In the first of these papers, a spectral editing sequence developed for a 2.1T system was modified for application at 1.5T (13). The original sequence, developed by Rothman *et al* (98), used a Delays Alternating with Nutation for Tailored Excitation (DANTE) inversion pulse centred on the 1.9ppm GABA resonance to induce J-modulation of the 3.01ppm GABA resonance. The DANTE sequence is made up of a series of N hard, very short duration RF pulses separated by regular periods for free precession of the magnetisation (76). After each pulse, the spins are flipped through a small angle and allowed to precess, so that the next RF pulse acts on the spins when they are in different phases of precession. Consequently, when viewed as Cartesian vectors in the rotating frame of reference, the spins follow a zigzag path determined by the offset from resonance before each RF pulse. By keeping the pulse amplitude constant while varying the pulse duration, DANTE can be used to shape pulses where amplitude modulation is not possible, and the pulse envelope may be shaped to meet a specific design. In this example, the DANTE pulse inverted the 1.9ppm GABA resonance and the sidebands of the 3.01ppm GABA resonance, resulting in an edited spectrum with the removal of all resonances *not* J-coupled to the 1.9ppm GABA resonance.

The application of this method at 1.5T is complicated by baseline distortions from the incomplete subtraction of NAA and choline, which degraded the appearance of

the difference spectrum around the 3.01ppm GABA resonance. Consequently, these contaminating resonances influenced the accuracy of quantification contributing to the large standard deviations (SDs) reported (46% for 8cc VOIs and 23% for 4cc VOIs). In addition, no attempt was made to discriminate GABA from the underlying macromolecule resonances (40), which probably contributed to the poor reproducibility of the results. Nevertheless, a GABA "peak" was identified in the edited spectra of all 10 normal volunteers.

As part of a study comparing techniques to identify low concentration metabolites, Weber *et al* developed an editing protocol by adapting the standard PRESS localisation sequence (15). The authors also targeted the 3.03ppm creatine peak to resolve the underlying 3.01ppm GABA resonance. The editing sequence was tested in five volunteers, and GABA concentrations between 0.7mM and 1.5mM were reported, with an "uncertainty" of 0.5mM. However, from the poorly resolved *in-vivo* example provided, it is difficult to see exactly what part of the GABA "peak" would have been quantified. Again, no correction for the underlying macromolecules was applied.

The same difference method was later applied to another set of five healthy volunteers undergoing both MRS and PET examinations to monitor the effects of the GABA-increasing drug vigabatrin (16). Each of the volunteers received different doses of the drug, and a near-linear trend was observed between dose increase and GABA measurement at low concentrations of vigabatrin. However, with only one experiment per volunteer, the reproducibility of the measurements could not be established. Baseline errors were less pronounced in the edited spectra presented here than in (13), but yet again, no account was taken of contamination of the GABA resonance from macromolecules or homocarnosine. Since earlier work by Petroff *et al* (88) had shown increases in homocarnosine with vigabatrin, it is possible that increases in this dipeptide contributed to the increased GABA measurements reported in (16).

Although Weber *et al* reported that "an adequate" SNR was acquired for all of their GABA measurements, the GABA peak in the difference spectrum provided post-drug administration was much more convincing that that pre-administration (16). It should also be noted that the increases in GABA were identified as *positive* peaks in the difference spectra. In a later study by the same group investigating the effects of vigabatrin in combination with the coenzyme pyridoxal 5'-phospate (14), an increase in the GABA+ / creatine signal was shown as a *negative* GABA+ resonance (GABA+ was used to acknowledge the contribution of macromolecules and homocarnosine to the "GABA" peak). Despite using the same acquisition protocol in both studies, different post-processing procedures were applied: In the first study, the difference spectra were the result of the nonedited – edited spectra (16). In this later work, the difference spectra resulted from the edited – nonedited spectra (14). Even with this change in analysis, the peak assignments pre-administration were again not clear and the spectra only marginally better post-drug administration. This may suggest that normal physiological GABA levels are just beyond the limits of detection using this spectral editing, difference method at 1.5T.

3.2.2.3 Technical limitations

The main disadvantage of this approach is that it only provides information about a single metabolite. In disease processes where the underlying metabolic changes are poorly understood, it is often useful to obtain information on *all* cerebral metabolites. Difference editing sequences, using specially tailored selective excitation pulses, permit the investigation of only one metabolite at a time (99). However, the acquisition of multiple difference editing spectra would be inefficient and with examination times quoted of up to 90 minutes (14), totally impractical. In such situations, it is more useful to apply a technique that allows the study of all metabolites simultaneously.

In addition to the inefficiency of the technique, application of difference-editing MRS relies on the acquisition of two separate spectra and this makes it extremely sensitive to motion (97). Any patient movement between the two sequences would

lead to subtraction errors, complicating the resulting spectra and resulting in inaccuracies in quantification (21).

It is clear from the literature that difference-editing techniques at 1.5T are not suitable for pure GABA measurement due to the indistinguishable J-modulations of the resonances from homocarnosine and macromolecules at 3.0ppm (11,12). However, from a scientific viewpoint, it is extremely interesting to evaluate new methods of GABA detection on clinical scanners. In collaboration with Dr. N. Sailasuta from General Electric Health Care (GEHC), a difference editing sequence was obtained for initial testing. Since the GABA editing pulse was designed for a 3T system, the failure of the sequence to work at 1.5T was not surprising.

The sequence provided by Dr. N. Sailasuta was based on the editing sequence by Hetherington *et al* (100). The homonuclear editing sequence uses specially designed Shinnar-Le Roux type pulses, which are polynomial in design and therefore have more optimised shapes when compared to the more conventional sinc or Gaussian RF pulses (64). The pulse consisted of specific frequencies for inversion and additional regions of non-inversion, to both invert the 1.9ppm macromolecule resonance and reduce the effect of the pulse on the 1.7ppm macromolecule resonance. Since the version of the sequence from Dr. Sailasuta was written for frequency bandwidths on a 3T scanner, the RF pulse was far too broad when applied at 1.5T, and so rather than refocusing only the spins of interest, the pulse wiped out almost the entire metabolite spectrum. With an editing pulse comprising a train of 30 pulses and 29 delays, optimisation of the pulse for 1.5T would be difficult at the best of times, and impossible without the necessary software. Even if a standard sinc RF pulse had been used for editing, production of a narrow pulse profile is not easy. To create a discrete and uniform frequency profile, an RF pulse of infinite duration and an infinite number of side lobes is required, which is clearly not realistic in an imaging system. In addition, increase in the pulse duration would require an increase in the echo time, ultimately leading to a reduction in the measured signal. DANTE RF pulses have been proposed as a method to overcome the drop in measured signal and deviations in the excitation profile arising from truncation artefacts. However,

results have not been entirely successful at 1.5T with incomplete subtraction of the metabolites close to GABA and baseline distortions (97).

3.2.3 Quantum filter techniques

3.2.3.1 Background

As described in the previous section, difference editing techniques exploit changes in frequency, induced by RF pulses, to simplify spectra. In contrast, multiple quantum filter methods (MQF) simplify spectra using a combination of RF pulses *and* magnetic field gradients to selectively rephase only spins from a specific coherence pathway (15). Equally important to this technique is the concept of coherence, and more specifically, the transfer of coherence between coupled spins.

To help explain the phenomenon of coherence, consider the application of a 90° pulse to a spin system at equilibrium. This RF pulse will force the magnetisation into the transverse plane, and if the spin system is coupled, may be represented by a specific number of energy level transitions as described in §2.4.3. In a conventional MRS experiment, the magnetisation observed on the resulting spectrum arises from the transition of spins between energy levels such that the change in magnetic quantum number, $\Delta m = \pm 1$ (70). Only single-quantum coherences (SQCs) are able to induce a voltage in the receiver coil, but this is not to say that other quantum coherences do not exist and cannot, with some manipulation, be observed.

Multiple quantum coherences (MQCs) arise when spins states are separated by $\Delta m \neq \pm 1$, where the spins are effectively forced to absorb more than one quantum of energy. In pulsed MR, this is achieved with application of a second RF pulse (101). This second pulse forces the spin states to absorb another quantum of energy, and therefore move to another energy level where the effect of this transition is no longer observable in the MR spectrum. However, the presence of these higher order quantum coherences can be detected indirectly by converting the spin states back to a SQC using RF pulses after manipulation of the spins by magnetic field gradients.

After the second RF pulse, both zero quantum coherences (ZQCs) and double quantum coherences (DQCs) are produced in equal proportions, and experience the first magnetic field gradient. For a DQ experiment, such as the one described by Knüttel *et al* (102), all coherences produced after the second RF pulse are "filtered", using magnetic field gradients, to obtain only DQCs, Figure 3.2. The selection of the DQ pathway leads to an automatic 50% loss in signal, since the other 50% of the available magnetisation was converted into ZQCs.

Theoretically, both coherence orders of $\Delta m = \pm 2$ are possible, but practically, only one of these pathways can be selected. Therefore, another 50% of the signal is lost. A third selective RF pulse, applied at the same frequency as the second, converts the DQCs into SQCs, allowing a theoretical maximum of 25% of the total magnetisation to be recorded in the MR spectrum.

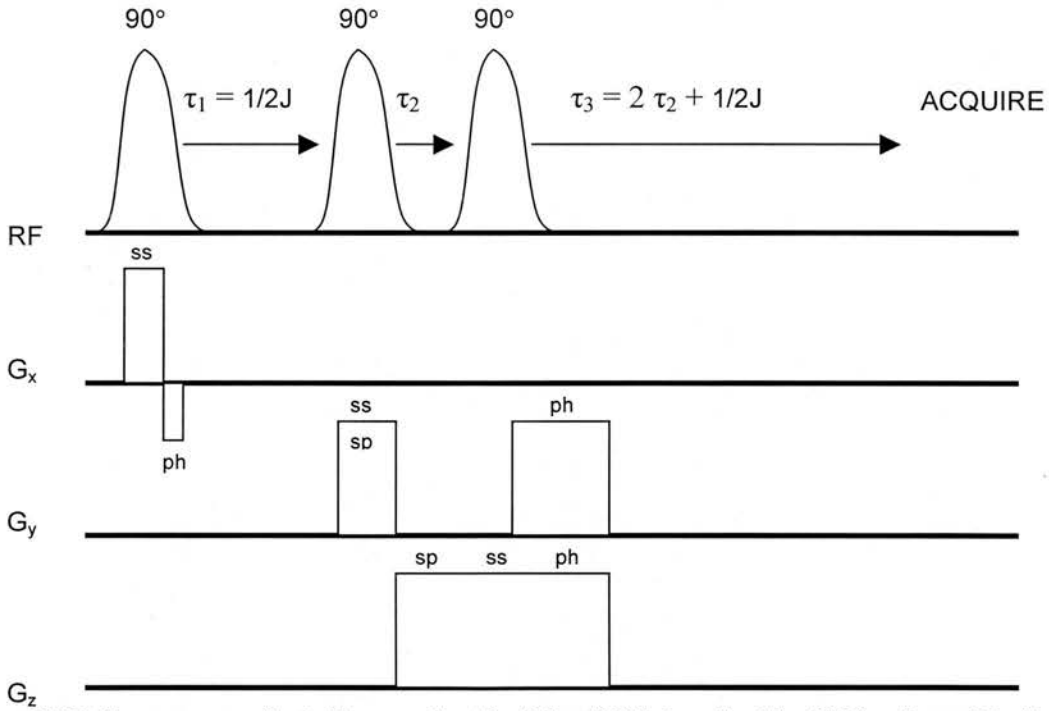

Figure 3.2 Pulse sequence (including gradients) of the DQF described in (102), where J is the spin-spin coupling constant of the spin-system of interest. The gradients served three purposes: slice-selection (ss), dephasing / rephasing intervals (ph) and homospoiling of the coherences (sp). For a weakly coupled spin system (e.g. lactate), after the first RF pulse, the spins evolve under chemical shift and spin-spin coupling interactions. The second RF pulse transfers the single quantum coherences into multiple quantum coherences. Since only the DQC pathway is being selected, all other pathways are dephased by the gradients in τ_1 and τ_3. The DQCs evolve in τ_2 (again due to spin-spin coupling and chemical shift differences). The third RF pulse transfers 50% of the DQCs into SQCs (see text). These are refocused in the time interval τ_3.

3.2.3.2 Clinical application

To date, all work using this technique at 1.5T uses DQF edited signals. Although ZQCs would permit an additional 25% of the total magnetisation to be retained, it has the disadvantage that uncoupled spins are not suppressed (97). During application of the only gradient used in ZQF after the second RF pulse, any spins from uncoupled resonances are aligned along the longitudinal axis and so do not experience the change in B_0. Without a second gradient pulse, these unwanted resonances are not dephased, and so remain in the recorded spectrum. This is particularly relevant when attempting to resolve GABA from the overlying creatine singlet.

One of the first reports specifically reporting GABA measurement using a quantum-filter method at 1.5T, was provided by Keltner *et al* (17). A frequency selective DQF pulse sequence was tuned to the 1.91ppm GABA resonance to facilitate the transfer of magnetisation from this resonance to the 3.01ppm GABA resonance, thereby improving its detection efficiency. In phantom work, this was cited as a "single-shot" technique, but *in-vivo,* two phase-calibration pulse sequences were required to ensure that the phase of the first 90° pulse matched that of the filter. *In-vivo*, the relative phases varied with voxel size and location, thought to be due to a transmitter delay causing a phase offset before application of the first slice-selective pulse. Using these two calibration sequences, and the water peak as reference, the phase was corrected prior to the DQF sequence. In all of the ten subjects scanned using this protocol, it was reported that the 3.01ppm resonance was visible on all the DQF spectra. (The appearance of the filtered GABA spectrum had been previously confirmed in *in-vitro* studies.)

This was an encouraging result when compared to the failure of Weber *et al* to yield any signal using their DQF (15). Their sequence was based on the difference editing pulse sequence mentioned in §3.2.2.2. Two additional 90° pulses and a single refocusing pulse were added (and additional gradients), with the timings and gradient strengths chosen for detection of the GABA signal between 1.7ppm - 3.0ppm. *In-*

vitro, the authors reported good singlet suppression and GABA identification, but this result was not replicated *in-vivo* (n = 1).

A slightly different approach was taken by McLean *et al* in their measurement of GABA using a localised DQF at 1.5T (19). As with (17), the DQF was based on PRESS localisation, but in this later sequence, the hard chemical shift refocusing pulse was removed. This, in conjunction with an increase in gradient strength, allowed a reduction in the TM from 14ms to 6ms to maximise the GABA yield. To avoid the additional phase calibration measurements, a series of *in-vitro* experiments were performed in order to obtain the phase settings required for specific voxel sizes and distances from the magnet isocentre. In acknowledgement of the contamination of the GABA signal from the peptides homocarnosine and glutathione, and the macromolecule peaks, the authors quantified "GABA+" in their resulting *in-vivo* spectra. In the 15 normal volunteers scanned, it was reported that GABA+ could be quantified in all the filtered spectra, with a repeatability of 38%.

This same DQF technique was applied by the same researchers to acquire spectra from the occipital lobe (103) and frontal lobe (104) in both epilepsy patients and healthy volunteers. Initial results following analysis of the occipital lobe spectra suggested that the GABA+ measurements in the group of epileptic patients were increased when compared to the control group, with a significant increase in the sub-group of patients with idiopathic generalised epilepsy (n = 15). However, after grey-white matter segmentation, there was no significant variation in any of the groups. No difference was observed in the GABA+ levels between the patients and healthy controls when studying spectra from the frontal lobe either (104). This also included a sub-group of patients with idiopathic generalised epilepsy whose mean GABA+ levels were the same as those in the control group. To date, no clinical applications of this method have been applied outside the group who developed this version of the DQF.

The literature thus far suggests that quantification of the results from quantum filtering methods at 1.5T rely heavily on the post-processing techniques applied.

Lack of spectral resolution prevents the acquisition of clear filtered GABA+ spectra, and the end results depend greatly on the prior knowledge included in modelling programmes, such as LCModel, (105), to extract the relevant GABA+ data from an otherwise noisy spectrum (19,103). Application of multiple quantum filtered techniques at higher field strengths immediately produces a discernible improvement in resolution, providing far more convincing results and facilitating more reliable quantification (106-110). In fact, it should be noted that at both 2.1T and 3T, CSI of GABA is possible using multiple quantum filter techniques (111,112)!

3.2.3.3 Technical limitations

As with spectral editing techniques using selective excitation pulses, the main limitation of this method is that it does not allow the study of multiple metabolites without performing several quantum filter experiments. Such pulse sequences have to be explicitly designed for each coupled spin-system under investigation, so that the detected signal will be a function of the coherence order and the evolution time. Thus, in order to gain a more complete biochemical description of the patient, including GABA, multiple sequences would need to be applied. Therefore, this inefficient approach was abandoned in preference for the more all-encompassing, two-dimensional MRS approach.

In addition to the lack of multiple metabolite information, the signal loss associated with the creation of the different coherence pathways is undesirable in human studies (21), particularly when measuring the lower concentration cerebral metabolites. Moreover, the repeatability of these techniques is non ideal, even at higher field strengths, with the application of a doubly selective pulse sequence at 2.1T producing a coefficient of variation of 23% for the *in-vivo* GABA-to-creatine ratios (106). This is comparable to the repeatability results calculated at clinical field strengths using spectral editing techniques, Table 7.1, suggesting that improvement in measurement reliability is not always associated with higher field strengths.

3.3 Two-dimensional techniques

3.3.1 2D Correlation Spectroscopy

3.3.1.1 Background

2D correlation spectroscopy (COSY) is the most widely used 2D technique, and is more often applied in high-resolution NMR experiments to determine the fine structure of the sample under study (113) than on clinical MRI scanners. COSY relies on the transfer of coherence between coupled spins that occurs during the evolution period, and since the interactions exist through the covalent bonds within the molecule, COSY produces "through-bond coherence transfer" (77).

Unlike conventional 1D MR spectra where peak assignment is made by the position of the chemical shift peaks, in 2D COSY, metabolites are identified by the correlation pattern arising from spins sharing a J-coupling (99). This is shown in Figure 3.3 showing the 2D COSY schematic and actual spectrum of lactate.

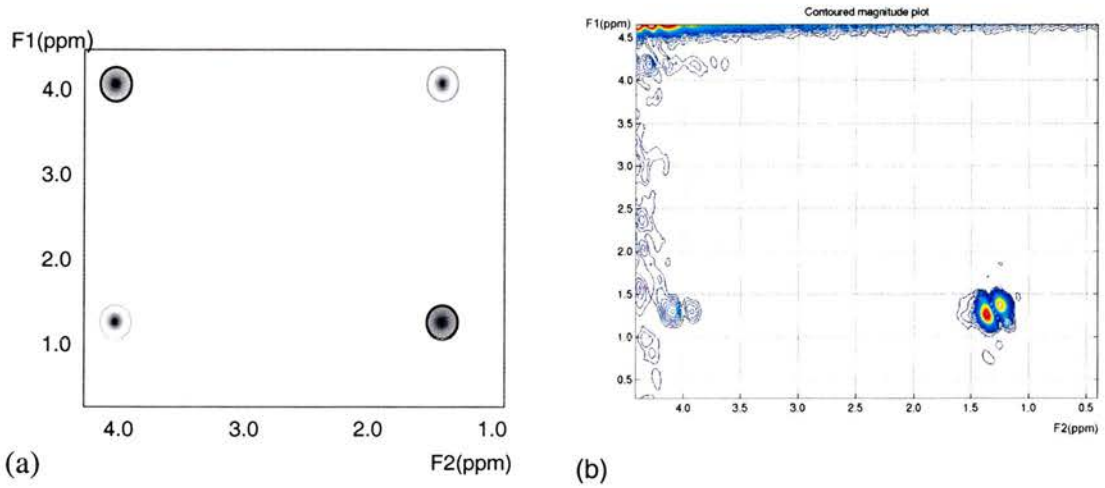

Figure 3.3 (a) schematic representation of 2D L-COSY spectrum of lactate, and (b) 2DLCOSY spectrum of a 3x3x3cm^3 voxel from phantom containing 5.0mM lactate (pH7, with all peaks shifted by ~0.1ppm in room temperature phantom).

In its most basic form, the COSY sequence comprises two 90° pulses separated by an evolution time, t_1, Figure 3.4 (76). Resuming the discussion of a weakly coupled two-spin system first introduced in §2, and applying the concept of coherence

transfer in §3.2.3.1, it is straightforward to see how this phenomenon is utilised in COSY.

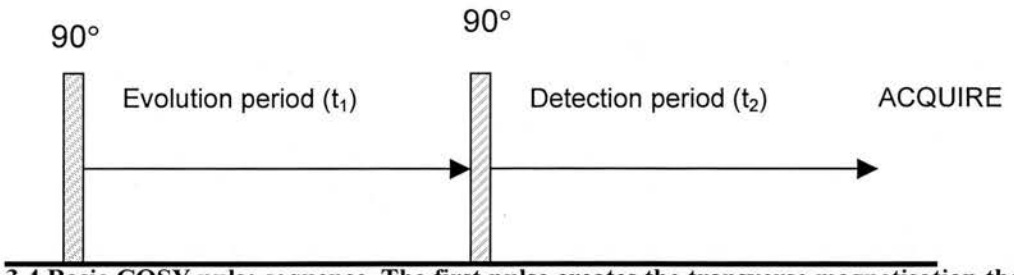

Figure 3.4 Basic COSY pulse sequence. The first pulse creates the transverse magnetisation that then precesses during the evolution time t_1. During this time, all of the individual spin components are "labelled" with their characteristic precession frequencies. After the second 90° pulse, the mixing pulse, transfer of magnetisation occurs between the coupled spins and they then precess during the detection period (t_2) at a new frequency.

After the first 90° pulse, the transverse magnetisation produced may be represented by each of the transitional changes listed in Table 2.4. This information can also be represented in terms of an energy level diagram, Figure 3.5. The SQCs from both spins S and I will freely precess under the influence of spin-spin coupling during time period t_1. Application of a second 90° pulse transfers the coherence from I_1 among the five possible transitions in the spin system (S_1, S_2, I_2, $\alpha\alpha - \beta\beta$ and $\alpha\beta$ - $\beta\alpha$) leaving a proportion with I_1 (113). Thus coherence is transferred between I to S in transitions S_1 and S_2, forcing Spin S to precess at the frequency of Spin I. These transitions correspond to SQCs and so after 2D FT, F1 $\neq$ F2, resulting in a peak that will reside at a point corresponding to the different chemical shifts of Spin S and I. This is away from the diagonal, hence the term "cross peak". The cross-peak provides evidence of coupling between the spins, and is why COSY has proven to be such a useful technique.

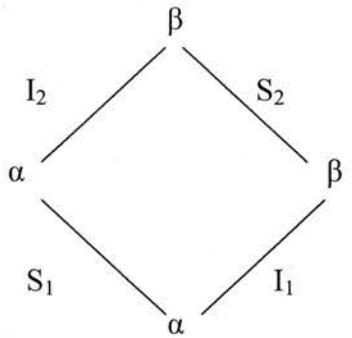

Figure 3.5 Energy level diagram for a coupled two-spin system IS described in Table 2.4.

Also during the detection period (t_2), the SQC remaining with spin I_1 or transferred to I_2 will continue to precess at its original Larmor frequency. That is, these SQC precess at the *same* frequency during t_1 *and* t_2, and in terms of the final 2D spectrum, will produce a peak on the line F1 = F2. This is equivalent to the peak that would be observed in an uncoupled spectrum, and due to its location on the 2D spectrum, is known as a "diagonal peak".

Finally, the transfer of coherence between $\alpha\alpha - \beta\beta$ and $\alpha\beta - \beta\alpha$ result in a DQC and ZQC respectively and will remain undetected without the addition of a third RF pulse.

3.3.1.2 High field and clinical application

Application of 2D COSY *in-vivo* has not been widespread, and at the time of writing, only two papers make reference to GABA measurement at 1.5T (20,21). Consequently, it is useful to include a more general discussion of COSY, including the development of the sequence.

As stated in the introduction, 2D COSY is more frequently applied on high resolution NMR systems, using homogeneous samples. One of the first examples of the acquisition of localised 2D COSY spectra from a heterogeneous sample was provided by Cohen *et al* in 1989 (114). Localisation was achieved using a 2cm diameter surface coil and used a conventional COSY sequence (90°- t_1 - 90° - acquire). All experiments were performed at 4.7T on a phantom containing separate containers of lactic acid and ethanol. Good localisation was achieved using the surface coil, and well-resolved 2D COSY spectra were acquired.

Following these encouraging results, Barrère *et al* performed a series of 2D COSY experiments on single metabolites *in-vitro* (phantom) and *ex-vivo* using rat brain tissue (99). This work culminated in the acquisition of 2D COSY *in-vivo* spectra from five rats using a 1.2cm diameter surface coil. All NMR experiments were performed on a 400MHz spectrometer and 2D COSY spectra were acquired using a SUPER COSY pulse sequence.

The SUPER COSY sequence was first described by Kumar *et al* and incorporated two additional time-delays around two refocusing pulses (115). These time-delays were optimised for a specific coupling constant to prevent the signal loss of cross-peaks associated with them being in antiphase during acquisition, as in a typical COSY experiment. By transferring the antiphase component from the cross-peaks to the diagonals, an increase in the intensity of the cross-peaks was observed compared to standard COSY. This aided detection of the cross-peaks, and particularly those close to the diagonal. The delays were also useful in suppressing the unwanted signal from water and lipids. In addition, since the intensity of the cross-peaks was no longer compromised, the acquisition time required for producing these peaks was also reduced, making the technique more feasible for detecting low concentration metabolites.

Comparison of the 1D and 2D spectra from the excised rat brain demonstrated the superior resolution of 2D COSY MRS and thus permitted the identification of metabolites otherwise hidden in the 1D spectrum (99). The results from the single metabolite 2D COSY experiments were superimposed onto the 2D COSY spectra from the *ex-vivo* and *in-vivo* rat brain spectra to aid metabolite identification. However, due to interactions between the metabolites that exist *in-vivo*, these reference spectra were incomplete. Despite this, GABA was identified in both 2D COSY rat spectra using this approach. In addition, the effects of ischaemia were also observed through the presence of lactate in the 2D COSY spectrum, and reductions in NAA. These spectral changes may also be observed on conventional 1D spectra, but of particular interest in this work, the authors also reported an increase in analine and GABA cross-peaks after ischaemia in all rats studied (n = 5).

Extensive pre-clinical work performed at 8.4T by Behar and Ogino permitted the assignment of chemical shift and spin-spin coupling constants for all the common cerebral metabolites, including GABA (116). High-resolution 2D COSY and 2D J-resolved spectra were acquired from tissue samples of the rat brain, and these have undoubtedly acted as an excellent source of reference for other workers in the field, be it animal or human study.

At the even higher field strength of 9.4T, 2D COSY was applied in conjunction with microdialysis to monitor the effects of pharmacological inhibition of GABA-transaminase *in-vivo*, in rats, leading to an increase in GABA levels (117). MRS was performed hourly after administration of the drug diluted in NaCl solution or the NaCl solution alone (as a control) to monitor changes in the intracellular GABA levels. Extracellular GABA was measured via the dialysates collected at the same time. Even before administration of the drug, the authors were able to measure GABA using 2D COSY with a sensitivity good enough to record the changes in intracellular GABA. Although these are exciting results, they cannot be compared directly to clinical work: As well as the very high magnetic field strength used, the SNR was also improved with direct contact between the rat skull and receiver coil, made possible by surgery – clearly not acceptable in clinical work in humans!

The first *in-vivo* 2D COSY spectrum of the human brain was acquired by Brereton *et al* in 1994 using a 2T magnet and surface coil (118). A large, 240cm^3 voxel was centred in the occipital cortex, although due to its size, it also included CSF signal from the ventricles, and lipids from subcutaneous fat. Further improvements in the SNR were attempted by acquiring each of the 128 increments with a NEX = 32, producing a scanning time for 2D spectroscopy alone of 102 minutes. Due to the short T_2 of the cerebral metabolites, the authors speculated that with the reduction in signal intensity associated with the longer TEs, the 2D experiment could be reduced to 64 increments without signal peak loss. More recent 2D COSY experiments have adopted this procedure, which among other factors has reduced the scanning time to more tolerable levels. Despite these drawbacks, the experiment was a success and peaks from aspartate, glutamate, glutamine and the α-CH resonances of NAA were identified on the 2D spectrum, as well as peaks from resonances normally found in conventional 1D spectroscopy.

Initial applications of a 2D COSY sequence at 1.5T did not seem very promising, with the authors of one of the first studies concluding that the technique was "not suitable for *in-vivo* work" (119). All the experiments in this study were performed

on a phantom containing a water / ethanol mix, but it was postulated that any *in-vivo* 2D spectra would contain artefacts from patient motion due to the long scanning time. This is despite the seemingly successful assignment of the CH_2 and CH_3 ethanol diagonal and cross-peaks. Thankfully not all research in this area was abandoned!

Two recent studies from the lab of Thomas *et al* have applied 2D COSY techniques at 1.5T for GABA measurement (20,21). Localised COSY (L-COSY) was performed in each case, allowing volume localisation *and* coherence transfer in a minimal time to prevent signal loss from the short T_2 cerebral metabolites. The sequence comprised three RF pulses (90° - 180° - t_1 - 90° - t_2 - acquire), and novel to this sequence, the last slice select RF pulse was dual purpose: It provided both coherence transfer for COSY and volume localisation of the voxel (21). This eliminated the need for additional RF pulses or gradients as described in (116,120).

Encouraging reproducibility results were obtained *in-vitro*, with within-run (that is, MRS of the same VOI in the same scanning session) coefficients of variation (CVs) for the diagonal and crosspeaks of < 2% and < 6% respectively (20). The CVs rose to between 7% – 15% for the between-days measurements (VOIs of the same size scanned on different days). *In-vivo*, the reproducibility of the higher concentration metabolites (NAA, choline and creatine) rose to < 13%, and the reproducibility of GABA was quoted as < 22%. These results at least suggest that *in-vivo* GABA measurement using 2D L-COSY at 1.5T is viable, and as such, will form part of the work in this thesis.

3.3.1.3 Limitations

2D COSY promises to be a useful tool for metabolite identification at 1.5T, but it is not without its drawbacks, the main one of which is the long scan time. With a TE_{min} = 30ms, TR = 2000ms, 64 Δt_1 increments and NEX = $16/t_1$, a scan time of 35 minutes was quoted (21). Although comparable to some of the scan times quoted for the spectral editing techniques (13,16), it is much longer than the time required for a conventional 1D spectrum (approximately three minutes). Therefore, it is possible

that some patient groups will not tolerate 2D L-COSY. However, the results from the two 1.5T studies presented suggest that with any fewer excitations, GABA is not observed in the 2D spectrum *in-vivo*.

Another disadvantage of this method is the loss of sensitivity when compared to 1D spectroscopy (121). 2D COSY relies on the transfer of coherence between different spins, and since only part of the magnetisation is transferred onto the coupled proton, there is a loss in the resulting signal. However, this reduction in sensitivity can be counter-acted with optimisation of the acquisition and processing parameters.

In common with the spectral editing sequence, another limiting factor of this 2D L-COSY is that a dedicated sequence is required, and without access to the programming skills or appropriately compiled sequence, 2D COSY measurements would not have been possible. Indeed, without the collaboration from Dr. M. Albert Thomas, University of California, the 2D COSY work in this thesis would not have been possible, and it is with thanks that the author acknowledges his assistance.

3.3.2 2D J-resolved spectroscopy

3.3.2.1 Background

J-resolved spectroscopy is another example of a "through-bond" 2D technique that can be utilised to reduce the complexity of spectra, by separating (or resolving) the chemical shifts of the multiplets from their scalar couplings. In doing so, it is possible to identify multiplets of similar chemical shift that are not normally resolved in a 1D spectrum (122). Of specific interest to this work is the 'Homonuclear J-resolved" technique where the homonuclear (usually H-H) couplings are resolved from the chemical shift information, thus allowing measurement of these couplings in decoupled spectra. So unlike 2D COSY spectra where both axes contain chemical shift *and* J-coupling information, after post-processing, 2D J-resolved spectra separate the J-coupling information (F1) from the chemical shift information (F2), Figure 3.6.

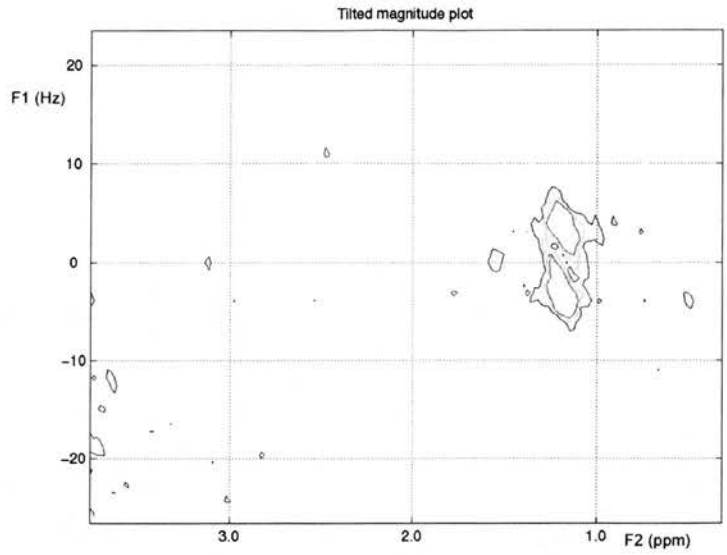

Figure 3.6 2D J-resolved spectrum of the weakly coupled metabolite lactate. The F1 dimension contains the J-coupling information (Hz) and the F2 dimension contains the chemical shift information (ppm). (All peaks are shifted by ~0.1ppm due to room temperature phantom.)

Aue *et al* first pioneered 2D Homonuclear J-Resolved Spectroscopy in the mid-1970's (58). In his communication, Aue described an indirect method of homonuclear broadband decoupling by acquiring a set of 64 echoes with uniformly incremented TEs, and then performing 2D FT to produce a 2D J-resolved spectrum. This was achieved using two basic pulse sequences: The first was a modified Hahn spin echo experiment, using only a 90° and 180° RF pulse, with echo acquisition after t_1, Figure 3.7(a). The second sequence contained multiple 180° pulses, and so more closely resembles the 2D J-resolved sequences currently used, Figure 3.7(b). The standard spin echo sequence was initially modified to include the second 180° pulse to provide the third orthogonal slice selective pulse, thereby obtaining a spectrum from a localised volume (123). This sequence is routinely applied as the standard PRESS spectroscopy sequence employed in conventional 1D spectroscopy, as described in §2.

Following 2D FT, Aue *et al* produced a stacked plot of the experimental sample, which contained chemical shift and J-coupling information along the ω_2 (or F2) axis, and J-coupling information only on the ω_1 (or F1) axis. After tilting, projection of the 2D spectrum along the ω_2 axis produced an entirely decoupled spectrum. Comparison of this result to the corresponding 1D spectrum, showed that the

decoupled spectrum appeared less complicated, thus allowing easier peak assignment.

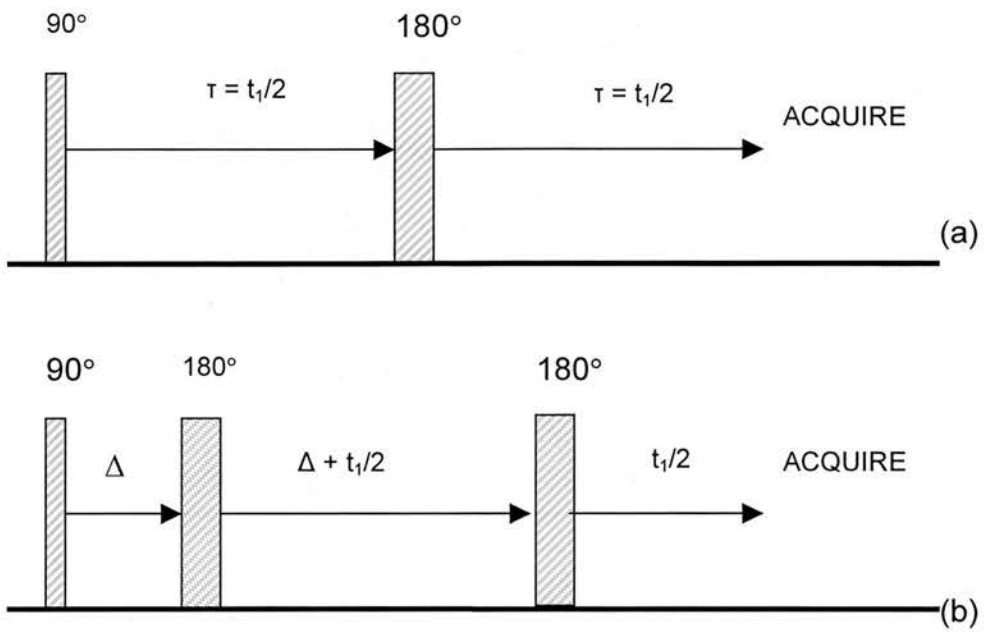

Figure 3.7 (a) The original homonuclear J-resolved experiment. (b) The spin-echo sequence for 2D J-resolved spectroscopy. Time Δ is the minumn time required to implement the RF pulses and gradients (22). The evolution time t_1 is split evenly across the last 180° pulse, and the echo collected after t_1 i.e. TE = 2Δ + t_1. GE's PRESS sequence follows the same formula for allocation of the components of TE between the RF pulses.

Review of the literature has shown that, to date, most of the 2D J-resolved sequences have been based on PRESS localisation (22-24,27,124). For simplicity, PRESS can be approximated by a standard spin-echo sequence, if the time between the 90° pulse and the first 180° pulse is short compared to 1/J (where J is the spin-spin coupling constant). As described previously, the application of the 90° pulse produces transverse magnetisation that may be represented by the transitional changes shown schematically in Figure 3.5. During τ in Figure 3.7(a), the magnetisation vectors are dephased both intentionally by the applied gradient, and unavoidably due to T_2* relaxation, Figure 3.8. Specific to coupled systems, in the time between the 90° and the following 180° pulse, the J-coupling between the nuclei force the transverse magnetisation to undergo periodic transformation into 'inphase' and 'antiphase' magnetisation, (125).

Inphase magnetisation occurs at even multiples of 1/J, i.e. $\tau = 0, 1/J, 2/J$ etc, where τ is the time between the 90° pulse and 180° pulse = time between 180° pulse and the echo. This type of magnetisation is similar to the transverse magnetisation observed in uncoupled systems, with a spin-echo resulting after time 2τ.

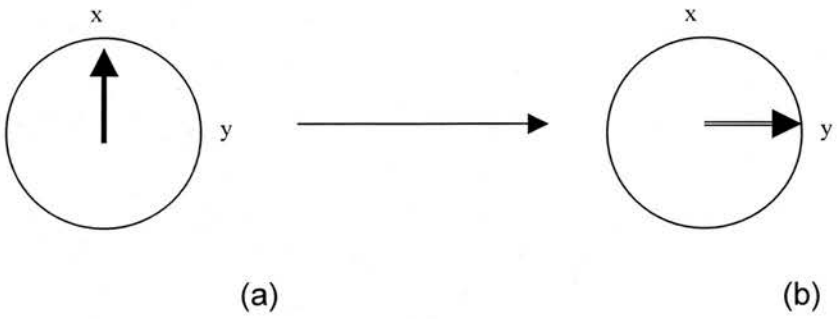

Figure 3.8 Evolution of anti-phase magnetisation of Spin A (M_A) in a weakly coupled AX spin system (a) at equilibrium, and (b) time τ after the 90° pulse. During τ the spin species are dephased due to the applied gradient Gx, T_2* relaxation and the J-coupling interactions between the spins.

Antiphase magnetisation is unique to J-coupled systems, and the effects of a non-ideal 180° pulse (as practically applied) on this type of magnetisation can be observed at odd multiples of 1/(2J) (90). The evolution of antiphase magnetisation is inherently more complicated, and to aid understanding, the process can be broken down into three different responses, Figure 3.9.

The first of these effects is similar to that experienced by the in-phase magnetisation, in that the vectors are partially refocused to produce a spin-echo after time 2τ, Figure 3.9 (a). Due to cosine modulation, refocusing of the spins is perfect but the signal is inverted by 180°. Secondly, incomplete refocusing of the antiphase magnetisation allows a proportion of the A_2 magnetisation vectors to continue precessing at their own Larmor frequency, are flipped by the non-ideal refocusing pulse, thus creating longitudinal magnetisation at time 2τ, Figure 3.9 (b). In addition, since a non-ideal 180° is used, the angles close to 90° in the transition band create MQCs. These are usually dephased by the gradients and their effects not observed. Both these responses relate to J-couplings *within* spins that are unaffected by the 180° pulse, and so they make no contribution to the recorded signal (126).

The third effect is that the non-ideal 180° pulse causes a population inversion of one the Spin A transitions, in a process known as polarisation transfer, Figure 3.9 (c). Thus magnetisation originally created on Spin A will be detected on Spin X, and vice versa. This effect can be observed in the recorded signal since, as with the first response, only the spin-spin couplings *between* spins inverted by the 180° pulse and those unaffected by the refocusing pulse are focused after 2τ.

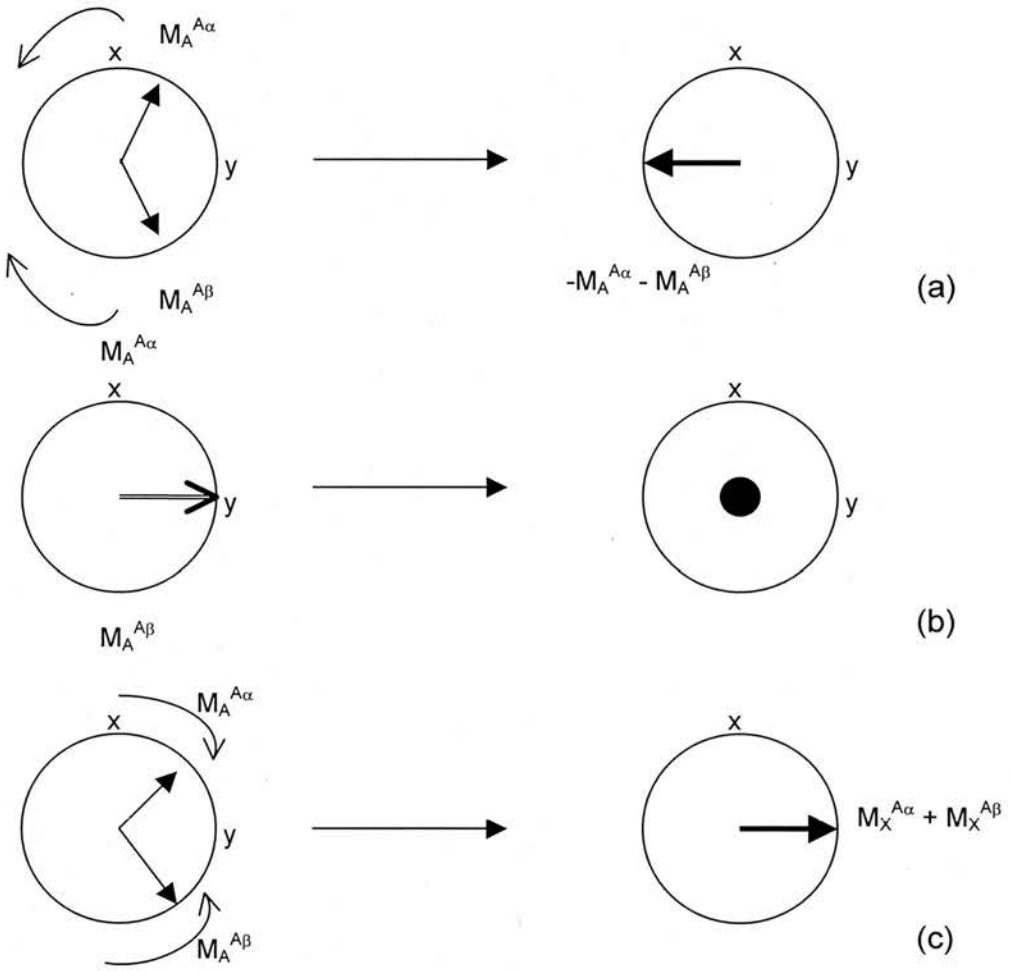

Figure 3.9 Evolution of anti-phase magnetisation of Spin A (M_A) in a weakly coupled AX spin system after application of a 180° pulse following Figure 3.8. (a) De-phased anti-phase magnetisation refocuses to produce spin echo at 2τ. (b) Creation of ZQCs and DQCs (which make no contribution to the recorded signal). (c) Polarization transfer, between Spin A to Spin X, also contributing to the observed signal at 2τ.

At echo times other than those specified, the resultant signals are comprised of a mixture of both in-phase and anti-phase polarisation. Consequently, signals collected at different echo times will contain information about the different phases of the

magnetisation vectors at the time when the refocusing pulse was applied. Since the change in phase is equivalent to the variation in coupling frequency, then measurement of the variation of phase with TE will provide information about the coupling of the system. This is the basis of the 2D J-resolved experiment.

Practically, the 2D J-resolved experiment can be performed by acquiring a series of PRESS MRS experiments, with the TE uniformly incremented between each one. In this way, the J-couplings can be evaluated by performing a FT with respect to the TE. The range of TE values and ΔTE are important as they determine the bandwidth and sensitivity of the F1 axis. The resulting bandwidth must be large enough to include the J-coupling frequency of the metabolites of interest, Equation 3.1. The number of individual experiments (nTE) performed must also be chosen with care as it is important that the F1 resolution is fine enough to show the point of maximum signal intensity of the resonance of interest, Equation 3.2.

$$Bandwidth = \frac{1}{\Delta TE}$$

Equation 3.1

$$F1 \quad Spectral \quad resolution = \frac{1}{nTE \times \Delta TE}$$

Equation 3.2

3.3.2.2 Clinical applications of technique

Due to the complexity of the spectra, and strong coupling patterns involved, applications of this technique *in-vivo* at field strengths as low as 1.5T has been difficult, and as such, very few studies investigating this method have been reported. Of the published work, there has been a trend to running multiple sequences using the standard PRESS spectroscopy sequence, either automatically as a self-written protocol, or as a series of individual experiments. In doing so, *in-vivo* measurements of metabolites including GABA have been reported.

Ryner *et al* were one of the first to publish *in-vivo* results using this technique (22). Their work comprised a comprehensive study of the individual metabolites commonly found *in-vivo* in separate phantom solutions, then as a composite solution, and the study was completed with the acquisition of *in-vivo* spectra. The standard PRESS sequence was modified to allow interleaved acquisition of 64 spectra, considerably reducing the scanning time required to perform a full 2D experiment using separate PRESS experiments. Individual phantoms were made containing common metabolites found in grey matter, at concentrations of 50mM. Of particular interest to this work, was the result pertaining to GABA. The 2D plot resulting from the *in-vitro* experiment of 50mM GABA clearly showed the splitting of GABA into three distinct groups at 3.01ppm, 2.28ppm and 1.91ppm, each assigned to the three CH_2 groups. The strong coupling patterns between each of the methylene groups was observed, with the strongest between the groups at 1.91ppm and 2.28ppm due to their close chemical shift proximity. These 2D assignments of GABA are comparable to those Behar and Ogino (116) in the acid extracts and extracted brain tissue of rats, performed at 8.4T.

In a brain phantom containing the same metabolites as previously studied in separate experiments, Ryner *et al* added GABA at a concentration of 0.5mM (22). Despite this being less than half the normal value quoted in (7), GABA resonances were identified at 3.01ppm and 1.91ppm (F1 = 7Hz), and a strong coupling set at 1.9ppm (F1 = 20Hz). The results from this phantom were compared to a composite 2D plot, constructed from the 2D spectra from the individual metabolites. Since the composite plot was derived from contours acquired separately, it lacked any information due to coupling between the metabolites, and so was easier to resolve. As such, the main use of this type of plot is to indicate the position of the different resonances. However, due to limitations in mimicking the physiological environment of the metabolites (including high concentration metabolites, the presence of macromolecules and trace paramagnetic materials, differences in viscosity and microscopic heterogeneity (25)), any further quantitative comparison with *in-vivo* data should be avoided.

Disappointingly, these results were not replicated *in-vivo*. Eight volunteers were scanned multiple times to acquire a total of 18 2D spectra. Using the same standard imaging set-up of the volume head coil, the authors reported that resonances due to NAA, glutamate / glutamine and, in some cases, lactate were readily identifiable on the 2D contour plots, although they were less confident when assigning resonances due to GABA and to taurine (an amino acid at concentrations similar to GABA (7)).

Lactate was also observed in a very small study (n = 3) using the 2D J-resolved technique at 1.5T in tumours (124). In this study, Thomas *et al* proposed that a major advantage of the technique was the ability to differentiate lactate from any lipid contamination that would have overlapped the lactate doublet at 1.31ppm in a standard 1D spectrum. On the resulting 2D plots, no resonances were assigned to other metabolites. However, from the 1D spectra, a decrease in all other metabolite concentrations was reported within the VOI, which may account for the apparent failure of further 2D assignment.

More recently, further work has been performed to validate this technique in healthy volunteers. Ke *et al* also used a modified PRESS sequence to perform 2D J-resolved MRS and extensive developmental work was carried out on both phantoms and *in-vivo* on healthy volunteers (24). In a slight variation to the earlier study by Ryner, a slightly longer TE_{min} of 48ms was used (compared to 25ms) and 14 extra spin-echoes were collected in a total of 64 experiments. In all instances the quadrature head coil was used. Phantoms were created with the concentrations of GABA well in excess of those found in normal physiological conditions (100mM), and separate phantoms were produced to investigate the effect of the overlying metabolites NAA, creatine, choline, glutamate and glutamine. Reassuringly, GABA was identified in each of the experiments. Moreover, the resonance at 3.01ppm was deemed the most suitable of the three GABA resonances for quantification as it was more easily discerned from the overlying creatine singlet using the 2D technique.

Using the same method, the *in-vivo* results also facilitated the identification of GABA at this peak position. The large volunteer group (n = 36) was evenly split between the sexes and following quantification of GABA, a difference was reported

between the two sub-groups (1.01±0.36 μmol/cm^3 for males; 1.16±0.43 μmol/cm^3 for females). It would be surprising if this difference was significant.

Ke reported that the major disadvantage of this technique was its acquisition time of 40 minutes – considerably longer than standard 1D spectroscopy – although not significantly longer than any of the aforementioned studies. Methods for reducing this time include the use of a surface coil to increase the sensitivity and thereby allow a decrease in NEX, and thus scan time. These issues had undergone some preliminary investigation in the previously discussed study of Ryner *et al* (22). In this study, one of the volunteers was re-scanned using a 8" transmit / 5" receive surface coil arrangement. The reported improvement in SNR facilitated a reduction in the NEX (and scan time) and a 60% decrease in voxel size. Comparable results were reported for all resonances apart from lactate where a reduction in signal intensity was observed. This was attributed to either an increase in signal loss, due to RF inhomogeneity associated with this coil arrangement, or an actual reduction in physiological concentration.

Further SNR investigations were performed by Ryner using the body coil transmit / 3" surface coil receive arrangement. Significant differences were reported between glutamate / glutamine and GABA peaks as seen using this set-up when compared to earlier *in-vitro* results, but not so for the NAA peaks. Differences in the T_2's of these metabolites were suggested as a possible cause for this dramatic reduction in intensity and peak resolution, although this later experiment had a reduced number of NEX per experiment (20 compared to 16), also reducing the SNR.

GABA measurements have been reported by Levy *et al* using the same 2D technique as first presented by Ryner, on a 1.5T GE scanner using the quadrature head coil (25), (26). However, the NEX was dramatically reduced to 2 which, whilst giving a more ideal scan time of 6 minutes, greatly reduced the quality of the resulting spectra. Spectra extracted at both J = 0Hz and J = 7.45Hz were studied to quantify NAA, choline and creatine in the former spectrum, and GABA in the latter. The authors reported a significant reduction in the mean GABA/creatine ratio as

measured between seven patients with focal dystonia and 17 age-matched controls in both the contralateral sensorimotor cortex ($p < 0.01$) and lenticular nucleus, ($p < 0.01$) (25). In a different study of 12 healthy volunteers who all underwent temporary forearm ischaemic nerve block to induce acute deafferentation, reductions in the GABA/creatine ratio immediately following deafferentation were also reported (26).

A similar technique was also used by Hurd *et al* at GE Medical Systems (now GE Healthcare), with the F1 created from timing parameters of either 128 evolution time increments of 2.5ms or 64 increments of 5ms. This was to produce oversampled, J-resolved spectra, again using a modified PRESS sequence (23). *In-vitro* spectra were obtained from the standard GE spectroscopy phantom with an addition of 5.0mM GABA (approximately x5 normal physiological concentration). In addition, spectra were collected from an unspecified number of healthy volunteers.

This method differed from that previously discussed, in that the collected spectra were not water suppressed, so were largely influenced by the water signal. This was to overcome base-line artefacts otherwise present due to gradient inaccuracies causing the production of spurious sidebands of water. It was found that the coherent water sidebands were modulated at the sideband frequency throughout the evolution time, and were present at two lines in the 2D spectrum: F1 = F2 and F1 = F2/2. It had been found previously that by oversampling in the F1 dimension, it was possible to resolve the artefacts from the signal of interest.

The authors reported an increase in resolution and specificity using this method, and were able to model both the water peak and the metabolites from the unsuppressed 2D data. This principle was applied to the *in-vitro* data, where the modelled GABA spectra at different J-coupling frequencies were superimposed on the phantom spectra to aid with identification. Application of the same technique to the *in-vivo* data facilitated identification of lactate, not normally easily distinguished above the noise in a healthy brain spectrum. Disappointingly, identification of the GABA peaks *in-vivo* was not attempted.

In a small study comparing spectral editing, double quantum filter techniques and 2D J-resolved spectroscopy, *in-vivo* GABA was not detected using the latter method (15). As with previous studies, a series of 64 experiments were performed, with the TE ranging from 35 to 665ms, NEX = 16, resulting in a scan time of 40 minutes. Of specific interest to this work, *in-vitro* experiments were performed on phantoms containing GABA only, and phantoms containing a mixture of alanine, GABA, NAA and creatine. In the composite phantom, GABA resonances were identified at 2.29ppm and 3.01ppm. Only a single *in-vivo* spectrum was obtained, from a 131.6ml voxel positioned to contain both grey and white matter. Although resonances from several metabolites were identified, no mention of GABA was made, suggesting that it was not identified by the authors. The 2D plots provided in the paper appeared noisy, and since no extracted spectra were provided, it is impossible to arrive at a definitive conclusion as to the success of the experiment with regards to GABA.

In a similar study by Ryner *et al* comparing 2D J-resolved spectroscopy to several different sequences, including multiple quantum filter techniques and COSY variations, no assignment was given to GABA in the resulting 2D J-resolved plot (123). Again, spectroscopy from a single voxel from only one volunteer was acquired. The 2D J-resolved sequence itself comprised of 50 individual experiments, with TE starting at 45ms, ΔTE = 10ms, TR = 2200ms, and NEX = 20, giving a scan time of 37 minutes. A grey matter phantom was constructed, including 0.5mM GABA, but this was only used in the COSY experiments and unfortunately there was no discussion of GABA in any of the results.

From reviewing the literature, it is apparent that very little work has been conducted into identifying GABA using this method at clinical field strengths. Consequently, there is a need for a full and logical investigation into the feasibility of generating a spectroscopy tool to quantify this metabolite that can be used routinely in the clinical setting. The development and reliability of such a technique will form the bulk of the work presented in this thesis.

3.3.2.3 Technical issues of 2D J-resolved MRS

The main advantage of employing 2D J-resolved MRS over the other available methods for detecting GABA (such as spectral editing and quantum filter techniques), is that 100% of the available GABA signal is maintained (123). In situations such as this where the metabolite only exists, *in-vivo,* in very small concentrations, this is a very important consideration. For example, the application of a zero quantum filter reduces the available sensitivity by 50% due to the coherence-transfer pathways selected (123). In a double quantum filter experiment, the efficiency is further reduced to 25%.

In addition, another of the disadvantages of the alternative techniques is that they are designed to select a single, specific metabolite. Whilst this work is primarily concerned with the investigation of GABA, application of 2D J-resolved MRS acquires J-coupling information from *all* metabolites in the sample. With the appropriate post-processing, this then allows analysis of any metabolite without the need for performing additional experiments.

The main disadvantage of the 2D J-resolved method is the scan time. Although in more recent papers, scan times of 6 minutes have been reported by reducing the NEX = 2, the resulting spectra are very poor. In studies where GABA has more convincingly been identified, the NEX varied between 8 – 20 (22), (24), resulting in acquisition times of between 15-37 minutes. This is considerably longer than the scan time required for a conventional 1D single voxel spectrum, and as such, may not be tolerated by unwell patients. However, if this experiment is to be performed at all, then it is important that the data acquired is of sufficient quality to provide convincing results, thereby justifying the longer scan times.

3.3.3 Two-dimensional Double Quantum Filter

3.3.3.1 Background

2D DQFs are an extension of the 1D DQF techniques described previously, Figure 3.10. The advantage of this type of 2D spectroscopy over, for example, COSY is the

removal of all uncoupled spins. In COSY, singlets produce prominent diagonal peaks that may obscure the signals from lower concentration metabolites nearby. In their absence, coupled spins can be more clearly observed. The description of this technique is included to provide a complete description of 2D techniques at 1.5T as results using 2D DQ-MRS for GABA measurement have been reported (127,128).

One of the first *in-vivo* applications of 2D DQ filtering, albeit immediately post-mortem and at 2T, was to measure lactate in a human neuroblastoma implanted onto the back of a mouse (129). The 2D DQF sequence used is shown in Figure 3.10 and lactate could clearly be distinguished from the lipid resonances in the resulting 2D DQ plot, whereas in the conventional 1D spectrum, the 1.31ppm lactate peak was obscured by the lipid presence. The presence of lactate was confirmed using enzymatic assaying. This lactic acid editing sequence was modified to improve the efficiency of lactate detection, reducing the extent of lipid overlap in the region of 1.4ppm and minimising the amount of residual water resulting in a better defined 2D spectrum (130). In addition, the acquisition time was reduced from around 30 minutes to just over one minute. A final modification was made to the original 1D sequence to allow CSI of lactate with the addition of phase and frequency encoding gradients.

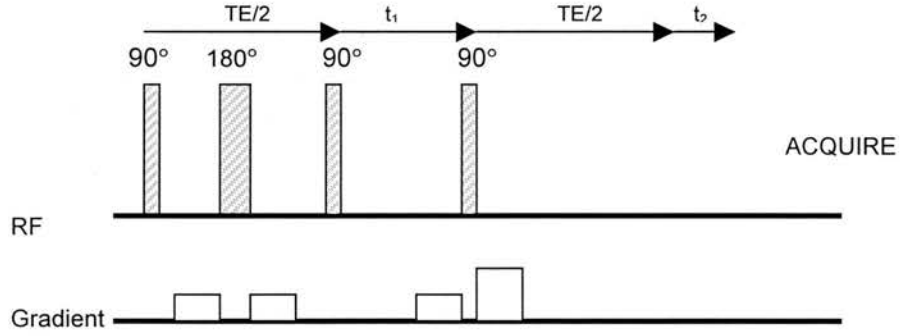

Figure 3.10 2D DQF pulse sequence, taken from (129): Pulse sequence repeated with successive increments of t_1.

Following the success of lactate editing, in mice *in-vivo*, a 2D multiple quantum filter editing sequence was optimised to identify the glutamate / glutamine resonances in rats at 4.7T (131).

In 2002, 2D MQ filtering techniques were being introduced at 3T for GABA measurement (132). This preliminary study only performed *in-vitro* measurements on two simple phantoms containing high concentrations of GABA and creatine, but was able to demonstrate effective GABA detection and an increased efficiency of water suppression. At the time of writing, it was disappointing to find no further GABA-related results using this sequence.

3.3.3.2 Clinical applications

In the only work to be published relating to GABA measurement at 1.5T, Wang *et al* modified the 1D DQF pulse sequence proposed by Keltner *et al* (17) to include a series of t_1 increments immediately after the second refocusing pulse (127,128). After FT, the F1 dimension therefore contained the DQ frequencies (in ppm) and the chemical shift information was held in F2. The aim of this method was to resolve the 3.01ppm GABA resonance from the underlying macromolecules. It has previously been shown in the 1D double quantum filter methods that identification of a GABA + macromolecule + homocarnosine signal is possible (17,19,103,104). Similarly, GABA without contamination was not resolved in the 2D DQF plots. However, from a purely scientific viewpoint, this is a very interesting extension of DQF techniques.

3.3.3.3 Technical limitations

The 2D DQF technique applied at 1.5T required 20 mins of scanning time. As with all 2D methods, it does have the advantage of acquiring information about several metabolites simultaneously, and so this time penalty can usually be justified. However, in view of the results from 2D COSY and 2D J-resolved MRS at this field strength, the associated loss of information from uncoupled metabolites may not.

Since 2D DQF MRS removes the contributions from uncoupled metabolites from the 2D spectrum, the creatine signal will no longer be available to act as an internal standard. This is a usual point of reference, and often helps with the general reading of the spectrum, but with training, this problem can easily be overcome. However, in

centres that insist on quoting *in-vivo* metabolites in ratios to creatine, this practice would not be possible.

Finally, another limitation of this sequence is, again, the need of a specialist pulse sequence. Unlike 2D J-resolved MRS, which can be performed with the manufacturer provided PRESS sequence, 2D DQF MRS requires extensive pulse sequence programming, which will be prohibitive for most clinical centres.

3.4 Conclusions

It has been established that additional MRS methods are required to reduce the complexity of spectra to facilitate the identification of certain metabolites in an otherwise overcrowded spectrum, and these are summarised in Table 3.1. Spectral editing techniques have the disadvantage in that they require prior knowledge of the metabolite of interest in order to design a sequence for selectively retaining the signal (116). This includes chemical shift information and coupling constants that are not available from conventional 1D spectroscopy, particularly where some of the resonances are overlapped by other metabolites.

The main advantage of the 2D COSY and 2D J-resolved methods over the spectral editing techniques is their ability to provide simultaneous assignment of resonances from several cerebral metabolites. To date, these include NAA, choline derivatives, creatine, glutamine, glutamate, lactate and GABA (133). Therefore, these 2D methods are studied in this thesis.

Table 3.1 Summary of methods of GABA measurement at 1.5T

Method	Pros	Cons
Difference editing	(1) Can be tailored to edit 3.01ppm GABA resonance	(1) Acquires information about only one metabolite (2) Requires the acquisition of two spectra: Susceptible to patient motion artefacts (3) SDs of *in-vivo* GABA measurement = 23% - 46% (4) Contamination of GABA resonance from macromolecules and homocarnosine (5) Scan times: 30 minutes – 90 minutes (6) Requires dedicated pulse sequence
Multiple Quantum Filters	(1) Can be designed to edit 3.01ppm GABA resonance (2) Scan times: 8.5minutes (+ phase calibration) – 17 minutes	(1) Acquires information about only one metabolite (2) Detection efficiency of only 25% (DQF) - 50% (ZQF) (3) Contamination of GABA resonance from macromolecules, homocarnosine and glutathione (4) Phase calibration sequences required *in-vivo* before application of DQF sequence (5) Repeatability of *in-vivo* GABA+ measurements = 38% (6) Requires dedicated pulse sequence
2D COSY	(1) Acquires information on all metabolites including 3.01ppm GABA resonance (2) Reproducibly of *in-vivo* GABA measurements < 22% (better than spectral editing methods)	(1) Signal loss associated with coherence transfer pathways (2) Requires manual pre-scan (3) Long scan time: 35 minutes + manual pre-scan (4) Requires dedicated sequence
2D J-resolved	(1) Acquires information on all metabolites including 3.01ppm GABA resonance (2) No inherent signal loss (3) Dedicated pulse sequence not essential	(1) Long scan time: 40 minutes (2) Contamination of 3.01ppm GABA resonance from macromolecules
2D DQF	(1) Allows identification of 3.01ppm GABA resonance + other coupled metabolites	(1) Removes all uncoupled spins from 2D plot: does not acquire information about all metabolites (2) Signal loss associated with coherence transfer pathways (3) Contamination of GABA resonance from macromolecules (4) Requires dedicated pulse sequence

4 2D J-resolved MRS using a protocol of 64 individual PRESS sequences

4.1 Introduction

This chapter describes the preliminary practical work of performing 2D J-resolved MRS *without* a dedicated sequence. This was accomplished using a series of standard PRESS MRS sequences. Initial validation of this approach was achieved by comparison of the resulting 2D J-resolved spectra against published data. Following this, the threshold of *in-vitro* GABA detection was determined, and an estimate of the general reproducibility of the method was obtained using a standard volume head coil. In all *in-vitro* work, the experiments were performed at room temperature and so include a ~0.1ppm shift. The results from a single healthy volunteer are presented. This chapter concludes by discussing different optimisation strategies for addressing the main disadvantages associated with this method.

4.2 Sequence description and post-processing

4.2.1 Background

As described in §3, 2D J-resolved MRS can be performed using a modified PRESS sequence, designed to uniformly increment the TE over a specific number of experiments. Such an approach relies on either having the expertise to successfully "modify" a PRESS sequence, or to obtain a suitable, pre-written, 2D J-resolved sequence. However, one of the over-riding advantages of this technique, compared to other GABA-detection methods reviewed in the previous chapter, is that the same result can be achieved *without* a dedicated J-resolved sequence. 2D J-resolved spectroscopy can be performed by manually incrementing the TE in an appropriate number of PRESS sequences.

Original investigation into the viability of using 2D J-resolved MRS to detect GABA at 1.5T was performed without a dedicated 2D sequence. Therefore, a protocol comprising 64 individual PRESS experiments was created, with the TE manually incremented (with values taken from the literature (23,24)) to create the required second dimension for the 2D J-resolved spectra.

As described in §2.6.2, the PRESS sequence consists of a 90° pulse followed by two 180° pulses. From the description of a general 2D experiment provided in the same chapter, it follows that in 2D J-resolved spectroscopy, the 90° pulse and first refocusing pulse constitute the preparation period, and the time either side of the second 180° pulse, equivalent to TE, comprises the evolution period. Since there is no polarisation or coherence transfer in this type of experiment, a mixing period is not required. Therefore, detection of the spin-echo occurs immediately after evolution, Figure 4.1. A numerical description of the designated timings shown in this figure can be found in Table 4.1.

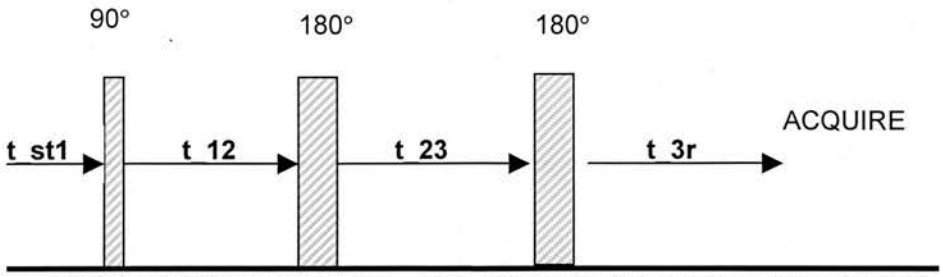

Figure 4.1 GE PRESS timing diagram. Taken from GE Spectroscopy Manual, 1999. The timing variables are described in Table 4.1.

Table 4.1 Description of timing parameters used in a GE PRESS pulse sequence. Numerical values and timing relationships were verified experimentally

Time	Description	Value
t_{st1}	Time from start to centre of pulse 1	Fixed at 2.548ms
t_{12}	Time from centre of pulse 1 to centre of pulse 2	Fixed at 9.392 ms
t_{23}	Time from centre of pulse 2 to centre of pulse 3	Varies according to $t_{23} = \frac{TE}{2}$
t_{3r}	Time from centre of pulse 3 to centre of the echo (when acquisition starts)	Varies according to $t_{3r} = \frac{TE}{2} - t_{12}$

§3.3.2 also states that the main aim of a 2D J-resolved experiment is to resolve the resonances so that there is *only* J-coupling information in the F1 dimension and chemical shift information in F2. This is achieved by applying the second refocusing pulse at the midpoint of the evolution period, t_1, to refocus only the chemical shifts, resulting in their removal from F1. The homonuclear couplings are unaffected by this 180° pulse and so appear in the final spectrum, (122). Therefore, in the detection period, only J modulation and Larmor frequency are effective. This does mean however, that initially both the F1 and F2 axes contain J-coupling information, producing multiplets that appear along the y = -x line (i.e. at 45° to either axis). If left in this way, the couplings will not appear where expected on the F1 axis, and F2 will contain both J-coupling and chemical shift information. Tilting the multiplets through an angle of 45° will remove the J-coupling contribution from the F2 axis, and align the coupling information correctly on F1 so projection onto the F2 axis will produce a decoupled spectrum, as desired. This is shown in the results from a

GAMMA (General Approach to Magnetic resonance Mathematical Analysis) simulation of GABA, Figure 4.2. (GAMMA is a C++ toolkit allowing the simulation of the behaviour of metabolites under various NMR experiments (134).)

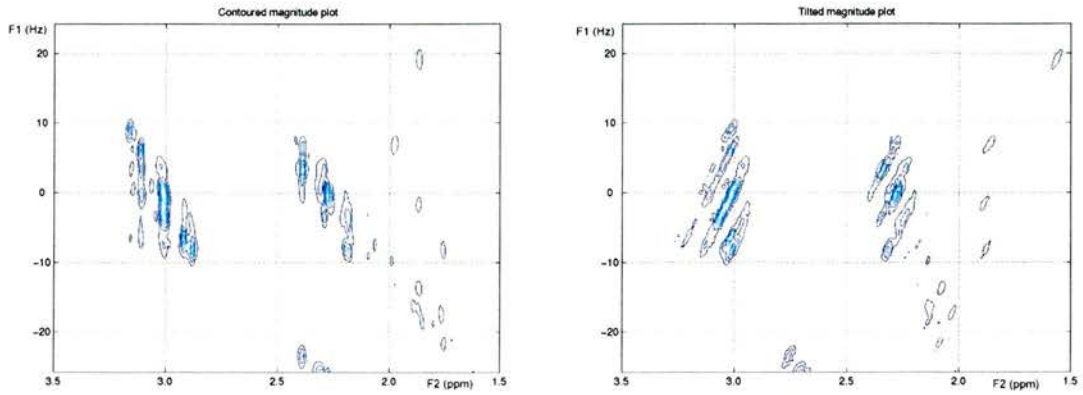

(a) (b)

Figure 4.2 Results from GAMMA spin-system simulation of GABA at 1.5T. The simulations were based on the standard, asymmetrical GE PRESS sequence, repeated for 64 echo times with a ΔTE of 10ms to mimic a 2D J-resolved experiment (135). (a) 2D J-resolved plot prior to tilting and (b) the same plot after tilting. Note how the resonances now line up in F1.

In terms of actually displaying the data, the recorded FIDs can be described by a combination of in-phase and anti-phase components, giving rise to a twisted lineshape (97). Consequently, it is not possible to display the spectra in pure-absorption mode and so 2D J-resolved spectra are always shown in absolute mode. An unavoidable disadvantage of this method of presentation is the decrease in spectral resolution, due to the broadening of the resonances associated with absolute mode display.

Another issue that can be at least partly addressed by post-processing is t_1 noise. This artefact appears from random fluctuations in the signal intensity arising from scanner instabilities during the evolution period, hence "t_1" noise, (113). Such scanner instabilities are evident as bands of noise, parallel to the F1 axis (prior to tilting), and occur in the same chemical shift positions as the genuine resonances. Another characteristic of this noise pattern is the intensity variation of the band: It is proportional to the amplitude of the corresponding resonance, and so the intense peaks of singlets are associated with stronger bands of noise. Since the actual stability of the scanner is the manufacturer's responsibility, where t_1 noise does exist,

it is very difficult to completely eliminate. Reproducibility between individual sequences can be improved by performing regular autoshims to maintain lineshape. Phantom stability – in terms of temperature and solvent equilibrium – is crucial, and it is also important to maintain magnetic stability. Thus the movement of magnetic materials in and around the magnet room is not recommended.

Post-processing methods can be used to reduce t_1-noise in the spectra, but may themselves give rise to artefacts. Exploitation of the symmetrical nature of the 2D J-resolved plot facilitates comparison of the data points either side of the diagonal, and then replacement of both with the smaller value. This method assumes that the difference between the two resonances is due to noise and if applied, must be done so with care to prevent regions of t_1 noise becoming enhanced with the multiplets. However, in the low F1 resolution *in-vivo* experiments, the resulting spectra are not entirely symmetrical around J = 0Hz. This is due to incomplete separation of the multiplet structures in both halves of the 2D spectrum, i.e. ±J Hz, so the intensities of the resonance pair are not identical. Therefore, "symmetricalisation" at clinical field strengths is not recommended.

Accurate phase correction can also lessen t_1 noise, by reducing the effects of phase changes occurring over the time series of FIDs. The exact procedure depends on the characteristics of the raw data, and more specifically, whether or not it has associated reference water information. In addition, the exact order in which the post-processing steps are applied will determine the type of phase correction applied (time domain or frequency domain). This subject is covered in greater depth in §5.

4.2.2 Scanning protocol

All experiments were performed on a 1.5T GE Signa Horizon scanner using a standard volume head coil. 2D J-resolved spectroscopy was achieved by performing 64 individual, single-voxel PRESS experiments: TE_{start} = 35ms, TR = 2000ms, number of excitations per frame of data (NEX) = 4, total number of excitations required for signal averaging (N_{scans}) = 32, VOI = 3 x 3 x 3 cm^3 and Δ TE = 10ms

giving rise to an F1 bandwidth of ± 50Hz, $t_{scan} \approx 2.5$hours. Initial 2D experiments were performed simply by loading the required number of PRESS sequences onto the desktop, setting the appropriate timing parameters and copying the graphic prescription from the first sequence to the 63 remaining sequences. (The manufacturer had warned against using the "copy and paste" tool as a method for repeating the sequences, since the software version at that time was unable to support this editing function.) After running a few preliminary experiments, the series was saved as a protocol for use in subsequent 2D J-resolved experiments. In this way, consistency between each of the 64 experiments and therefore the 2D experiments was ensured, with only the VOI needing to be copied onto each prescription.

With a set protocol and once the VOI had been prescribed for each experiment, it was possible to automate the 2D J-resolved experiment by selecting the "autoscan" mode, thereby allowing each sequence to run sequentially without any operator input. However, this would have meant that before every sequence, a full prescan would have been performed. This involves setting the centre frequency, the transmit- and two receive-gains, and optimisation of the voxel localisation shim and water suppression. For this 2D experiment, allowing 64 full prescans would add an extra hour to an already excessive scan time. Since the data were being collected from the same VOI in a phantom, it was not necessary to re-shim the voxel between every PRESS experiment, based on the assumption that the subject did not move, and that there was no significant drift of the scanner settings. Consequently, it was possible to interrupt the pre-scan as soon as it started (by starting a manual pre-scan and immediately selecting "Done"), and thus dramatically reduce the amount of time spent in pre-scan optimisation.

4.2.3 Post-processing Protocol

Following acquisition, each 2D experiment had 64 raw data files, known as "P-files" on a GE scanner. There are only 196 unique p-file identifiers, starting at P00000.7 and incremented by approximately 512 each time a new file is created. Thus, once p-file P99840.7 is named, the next P-file created is P00000.7 and so on. If this raw data

file already exists, then it is over-written by a new version, and the raw data from the old file is lost. Thus, in a 2D experiment where at least 64 spectroscopy sequences were being performed, extreme care was taken to ensure that the p-files were transferred to another location at regular intervals to prevent data loss due to file over-writing.

To ensure that the p-files were processed in the correct order, that is the order of acquisition with increasing TE, each of the p-files were renamed according to the TE used, into the form te###ms.raw, e.g. te35ms.raw, te45ms.raw etc. In-house software previously developed for processing single-voxel spectroscopy and CSI data was adapted to automatically process the 64 renamed raw data files. The main functions of this programme (Jresolved.c, written by Ian Marshall) were to: -

i. Read in the renamed raw data files
ii. Phase correct the FIDs using the water FID as reference
iii. Scale the phase-corrected FIDs according the pre-scan parameters (transmitter gain (TG) and receiver gain (R1 and R2)) and the spectroscopy voxel volume
iv. Remove the residual water signal
v. Cumulatively save all the processed FIDs in one large text file for further processing in Matlab (The Mathworks Inc).

Phase correction was based on the well-documented method by Ordidge and Cresshull (136). This relies on the acquisition of a water reference signal at the same time as a water-suppressed, metabolite signal. Information about the phase distortions arising from field inhomogeneities and eddy currents can be obtained from the phase angle of the reference signal, analysed on a point-by-point basis. Since the water-suppressed signal experiences phase distortions due to the same field inhomogeneities and eddy currents, as well as the phase information from the metabolites, subtraction of the phase angles from the reference signal results in a phase-corrected metabolite FID. The main disadvantage of this method is the extra time needed to acquire the reference signal. However, standard PRESS acquisition on the GE scanner automatically includes a number of frames (set by the total number of scans / total number of excitations for a single frame of data) of non-water

suppressed data that can be extracted from the same p-file as the water-suppressed data and used for phase correction.

Even with the application of a CHESS pulse, the water signal remains dominant in the resulting spectrum, and so further post-processing is required to remove the residual water peak. It is well established that an FID can be modelled as a sum of complex, exponentially damped sinusoids, giving rise to a series of frequency-domain Lorenzian lines (67), so the FID can be accurately modelled to remove the water peak. One such method of achieving this is using the Hankel Lanczos singular value decomposition method (HLSVD) (137,138). Using the known characteristics of the time domain signal, HLSVD can be used to model the FID using a limited number of singular values. The time-domain suppressed water signal can be identified from the central frequencies of the water resonance and from its larger amplitude sinusoids (compared to those from the metabolites). Once the residual water is subtracted from the original FID, the predominant information in the resulting FID will be from the metabolites. The advantage of performing the modelling and subtraction in the time-domain is that both the main water peak and its tail are removed from the frequency-domain spectrum, without affecting the metabolite signals (since these lie outside the water region). Consequently, if the algorithm performs effectively, there should be no baseline artefacts from the residual water signal complicating measurement of the metabolites.

In terms of the practical aspects of post-processing the spectroscopy raw data, especially with a single 2D experiment requiring 64 individual spectra, it was advantageous that HLSVD was fully automated. In-house software previously written for spectroscopic analysis was applied (139), using the same initial modelling parameters and number of iterations.

Once these time domain corrections had been made, the processed FIDs were saved in a text file, ready for importation into Matlab for frequency domain manipulation.

In Matlab, a second programme (Jres_mag) was applied, performing: -

i. Apodization of the data using a simple sine bell in the F1 dimension, and a Lorenzian-Gaussian combination in the F2 dimension. This enabled an optimum compromise between line width and resolution to be obtained.
ii. 1D FT on the FIDs to allow observation of the spectra as typically seen in an MRS experiment.
iii. Second dimension FT on the results from (ii) to display the complete results from the 2D J-resolved experiment.

The conventional method of displaying 2D spectra is on a contour plot, with an appropriate "cut-through" level determined by the concentration of the metabolites under study. A 2D contour plot is analogous to an Ordnance Survey map, with the peaks and troughs of the metabolite peaks akin to the peaks and troughs of mountains and valleys. To represent the 3D information in 2D, it is necessary to choose a height at which to "cut-through" the plot and thus observe the 2D projection of the 'landscape' at that level, Figure 4.3. Higher up the plot, information is gained about metabolites with large peaks i.e. those present in high concentrations. As the "cut-through" level is reduced, more information is obtained about lower concentration peaks until eventually all information is lost to noise. Once the plot had been constructed, individual spectra were extracted at rows corresponding primarily to the GABA J-coupling frequency, although spectra from any other J-coupling frequency are also possible.

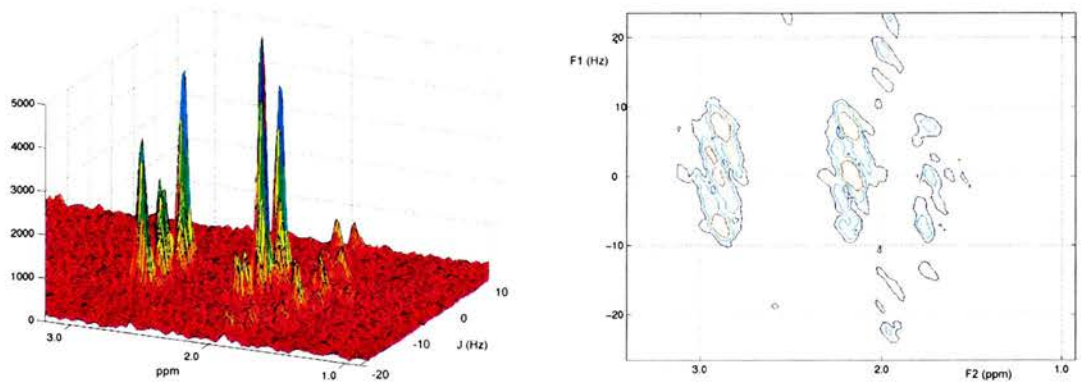

(a) (b)

Figure 4.3 (a) 3D surface plot and (b) 2D J-resolved contour plot from the same 3 x 3 x 3cm^3 VOI in a phantom containing 10mM GABA. The metabolite peaks at 3.01ppm, 2.28ppm and 1.89ppm are clearly seen.

Quantification of the extracted spectra was achieved in Magnetic Resonance User Interface (MRUI) (http://carbon.uab.es/mrui/). The matlab spectra were converted to ascii files of the correct form, header layout and size to be properly processed in MRUI by a function called lineSelect.m, written by the author. Prior knowledge files were created from 2D J-resolved experiments on high concentration individual phantoms, with files created for the metabolite resonances both at J = 0Hz (i.e. uncoupled spectra) and J = 7.4Hz (GABA J-coupling frequency). Once the acquisition of the prior knowledge was complete, the quantification process was semi-automated, requiring no additional data input, thus standardising the procedure.

4.3 *In-vitro* experiments using 64 PRESS experiments

4.3.1 Individual metabolite phantoms

4.3.1.1 Methods

A number of experiments were performed to establish the validity of 2D J-resolved MRS from 64 individual PRESS sequences. The first of these involved comparing the experimental results from the individual metabolites to the published literature, to confirm their appearance on 2D J-resolved spectra (22). Aqueous solutions of 50mM creatine, 50mM choline and 100mM of GABA all underwent 2D J-resolved spectroscopy using the acquisition parameters given in §4.2.2. In addition, 2D J-resolved spectra were acquired from aqueous solutions of glutamate and glutamine, both at concentrations of 25mM.

4.3.1.2 Results

Figure 4.4 shows the 2D J-resolved spectra from individual phantoms containing 50mM of both choline and creatine. The 2D J-resolved plot from 100mM GABA is given in Figure 4.5 (a), and Figure 4.5 (b) shows the spectrum extracted from the 2D plot, corresponding to the J-coupling frequency of GABA: J = 7.4Hz. Finally, the complex coupling patterns from the phantoms containing glutamate and glutamine are shown in Figure 4.6 (a) and (b) respectively.

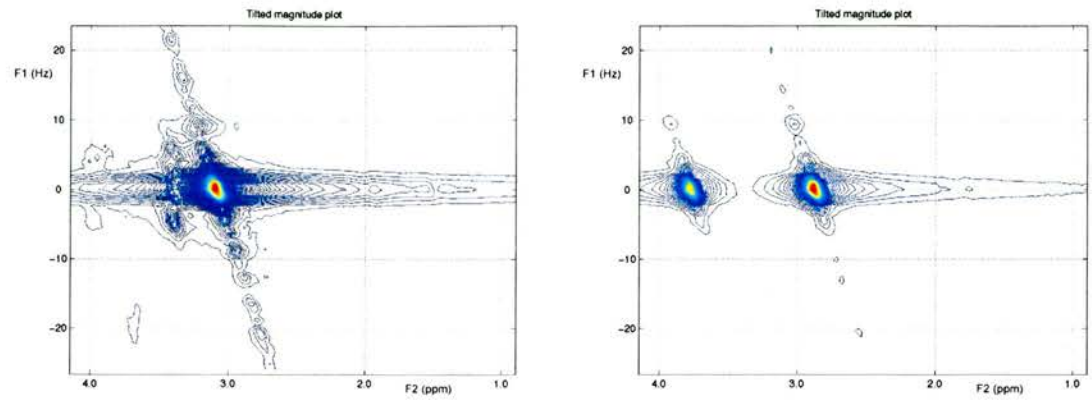

(a) (b)

Figure 4.4 2D J-resolved plot from a 3x3x3 cm^3 VOI positioned in a phantom containing (a) 50mM choline and (b) 50mM creatine. Both experiments were performed using a standard volume head coil (with all peaks shifted by ~0.1ppm in room temperature phantoms).

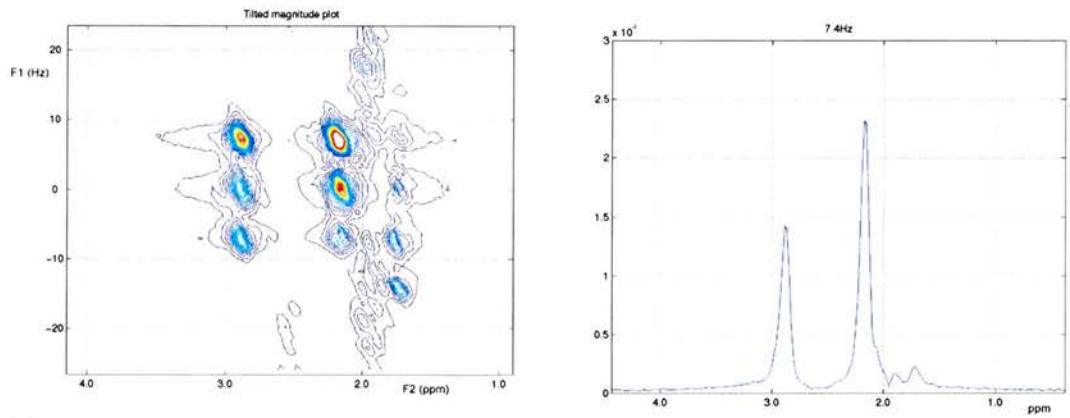

(a) (b)

Figure 4.5 (a) 2D J-resolved plot from a 3x3x3 cm^3 VOI positioned in a phantom containing 100mM GABA, using a standard volume head coil. (b) Extracted row corresponding to GABA J-coupling frequency (7.4Hz) – the 3.01ppm and 2.28ppm GABA peaks are clearly visible (with all peaks shifted by ~0.1ppm in room temperature phantoms).

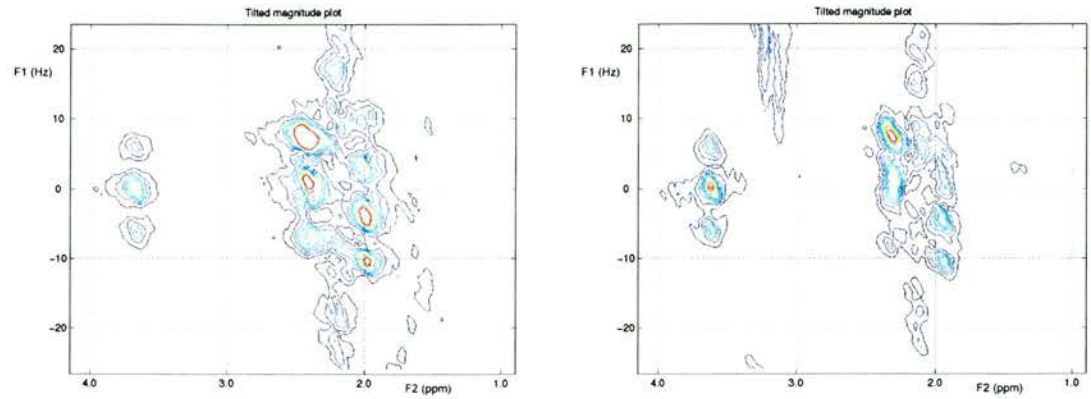

(a) (b)

Figure 4.6 2D J-resolved plot from a 3x3x3 cm^3 VOI positioned in a phantom containing (a) 25mM glutamate and (b) 25mM glutamine. Both experiments were performed using a standard volume head coil (with all peaks shifted by ~0.1ppm in room temperature phantoms).

4.3.1.3 Discussion

From 1D MRS, we know that creatine has a prominent singlet at 3.03ppm. As it is uncoupled, only a single creatine peak is expected on a 2D J-resolved spectrum, and this is confirmed by the experimental work, Figure 4.4 (b). However, this spectrum was not ideal due to the large F1 and F2 artefacts arising from t_1 noise (as previously discussed) and truncation artefacts. This may be due to heating of the gradient coils or indicative of the irregular autoshimming of the voxel, but nevertheless, was of concern. Once the voxel has been shimmed in a stationary phantom, it should not need to be reshimmed unless the scanner pre-scan parameters were susceptible to drift. However, even without deuterium field locks to provide temporal stability, such as those used in high resolution spectrometers (123), it is unlikely that the B_0 field will drift to an observable extent.

Overall, the general pattern of the metabolites tested was as expected, with their coupling patterns similar to those published by Ryner *et al* (22). This favourable comparison permitted initial validation of this method of acquiring and processing 64 individual PRESS sequences to form a single 2D J-resolved experiment. In light of this, it was appropriate to evaluate the technique's performance specific to GABA measurement.

4.3.2 Threshold of GABA detection

4.3.2.1 Introduction

Before this technique could be applied *in-vivo*, it was important to establish whether or not this approach was sensitive enough to detect GABA at normal physiological concentrations. Therefore, a series of experiments were performed to determine the threshold at which GABA can be detected *in-vitro*, and from these results, consider the suitability of the method *in-vivo*.

4.3.2.2 Materials and Methods

All experiments were performed following the protocol given in §4.2.2. 2D J-resolved spectra were acquired from a 3x3x3cm^3 voxel in the centre of the phantom, using a standard volume head coil.

Fourteen individual phantoms were made each containing physiological concentrations of choline and creatine (3mM and 9mM respectively) and GABA at concentrations as listed in Table 4.2. The actual concentrations of choline and creatine were chosen to represent the upper boundaries of normal physiological concentrations, in all brain regions (140). The metabolite concentrations were calculated from masses of the dry chemicals (Sigma-Aldrich).

Table 4.2 Phantom metabolite concentration for threshold of GABA detection experiments

Phantom number	Metabolite concentration (mM)		
	Choline	Creatine	GABA
1	3	9	20.0
2	3	9	5.0
3	3	9	3.0
4	3	9	2.0
5	3	9	1.9
6	3	9	1.8
7	3	9	1.7
8	3	9	1.6
9	3	9	1.5
10	3	9	1.4
11	3	9	1.3
12	3	9	1.2
13	3	9	1.1
14	3	9	1.0

4.3.2.3 Results

To aid identification and quantification of GABA, an initial phantom containing 20mM GABA and physiological concentrations of choline and creatine was investigated, Figure 4.7. GABA can be clearly identified in both the 2D J-resolved plot and the extracted spectrum.

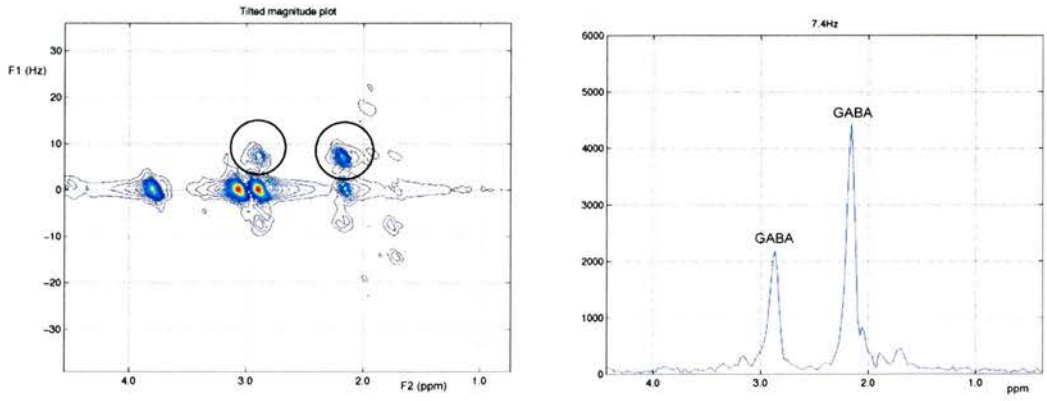

(a) (b)

Figure 4.7 (a) 2D J-resolved plot from 3x3x3 cm^3 VOI positioned in a phantom containing 3mM choline, 9mM creatine and 20mM GABA. The 3.01ppm and 2.28ppm GABA resonances are highlighted by the circular markers. (b) Extracted row corresponding to GABA J-coupling frequency – the 3.01ppm and 2.28ppm GABA peaks are clearly visible (with all peaks shifted by ~0.1ppm in room temperature phantoms).

Figure 4.8 shows the 2D plot from the phantom containing the lowest detectable concentration of GABA in this experimental set-up, that is 1.2mM. The 3.01ppm GABA resonance is clearly seen on both the 2D contour plot and the extracted spectrum in Figure 4.8 (b). Figure 4.8 (c) displays the results after quantification of the peaks in the extracted spectrum using MRUI. Using the same method, the 3.01ppm GABA peak was quantified in all spectra where it was visible and the results plotted in Figure 4.9.

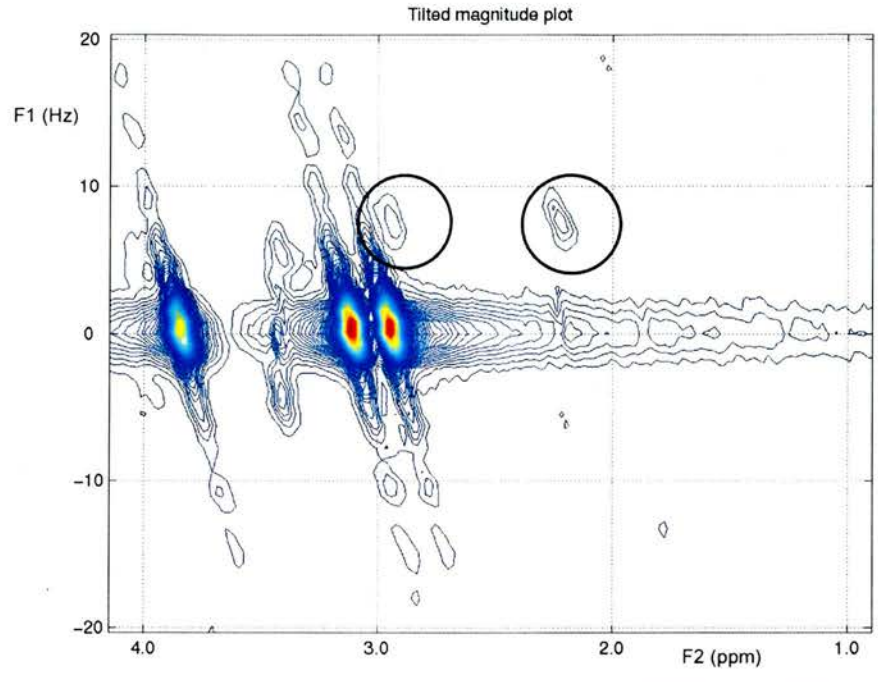

(a)

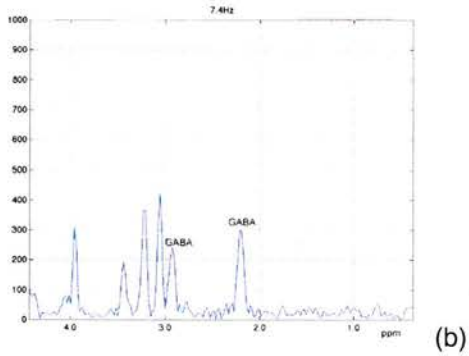

(b)

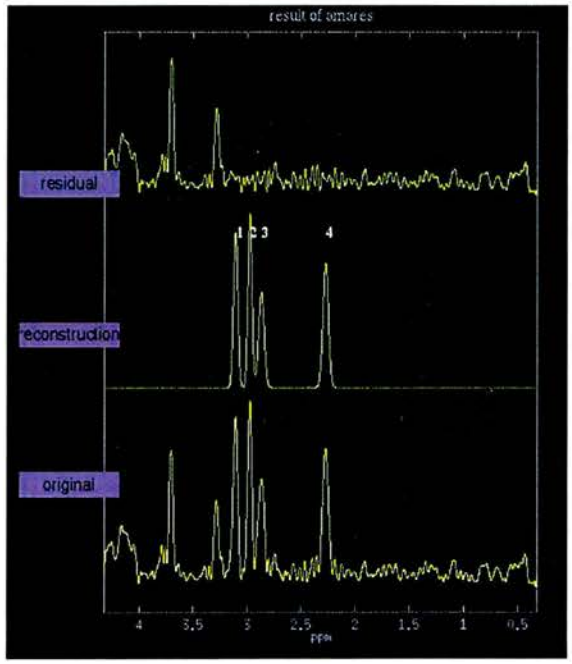

(c)

Figure 4.8 (a) 2D J-resolved plot from 3x3x3 cm^3 VOI centrally positioned in a phantom containing 3mM choline, 9mM creatine and 1.2mM GABA. The 3.01ppm and 2.28ppm GABA resonances are highlighted by the circular markers. Extracted GABA (J = 7.4Hz) spectrum from same phantom: (b) Matlab raw data. (c) After quantification in MRUI: Peaks 1 and 2 correspond to the residual peaks from choline and creatine respectively; Peak 3 is the 3.01ppm GABA and peak 4 is the 2.28ppm GABA peak (with all peaks shifted by ~0.1ppm in room temperature phantoms). The original (bottom), modelled (centre) and residual = original – modelled (top) spectra are shown.

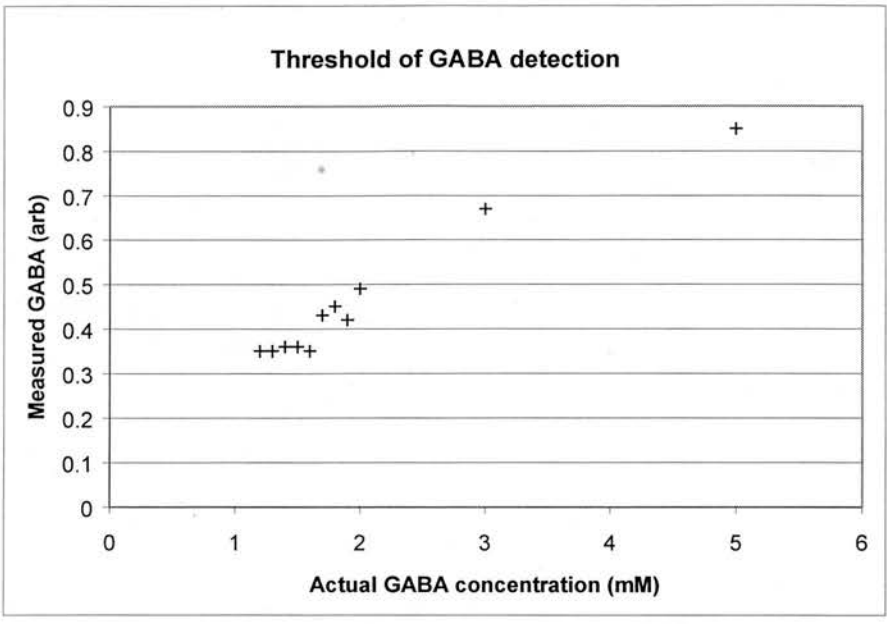

Figure 4.9 Results of *in-vitro* GABA measurement from a 3x3x3 cm^3 voxel in 14 phantoms of decreasing GABA concentration, using 2D J-resolved MRS (64 individual sequences), in a volume head coil.

4.3.2.4 Discussion

This series of *in-vitro* experiments has shown that that GABA can be resolved from the neighbouring resonances of choline and creatine *in-vitro*, and at concentrations approaching those found in normal human brains. However, as Figure 4.9 shows, it is very difficult to discriminate between the actual concentrations of GABA at the very low concentrations, i.e. less than 1.6mM. Therefore it is important to establish the reproducibility of these results, before any conclusions can be drawn regarding the reliability of future *in-vivo* measurements. This issue of reproducibility is addressed in the next section.

4.3.3 Reproducibility

4.3.3.1 Introduction

Before applying any new method clinically, it is essential to determine the reproducibility of the entire process, including acquisition and post-processing. A comprehensive background into the reproducibility of spectroscopy techniques is

given in §7, preceding a thorough study of the reproducibility of GABA measurements using a dedicated 2D J-resolved MRS sequence, to which the reader is directed for a more complete introduction.

Since the ultimate aim was to apply this method in a clinical environment where scans are repeated in different sessions over many days and weeks (so called "between-days" reproducibility), a small study (n = 5) was performed to determine the reproducibility of such measurements, also over many scan sessions.

4.3.3.2 Materials and Methods

2D J-resolved spectra were acquired from a volume head coil, using the same protocol as given in §4.2.2. A single phantom was made containing physiological concentrations of the most common cerebral metabolites, as listed in Table 4.3. To obtain an indication of the general reproducibility of the technique, preliminary measurements were taken from only acetate (substituted for NAA), choline and creatine. In light of the previous results with artefacts appearing in both F1 and F2, extra care was taken with the experimental set-up on each occasion. Temperature consistency was achieved by allowing the solution to stabilise at magnet room temperature for at least 24 hours before the experiment, and motion artefacts were reduced by positioning the phantom within the magnet bore (in the volume head coil) for a minimum of 15 minutes before commencing scanning.

Table 4.3 Metabolites included in phantom for reproducibility study. Concentrations taken from (123).

Metabolite	Concentration (mM)
Acetate	11.7
choline	1.4
total creatine	8.2
myo-inositol	6.2
glutamate	12.5
glutamine	1.8
GABA	0.5
lactate	0.5

To obtain a measure of the between-days reproducibility, five 2D J-resolved spectra were acquired over a period of nine days. The resulting raw data files were then transferred to a SUN Ultra workstation and processed as previously described in §4.2.3. From the J = 0Hz spectra, the acetate, choline and creatine peaks were quantified in MRUI, using prior knowledge files as previously described. Coefficients of variation (CVs), defined as the percentage ratio of the standard deviation to the mean, were calculated for all three metabolites from all five 2D J-resolved spectra.

4.3.3.3 Results

The results from the five between-days 2D J-resolved experiments are summarised in Table 4.4. Figure 4.10 shows representative results from the reproducibility study, showing a 2D J-resolved and an extracted spectrum (at J = 0Hz) respectively.

Table 4.4 Peak areas (arb), as quantified in MRUI, from *in-vitro* between-days reproducibility experiments

Metabolite	Between-days experiment					Mean	SD	CV(%)
	1	2	3	4	5			
choline	14.54	11.88	11.05	12.57	14.33	12.87	1.53	11.8
creatine	24.29	19.63	18.39	17.58	19.47	19.87	2.61	13.1
acetate	31.27	24.88	22.78	24.4	27.31	26.13	3.30	12.6

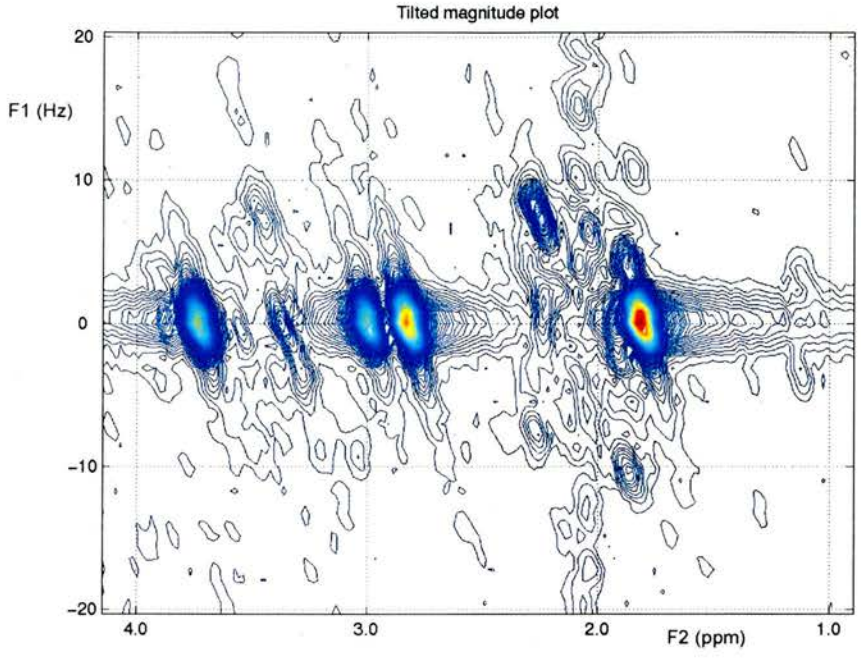

(a)

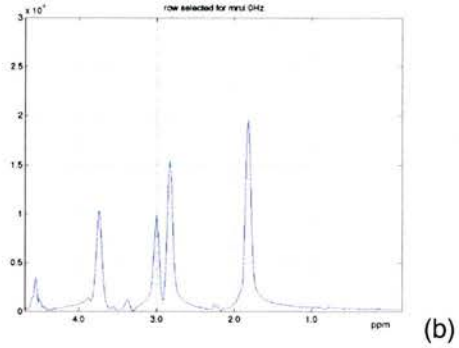

(b)

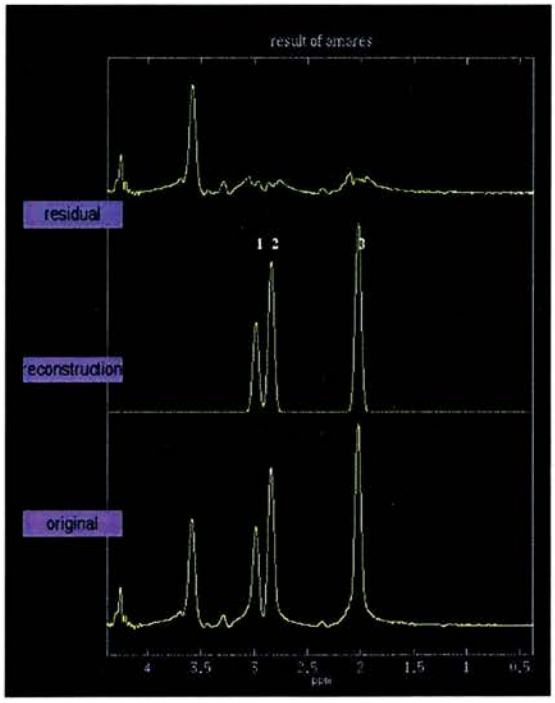

(c)

Figure 4.10 2D J-resolved spectrum from 3x3x3 cm^3 VOI centrally positioned in a phantom containing physiological concentrations of choline, creatine, acetate (in lieu of NAA), glutamate, glutamine, myo-inositol, GABA and lactate, Table 4.3. Extracted uncoupled (J = 0Hz) spectrum from same phantom: (b) Matlab raw data (c) After quantification in MRUI Peaks 1, 2 and 3 correspond to choline, creatine and acetate respectively (with all peaks shifted by ~0.1ppm in room temperature phantoms).

4.3.3.4 Discussion

As will be discussed in §7, large variations in the CVs for *in-vivo* NAA, choline and creatine have been detailed, but *in-vitro*, CVs of < 5% have been reported using conventional 1D methods (141,142). It is somewhat disappointing, therefore, that the reproducibility of acetate, choline and creatine are all > 10% using this 2D method. This may reflect scanner instabilities over the 2.5 hour acquisition process. Without comprehensive study, the reproducibility of GABA measurement using this technique cannot be established, but it is likely that it will be worse than the measured CVs of the higher concentration metabolites. If confirmed, then this has important implications on the appropriateness of applying this protocol to human subjects.

4.4 *In-vivo* results

4.4.1 Introduction

The ultimate aim of this project was to obtain 2D J-resolved spectra from human volunteers and patients for *in-vivo* GABA measurement. Although as it stands, this protocol cannot be clinically applied, it was of interest to acquire at least a single *in-vivo* 2D spectrum to relate the results to the *in-vitro* work.

4.4.2 Methods

A single healthy volunteer was recruited to test this approach *in-vivo*, and written informed consent was obtained. Sixty-four PRESS spectra were acquired from a $3x3x3cm^3$ voxel positioned in the occipital cortex using a series of T_2, 3-plane localising images acquired using a volume head coil, and following the protocol detailed in §4.2.2. Following post-processing of the raw data files as previously described in §4.2.3, a 2D J-resolved spectrum and extracted spectrum corresponding to the J-coupling frequency of GABA were produced.

4.4.3 Results

The resulting 2D J-resolved spectrum is shown in Figure 4.11 (a). Figure 4.11 (b) provides the spectrum extracted from the 2D contour plot corresponding to the J-coupling frequency of GABA. Comparison to the available 2D J-resolved spectra in the literature allowed assignment of the 3.01ppm GABA peak. Examination of the individual 1D spectra prior to 2D FT showed that almost all metabolite signal had disappeared by TE = 475ms, with little evidence of either the choline or creatine peak after TE = 415ms, Figure 4.12.

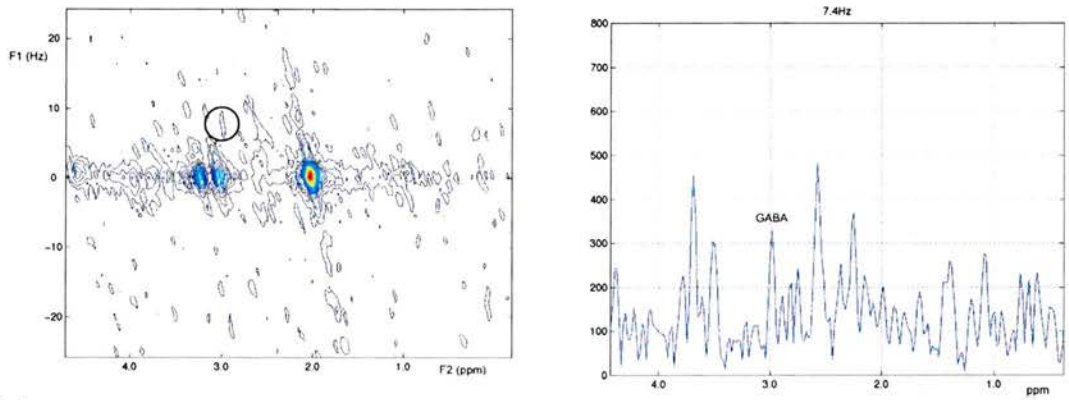

(a) (b)

Figure 4.11 (a) 2D J-resolved spectrum and (b) extracted row corresponding to the J-coupling frequency of GABA from a 3x3x3cm^3 VOI in a normal, healthy volunteer. Provisional assignments have been made for the 3.01ppm GABA resonance.

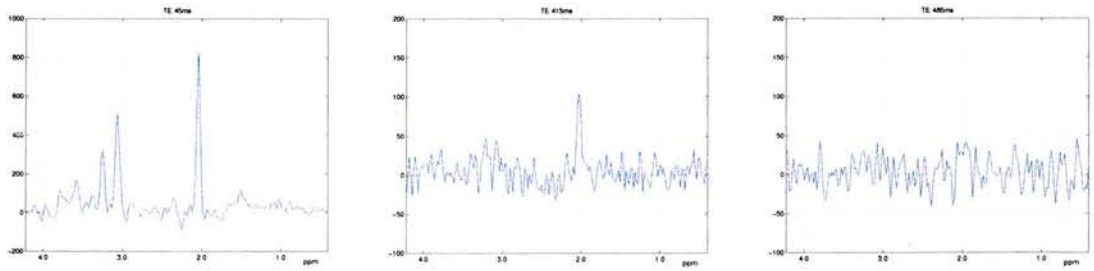

(a) (b) (c)

Figure 4.12 Conventional 1D *in-vivo* spectra using the 2D J-resolved experiment with TE (a) 45ms, (b) 415ms and (c) 485ms demonstrating the loss in metabolite signal

4.4.4 Discussion

The success of 2D J-resolved spectroscopy, using a composite of individual PRESS sequences, for *in-vivo* GABA measurement is not conclusive. A peak assignment to

GABA has been made at its F1 = 7.4Hz and F2 = 3.01ppm position. The extracted spectrum shows a distinct peak at ~ 3.0ppm and the corresponding assignment has been made to GABA. However, the extent of the contribution from contaminating resonances (such as macromolecules, glutathione and homocarnosine (19)) has not been established, and it may be that these form the bulk of the observed peak. Clearly, further work is required.

This experiment has shown though, that it is possible to acquire a 2D J-resolved spectrum from a normal volunteer using a protocol of 64 PRESS experiments with the manual increase of TE. That in itself is a result worth achieving, and suggests that on conventional clinical scanners, with only standard spectroscopy sequences, *in-vivo* 2D J-resolved spectroscopy is possible.

4.5 Sequence optimisation

4.5.1 Introduction

The results from the experiments using 64 PRESS sequences to create a 2D J-resolved experiment have shown that, in principle, the approach works. However, one of its major disadvantages is the scan time needed to acquire all 64 spectra. Therefore, an obvious remedy would be to acquire fewer spectra, but this would only be useful if a similar result could be achieved. Study of the literature has shown that while most investigators used 64 TEs, variations have been used: Ryner *et al* used between 40 and 64 increments, all in 10ms steps (22). Without changing the stepsize, this variation in step count has direct implications on the achievable resolution. Despite this, the authors used 50 TE steps in all of their *in-vivo* work and were still able to make tentative assignments to taurine and GABA cross-peaks.

Post-processing techniques can also offer a method of reducing the time actually required in the scanner. Since the metabolite signal has diminished after approximately TE = 485ms, the remaining spectra could be zero-filled to complete the matrix, and preserve the F1 resolution. Both these approaches were investigated using GAMNA simulations and the raw data from results presented thus far.

Another general method of reducing the total acquisition time is to collect fewer excitations at each TE. When attempting to measure signals from low concentration metabolites, this can have a detrimental effect on the end result. This can be compensated for by exchanging the volume head coil for a more sensitive surface coil. The application of different coils to the measurement of GABA is investigated in §6.

4.5.2 Methods

GABA spin-system simulations in GAMMA based on (135) were acquired under standard conditions (TE_{start}= 35ms, number of experiments = 64, ΔTE = 10ms) and the results were re-processed in two ways:

(1) Including fewer PRESS experiments in the final analysis to observe the effect of changing F1 resolution on the resulting spectra.

(2) Substituting the end portion of the original raw data with zeros to mimic the effect of acquiring a reduced dataset and then zero-filling. In this way, the F1 resolution is preserved at 1.56Hz.

The same post-processing protocol was then applied to a series of *in-vitro* and *in-vivo* data.

4.5.3 Results

Results from applying the optimisation methods to the GAMMA simulations are shown in Figure 4.13 and Figure 4.14. Representative results from the *in-vitro* work are given in Figure 4.15 and Figure 4.16 from a phantom containing 1.2mM GABA with choline and creatine. The same post-processing applied to the *in-vivo* dataset are shown in Figure 4.17 and Figure 4.18.

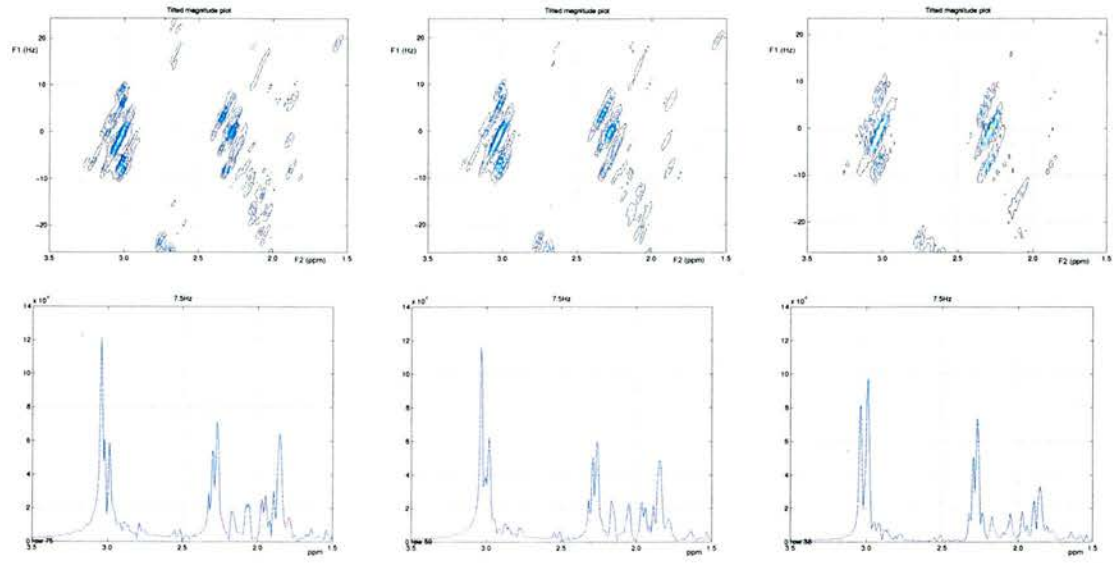

(a) (b) (c)

Figure 4.13 Result from reducing the number of TEs simulated: (a) 64 TEs (resolution = 1.56Hz); (b) 50 TEs (resolution = 2Hz) and (c) 32TEs (resolution = 3.13Hz)

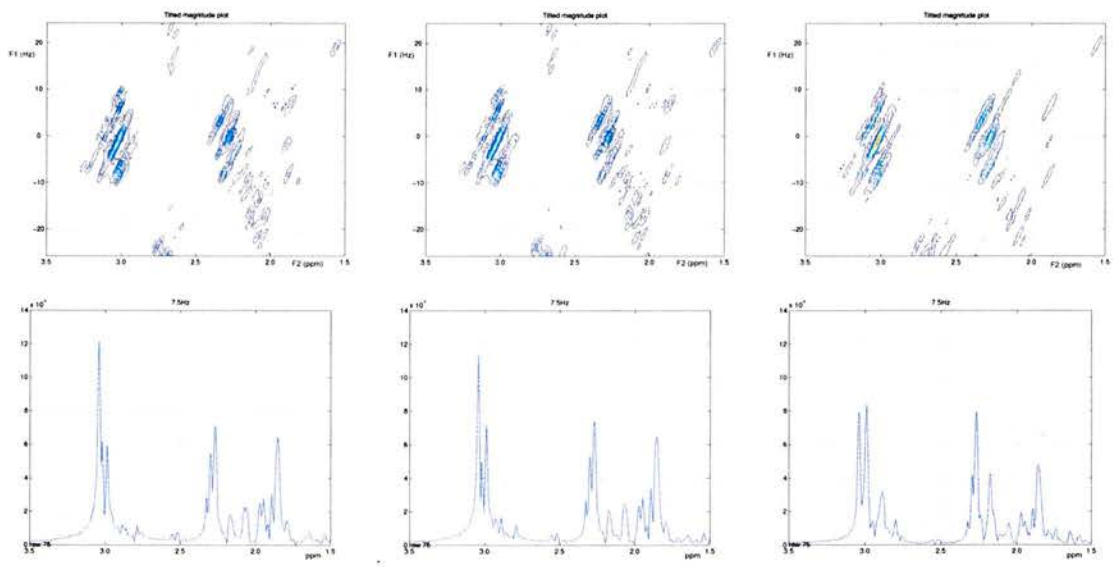

(a) (b) (c)

Figure 4.14 Results from zero-filling the *simulated* data (a) no zero-filling, (b) zero-filling from TE 525ms onwards and (c) zero-filling from TE 355ms onwards (i.e. at experiment 32).

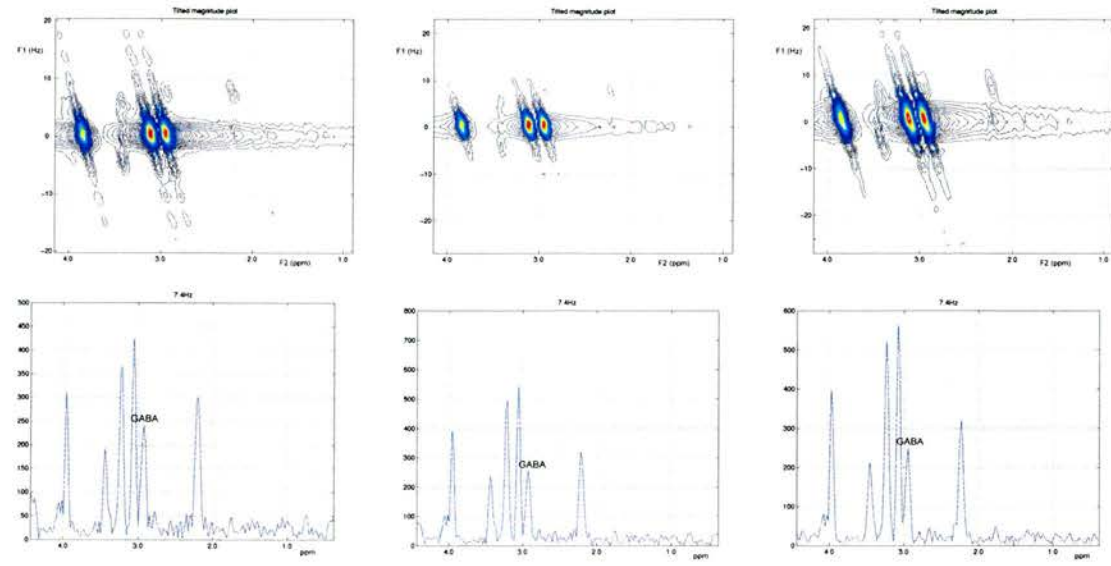

(a) (b) (c)

Figure 4.15 Result from reducing the number of TEs acquired in a phantom containing 3mM choline, 9mM creatine and 1.2mM GABA: (a) 64 TEs (resolution = 1.56Hz); (b) 50 TEs (resolution = 2Hz) and (c) 32TEs (resolution = 3.13Hz) (with all peaks shifted by ~0.1ppm in room temperature phantoms)

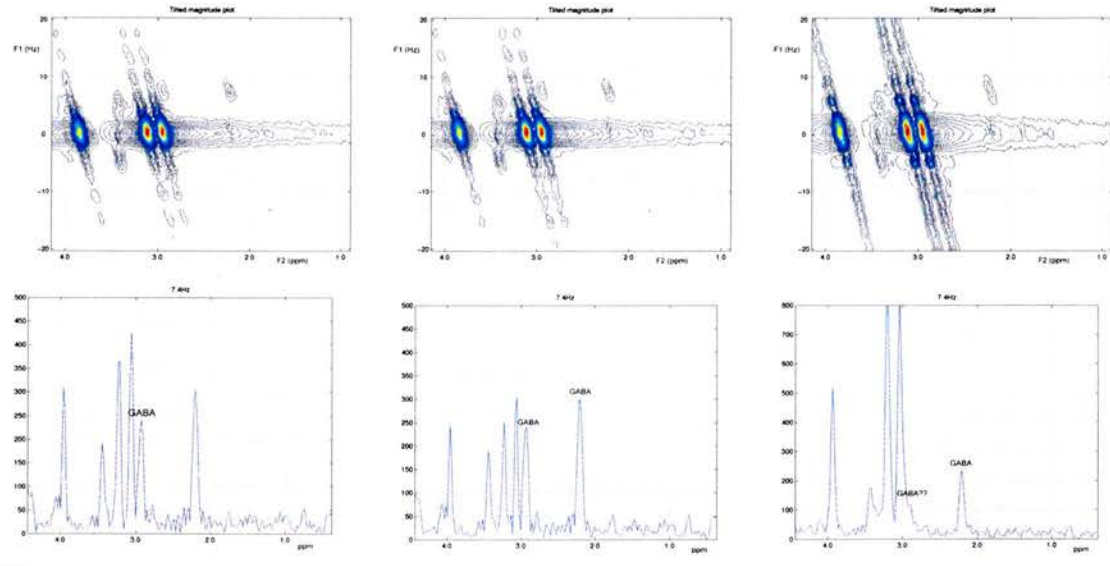

(a) (b) (c)

Figure 4.16 Results from zero-filling the data acquired in a phantom containing 3mM choline, 9mM creatine and 1.2mM GABA: (a) no zero-filling, (b) zero-filling from TE 525ms onwards and (c) zero-filling from TE 355ms onwards (i.e. at experiment 32) (with all peaks shifted by ~0.1ppm in room temperature phantoms).

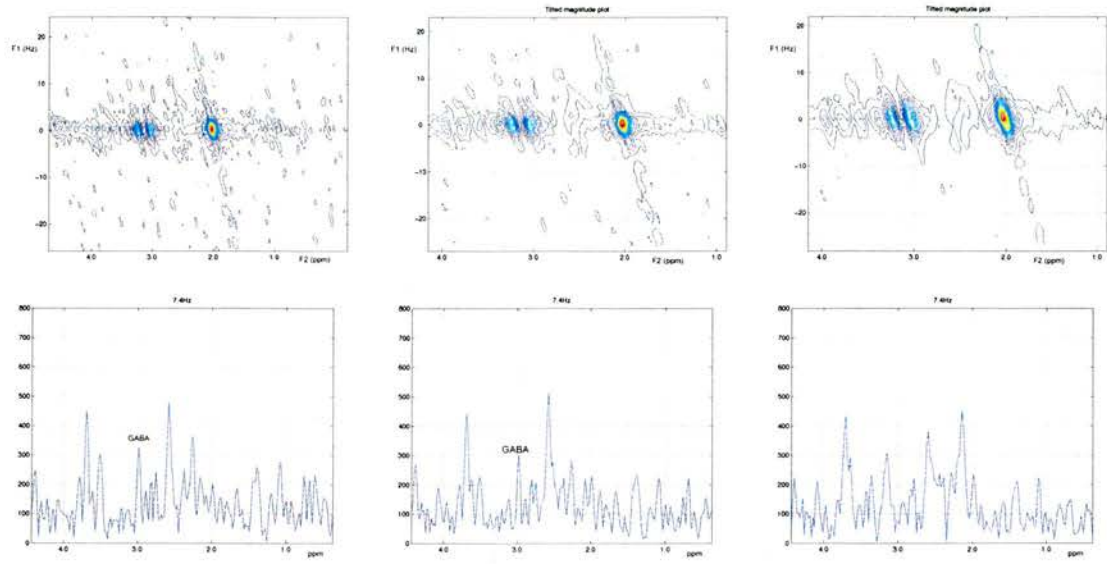

(a) (b) (c)

Figure 4.17 Result from reducing the number of TEs *in-vivo*: (a) 64 TEs (resolution = 1.56Hz); (b) 50 TEs (resolution = 2Hz) and (c) 32TEs (resolution = 3.13Hz)

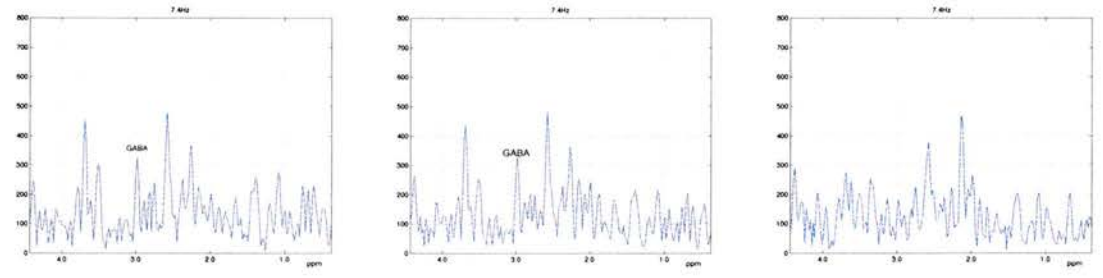

(a) (b) (c)

Figure 4.18 Results from zero-filling the *in-vivo* data (a) no zero-filling, (b) zero-filling from TE 485ms onwards and (c) zero-filling from TE 355ms onwards (i.e. at experiment 32).

4.5.4 Discussion

As expected, by far the worst result in all cases was the acquisition of only 32 spin-echoes. When zero-filled to the equivalent of 64 spin-echoes, a GABA peak is not visible in either the *in-vitro* and *in-vivo* datasets. Without zero-filling, not only is there a decrease in the available F1 resolution, but there is considerable spread of the singlet resonances. In the *in-vivo* experiment with broader linewidths, this F1 spread could potentially lead to occlusion of the GABA peak, and so as a post-processing strategy should be abandoned.

The results from acquiring 50 FIDs are far more encouraging. Although GABA is readily identifiable in all examples, the zero-filling option may be preferred as it allows an F1 resolution of 1.56Hz. This is important, as one of the major advantages of 2D J-resolved spectroscopy is that information on *all* the metabolites is acquired, and so large decreases in the F1 resolution may prevent other metabolites from being identified. With little differences observed between the complete data set and the result from zero-filling only the last 18 experiments, this suggests that this approach may be an acceptable means of decreasing the scanning time. However, further clarification is required before this approach is adopted for routine *in-vivo* data collection.

4.6 Discussion and conclusions

Despite the success of developing a protocol to replicate 2D J-resolved MRS, it was clear from the start, that such an approach was not going to be viable in the clinical domain. A "sequence" of over 2.5 hours (excluding patient set-up and localising scans) was never going to be acceptable to a patient population, and was just barely so for a healthy volunteer. Nevertheless, it was a very interesting and beneficial exercise.

The results from the experimental work in this chapter have demonstrated that 2D J-resolved spectroscopy can be performed *without* a dedicated sequence. Moreover, in the single volunteer scanned, a peak assignment to GABA was made. Perhaps with further optimisation of the protocol, incorporating more sensitive coils and reduced raw data acquisition, it may be possible to decrease the scanning time further. However, it is unlikely that these measures alone will reduce the scan time sufficiently while maintaining adequate resolution and SNR, to allow employment of this method outside the research environment.

5 2D J-resolved MRS using a dedicated sequence

5.1 Introduction

The results from §4 demonstrated that it is possible to perform 2D J-resolved spectroscopy without a dedicated sequence. However, such an approach is not practically viable as it requires over two and a half hours of scan time. To facilitate a more viable transition of this method into the clinical environment, a dedicated 2D J-resolved PRESS sequence was obtained for testing. This is a research sequence, developed by Dr. N. Sailasuta at GEHC, initially for use at 3T and generously made available for testing on the university's 1.5T research scanner.

This chapter describes the initial testing and validation work of the dedicated 2D J-resolved sequence. Detailed descriptions of the acquisition and post-processing protocols are provided, with particular attention to the differences between the dedicated sequence and 64 individual sequences. Following a similar pattern as §4, the results from individual metabolite solutions are presented, the threshold of *in-vitro* GABA detection is determined and an estimation of the general reproducibility of the sequence obtained.

5.2 Sequence description

5.2.1 Background

As stated in the introduction, the dedicated 2D J-resolved PRESS sequence is a research sequence, so cannot be used without a research "key": An agreement between the institution and scanner manufacturer allowing the MRI system to be used for research. Since all work was performed on the university's dedicated research scanner, the key was already in place and the research agreement was updated to include the recent acquisition of the 2D J-resolved sequence.

The dedicated 2D J-resolved sequence is based on the standard PRESS sequence, modified to allow the time either side of the second refocusing pulse to be uniformly incremented (90°-180°-t_1/2-180°-t_1/2-acquire). Fundamentally, the two sequences are very similar. Both use the same fat and water suppression parameters, and prior to a scanner software upgrade, the saturation bands were the same too. The same RF pulses and slice-select gradients are also used. In a standard PRESS sequence, there are two loops controlling data acquisition: The first is determined by the number of excitations as specified by the user. The second controls the number of water reference spectra acquired. This first loop is common to the 2D J-resolved sequence, but in contrast, the second loop is used to control the number of spectra acquired in the 2D experiment. I.e. the number of TE steps, known as steps2d. Echo detection then proceeds along a common route. Since the sequences are so alike, the 2D version is appropriately named 2D J-resolved PRESS.

5.2.2 Scanning protocol

All experiments were performed on a 1.5T GE Signa Horizon scanner, operating in research mode. 2D J-resolved spectroscopy was performed using a dedicated sequence with the following scan parameters: TR = 2000ms, TE_{start} = 35ms, ΔTE = 10ms, NEX = 16 at each TE. The scanning time for each 2D experiment was approximately 35 minutes. In all experiments, a 3x3x3cm^3 VOI was placed in the

centre of the phantom using a 3-plane localising image from a standard volume head coil for localisation, i.e. the same set-up as described in §4.

5.2.3 Post-processing

After transfer of the raw data files to a Sun Ultra workstation, the same general post-processing routine as described in §4.2.3 was applied. This consisted of removal of the water components using HLSVD and scaling of the FID to take into account the pre-scan parameters. Prior to 2D FT the data were zero-filled and apodized in both F1 and F2 dimensions using a simple sine-bell filter and Lorenzian-Gaussian enhancement respectively. After 2D FT, the dataset was tilted to remove the J-coupling contribution on the resulting 2D plot, and spectra were extracted at J = 7.4Hz for GABA measurement.

Quantification of the metabolite areas in MRUI was extended to include the conventional, 1D spectra prior to FT. The FID raw data was extracted from the composite text file containing the information from all 64 experiments, and converted into the appropriate ascii format. Prior knowledge files for the metabolites at representative long and short TEs (35ms and 135ms respectively) were created in the same way as previously described in §4.

However, the water reference spectra required for phase correction were no longer acquired as part of the 2D J-resolved sequence. This meant that the automatic time domain phase correction as applied to the 64 individual sequences had to be changed to account for this. As a result, a more in depth study of phase correction methods was required.

5.2.3.1 Phase correction: Background

As stated earlier, an FID can be modelled as a series of damped sinusoids, but for various practical reasons, the phase of these signals may not all be zero. Possible causes of phase shifts include a delay between the start of the RF pulse sequence and data acquisition, or misadjustment of the phase detector (143). In the latter case, the

phase distortion will produce a uniform error across the entire spectrum, meaning that the mixture of absorption and dispersion will be the same for all peaks. This is a zero-order, frequency-independent phase shift, and can be corrected by a complex rotation of the signal. Correcting this type of phase shift is of primary concern in this section.

There is a plethora of work applying time domain phase correction to FIDs using information from a reference signal e.g. (136,144-148). As discussed in the previous chapter, the technique of using a reference signal to acquire the necessary information for zero-order phase correction was introduced by Oriddige and Cresshull (136). Application of the same phase angles from the reference signal to the water-suppressed signal on a point-by-point basis provides a reliable approximation of zero-order phase correction. However, in the absence of a reference signal, such methods cannot be directly applied. One solution is to treat the metabolite signal as the reference, since without additional processing, the residual water signal will still dominate the FID. Thus, the metabolite FID will effectively phase correct itself.

Frequency domain methods of phase correction often rely only on the water-suppressed, metabolite spectra and not a reference signal. Siegel used a modified simplex method to optimise the angles needed to phase correct the spectra using pre-set criteria based on the area of the absorption (real) signal (149). The actual criteria on which the phase correction was based originated from the much earlier work by Ernst (150). In this, Ernst found that a spectrum was correctly phased if the ratio of the area above the real-mode spectrum to that below was maximum. This approach was utilised by Chen and Kan to apply both zero and first order corrections to their spectra (151). In addition, Balacoo used this method as a starting point for his automatic phase correction method, but went on to optimise the technique for high resolution spectra (152). Although this method is not without its problems, generally caused by baseline distortions and noisy spectra (153), it does in theory provide a logical way of phase correcting spectra without needing the additional information

from a reference signal. With appropriate selection of the spectral region chosen for phase correction, it may also be possible to avoid these common pitfalls.

5.2.4 Phase correction testing

It was important to establish a reliable post-processing protocol as quickly as possible, to allow *all* the data to be consistently processed. Consequently, two methods of phase correction were tested on the initial phantom data to allow a decision to be made early on in the acquisition of data.

5.2.4.1 Time-domain phase correction

The time-domain Ordidge and Cresshull method was adapted to obtain the phase angle for zero-order phase correction from the water-suppressed signal and then apply it back onto the FID. This modified version of the original time-domain method was written by Ian Marshall and included as part of the original post-processing C program.

5.2.4.2 Frequency-domain phase correction

Chen and Kan developed an iterative algorithm for the automatic phase correction of NMR spectra as they were being acquired from the spectrometer (151). This is a frequency domain method, where the spectra are assumed to be properly phased when the ratio of the area *above* the x-axes in the absorption curve to that *under* the x-axis is maximum, Figure 5.1. This principle can be applied for both zero and first order correction.

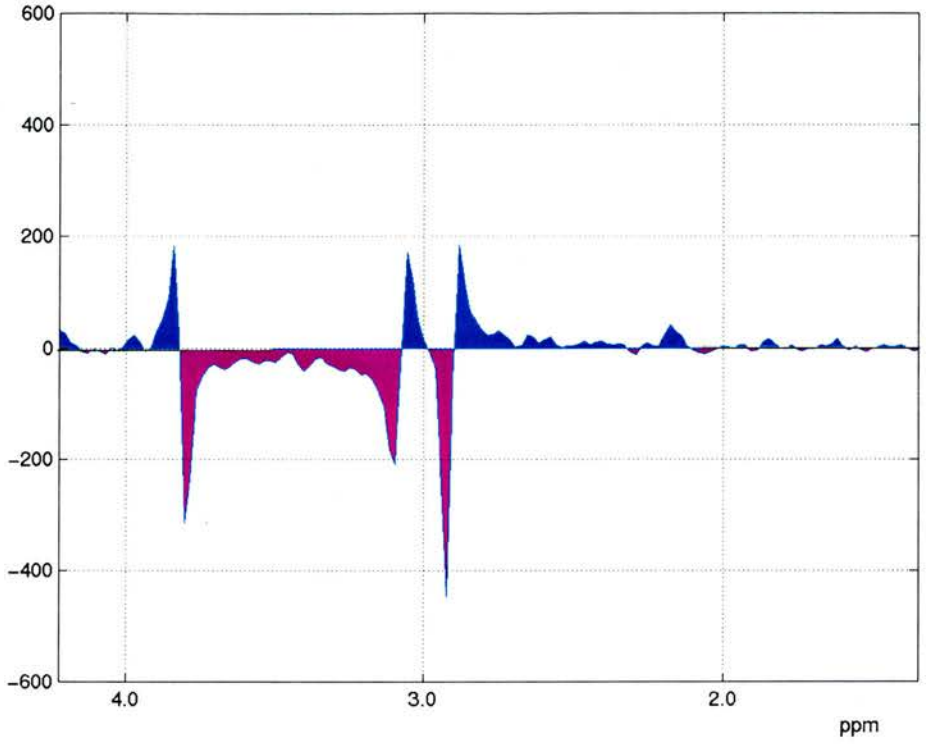

Figure 5.1 Unphased spectrum from a phantom containing choline, creatine and GABA. For the purposes of the Chen, Kan algorithm, the areas above the absorption curve are shaded in blue, and the areas below the curve in purple. Phase correction is achieved when the ratio of the areas above and below the curve is at maximum.

This program was adapted to phase correct the data *after* acquisition, i.e. as part of post-processing prior to 2D FT. In addition, zero order phase correction was initially performed on a specific singlet contained within the spectrum and then the calculated phase applied to the rest of the spectrum. Figure 5.2 shows the scheme behind zero order phase correction using this method.

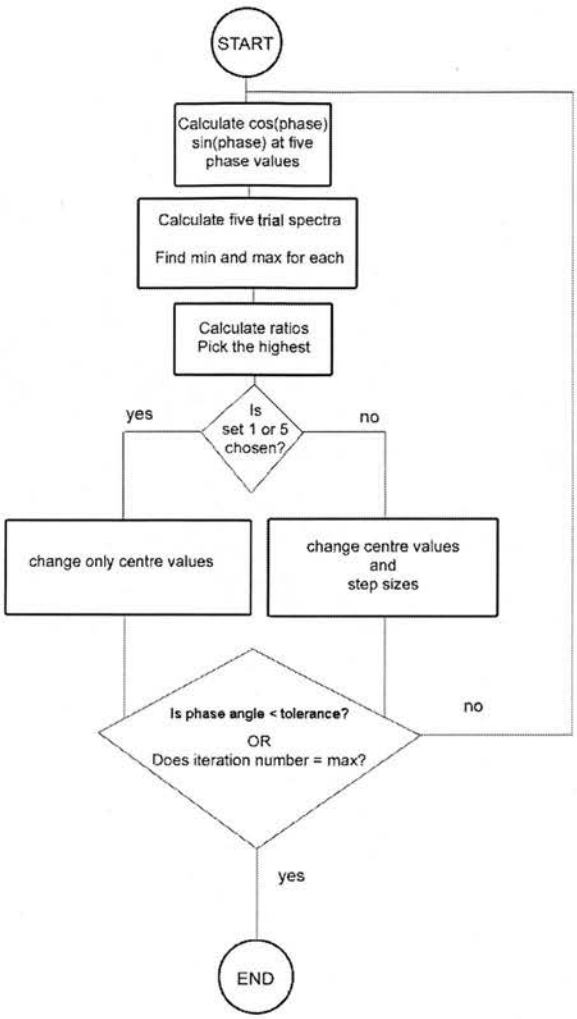

Figure 5.2 Flow chart demonstrating how zero order phase correction was performed

Rather than applying the routine to the entire spectrum, as described in the original paper, the region around creatine was selected. Creatine is a singlet and, as such, is immune to complicated coupling interactions altering the appearance of its peak with increasing TE. This means that the correctly phased peak is consistently positive, making it the most reliable peak upon which to apply the algorithm. In addition, since this peak is in the closest proximity to the 3.01ppm GABA peak, it is important to correctly phase this peak to aid GABA identification. Frequency-domain phase correction was tested using the Matlab functions, PhaseCorrect.m and RotateSpectrum.m, written by the author.

5.2.5 Phase correction: results

5.2.5.1 Frequency-domain phase correction: initial results

The Chen and Kan method was based on selecting the best phased spectrum from a group of five, and then testing this result against a newly selected set of spectra until the maximum area ratio is found. The advantage of this iterative approach is that the optimum phase angle for correction can usually be found within a few iterations, typically less than six.

Another advantage of this method over a non-iterative approach calculating, for example, the area ratio for all 360° rotation, is that it is possible to obtain angles of arbitrary accuracy. To achieve 0.1° resolution non-iteratively would required 3600 calculations but using the iterative algorithm, can usually be obtained in less than ten steps, making it more efficient. However, with only one global solution possible, in terms of the specifics of the algorithm, the same solution is found, Figure 5.3.

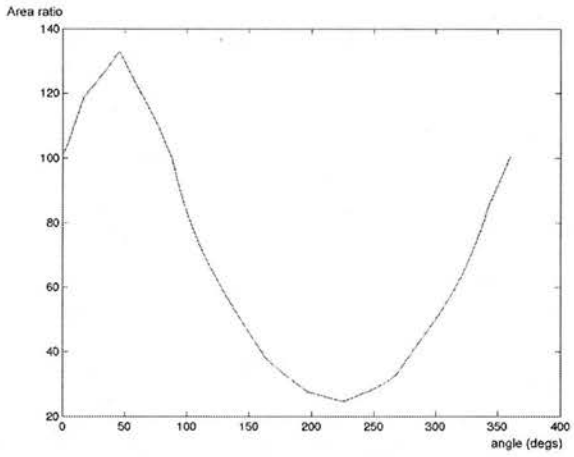

Figure 5.3 Results from calculation of the area ratio across all 360° of rotation. In all data tested, there was only a single global solution, meaning that incorrect results were not going to be produced from being trapped in local maxima / minima.

As stated in the method, it was originally planned to perform phase correction on the creatine singlet alone. Preliminary testing on the entire spectrum failed due to the excessively noisy nature of the water peak, causing over-estimation of the phase angle. An improvement was seen when phasing the spectral region containing only the metabolites, but this was only marginal when tested in spectra containing a near

complete cerebral metabolite set. It was thought that this was due to the complicated nature of the spectra, with many overlapping peaks, and coupled multiplets that do not follow a simple pattern of evolution with increasing TE. This poor result led to considerable bleed in the F1 dimension.

Purely for interest, the algorithm was applied to the acetate (≈ NAA) peak only. This showed an improvement in the results from data sets with multiple metabolites, but it was difficult to determine the exact start and end positions of the peak. *In-vivo*, and particularly at short TEs, this will also be problematic, due to the underlying macromolecules and metabolites complicating the appearance of the peak. In trying to optimise the region of the acetate peak, the results showed how sensitive the algorithm was to the spectral length on which it had to act. Addition or subtraction of only a few data points changed the phase angle applied to the spectrum for correction.

As in the original description of the proposed adaptation of the method, the creatine peak was isolated. Again there was an improvement in the results, Figure 5.4, but the F1 bleed in the resulting 2D spectrum proved that the phasing was still not entirely accurate. Consequently, the region of analysis was extended to include the 3.2ppm choline peak. This dramatically improved the phasing of the individual spectra (Figure 5.5) and this enhancement was carried through into the 2D J-resolved spectra.

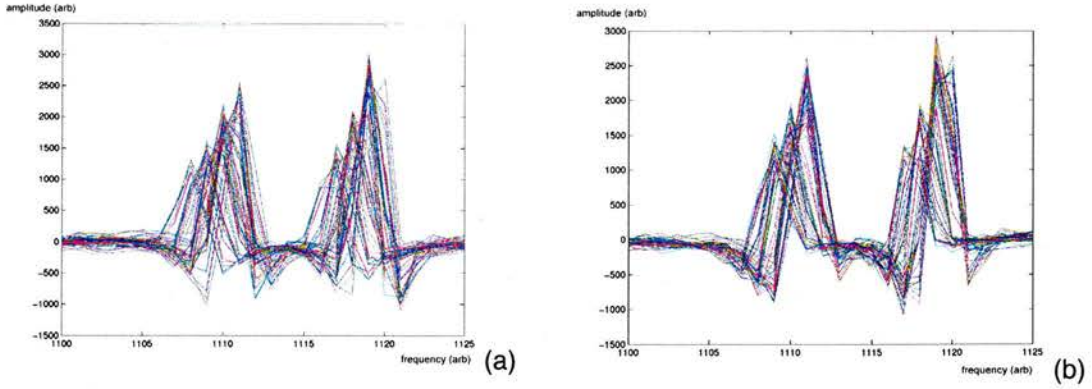

Figure 5.4 Results from phasing on only the creatine peak, real parts (a) before phase correction and (b) after phase correction. Although there is some "neatening" of the two peaks after phase correction, there is still considerable variation in the baseline causing artefacts in the 2D J-resolved spectra.

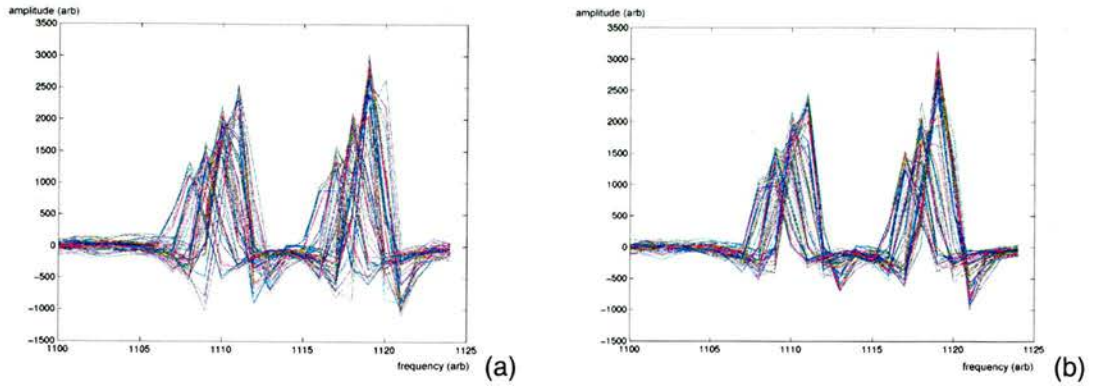

Figure 5.5 Results from phasing on the 3.2ppm choline and 3.0ppm creatine peaks, real parts (a) before phase correction and (b) after phase correction. Both peaks are better phased when compared to Figure 5.4 and there is less variation in the baseline, producing much clearer 2D J-resolved spectra.

5.2.5.2 A comparison of the results between two techniques

Having developed the Chen and Kan zero-order phasing routine to its optimum level of performance, both the time-domain and frequency-domain methods were tested on a series of *in-vitro* data, ranging from single metabolite solutions, phantoms containing physiological concentrations of choline and creatine with varying GABA concentrations, to a full physiological phantom. Representative results from these experiments are shown below. Figure 5.6 shows some of the initial results from phasing the singlet creatine. The 2D spectra and extracted GABA rows are shown in Figure 5.7, from a phantom containing physiological concentrations of choline and creatine and 5mM GABA. Finally, Figure 5.8 shows the spectra acquired from phasing the results from a physiological phantom.

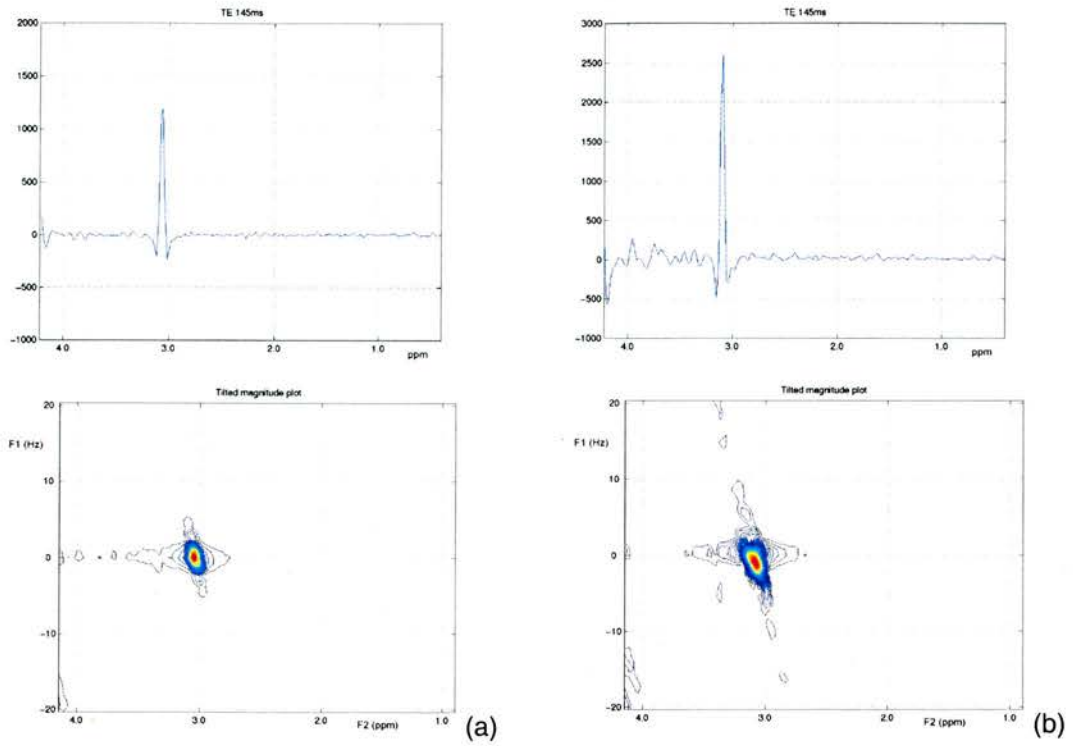

Figure 5.6 Conventional 1D spectra (TE 145ms) and 2D J-resolved plot from phantom containing creatine only using (a) time-domain phase correction and (b) frequency-domain phase correction

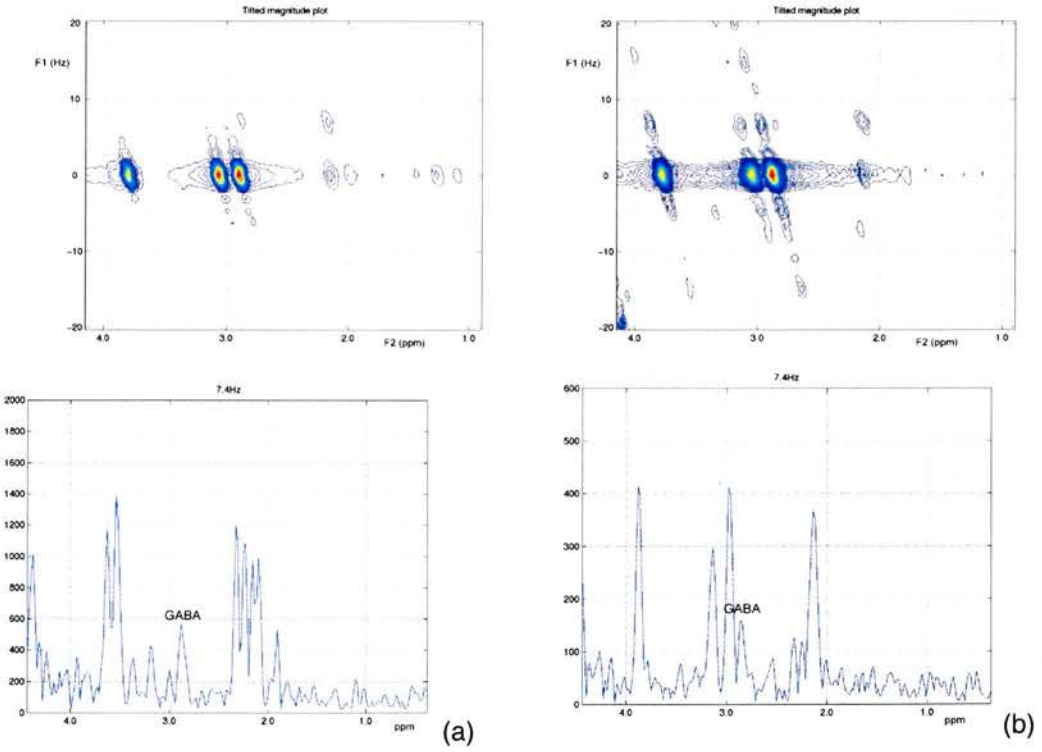

Figure 5.7 2D J-resolved plot and extracted GABA row from phantom contacting choline, creatine and 5mM GABA using (a) time-domain phase correction and (b) frequency-domain phase correction

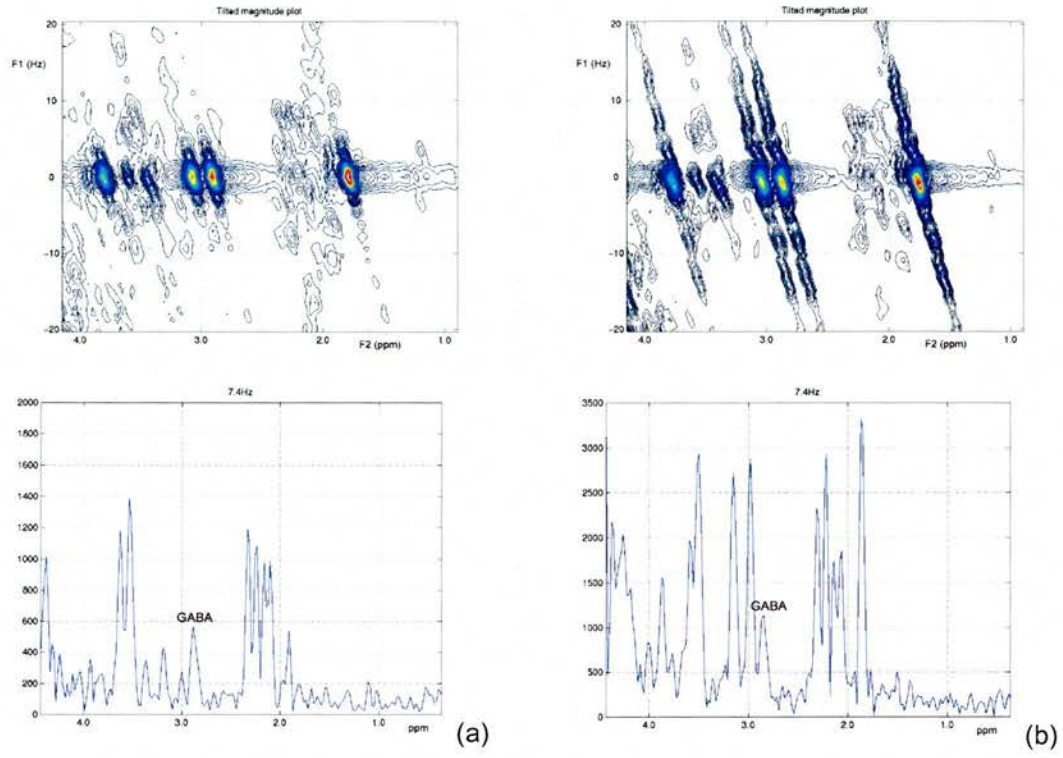

Figure 5.8 2D J-resolved spectra and extracted GABA rows from physiological phantom phase corrected using (a) time domain and (b) frequency domain methods as described in text.

5.2.5.3 Phase correction: Discussion

It is clear from the presented results that the adapted Ordidge and Cresshull time-domain method has the most success in phasing the data. T_1 noise is considerably reduced in the resulting 2D J-resolved spectra, confining the singlet resonances around the J = 0Hz line. Excessive spread of the data in the F1 dimension can cause contamination of the extracted spectra, leading to unreliable quantification of the metabolites of interest.

Zero-order phase correction using the frequency-domain methods was less successful than its time domain counterpart over the entire spectrum. For the spectral region at which it was applied, the spectrum is correctly phased, but at other frequencies, this was not the case. The algorithm does, however, ensure that the real part of the signal is closer to absorption mode than the imaginary part, and as such, may provide a good first approximation of the phase before applying additional first-order techniques. However, in light of such encouraging results from the time-domain method, further exploration of this algorithm was superfluous. Therefore, in all

subsequent work, the time-domain routine was routinely applied in the post-processing of the 2D J-resolved data.

5.3 Individual metabolite phantoms

5.3.1 Introduction

As stated in §4, it was important to establish the validity of the 2D J-resolved acquisition and post-processing protocols by performing a series of experiments to compare to the results in the published literature. For this reason, aqueous metabolite solutions were studied on an individual basis to obtain an indication of the performance of the technique as a whole.

5.3.2 Methods

2D J-resolved MR spectra were acquired using the specific GE pulse sequence as described in §5.2. In each case, 64 t_1 increments were collected with NEX = 16 (TE_{start} = 35ms, ΔTE = 10ms, TR = 2000ms) resulting in an acquisition time of 35 minutes. The raw data files were then transferred to a Sun Ultra Workstation (Sun Microsystems, Mountain View, CA) where the data were processed using the protocol defined in §5.2.3.

Aqueous solutions of the commonly investigated cerebral metabolites (choline, creatine, myo-inositol, glutamate and glutamine) were prepared at physiological concentrations in 3.6 litre spherical, glass containers. GABA was investigated at a concentration of 10mM. The solutions were adjusted to physiological pH of 7.2 using a combination of hydrochloric acid and sodium hydroxide. No attempt was made to mimic physiological relaxation times in the phantoms. Finally, a 2D J-resolved dataset was acquired from the commercially available GE spectroscopy phantom, the contents of which are listed in Table 5.1.

Table 5.1 GE MRS Head sphere contents, as listed in the GE spectroscopy manual, 2001

Chemical name	Concentration (mM)
Potassium phosphate monobasic	50mM
Sodium hydroxide	56mM
N-acetyl-aspartic acid	12.5mM
Creatine hydrate	10mM
Choline chloride	3mM
Myo-inositol	7.5mM
L-Glutamic acid (monosodium salt)	12.5mM
DL-lactic acid (lithium salt)	5mM
Sodium azide	0.10%
Magnavest	0.10%

5.3.3 Results

The 2D J-resolved spectra resulting from the individual metabolite experiments are provided in Figure 5.9 to Figure 5.11. Figure 5.12 shows the resulting 2D spectrum from the same experiment carried out on the standard GE spectroscopy phantom.

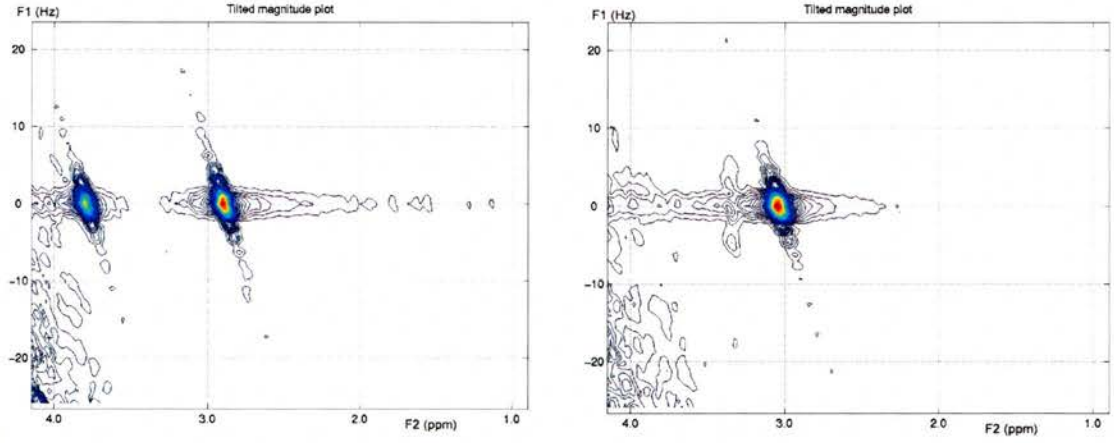

(a) (b)

Figure 5.9 2D J-resolved plot from a 3x3x3 cm^3 VOI positioned in a phantom containing (a) 9mM creatine and (b) 3mM choline. Both experiments were performed using a standard volume head coil (with all peaks shifted by ~0.1ppm in room temperature phantoms).

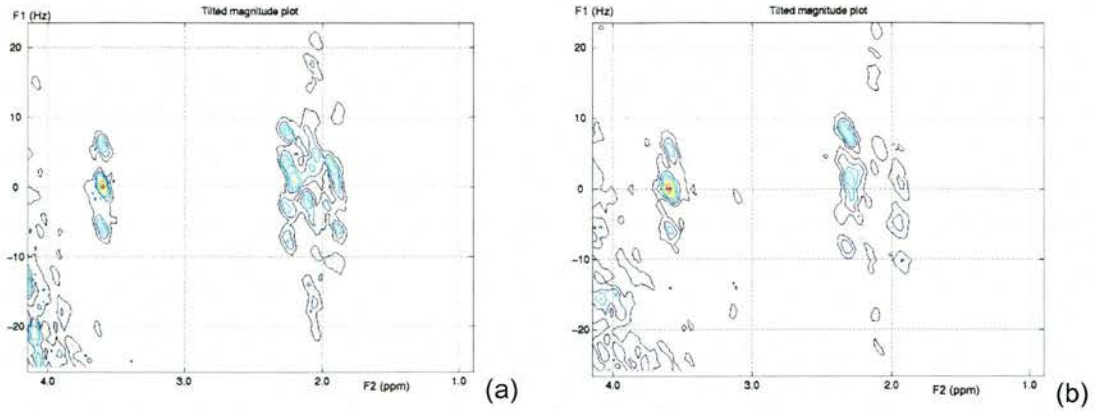

Figure 5.10 2D J-resolved plot from a 3x3x3 cm^3 VOI positioned in a phantom containing (a) 12.5mM glutamate and (b) 5.8mM glutamine. Both experiments were performed using a standard volume head coil (with all peaks shifted by ~0.1ppm in room temperature phantoms).

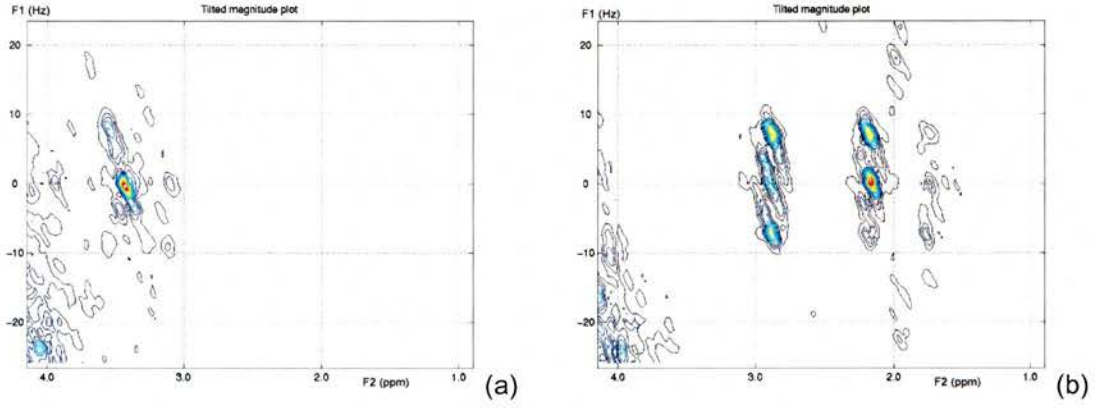

Figure 5.11 2D J-resolved plot from a 3x3x3 cm^3 VOI positioned in a phantom containing (a) 8.1mM myo-inositol and (b) 10mM GABA. Both experiments were performed using a standard volume head coil (with all peaks shifted by ~0.1ppm in room temperature phantoms).

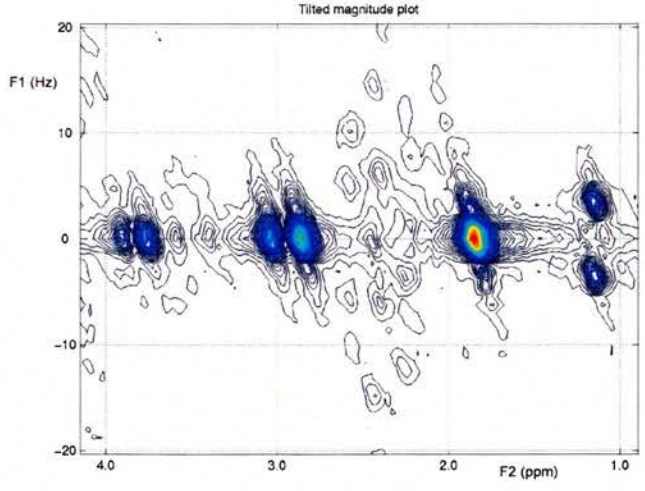

Figure 5.12 2D J-resolved plot from a 3x3x3 cm^3 VOI positioned in a standard GE spectroscopy phantom (contents given in Table 5.1Table 5.1) (with all peaks shifted by ~0.1ppm in room temperature phantoms).

5.3.4 Discussion

Overall, the coupling patterns observed in the 2D spectra agree with those in the literature (22) and are similar to those produced from the 64 individual experiment protocol (§4.3.1). There is, however, evidence of a larger residual water peak in these results compared to those presented in §4. This is probably due to the auto water suppression (AWS) optimisation in the individual PRESS experiments, which wasn't applied in the dedicated sequence. It may also indicate poorer shimming of the voxels in some of the experiments.

5.4 GABA threshold

5.4.1 Introduction

As described in the previous chapter, the threshold of GABA detection needs to be established using the dedicated 2D J-resolved sequence in a standard brain imaging set-up. Knowing that high concentrations of GABA can be detected using this method, the experiments focussed on physiological concentrations of the metabolite.

5.4.2 Materials and methods

All experiments were performed following the acquisition protocol set out in §5.2.2. 2D J-resolved spectra were acquired from a $3x3x3cm^3$ voxel in the centre of the phantoms, using a standard volume head coil.

Eleven individual phantoms were made, each containing physiological concentrations of choline and creatine (3mM and 9mM respectively). As with the corresponding experiments described in §4.3.2, the concentrations of these metabolites were chosen to encompass the normal range of physiological concentrations in all brain regions (140). GABA was added in different concentrations to each, from 2.0mM to 1.0mM GABA, at 0.1mM intervals. The aqueous solutions were calculated from the dry masses of the chosen chemicals (Sigma-Aldrich).

Post-processing and quantification of the extracted spectra followed the method described in §5.2.3.

5.4.3 Results

A summary of all the quantifiable results is shown in Figure 5.13, with a minimum identifiable GABA concentration of 1.2mM. The minimum threshold of GABA detection was determined by visual assessment: The 3.01ppm GABA resonance was identified by a separate and distinct contour on the 2D plot, at 7.4Hz, with a corresponding peak on the extracted spectrum. The 2D J-resolved spectrum corresponding to this concentration of GABA, with extracted GABA row (pre- and post-quantification) are shown in Figure 5.14.

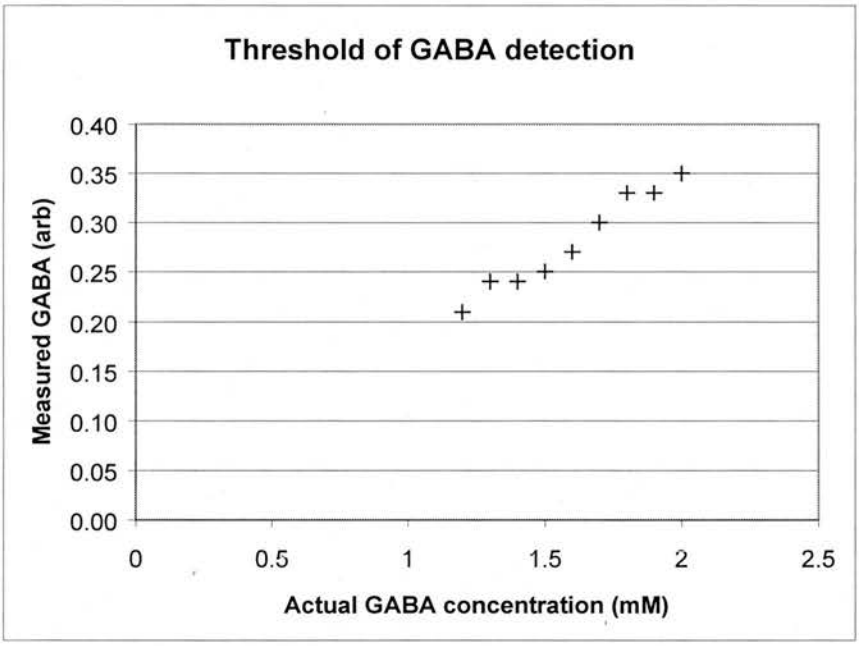

Figure 5.13 Results of *in-vitro* GABA measurement from a 3x3x3cm^3 voxel in 11 phantoms of decreasing GABA concentration, using a dedicated 2D J-resolved MRS sequence in a volume head coil.

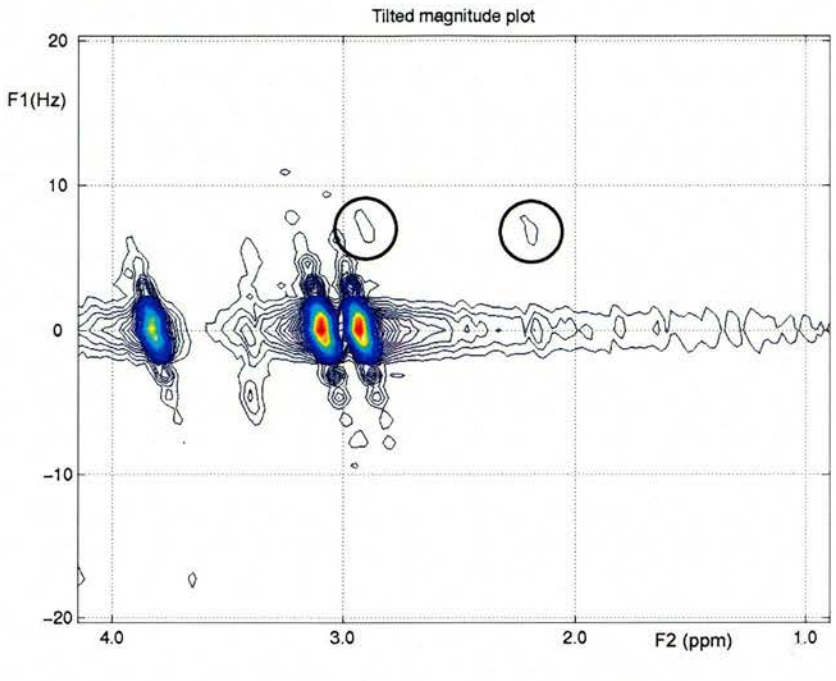

(a)

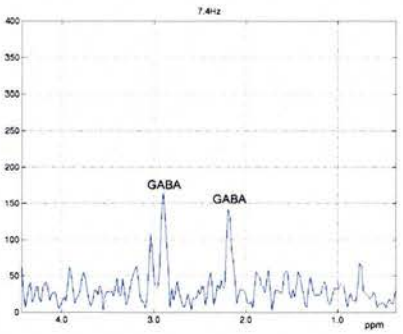

(b)

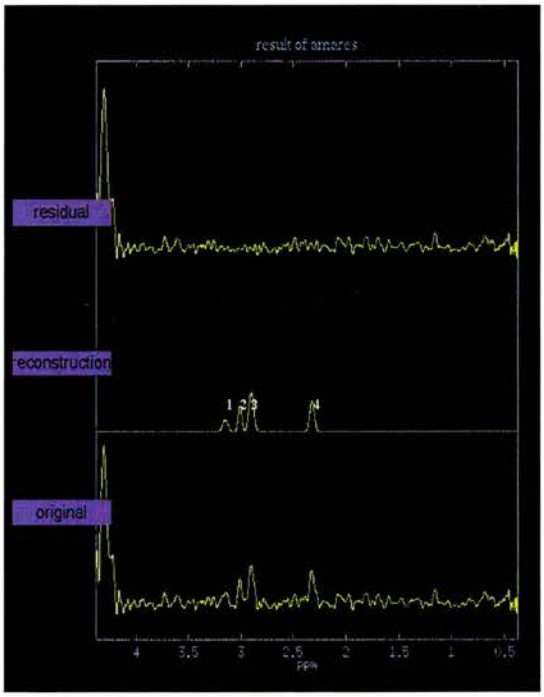

(c)

Figure 5.14 2D J-resolved spectrum from a 3x3x3cm^3 VOI centrally positioned in a phantom containing 3mM choline, 9mM creatine and 1.2mM GABA. The 3.01ppm and 2.29ppm GABA resonances are identified by the circular markers. Extracted GABA spectrum (J = 7.4Hz) from the same phantom: (b) Matlab raw data and (c) After quantification in MRUI (with all peaks shifted by ~0.1ppm in room temperature phantoms). Peaks 1 and 2 correspond to the residual peaks from choline and creatine; Peak 3 is the 3.01pm peak and peak 4 is the 2.28ppm GABA peak.

5.4.4 Discussion

It is interesting to note that the same threshold of GABA detection has been shown in both the series of experiments using a composite and a dedicated 2D J-resolved sequence. Thus, in the standard clinical brain-imaging set-up, that is using a volume head coil at 1.5T, concentrations of GABA can be detected as low as 1.2mM. This is within physiological concentration as cited in (7) but may not be sensitive enough to detect the reductions in GABA associated with depressive disorders (8).

Although these are encouraging results, the reliability of such measurements need to be established before applying the work *in-vivo*. Preliminary results from a reproducibility study addressing this issue are presented in the next section.

5.5 Reproducibility

5.5.1 Introduction

As part of a much larger study looking at the reproducibility of GABA measurement using the dedicated 2D J-resolved sequence, a general indication of the reproducibility of the technique was obtained by quantifying the peak areas of choline and creatine. The results from this work are included here to establish the background on which the GABA-specific reproducibility work is set (§7).

5.5.2 Materials and methods

2D J-resolved spectra were acquired following the protocol outlined in §5.2.2. Five phantoms containing physiological concentrations of choline and creatine (3mM and 9mM respectively) were made in the same 3mm thick, 3.6 litre, glass, spherical shell.

Three measures of reproducibility were taken:

(1) Within-run reproducibility: Variation due to scanner instability alone (same scan session).

(2) Within-session reproducibility: Variation due to scanner instability and voxel re-positioning (in the same scan session).

(3) Between-days reproducibility: Both scanner and set-up variation over several days.

In each of the three sets of reproducibility measurements, five 2D J-resolved spectra were acquired. Each experimental set was repeated for all five phantoms, giving rise to a total of 75 experiments performed in the volume head coil.

The resulting raw data files were transferred to a Sun Ultra workstation and processed as described in §5.2.3. Uncoupled spectra were extracted at J = 0Hz for quantification of choline and creatine. CVs were calculated for both metabolites in each of the within-run, within-session and between-days reproducibility experiments.

5.5.3 Results

A representative uncoupled spectrum following quantification in MRUI is shown in Figure 5.15. To ensure that the correct row was selected for quantification, rows either side of the central row were extracted and quantified for comparison. In all cases, the original selection of the central row was correct. Table 5.2 lists the CVs calculated in all of the reproducibility experiments, with the CVs ranging from 0.86% to 9.57%.

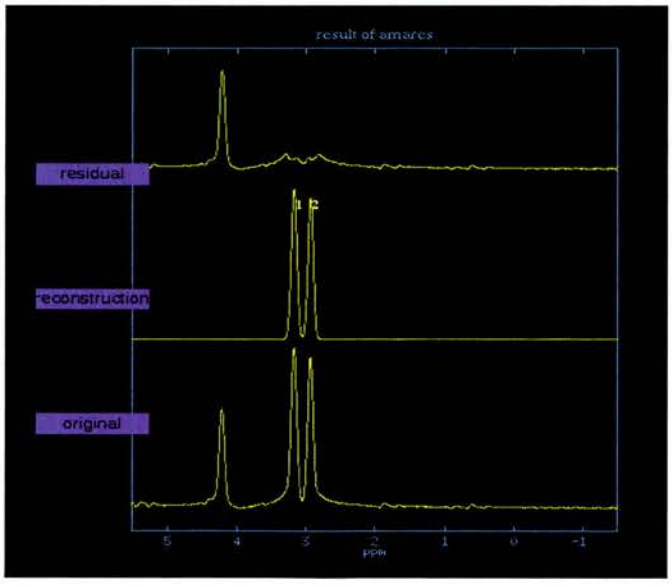

Figure 5.15 showing example uncoupled spectrum from phantom containing physiological concentrations of 3mM choline and 9mM creatine (peaks 1 and 2 respectively).

Table 5.2 Summary measures of the five phantoms containing the 3mM choline and 9mM creatine in all 75 experiments in the volume head coil

Metabolite	Phantom number	CV (%)		
		within-run	within-session	between-days
choline	1	3.17	6.37	8.02
	2	9.06	9.09	9.36
	3	5.51	4.75	4.34
	4	2.47	3.01	8.19
	5	0.86	6.67	8.28
creatine	1	2.78	7.49	5.50
	2	8.74	9.57	9.22
	3	4.38	4.78	3.58
	4	3.22	2.98	9.21
	5	1.35	6.04	7.76

5.5.4 Discussion

In relation to phantom work, a between-days CV of less than 5% is expected for the three main metabolite peaks, including choline and creatine (142). This result was not reflected in the quantified data, with over half the CVs > 5% and the largest rising to 9.57%. This may suggest an overall decrease in the reproducibility of 2D MRS or indicate problems with scanner stability over the acquisition time. However, with such a wide variation in reproducibility values published for conventional 1D MRS (154), these results do not exceed any the outer limits of the quoted reproducibility ranges.

5.6 Discussion and conclusions

The most obvious advantage of the dedicated 2D J-resolved sequence over the composite sequence described in the last chapter, is the decrease in acquisition time. This is due to the continuous acquisition of data during the scan time, with the automatic loop through of TEs, and the requirement of only one pre-scan. Although 35 minutes is still long when compared to other imaging and spectroscopy sequences, it is a very efficient method of collecting both chemical shift and J-coupling information over the entire ppm range. From a clinical viewpoint, it is clear that this sequence would dominate any scanning session, with perhaps only time for

a localising and T_2-weighted image, but it is certainly more viable than an in-magnet time of over three hours!

Of course, the time gain would be of no advantage if the sequence didn't perform as expected. These initial results have shown that both the acquisition and post-processing protocols are able to produce 2D spectra allowing differentiation of the metabolites by their J-couplings. In addition, the reproducibility of the results for choline and creatine are within acceptable limits.

Having established the validity of the method in theory and *in-vitro*, further investigation needs to be performed to assess its applicability to *in-vivo* GABA detection. The optimisation strategies employed to meet this aim are the focus of the next chapter.

6 Optimisation of 2D J-resolved MRS for GABA measurement

6.1 Introduction

Results from the previous chapter have established that a dedicated 2D J-resolved sequence is able to measure GABA in phantoms at concentrations approaching those *in-vivo*, in an acceptable scanning time. However, there are many factors that need to be addressed before translating this work *in-vivo*.

GABA is a very low concentration metabolite, and so improvements in the SNR during acquisition would aid its detection. In principle, this can be achieved using surface coils and prescribing large spectroscopy VOI. The advantages of using such approaches are discussed in §6.2 and §6.3. The TE / ΔTE / TR timings were optimised to record the largest available GABA signal whilst at the same time, reducing the contribution from the underlying macromolecule resonances, shown in §6.4. In all cases, a compromise had to be found between the theoretical and physiological / anatomical limitations, to arrive at the optimum protocol for *in-vivo*

work. Once established, the protocol was tested on a phantom containing physiological concentrations of all the common cerebral metabolites, §6.5.

6.2 Coil arrangement

6.2.1 Introduction

In standard MR brain imaging, a volume (birdcage) head coil is used as it gives full coverage of the brain for both imaging and spectroscopy purposes. However, for single-voxel spectroscopy experiments, it is often useful to use a surface coil, exploiting the increase in SNR associated with the excitation of a smaller localised volume. This is particularly useful when aiming to record signals from low concentration metabolites. Therefore, a series of *in-vitro* experiments were performed to measure the variations in 2D J-resolved MRS introduced with different coil arrangements.

6.2.2 *In-vitro* experiments

All experiments were carried out on the centre's 1.5T GE Signa Horizon scanner, operating in research mode and using a dedicated 2D J-resolved sequence as previously described (§5) (TE_{start} = 35ms, TR = 2000ms, ΔTE = 10ms, number of TEs (steps2d = 64)). Two sets of experiments were conducted: First, a general measurement of changes in SNR of GABA signals from the same phantom using different coil arrangements. Secondly, a series of *in-vitro* experiments using decreasing concentrations of GABA to see how these changes translated into differences in the threshold of GABA detection.

6.2.2.1 GABA SNR in each coil arrangement

2D J-resolved spectra were acquired from a single phantom containing 10mM GABA in a standard volume head coil, 3" and 5" surface coil. The experiments were performed consecutively, using the same acquisition parameters. To replicate *in-vivo* set-up with a voxel placed in the occipital cortex, a VOI was positioned in the lower

half of the phantom (equivalent to the high signal region in the surface coils) for all three coil arrangements. In each case, the same 3x3x3cm^3 voxel was prescribed.

As expected, all three 2D J-resolved spectra were similar in appearance, Figure 6.1. However, the increase in sensitivity of the surface coils was translated into an increase in the GABA peak areas after quantification, Figure 6.2 and Table 6.1, with a corresponding increase in the SNR.

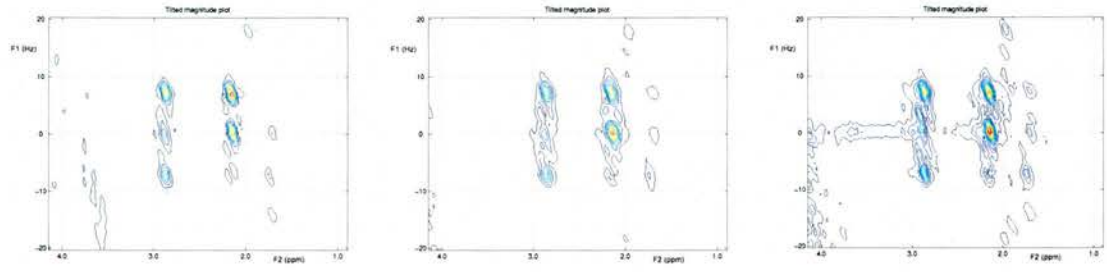

(a) (b) (c)

Figure 6.1 2D J-resolved spectra from 3x3x3 cm^3 VOI in 10mM GABA phantom using (a) standard volume head coil, (b) 5" surface coil and (c) 3" surface coil (with all peaks shifted by ~0.1ppm in room temperature phantoms).

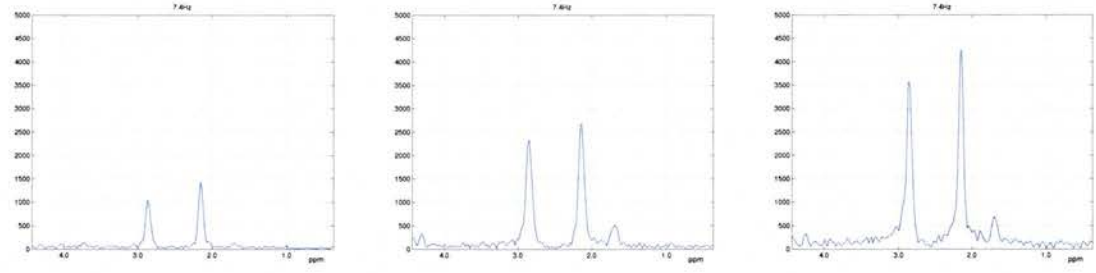

(a) (b) (c)

Figure 6.2 Extracted spectra from 2D J-resolved spectra from 10mM GABA phantom using (a) standard volume head coil, (b) 5" surface coil and (c) 3" surface coil (with all peaks shifted by ~0.1ppm in room temperature phantoms).

Table 6.1 Quantification of GABA peaks, *in-vitro*, using three different coil arrangements

Coil arrangement	GABA peak area (arb)			mean noise (arb)	SNR 3.01ppm GABA peak
	3.01ppm	2.28ppm	1.89ppm		
Volume head coil	1.61	2.13	0.13	0.03	67.1
5" surface coil	4.32	4.82	0.89	0.06	90.0
3" surface coil	5.60	5.98	0.90	0.06	116.7

The results confirm that the highest SNR is obtained using the 3" surface coil, as would be expected. However, the overall excited volume is smaller in this coil compared to the both the 5" surface coil and the head coil. As a result, the VOI used – that is $3x3x3cm^3$ – encompassed almost the entire high signal volume. Although not an issue *in-vitro*, *in-vivo* it is desirable to have a large high-signal region in which to place a large VOI, to allow changes in exact VOI locations to account for variations in anatomy. Therefore, it might prove that the 5" surface coil provides the best compromise between increased SNR and excited volume.

6.2.2.2 Threshold of GABA detection in each coil arrangement

The threshold for *in-vitro* GABA detection using a standard volume head coil has previously been determined at 1.2mM, §5.4. Given the increase in sensitivity associated with the surface coils compared to the volume head coil, it was of interest to investigate the limit of GABA detection using 2D J-resolved MRS and a surface coil arrangement.

Results from the literature suggest that *in-vivo* GABA concentrations as low as 0.8mM have been recorded (6,11). Since it is already known that concentrations of 1.2mM can be observed in the volume head coil, three additional experiments were carried out in the 5" surface coil using GABA concentrations as low as 0.8mM, Table 6.2. For comparison, 2D J-resolved spectra were also acquired from phantoms four and five using a 3" surface coil.

Table 6.2 Phantom metabolite concentration for threshold of GABA detection experiments using a 5" surface coil.

Phantom number	Metabolite concentration (mM)		
	Choline	Creatine	GABA
1	3	9	2
2	3	9	1.5
3	3	9	1.2
4	3	9	1.0
5	3	9	0.8

A summary of the results is given in Figure 6.3. The minimum concentration of *in-vivo* GABA reported in the literature (0.8mM) was detected using the surface coils, and the 2D J-resolved spectra and extracted rows corresponding to this concentration are shown in Figure 6.4 (for the 3" surface coil) and Figure 6.5 (for the 5" surface coil). A two-fold increase in the SNR was calculated for the lowest two concentrations of GABA when using the 3" surface coil compared to the 5" coil, Table 6.3.

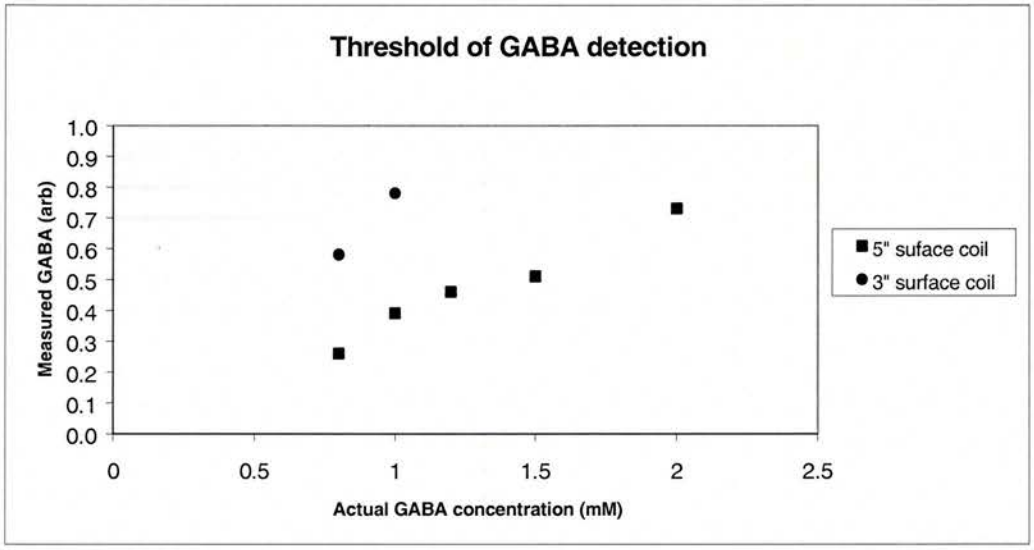

Figure 6.3 Results of *in-vitro* GABA measurement from a 3x3x3 cm^3 voxel in five phantoms of decreasing GABA concentration, using a dedicated 2D J-resolved MRS sequence in two different sized surface coils.

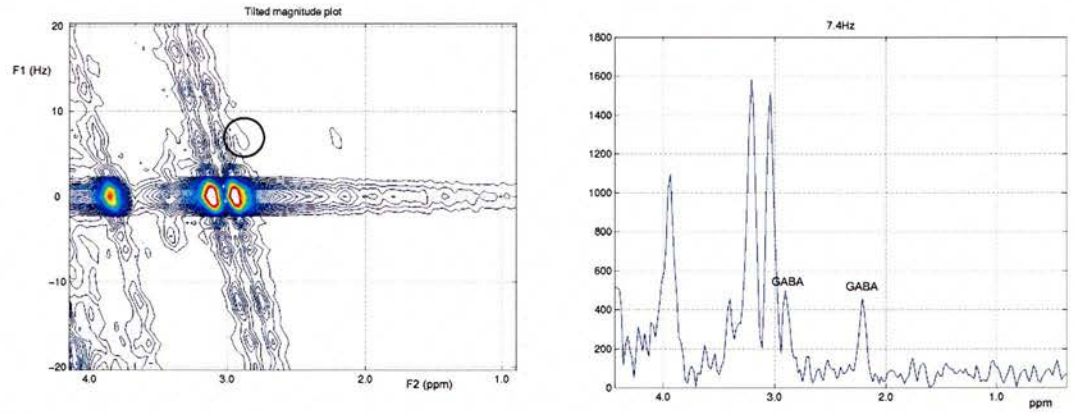

(a) (b)

Figure 6.4 (a) 2D J-resolved spectra from 3x3x3 cm^3 VOI in a phantom containing 3mM choline, 9mM creatine and 0.8mM GABA phantom using a 3" surface coil. The circular marker identifies the 3.01ppm GABA resonance. (b) Extracted GABA row from same phantom (with all peaks shifted by ~0.1ppm in room temperature phantoms)

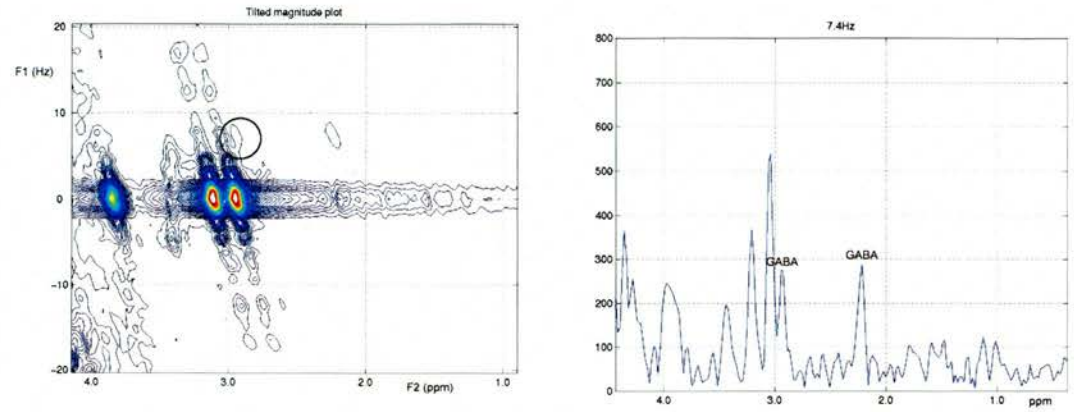

Figure 6.5 (a) 2D J-resolved spectra from 3x3x3 cm^3 VOI in a phantom containing 3mM choline, 9mM creatine and 0.8mM GABA using a 5" surface coil. The circular marker identifies the 3.01ppm GABA resonance. (b) Extracted GABA row from same phantom (with all peaks shifted by ~0.1ppm in room temperature phantoms)

Table 6.3 Peak areas (arb), as quantified in MRUI, of GABA, *in-vitro*, using two surface coils

Actual GABA conc (mM)	5" surface coil			3" surface coil			% increase in SNR (3" to 5")
	3.01ppm GABA pk	mean noise	SNR 3.01ppm GABA pk	3.01ppm GABA pk	mean noise	SNR 3.01ppm GABA pk	
1	0.39	0.04	9.0	0.78	0.04	19.5	216.7
0.8	0.26	0.03	7.8	0.58	0.04	15.8	202.8

It is reassuring that GABA concentrations as low as 0.8mM can be detected using both sizes of surface coil. Since only a single experiment was performed at each concentration in each coil arrangement, no measure of the reproducibility was obtained. However, this is addressed in the formal reproducibility study described in §7. In terms of the *in-vivo* work, these initial results are encouraging. They suggest that the entire normal physiological range of GABA concentrations can be studied using 2D J-resolved MRS, as reported by recent spectral editing studies (6,11,98,100).

6.2.3 *In-vivo* experiments

6.2.3.1 Introduction

The results from the *in-vitro* work suggest that in terms of SNR, the better coil to use would be the 3" surface coil. To estimate the improvement in sensitivity seen *in-vivo*, single voxel spectra were acquired from the same brain region, using the same acquisition parameters in both a volume head coil and 3" surface coil in four normal volunteers.

6.2.3.2 Scanning protocol

Written informed consent was obtained from all four volunteers. In each case, the volunteer was set-up in a volume head coil and a series of T_2 FSE images obtained to verify their neuro-radiological status. Using these as the localising images, a $3x3x3cm^3$ VOI was placed in the occipital cortex and a single voxel spectrum acquired (TE = 55ms, TR = 2640ms, NEX = 16). The scan series was then repeated using a 3" surface coil.

6.2.3.3 Post-processing

Following acquisition, the raw data files were transferred to a Sun Ultra Workstation and were processed as described in §5. In summary, this consisted of automatic time-domain phase correction and removal of the water peak (using HLSVD). The files were then converted into ascii format for quantification in MRUI. Due to the poor baseline in the spectra from the surface coil, it was not always possible to accurately separate the choline and creatine peaks. Therefore only the NAA peak was quantified in all spectra. MRUI prior knowledge files were created for each coil arrangement to ensure that the same peak parameters were applied in case.

6.2.3.4 Results

The results from all four volunteers following quantification of the NAA peak are provided in Table 6.4. In all cases, at least a 133% increase in SNR is observed

when using the surface coil instead of the volume head coil. Figure 6.6 shows a set of representative spectra from one of the volunteers in both coil arrangements.

Table 6.4 Peak areas (arb), as quantified in MRUI, of the NAA peak from four healthy volunteers.

Volunteer	volume head coil		3" surface coil		% increase in SNR (3" to volume)
	NAA peak (arb)	mean noise (arb)	NAA peak (arb)	mean noise (arb)	
1	1.67	0.07	3.56	0.11	135.7
2	1.62	0.13	4.85	0.24	162.2
3	1.83	0.07	3.95	0.11	137.4
4	1.74	0.13	3.74	0.18	155.2

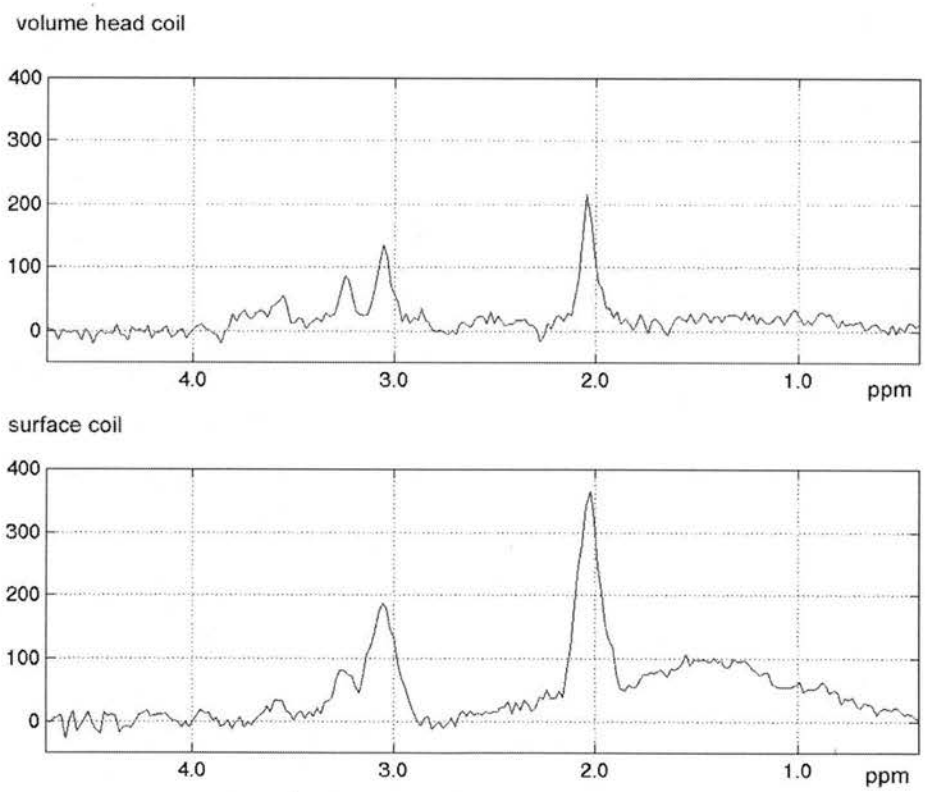

Figure 6.6 Conventional 1D spectra (TE = 58ms, TR = 2640ms, NEX = 16) from a 3x3x3cm^3 VOI located in the occipital lobe of a healthy volunteer using (a) volume head coil and (b) 3" surface coil.

6.2.4 Discussion and conclusion

It is expected that an increase in SNR of the 3.01ppm GABA peak will be measured *in-vivo*, albeit not to the same extent as that seen *in-vitro*. However, the size and location of the voxel must also be taken into consideration. Figure 6.7 shows the images acquired from the same volunteer using both the 3" and the 5" surface coils. Since the sensitive volume of the coil is determined by the coil radius (155), it is immediately obvious that the 5" allows excitation of a larger voxel, which is also important for improving the SNR. In addition, the larger excited volume allows more freedom with regard to actual voxel location, with more opportunity for the operator to fit the voxel around the unique anatomy of the patient, e.g. avoiding large blood vessels or ventricles.

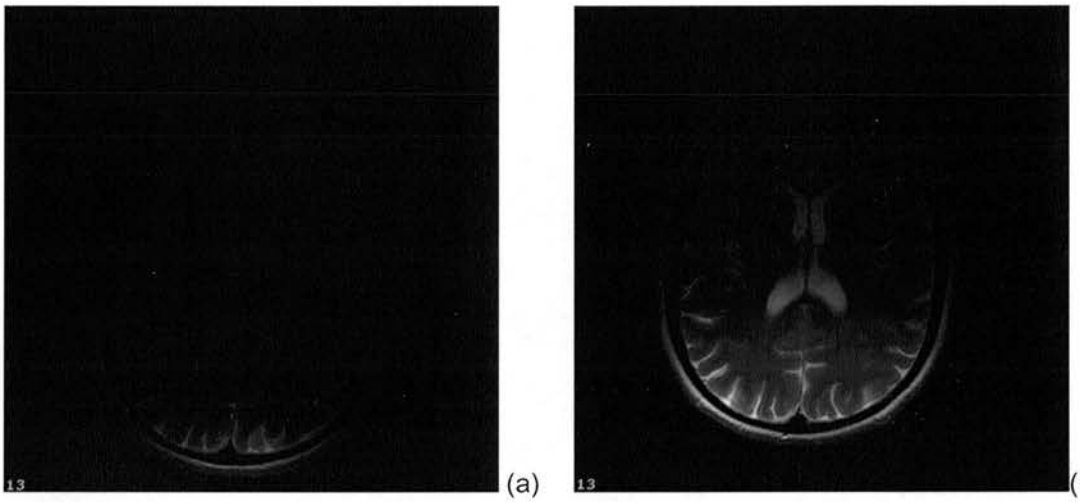

Figure 6.7 T_2 axial FSE localising images for spectroscopy using (a) a 3" surface coil and (b) a 5" general-purpose surface coil.

Overall, these results have confirmed that surface coils are more sensitive than a volume head coil for performing 2D J-resolved MRS, a characteristic that is particularly useful when attempting to quantify low-concentration metabolites such as GABA. Although the 3" surface coil shows further improvement in SNR over the 5" coil, for *in-vivo* applications, the 5" coil is more suitable as it allows the individual placement of larger voxels as dictated by the neuro-anatomy. Therefore, a 5" surface coil should be considered as standard when acquiring 2D J-resolved spectra *in-vivo*.

6.3 VOI size

6.3.1 Introduction

Performing MRS experiments in a homogenous, aqueous phantom allows a countless number of voxel sizes, limited only by the size of the outer walls of the phantom. *In-vivo*, this is clearly not the case. Not only are the voxel sizes limited by the size and shape of the brain mass, the specific dimensions of the voxel are also bound by the anatomy of the brain, and in particular, in the avoidance of ventricles, large sulci and blood vessels. In addition, it is important to position the voxel away from the scalp to avoid contamination of the spectra from scalp lipids. These problems are accentuated when acquiring spectra from patients with abnormal brain tissue, e.g. lesions arising from acute brain infarcts, as the investigator may wish to include mostly tissue from these regions or avoid them altogether. Clearly voxel set-up *in-vivo* is much more complicated than in a glass bowl full of chemicals!

Since MRS allows the acquisition of signals from low concentration metabolites, it is desirable to excite a large volume of tissue, to increase the SNR of the measurement. Given the constraints of voxel size and placement that exist *in-vivo*, especially in the abnormal brain, it is important to establish the minimum voxel size feasible for GABA measurement.

6.3.2 Methods

To investigate the effect of VOI size on the GABA signal quantified, a phantom containing 1.2mM GABA was made. 2D J-resolved spectra were acquired using a dedicated sequence (TE_{start} = 35ms, TR = 2000ms, ΔTE = 10ms, steps2d = 64) and a 5" surface coil, following the protocol given in Table 6.5. After acquisition, the extracted GABA row was quantified in MRUI as previously described in §5.

Table 6.5 Protocol for the investigation of measured GABA signal with VOI size

Experiment	1	2	3	4	5	6	7	8	9	10	11
VOI (cm^3)	27.7	24.7	22.3	19.7	17.6	15.6	13.8	12.2	10.6	9.3	8.0

6.3.3 Results

Figure 6.8 shows the results following quantification of the 3.01ppm GABA peak, with increasing voxel size. As described in §4.2.3, part of the initial post-processing involves normalisation of the signal to take into account the calibration values set in the individual MRS experiments, and this includes VOI size. Therefore, a flat horizontal line would be expected if consistent GABA measurement had been achieved.

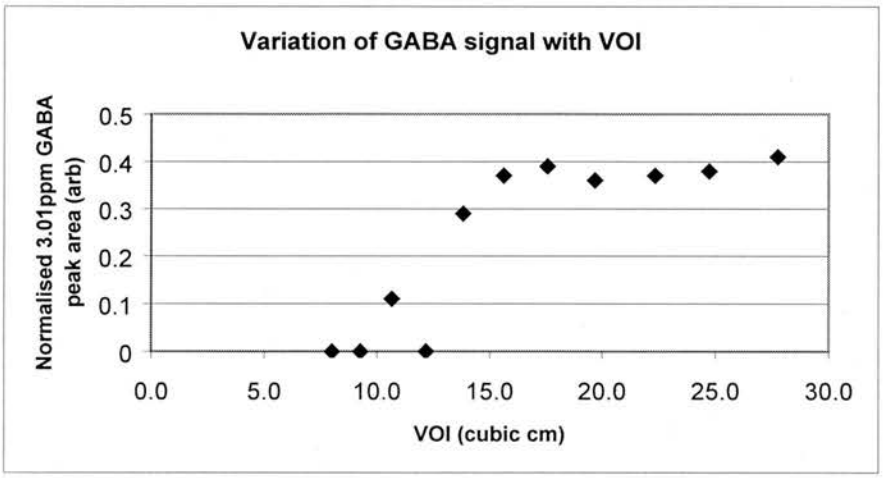

Figure 6.8 Results of *in-vitro* GABA measurement from increasing voxel sizes in a single phantom containing 1.2mM GABA. 2D J-resolved spectra were obtained using a dedicated 2D J-resolved MRS sequence in a 5" surface coil (see text for details).

6.3.4 Discussion and conclusions

These results clearly show that *in-vitro*, GABA measurement begins to breakdown in voxels below 15cm^3. Repetition of these experiments in a high concentration GABA phantom Figure 6.9, showed that this was due to the poor SNR at 1.2mM GABA, leading to failure to quantify any discernible GABA peak in MRUI or an inaccurate measurement. Either way, when translating this work *in-vivo*, at all times voxels larger than 15cm^3 should be prescribed, and unless designated by a set protocol, the user should be encouraged to make the voxel dimensions as large as possible, within the anatomical limits.

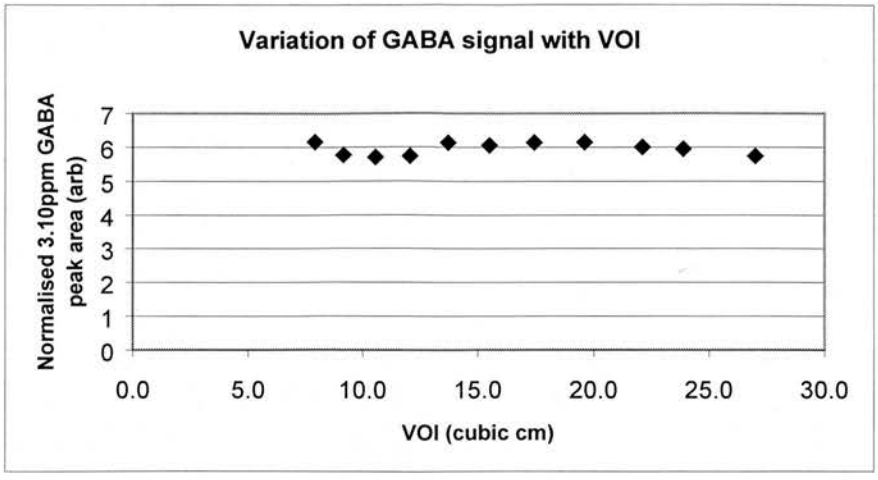

Figure 6.9 Results of *in-vitro* GABA measurement from increasing sizes in voxel in a single phantom containing 10mM GABA. 2D J-resolved spectra were obtained using the same protocol as for the phantom used described previously

6.4 Acquisition parameters

6.4.1 Introduction

At the time of writing, five variations of performing 2D J-resolved spectroscopy had been published, and these were discussed in §3. Although all were based on the same pulse sequence, there were three main differences in the timing parameters used. To determine the effect this had on the resulting spectra, a series of GAMMA simulations (135) and *in-vitro* experiments were performed using each set of timings. The *in-vitro* experiments were performed on a 10mM GABA phantom, in the same scanning session with prescription of the same voxel. Thus, in the absence of any significant scanner fluctuations, any changes in the results following quantification of the GABA peaks were due to the changes in applied timings.

6.4.2 Materials and methods

As described in §4, results from GAMMA simulations of GABA at 1.5T have been previously reported. It was possible, therefore, to adapt the modelling parameters of the 2D J-resolved sequence to replicate the timing parameters used in literature, to predict what effects these would have on real data. Since the GAMMA modelling ignored the effects of relaxation, only three of the five variations were simulated as

used in (23,25-27). The remaining two differed only in the TE_{start} used (22,24), and any differences would not been shown without taking into account GABA relaxation characteristics.

Three different acquisition models were tested, the details of which are given in Table 6.6. The experiments were then repeated *in-vitro* using a 3.6l, glass spherical phantom containing 10mM GABA. The phantom was positioned on a specially designed headrest that was placed directly on a 5" surface coil. Using a localiser image, a $3x3x3cm^3$ voxel was positioned in the region of high signal intensity in the lower half of the phantom. The set-up was the same in all experiments. A modified set of these experiments, designed to more clearly show the differences resulting from changes in TE, were conducted on a phantom containing 1.2mM GABA, Table 6.7.

To aid quantification of the resulting spectra, a prior knowledge file was created in MRUI. Each of the three GABA peaks were quantified (3.01ppm, 2.28ppm and 1.89ppm), although since only the 3.01ppm peak will be visible *in-vivo*, particular attention was paid to the effects of the timing variables at this resonance.

Table 6.6 Timing parameters used in all of the published methods of 2D J-resolved MRS

Timing method	TE_{min} (ms)	TR (ms)	ΔTE (ms)	steps2d	Reference	GAMMA simulated?
1	35	2000	10	64	(25,26)	Yes
2	35	2000	5	64	(23)	Yes
3	35	2000	2.5	128	(23,27)	Yes
4	25	2200	10	64	(22)	No
5	48	2640	10	64	(24)	No

Table 6.7 Second set of timing experiments performed on a phantom containing 1.2mM GABA only

Timing method	TE_{start} (ms)	TR (ms)	ΔTE (ms)	steps2d	NEX
1	35	2000	10	64	16
2	35	2000	5	64	16
3	35	2000	2.5	128	16
4	35	2000	5	128	16

This work was then extended to investigate the practical implications of changing the NEX, Table 6.8, and TR (to min TR for longest TE), Table 6.9.

Table 6.8 Protocol for the investigation of NEX on GABA measurement using 2D J-resolved MRS

TE_{min} (ms)	TR (ms)	ΔTE (ms)	steps2d	NEX	t_scan (min:sec)
35	2000	10	64	8	17:20
35	2000	5	64	8	17:20
35	2000	2.5	128	8	34:24
35	2000	10	64	16	34.:40
35	2000	5	64	16	34:40
35	2000	2.5	128	16	68:48

Table 6.9 Protocol for investigation of TR_{min} on GABA measurement using 2D J resolved MRS

TE_{min} (ms)	TR (ms)	ΔTE (ms)	steps2d	NEX	t_scan (min:sec)
35	1800	10	64	8	15:36
35	1800	5	64	8	15:36
35	2000	10	64	8	17:20
35	2000	5	64	8	17:20
35	2200	10	64	8	19:04
35	2200	5	64	8	19:04
35	2500	10	64	8	21:40
35	2500	5	64	8	21:40

6.4.3 Results

The 2D J-resolved spectra and corresponding extracted GABA rows resulting from the GAMMA simulations of the published timings are shown in Figure 6.10. Table 6.10 lists the results post-quantification of the simulated GABA peaks. Figure 6.11 gives a representative 2D J-resolved plot, and associated GABA row, from the series of *in-vitro* experiments using the same published timings as the simulations. The extracted spectra from all five 2D J-resolved plots are overlaid in Figure 6.12 and the results from quantification in Table 6.11.

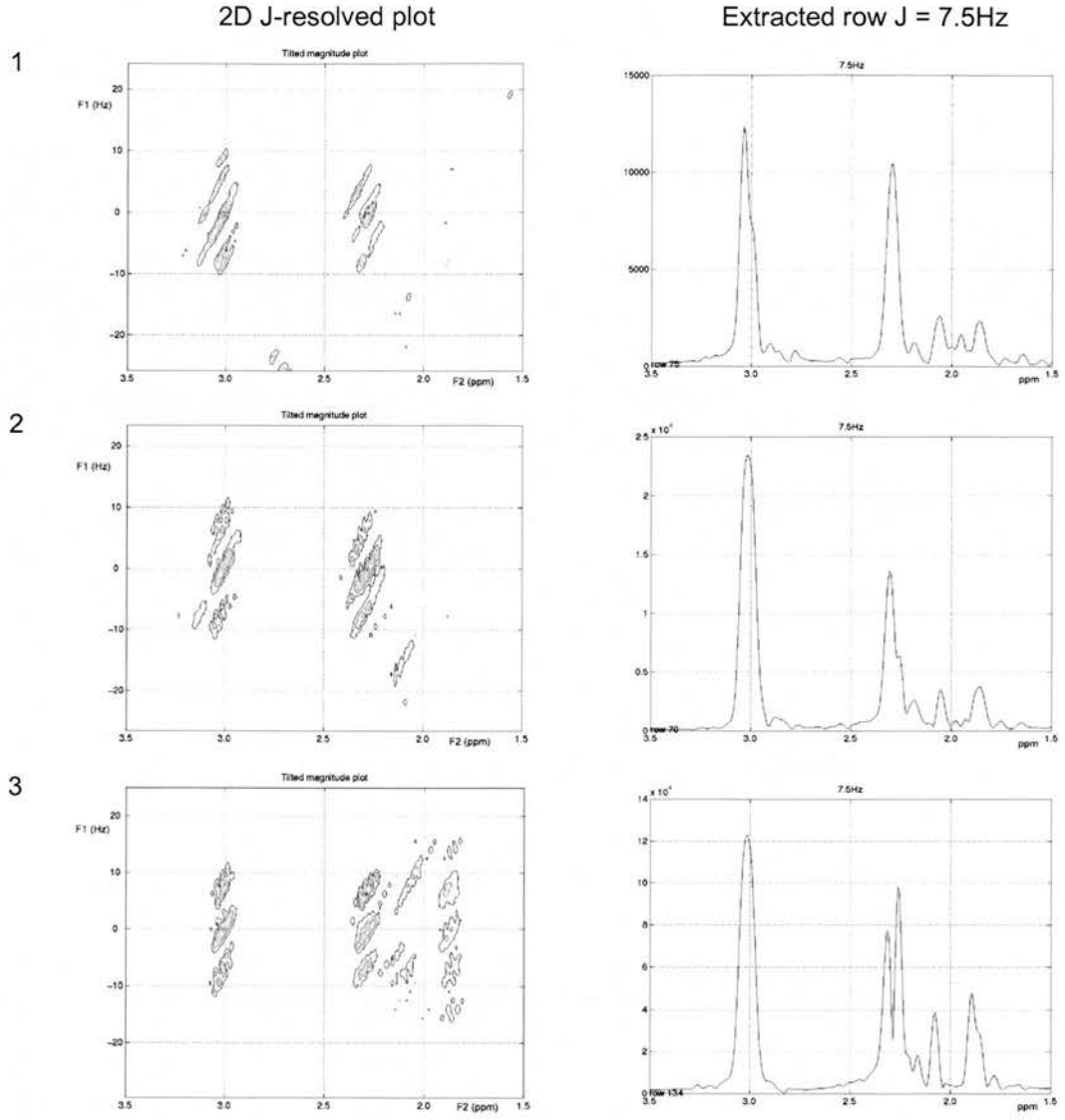

Figure 6.10 Results from GABA simulations of literature timings for 2D J-resolved experiments. The numbers in the left-hand column correspond to the timing numbers in Table 6.6. All 2D spectra have been scaled to the 2.28ppm GABA peak. To obtain results more akin to those obtained from practice, F1 and F2 apodization (Lorentzian and Gaussian respectively) = 2.6Hz was used in each dimension.

Table 6.10 Peak areas (arb), as quantified in MRUI, of the simulated 3.01ppm and 2.28ppm GABA peaks, from the extracted J = 7.45Hz row, in the timing variations listed in Table 6.6

Timings	TE_{start} (ms)	ΔTE (ms)	steps2d	GABA	
				3.01ppm	2.28ppm
1	35	10	64	5.65	4.19
2	35	5	64	6.23	4.59
3	35	2.5	128	6.61	4.88

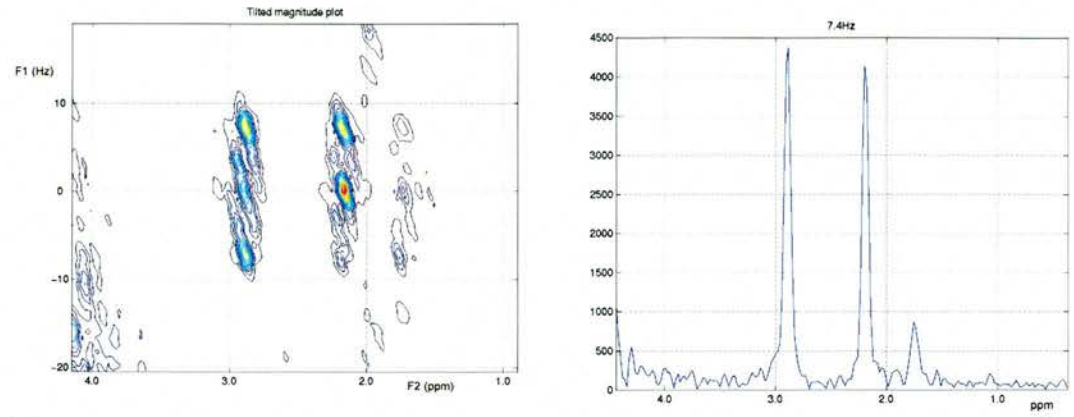

(a) (b)

Figure 6.11 Representative results from phantom containing 10mM GABA only; Timing parameters 1: TE_{min} = 35ms, TR = 2000ms; ΔTE = 10ms; steps2d = 64; NEX = 16. (a) 2D J-resolved plot and (b) the extracted 1D spectrum at the GABA J-coupling frequency (J = 7.45Hz) (with all peaks shifted by ~0.1ppm in room temperature phantoms).

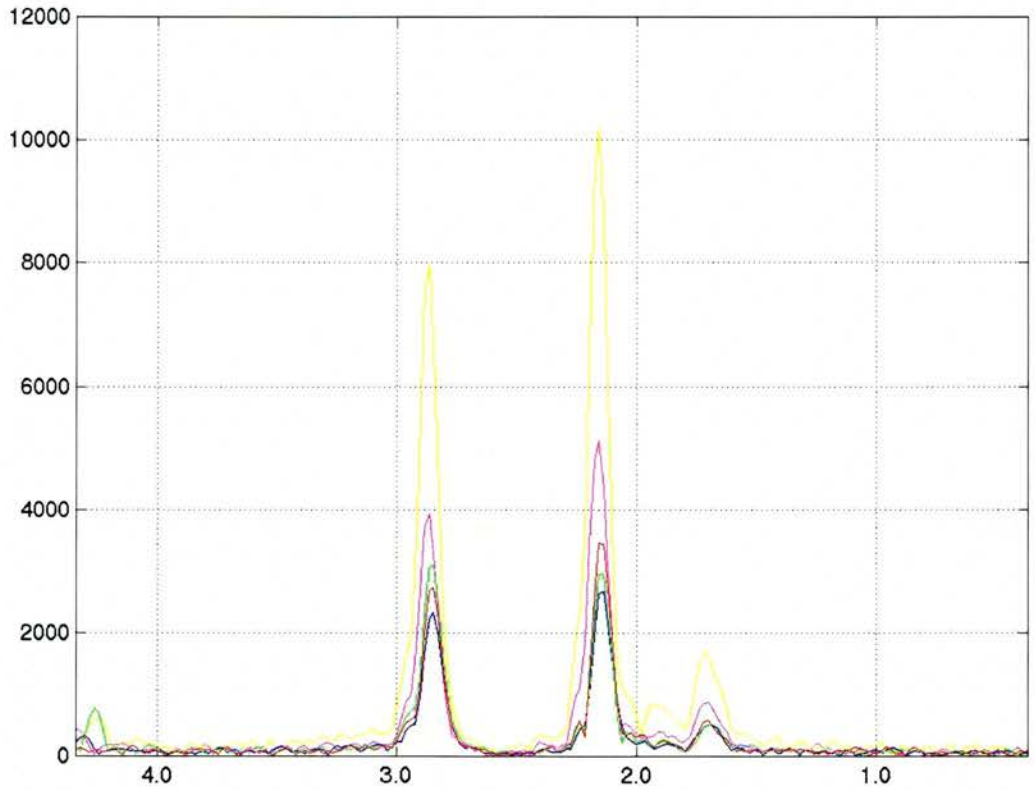

Figure 6.12 Extracted spectra at 7.4Hz for all timing experiments: Timing 1; timing 2; timing 3; timing 4; timing 5. Phantom = 10mM GABA only (with all peaks shifted by ~0.1ppm in room temperature phantoms).

Table 6.11 Results from quantification of the 3.01ppm GABA peak, from the extracted J = 7.45Hz row, for the timing variations listed in Table 6.6.

Timing set	SNR 3.01ppm GABA peak
1	144.0
2	105.3
3	159.9
4	164.4
5	145.2

The extracted spectra corresponding to J = 7.45Hz from the 1.2mM GABA phantom are overlaid in Figure 6.13, and Table 6.12 summarises the results following quantification of the 3.01ppm GABA peak.

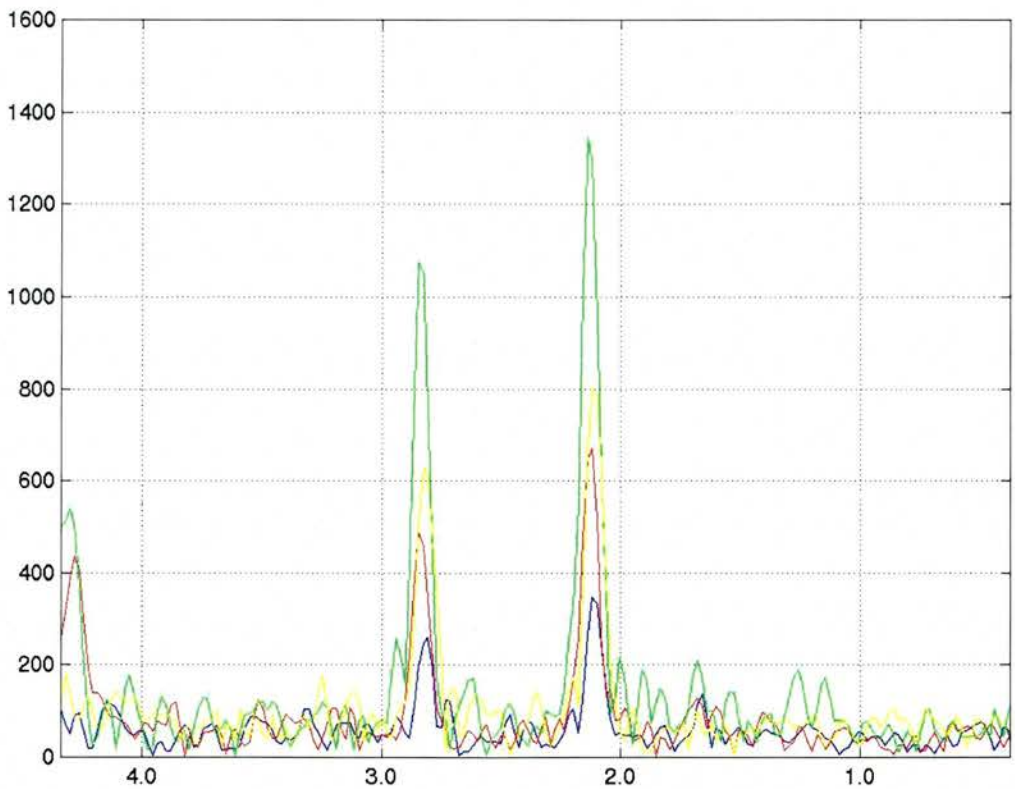

Figure 6.13 Extracted spectra at 7.4Hz for timing experiments on phantom containing 1.2mM GABA only: timing1, timing2, timing3, timing4 (with all peaks shifted by ~0.1ppm in room temperature phantoms)

Table 6.12 Results from quantification of the 3.01ppm GABA peak, from the extracted J = 7.45Hz row, in the timing variations listed in Table 6.7

Timing set	SNR 3.01ppm GABA peak
1	19.5
2	20.3
3	28.2
4	22.3

The results following variation of the NEX and TR are shown in Table 6.13 and Table 6.14 respectively.

Table 6.13 Peak areas (arb), as quantified in MRUI, of the 3.01ppm GABA peak, extracted from the J = 7.45Hz row, after reduction of the NEX. All other experimental parameters remained constant.

TE_{start} (ms)	ΔTE (ms)	steps2d	TR (ms)	SNR 3.01ppm GABA peak	
				NEX = 16	NEX = 8
35	10	64	2000	19.5	10.3
35	2	64	2000	20.3	12.5
35	2.5	128	2000	28.2	11.9

Table 6.14 Peak areas (arb), as quantified in MRUI, of the 3.01ppm GABA peak, extracted from J = 7.45Hz row, with increasing TR. All other experimental parameters remained constant.

TR (ms)	3.01ppm GABA peak (arb)	
	ΔTE = 10ms	ΔTE = 5ms
1800	0.74	1.03
2000	0.77	1.08
2200	0.76	1.06
2500	0.79	1.10

6.4.4 Discussion and conclusions

At first sight of the results from the simulations, it would appear as though the method using 128 steps of 2.5ms (timings 3) yields the higher GABA peak in the extracted spectrum, Figure 6.12. However, this is deceiving as there is a corresponding increase in the noise, resulting in only a ~ 17% increase in the SNR,

Table 6.10. Similar results were obtained in the *in-vitro* work Figure 6.12, although the SNR increase between timing set one and three are less (~10%), Table 6.11.

Although any SNR increase is desirable for translation of this work *in-vivo*, it is also important to consider the loss of F1 resolution using these acquisition parameters, which may prevent the measurement of metabolites at different J-coupling frequencies. In view of this limitation, the small decrease in SNR associated with acquiring 64 steps at 10ms intervals as seen in the phantom experiments, is an acceptable compromise to maintain the F1 resolution necessary to adequately differentiate between J-coupling frequencies, and therefore resolve multiple metabolites using this technique.

In spectroscopy experiments, the value of the number of excitations, "NEX", determines the phase cycling used, to exploit the advantages of signal averaging every time an RF pulse is applied. A NEX = 8 means that phase cycling (in a cycle of 2) is performed on all three RF pulses. In practice, this means that for each pulse, the phase is altered so that the frame consists of 8 excitations. By using NEX = 16, the phase cycling scheme applied when NEX = 8 is repeated for a second time.

As expected, the results from NEX = 8 all show large reductions in the 3.01ppm GABA peak compared to NEX = 16, Table 6.13. This would contraindicate changing the NEX for the 2D J-resolved experiment. 2D COSY *in-vivo* results from Thomas *et al* also suggest that GABA measurement is more reliable when using NEX = 16 compared to NEX = 8 (21), although in more recent work, GABA peak assignments have been made using an NEX = 8 (20). Since some uncertainty exists as to the effectiveness of GABA measurements at 1.5T with a reduced NEX (albeit using COSY), it would seem prudent to perform all 2D J-resolved experiments with an NEX = 16, at least until there is sufficient evidence to suggest otherwise.

As with decreasing the NEX, a reduction in the scanning time associated with a decrease in TR would only be truly beneficial in the absence of any detrimental effects on the resulting spectra. Again, this is not the case, Table 6.14. Over the

range of TRs investigated, a change in GABA signal of ~ 6% is seen for both acquisition sets. This suggests that particularly for the last three experiments, full recovery of the longitudinal relaxation had been achieved, giving maximum SNR. Therefore, in the absence of any significant gain in signal by using the longest TR, a TR of 2000ms is an appropriate compromise between the GABA SNR and scan time.

In conclusion, the results presented thus far would suggest use of the acquisition parameters given in Table 6.15 for optimum GABA measurement using 2D J-resolved MRS at 1.5T.

Table 6.15 Protocol for optimum *in-vitro* GABA measurement

Coil	5" GP surface coil
VOI	Not less than $15cm^3$
TE_{start}	35ms
Δ TE	10ms
steps2d	64
TR	2000ms
NEX	16
t_{scan}	34:24 minutes

6.4.5 Elimination of macromolecule contributions

6.4.5.1 Introduction

During the comparison of MRS techniques for GABA measurement in §3, the problem of contamination of the 3.01ppm GABA peak was highlighted. This is due to contributions from macromolecules, and the peptides homocarnosine and glutathione (GSH) (19).

"Macromolecule" is a general term covering the high molecular weight proteins and nucleic acids that exist across the entire MR spectrum, including a distinct resonance at 3.00ppm (40). Since macromolecules have shorter T_2 relaxation times than the lower molecular weight cerebral metabolites, they can be eliminated from MR

spectra by using long TEs. At short TEs, the presence of macromolecules will complicate quantification and identification of the over-lying metabolites (43).

Measurements of the coupling constants of GSH specify that the 2.93ppm and 2.98ppm resonances have J-coupling frequencies distant to that from GABA (at 4.71Hz and 14.06Hz) so can easily be separated from GABA using 2D J-resolved MRS (40). However, similar measurements of the prominent macromolecule resonances indicate that the 3.00ppm resonance has a J-coupling frequency of 7.8Hz, very close to that of GABA at 7.4Hz (40). High-resolution 2D J-resolved spectra also show distinct macromolecule resonances exactly where GABA would appear *in-vivo* (40). This suggests that the inclusion of short TEs in the 2D J-resolved acquisition protocol prevents the designation of the observed resonance at F1 = 7.5Hz, F2 = 3.01ppm solely to GABA. Therefore the minimum TE for the 2D J-resolved experiment should be a compromise between the absence of macromolecules and loss of metabolite signal. This approach was first applied in 2D J-resolved MRS by Lymer *et al* in 2003 (156).

6.4.5.2 Scanning protocol for 1D *in-vivo* MRS of macromolecules

Five healthy volunteers were recruited for this study and from each, written informed consent was obtained. MRI was performed on a 1.5T GE Signa Horizon Scanner, using a standard volume head coil to acquire a series of axial T_2 image to confirm the neuro-radiological status of the volunteers.

MRS was performed using a 3" surface coil for localisation. In each volunteer a $3x3x3cm^3$ VOI was placed in the occipital cortex, using a 3-plane localiser for positioning.

To obtain a spectrum containing only resonances from macromolecules, an inversion recovery (IR) sequence was employed. This uses a 180° pulse to invert the longitudinal magnetisation after which their recovery is determined by the T_1 of the individual tissues. Macromolecules have a shorter T_1 than the cerebral metabolites, so its recovery is faster. Careful choice of the time delay between the inversion pulse

and preceeding 90° pulse allows excitation of the macromolecule signal once it has almost recovered and nulling of the signal from the metabolites (40,41,44,87). This time delay between the two pulses is known as the inversion time (TI).

To determine an optimum TI for full inversion of the metabolite signal whilst maintaining the macromolecule contribution, preliminary experiments were conducted on both the standard GE spectroscopy phantom (metabolite only) (see Table 5.1 for listing of phantom contents) and a volunteer. From this work, a TI of 675ms was chosen.

Each subject underwent a series of 1D MRS experiments, with the TE ranging from 35ms – 85ms (TR = 2640ms, NEX = 16). IR spectra were also acquired contiguously at every TE to obtain metabolite-nulled spectra.

6.4.5.3 Post-processing

The raw data files were transferred to a Sun Ultra Workstation for processing using a combination of in-house and commercially available software. In-house software was used to automatically phase correct and remove the residual water peak using HLSVD, §5. The metabolite-nulled spectra were quantified in both MRUI and SAGE (GE Medical Systems).

6.4.5.4 Results

A summary of all the results from all five volunteers is given in Figure 6.16. Figure 6.14 provides representative IR spectra from one of the volunteers and the corresponding metabolite plus macromolecule spectra are shown in Figure 6.15.

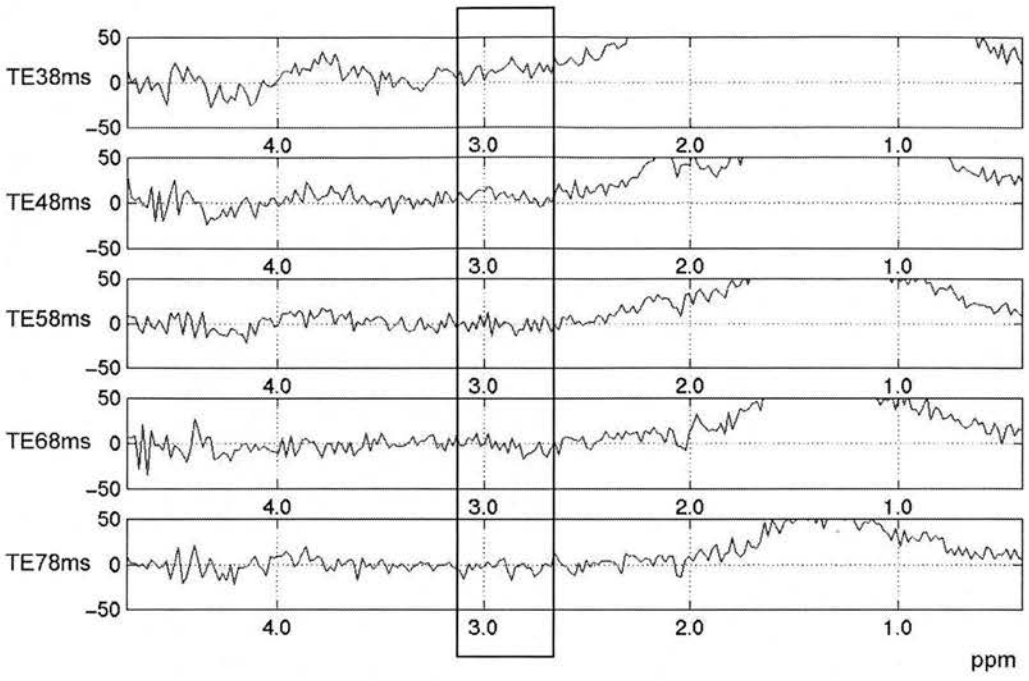

Figure 6.14 Metabolite-nulled data from one of the volunteers for the first five IR experiments.

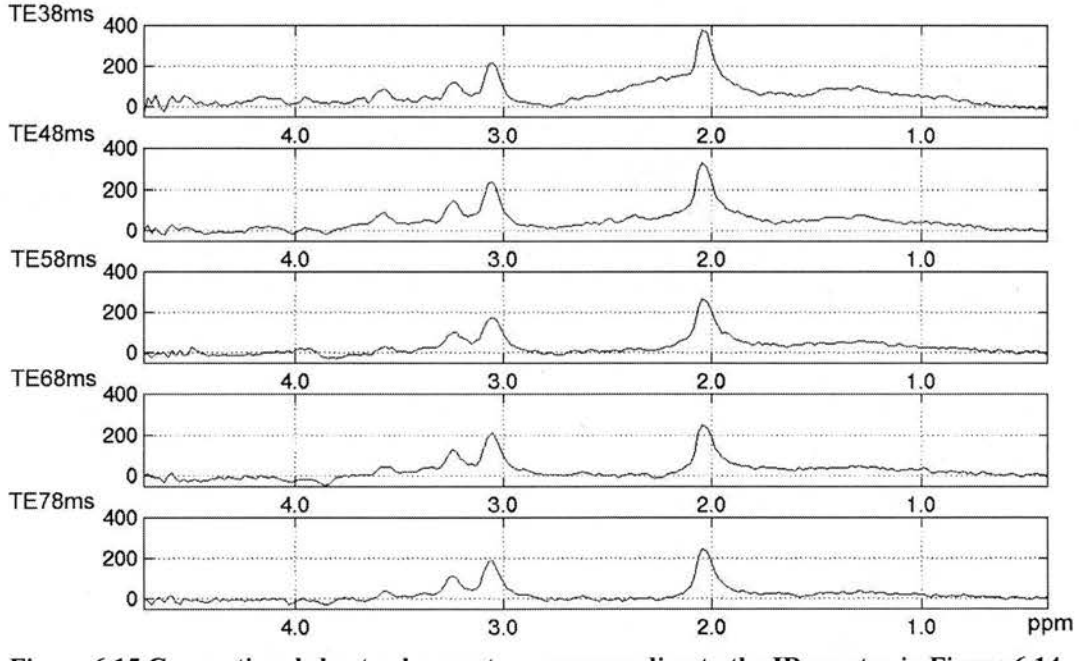

Figure 6.15 Conventional short-echo spectra corresponding to the IR spectra in Figure 6.14.

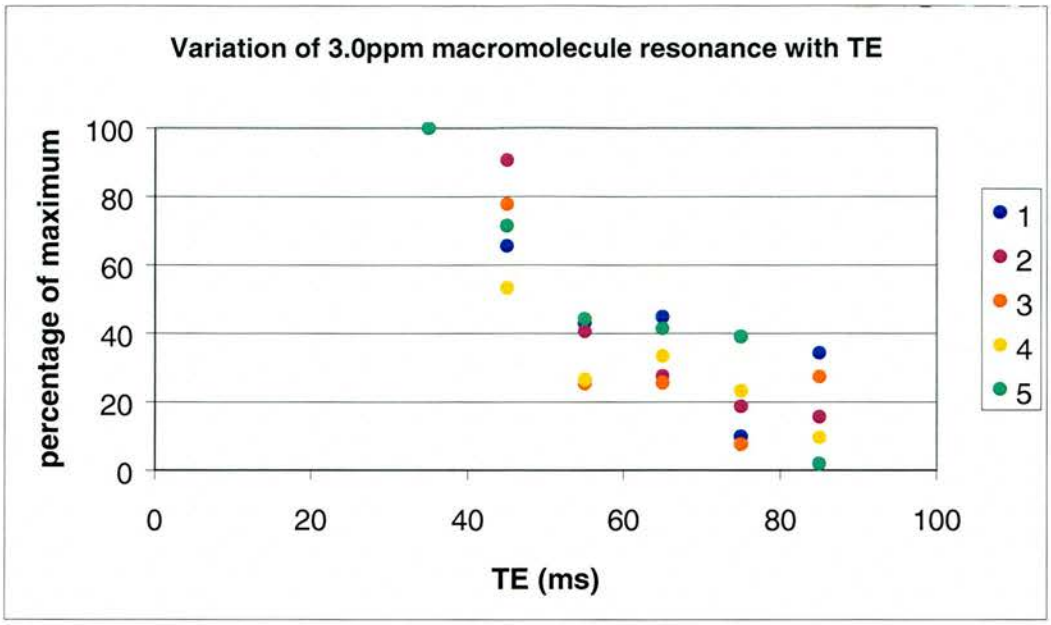

Figure 6.16 Summary of quantification of the 3.0ppm macromolecule peak, in all five volunteers. Results are given as a percentage of the maximum macromolecule signal at TE = 38ms.

The *in-vivo* results show a large reduction in the macromolecule signal at around 55ms. It was important therefore, to establish whether or not a delay of 20ms on the onset of the 2D J-resolved experiment would have a sufficiently negative impact to prevent GABA detection. To test this, a series of *in-vitro* experiments was performed encompassing the entire TE range of interest: That is from 35ms to 685ms, Figure 6.17 and Figure 6.18.

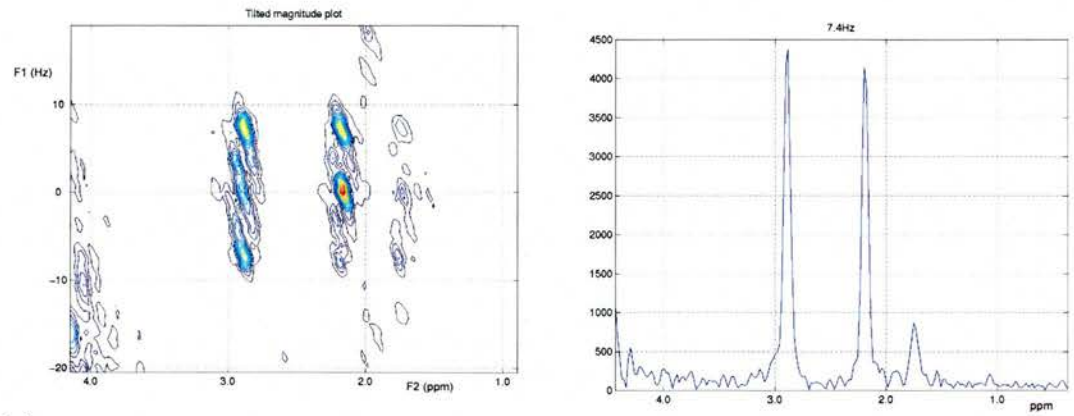

(a)

(b)

Figure 6.17 Results from *in-vitro* 2D J-resolved experiment with 10mM GABA (64TEs, TE_{min} = 35ms and ΔTE = 10ms): (a) 2D J-resolved spectrum and (b) extracted GABA row (with all peaks shifted by ~0.1ppm in room temperature phantoms).

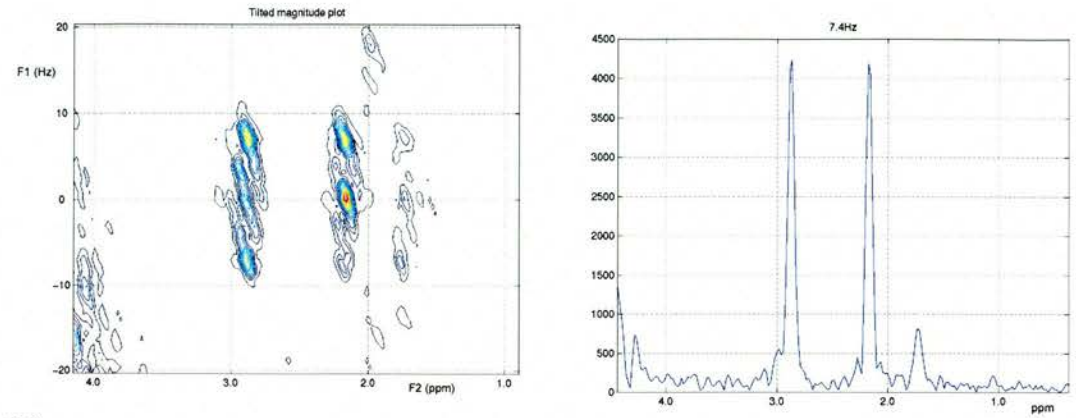

(a) (b)

Figure 6.18 Results from *in-vitro* 2D J-resolved experiment with 10mM GABA (64TEs, TE_{min} = 55ms and Δ TE = 10ms): (a) 2D J-resolved spectrum and (b) extracted GABA row (with all peaks shifted by ~0.1ppm in room temperature phantoms).

Table 6.16 Summary of results following quantification of the 3.01ppm GABA peak area in MRUI using different acquisition protocols.

peak (arb)	TE_{start}	
	35ms	55ms
3.01ppm GABA	5.59	5.56

6.4.5.5 Discussion and conclusions

The general trend was as expected with a decrease in macromolecule resonance with increasing TE, Figure 6.16. A distinct reduction in the macromolecule presence was observed at TE = 55ms, with results from all volunteers falling to below 45% of the maximum (recorded at TE = 35ms). After this TE, the same general trend was observed, although quantification was more difficult as the macromolecule resonance approached the level of noise. The results demonstrate that by starting acquisition after TE = 55ms, the contribution of macromolecules to the GABA resonance will be reduced.

A 20ms delay in the start of acquisition of data for the *in-vitro* 2D J-resolved experiment (TE_{start} = 55ms not 35ms) makes only a very small difference to the 3.01ppm GABA peak area in the extracted spectrum (<1%). However, with only 1:04 minutes difference in the actual acquisition time between collecting 64 TEs (35ms – 665ms) and 66 TEs (55ms – 685ms), it would be interesting to acquire *in-*

vivo data over both ranges to compare any differences in the 2D results. Consequently, the optimised protocol for *in-vivo* GABA measurement is given in Table 6.17.

Table 6.17 Protocol for *in-vivo* GABA measurement

Coil	5" surface coil
VOI	Not less than $15cm^3$
TE_{start}	35ms
Δ TE	10ms
TR	2000ms
steps2d	66
NEX	16
t_{scan}	35:28 minutes

6.5 Optimised protocol test

6.5.1 Introduction

In the preceding sections in this chapter, a number of experiments have been performed to determine the optimum protocol for GABA measurement, *in-vivo*, using 2D J-resolved MRS at 1.5T. Before applying this procedure to a volunteer, it was prudent to test the protocol on a phantom containing physiological concentrations of *all* the common cerebral metabolites, corrected to physiological pH. Although relaxation effects were unaccounted for, the results from this experiment allowed the complete acquisition and post-processing method to be validated *in-vitro*, offering the best possible results before *in-vivo* translation.

6.5.2 Methods

2D J-resolved MRS was performed on a 1.5T GE Signa Horizon scanner, operating in research mode and using a 5" surface coil. The acquisition parameters were as listed in Table 6.17.

An aqueous solution containing the cerebral metabolites listed in Table 6.18 were placed into a 3.6l, glass spherical phantom. The pH of the solution was adjusted to pH 7 using a mixture of sodium hydroxide and hydrochloric acid. After allowing the temperature of the solution to stabilise at the magnet room temperature, the phantom was set-up on a specially designed headrest that was placed directly on a 5" surface coil. This was positioned in the magnet and left to settle for approximately 20 minutes to reduce artefacts arising from solution movement. Using the localiser image, a 3x3x3cm^3 voxel was prescribed in the lower half of the phantom, in the region of high signal intensity, from which a 2D J-resolved spectrum was acquired.

Table 6.18 Concentrations of metabolites used to make the physiological phantom

Metabolite	Concentration (mM)
choline	2.5
creatine	9
GABA	1.5
acetate (in lieu of NAA)	12.5
glutamine	5.8
glutamate	12.5
myo-inositol	8.1
lactate	0.4

Acquisition of spin-echoes across the range TE = 35ms - 685ms, allowed two 2D J-resolved spectra to be processed. The first, from TE = 35ms (steps2d = 64) and the second, as if avoiding macromolecule contribution with a TE_{start} = 55ms (steps2d = 64).

Note on phantom preparation.

Previous to this experiment, all *in-vitro* experiments thus far had consisted of simple hand-made phantom solutions or the commercially available GE spectroscopy phantom. With the spectral peaks appearing at the expected chemical shifts (given an approximate 0.1ppm shift due to room temperature phantoms not body temperature brains) in all spectra, it had not been deemed necessary to routinely perform additional adjustments to the solutions (e.g. temperature, pH). However, the

situation was hugely complicated with the introduction of glutamate to the stock metabolite solutions.

Initial experiments revealed that on addition of glutamate to a mixed metabolite solution, the 3.01ppm GABA peak "disappeared", even with GABA at concentrations several orders of magnitude higher than physiological levels that had previously been detected. Simulations of the two chemicals demonstrated that there should be no overlap of the 3.01ppm GABA peak from glutamate in the extracted spectrum, Figure 6.19.

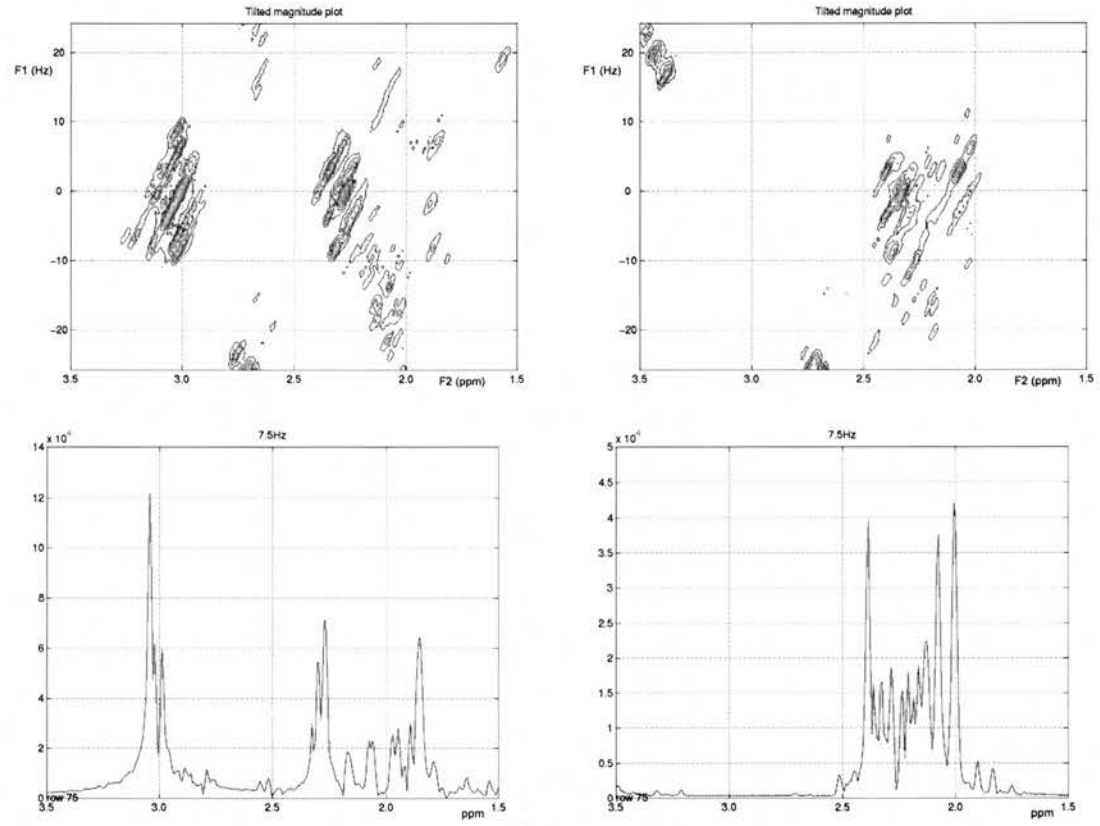

(a) (b)

Figure 6.19 Results from spin-system simulations of (a) GABA and (b) glutamate. The extracted spectra show a distinct separation between the 3.01ppm GABA resonance and glutamate at J = 7.5Hz.

The solution to this problem was found from helpful discussions with Professor Peter Sadler and Dr. Vivienne Munk, School of Chemistry, The University of Edinburgh, and the results from NMR performed on a Bruker 800 MHz spectrometer (~18.8T),

performed by Dr. Munk. The author is indebted to them both for their valuable contributions to this work.

The high-resolution spectra from aqueous solutions of GABA, glutamate and then GABA and glutamate combined are shown in Figure 6.20. The spectra have been expanded across the 1.9ppm to 3.9ppm range to focus in on the chemical shifts of interest when using a clinical MRI scanner.

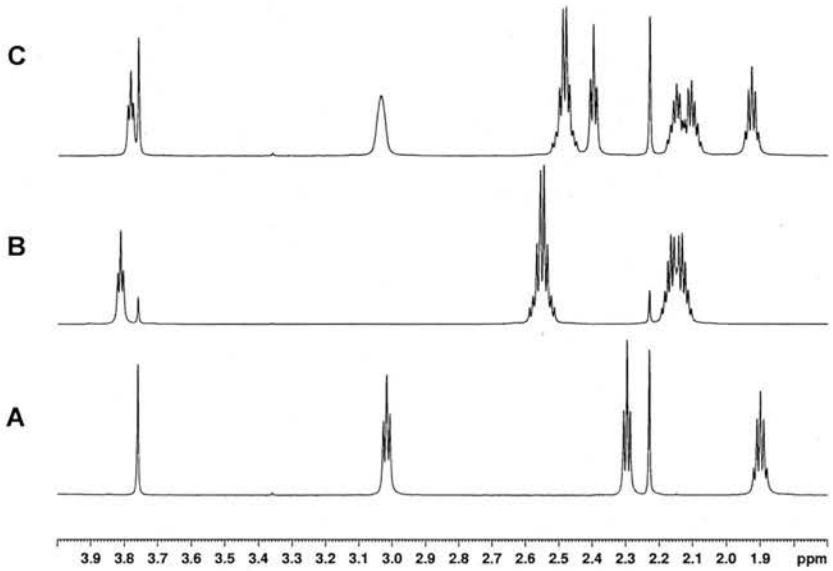

Figure 6.20 High-resolution spectra (800Mz) of (A) 1.5mM GABA, (B) 12.5mM glutamate and (C) a mixture of both metabolites. Dioxane was added as an internal standard (3.76ppm). All experiments performed by Dr. V. Munk, School of Chemistry.

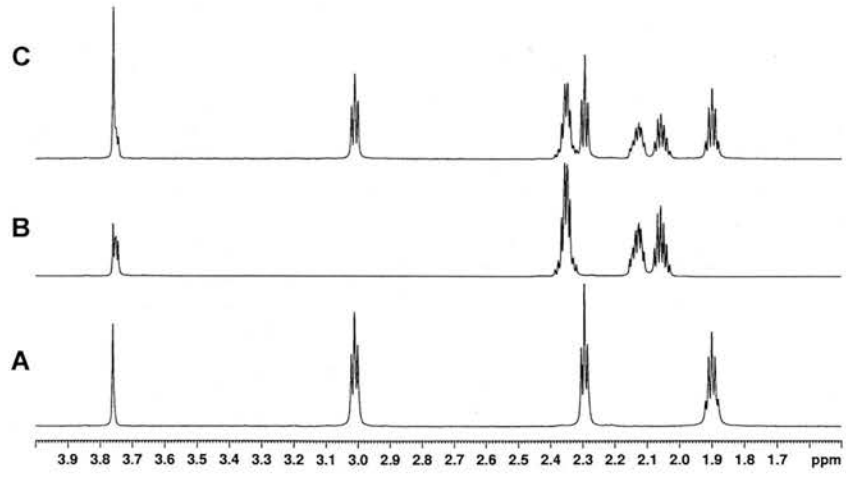

Figure 6.21 High-resolution spectra (800mHz) of (A) 1.5mM GABA, (B) 12.5mM glutamate and (C) a mixture of both metabolites *after* pH correction. Dioxane was added as an internal standard (3.76ppm). All experiments performed by Dr. V. Munk, School of Chemistry.

Without regulation of the pH, the chemical shifts of some of the peaks (including the 3.01ppm GABA peak) changed when the two metabolites were mixed. Specific to the GABA peak of interest, the distinct triplet significantly broadened when in mixture with glutamate. The results after pH adjustment to pH 7.4 are shown in Figure 6.21. With no differences in the chemical shifts in the spectrum from the chemical mixture, these results clearly show the importance of pH correction.

6.5.3 Results

The 2D J-resolved spectra and corresponding extracted GABA rows from both TE ranges are shown in Figure 6.22. Table 6.19 summarises the results post-quantification.

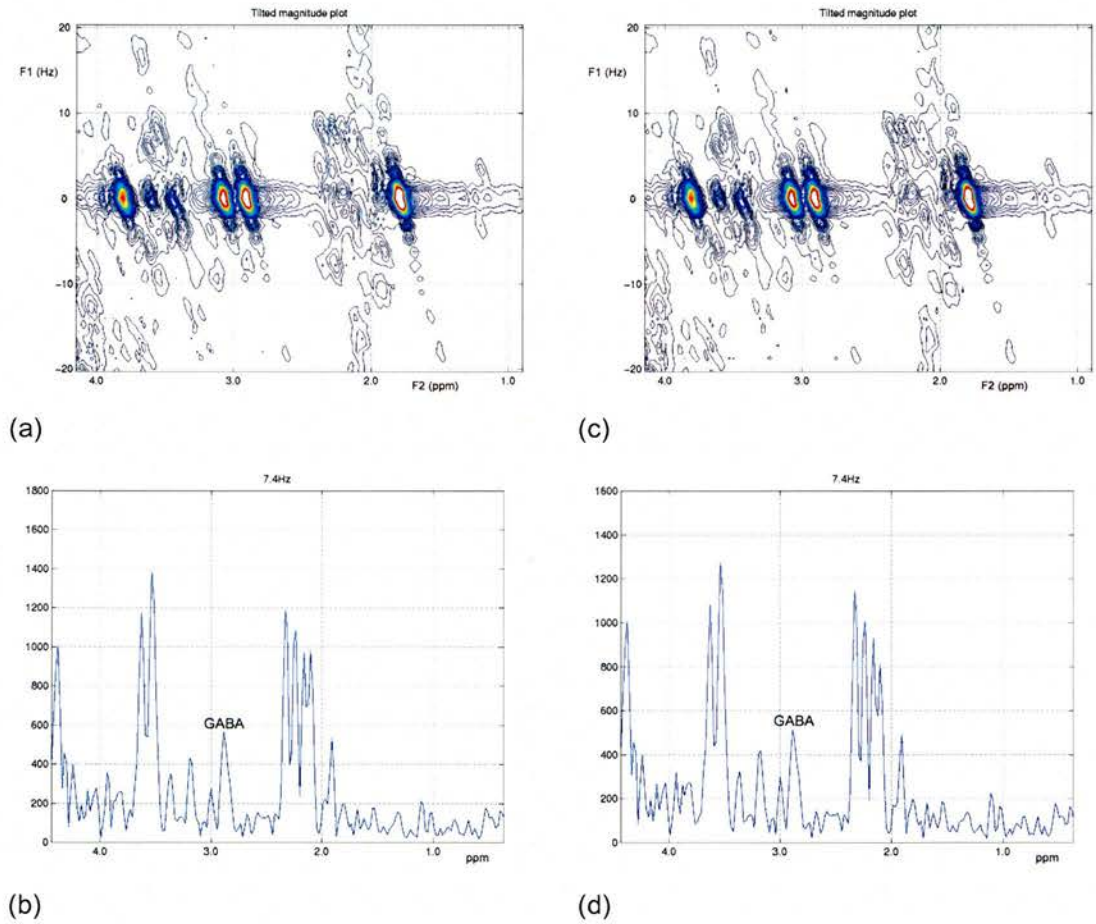

Figure 6.22 (a) 2D J-resolved plot and (b) extracted GABA row from analysis of data with TE_{start} = 35ms. (c) 2D J-resolved plot and (d) extracted GABA row from analysis of data with TE_{start} = 55ms. All results from a 3x3x3cm^3 VOI in a physiological phantom containing the metabolites listed in Table 6.18 (with all peaks shifted by ~0.1ppm in room temperature phantoms).

Table 6.19 Quantification of 3.01ppm GABA peak area (in MRUI) in both datasets

TE_{start} (ms)	ΔTE (ms)	steps2d	TR (ms)	NEX	3.01ppm GABA peak (arb)
35	10	64	2000	16	0.80
55	10	64	2000	16	0.73

An alternative to collecting 64 spin-echoes was proposed in §4.5, whereby only 40 spin-echoes were acquired and then the dataset zero-filled to 64 to achieve the same F1 resolution. This approach was applied to the physiological phantom and the results are presented in Figure 6.23 and Table 6.20.

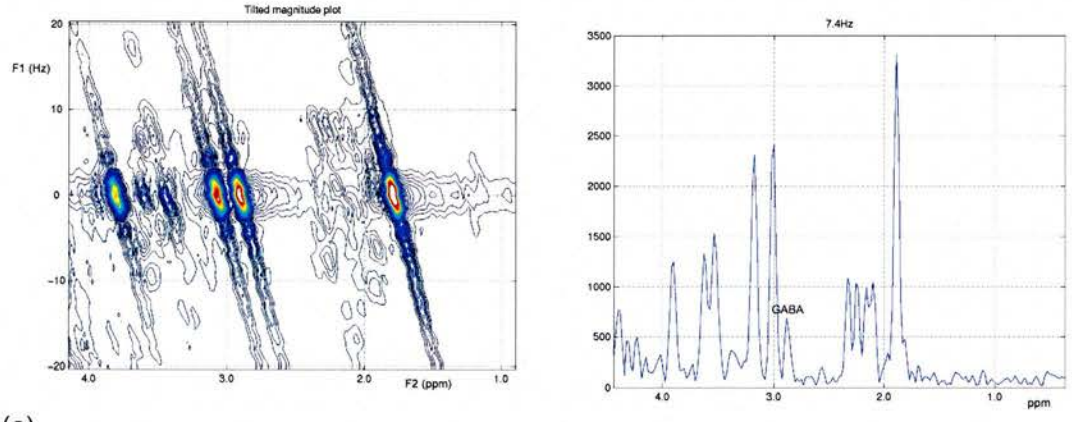

(a) (b)

Figure 6.23 (a) 2D J-resolved plot and (b) extracted GABA row from same physiological phantom. Only the first 40 spin-echoes were included in the analysis, with the remainder of the dataset zero-filled to maintain the F1 resolution achieved with 64 spin-echoes (with all peaks shifted by ~0.1ppm in room temperature phantoms).

Table 6.20 Quantification of 3.01ppm GABA peak area (in MRUI) when post-processing only the first 40 spin-echoes

TE_{start} (ms)	ΔTE (ms)	steps2d	TR (ms)	NEX	3.01ppm GABA peak (arb)
35	10	40	2000	16	0.56

6.5.4 Discussion and conclusions

The results from the physiological phantom demonstrate that GABA measurements can be made from 2D J-resolved spectra acquired at 1.5T. Using an optimised

protocol based on a dedicated 2D J-resolved sequence, the total number of spin-echoes required for post-processing can be obtained in 35:28 minutes.

As expected, there is a small decrease in the peak area of the 3.01ppm GABA peak acquired with a TE_{start} = 55ms (< 10%). With only an extra one minute to acquire the additional two spin-echoes required for dual analysis, it would be extremely useful to collect the full range of spin-echoes to allow comparison between 2D J-resolved spectra both with and without macromolecule contributions.

A reduction in the number of spin-echoes and zero-filling the remaining dataset was proposed as a technique for reducing the acquisition time while maintaining the F1 resolution required to measure GABA, §4. Application of this approach on the physiological phantom shows considerable F1 bleed from the three main metabolite peaks of choline, creatine and acetate (~ NAA *in-vivo*). With such spread of the resonances, there is a real danger than the 3.01ppm GABA resonance would be obscured. Although not the case in this example, the measured GABA peak did show a 30% reduction compared to the equivalent peak from a full 64 spin-echo acquisition, and the broader linewidths obtained *in-vivo* are likely to further complicate the issue. Consequently, acquisition of the full 64 spin-echoes (or 66 spin-echoes for with / without macromolecule data processing) is recommended.

Overall, the results from this final experiment are very encouraging for *in-vivo* translation. However, before doing so, it is important to establish the reproducibility of the technique, a matter that is formally addressed in §7.

7 2D J-resolved reproducibility of *in-vitro* GABA measurement

7.1 Introduction

It has been established in §3 that results from 2D spectroscopy techniques are being increasingly reported (13,17,19,22-24). However, there has been very little published work regarding the reproducibility of these methods. As with all new procedures, it is important to evaluate the associated reliability and reproducibility of the technique before it can be applied routinely as a research or clinical tool. Therefore, any observed changes can be attributed to true physiological changes rather than systematic variation. This is particularly important for 2D MRS techniques as these aim to quantify peaks from low concentration metabolites, using protocols that have inherent differences in their methodology and sensitivity.

Most previous single-voxel proton MRS reproducibility studies have been concerned with 1D techniques, both *in-vitro* and *in-vivo* using short and long TEs. Since 1D MRS is a well understood technique, using established acquisition and post-

processing methods, the coefficients of variation (CVs) obtained from such studies may reflect the optimum achievable reproducibility in 2D MRS, so it is useful to examine these studies in more detail.

Many of the factors affecting reproducibility in 1D experiments are common to 2D investigations, therefore it is important that these components are investigated as fully as possible in a well-constructed protocol. Brooks *et al* (157) listed five possible causes of variation among quantified spectroscopy results. These are:

1. Instrument variability
2. Biological variability
3. Voxel variability – i.e. errors associated with volume of interest (VOI) placement on repeated scans
4. Operator variability with regard to scanning protocols
5. Differences in data analysis procedures

Since biological variation is the factor of interest, it is desirable to minimise all other variables so that the measured result reflects only physiological changes.

Within the same research / clinical centre, any differences in the data analysis procedure can be eliminated by adopting a standard post-processing protocol, ideally fully-automated to reduce any operator bias or variability. The same principle can be applied to the scanning protocol to reduce differences in acquisition parameters. Hence, with standardisation of data acquisition and post-processing, it is the voxel positioning and instrument variability that have the most influence on the reproducibility, particularly in serial studies, and it is these factors that need to be investigated.

Marshall *et al* specifically addressed these issues by measuring both "within-run" and "between-days" reproducibility (141). The former relates to successive measurements of the subject without any movement or re-positioning of the voxel, therefore any variation in the results should reflect only the scanner instability. "Between-days" reproducibility refers to measurements made on different days, thus necessitating both subject and voxel re-positioning. Therefore, the calculated CVs

reflect both set-up and instrument variability. Results from *in-vitro* work using the scanner manufacturer's standard spectroscopy phantom containing only acetate and lactate showed that, as expected, the between-days reproducibility was in most cases, worse than the within-run. Moreover, the largest measured between-day CV was only 3.3% (standard PRESS, TE/TR = 135 / 1600 ms, VOI = 8ml, $N_{acquisitions}$ = 16).

Disappointingly, these results were not reflected *in-vivo*. In a small group of 12 healthy volunteers, spectra were obtained from an 8ml VOI placed in the left or right parietal matter (PRESS, TE/TR = 135 / 1600 ms, VOI = 8ml, $N_{acquisitions}$ = 256). The CVs of the absolute metabolite peak areas for NAA, choline and creatine rose to 18%, with the lowest CV having a value of 9%. Repeated measurement of the same volunteers on a second day showed no significant differences between the data for both days. In a second group of four volunteers, six spectra were acquired from each subject on four different days from an 8ml VOI placed in the right parietal white matter. Again, the between-day reproducibility was larger than the within-run, and with a change in acquisition parameters to reduce the scan time (PRESS, TE/TR = 135 / 1600 ms, VOI = 8ml, $N_{acquisitions}$ = 64), the CVs fell as low as 4.4%, although extremely large CVs were quoted for creatine (up to 25.8%). This was attributed to post-processing problems of fitting the creatine peak using the modelling software.

In the most recent of the 1D reproducibility studies, Schirmer *et al* investigated several different aspects of reproducibility at 1.5T, in three series of phantom and volunteer studies (142). All experiments used the quadrature head coil and the PRESS spectroscopy sequence (VOI = 8ml, $N_{acquisitions}$ = 128). The first part was an *in-vitro* study using the standard GE spectroscopy phantom (TE/TR = 30/1500ms). Over a period of 13 months, 84 spectra were acquired using two different scanner software versions (due to an upgrade approximately half-way through the experimental period). Since spectra from the same phantom were collected, the changes in the measured metabolite concentrations from phantoms using the same software version could only be attributed to scanner instabilities and set-up variations. As expected, there were significant differences between the metabolite concentrations between software versions. However, CVs of 3.8%, 4.0%, 3.3% and

6.1% were obtained for choline, creatine, NAA and myo-Inositol (mI) respectively following analysis from both software versions.

In the first series of *in-vivo* results reported, five spectra (TE/TR = 35/2000ms) from the same volunteer in six separate scanning sessions over 10 days (at the same time of day) were acquired, thus providing a total of 30 spectra. All VOIs were positioned in the right parietal white matter using anatomical landmarks from the scout images for positioning. In this respect, variations due to patient set-up and scanner instability would be expected, but over such a short time period and with efforts to maintain a consistent nutritional state, physiological changes in the measured metabolites are not. For the same four metabolites, CVs (following analysis of all 30 spectra from the same individual) of 4.9% (choline), 6.4% (creatine), 3.8% (NAA) and 7.7% (mI) were obtained. These results are comparable to those obtained from the phantom study. Since both involved the repeated scanning of the same subject (be it phantom or human head), they reflect changes in scanner performance and repositioning, not physiological changes, and so the similarity in results should be expected. However, exact interpretation of these results is difficult since they are from spectra both within the same scanning session *and* in different sessions, with some results being influenced by set-up variations and others not. Still, as an overall estimation of the in-vivo CV obtained, these results are encouraging.

Similar results were obtained by Brooks *et al* in a study of neurologically normal volunteers (n = 10) also conducted at 1.5T, using the volume head coil but using the STEAM spectroscopy sequence (157). Each subject was scanned at three time points, the second scan an hour after the first, and the third approximately a month later. Six spectra from the same VOI were acquired in each scanning session. Again, mean coefficient of variations (CV) were reported of 5.30%, 4.33% and 3.30% for choline, creatine and NAA, and 8.10% for mI. Following analysis of the mean variance from the between-sessions results, it was suggested that differences in concentration of choline, creatine, NAA and mI above 20.1%, 16.7%, 12.8% and 20.8% respectively could be attributed to physiological changes

In the last part of Schirmer's study, spectra from 35 healthy volunteers were acquired (142). In all cases, a single spectrum (TE/TR = 35/2000ms) was acquired from the parietal white matter. In 12 subjects, a second spectrum was obtained immediately following the first, in the same brain region, but following re-positioning of the subject. Eight volunteers were re-scanned 8-14 days after the first session, again acquiring spectra from the same brain region. In the single voxel from all 34 volunteers, the CVs for choline, creatine, NAA and mI were 15.0%, 10.3%, 7.6% and 14.6% respectively. These show a large increase in CV when compared to the results from the same subject, but are more realistic in terms of the clinical environment: Different subjects (age and sex) scanned at different times of day, with different operators responsible for patient positioning and adhering to the scanning protocol. It is therefore possible that these CVs may reflect actual changes in metabolite concentration, in addition to previously mentioned causes of variation. However, since no brain matter segmentation was applied, these differences may also indicate changes in the white / grey matter brain composition and CSF content of the VOI between the subjects. In addition, it is possible that differences in the relaxation rates of the metabolites between volunteers may have some influence on the results. In the sub-set of eight volunteers that were rescanned approximately a fortnight after the first scan, the CVs were < 7% for choline, creatine and NAA and < 9% for mI, results approaching those for the first and second parts of the study.

However, these three studies by no means reflect the extent of the reproducibility results reported. In a letter to the editor, Wardlaw *et al* included a table of results from 11 1D reproducibility studies performed between 1991 and 1998 (154). For NAA alone, CVs from absolute values ranged from 13% to 29%, with one study quoting a general error of 39%. In terms of 2D, no less variation should be expected.

Pertaining to reproducibility in 2D J-resolved MRS, only Ke *et al* performed any quantitative analysis of their results, and for the mean detected GABA concentrations, a 36.5% standard deviation (SD) was quoted (24). This is considerably poorer than that reported using other techniques, Table 7.1. This disappointing result was attributed to the decrease in sensitivity due to use of the

volume head coil compared to a surface coil, and a smaller VOI. In addition, it was suggested that the longer scan time required for this J-resolved method encouraged patient motion, thus further reducing the SD.

Table 7.1 Comparison of published reproducibility results for 2D MRS techniques

Method	number of subjects	SD and range of measured GABA	Reference
Spectral editing at 1.5T	10	mean: 0.12 ± 0.05(SD) range: 0.04 – 0.20	(13)
Spectral editing at 1.5T	8	SD 20% reliability coefficient of repeated experiments = 0.7	(14)
DQF at 1.5T	15	SD = 0.2mM (repeatability = 38%)	(19)
DQF at 1.5T	10	mean: 0.20 ± 0.05 (SD)	(17)

The specific topic of reproducibility in 2D MRS was addressed by Binesh *et al*, using a 2D L-COSY sequence in 40 *in-vitro* experiments and on 10 volunteers, each scanned four times (20). The spectra were acquired on a 1.5T GE scanner using body coil transmit / 3" surface coil receive set-up, thus providing an increased SNR compared to results from the head coil. The phantom used was the standard GE spectroscopy phantom, which does not contain GABA, and as such, no results were quoted specifically for GABA in *in-vitro* experiments.

In the within-run *in-vitro* experiments performed, CVs of less than 2% were observed for the diagonal metabolite peaks and less than 6% for the cross-peaks. Since the volume selection and data processing methods were unchanged, these differences were accounted for by temporal instability of the scanner, affecting the quality of shim and water suppression. Comparison of measurements taken over the eight-month period gave CVs of between 7% - 15%. Differences in the phantom set-up, or changes in the transmit gain, as well as small daily fluctuations in the magnetic field inhomogeneity or RF power could account for this poorer CV. Marshall *et al* recently presented data showing a clear increasing trend in spectroscopy QA results, accounted for by temporal changes in the RF transmitter causing a drift in the transmit gain (158). So, without regular checks (and re-calibration where necessary),

such factors may remain unaccounted for leading to an over-estimation of any physiological changes.

In terms of the 2D COSY *in-vivo* work, there was a large range of CVs for each metabolite (20). For example, the CV for the diagonal peaks of choline, creatine and NAA were less than 9% in both the intra- and inter-subject experiments. This figure rose to about 17% for the cross-peaks from glutamine / glutamate, mI, asparate and threonine / lactate. The results for GABA showed an increased variation again; both intra-and inter-subject experiments gave a mean CV of about 22%. This higher CV was attributed to possible overlap of the GABA cross peak from ridges of the nearby creatine and NAA.

As an additional part to this work, the intra-class correlation was calculated using the *in-vivo* peak integrals and metabolite ratios (with creatine taken as reference). All the major metabolites (NAA (diagonal and cross-peak), creatine, Glx) demonstrated significant correlations of the measured ratios with respect to the diagonal peak of creatine, yet this was not true of the lower concentration metabolites. Thus, the lower SNR of these peaks prevents the difference of these peaks between subjects to be significant when compared to the peaks from the same subject at different times. It was suggested that improvement in coil design might improve the CV of the cross-peaks by increasing the SNR.

It is against this background, that a series of local reproducibility experiments was conducted, to identify the reliability of 2D J-resolved MRS, particularly for the detection and quantification of GABA, on the centre's 1.5T scanner.

7.2 Method

7.2.1 Scanning protocol

As have been previously discussed in §3, identification of the 3.01ppm GABA resonance was chosen as initial experiments had shown that it was possible to resolve this resonance from the overlapping resonance using the 2D J-resolved technique.

To test the reproducibility of this approach, five spherical phantoms containing physiological concentrations of choline and creatine (3mM and 9mM respectively) and concentrations of GABA of 10mM, 5mM, 2mM, 1.5mM and 1.2mM were evaluated. The GABA concentration of 1.2mM had been previously shown to be the lowest detectable concentration using the volume head coil, §5. Since GABA at a lower concentration of 0.8mM had been detected using a 5" surface coil, §6, reproducibility measurements were also taken at this concentration in the surface coil. For comparison, these experiments were also repeated in a 3" surface coil.

Three measures of reproducibility were taken: (1) Variation due to scanner instability alone (within-run reproducibility); (2) variation due to scanner instability and voxel re-positioning (within-session reproducibility); (3) both scanner and set-up variation over several days (between-days reproducibility). In each of the three sets of experiments, five 2D J-resolved spectra were acquired, Table 7.2. Results from §6 have shown that the optimum scanning protocol for GABA measurement uses a 5" surface coil. However, since this is a formal reproducibility study, each experimental set from 10mM GABA to 1.2mM GABA was carried out in both 5" surface coil and a volume head coil since this is used for standard neuro-imaging / spectroscopy. With the additional very low GABA concentration experiments in two sizes of surface coil, a total of 180 separate experiments were performed.

For experiments using the volume head coil, the phantom was positioned in the centre of the coil, which in turn was positioned in the isocentre of the magnet, and a $3x3x3cm^3$ voxel was centred in the phantom using a 3-plane localising image. In experiments using the surface coils, the phantom was placed on a specially designed headrest, and once positioned in the centre of the magnet, a $3x3x3cm^3$ voxel was placed in the central part of the lower half of the phantom. Consequently, in all cases, the ideal set-up for each coil arrangement was chosen.

All experiments were performed on a clinical 1.5T GE Signa Horizon system using a dedicated 2D J-resolved spectroscopy sequence [N. Sailasuta, GE Healthcare] as described in §5. 2D J-resolved spectra were obtained with the optimised protocol

given in Table 6.17, i.e.: TE_{start} = 35ms, ΔTE = 10ms, steps2d = 66, TR = 2000ms, NEX = 16. The total scanning time for each experiment was approximately 35 minutes.

Table 7.2 Number of experiments made for the calculation of within-run, within-session and between-days reproducibility, in both a volume head coil (VHC) and 5" general-purpose surface coil (5"GP), for all five GABA concentrations investigated in both coil arrangements

GABA concentration (mM)	within-run		within-session		between-days	
	VHC	5"GP	VHC	5"GP	VHC	5"GP
1.2	5	5	5	5	5	5
1.5	5	5	5	5	5	5
2.0	5	5	5	5	5	5
5.0	5	5	5	5	5	5
10.0	5	5	5	5	5	5
Total	**25**	**25**	**25**	**25**	**25**	**25**

7.2.2 Post-processing

As described in previous chapters, the resulting P-files from each scan were transferred to a SUN Ultra workstation where the FIDs underwent automatic time-domain phase correction, removal of water components using HLSVD and apodization in both the F1 and F2 dimensions. Following 2D Fourier Transform of the data, 2D magnitude contour plots were produced, allowing the identification of the metabolites. Spectra were then extracted at J = 0Hz (providing an uncoupled spectrum) and J = 7.4Hz, the J-coupling frequency of GABA. Conversion of these spectra to MRUI format facilitated quantification in MRUI to obtain integral peak values for each of the metabolites. In addition, ratios to creatine were obtained for the GABA measurements.

Using the data acquired from experiments of individual metabolites, prior knowledge files were created in MRUI to allow the automatic quantification of the extracted spectra. In the J = 0Hz spectra, the choline and creatine peaks were quantified, and the results were presented in §5. In the J = 7.4Hz extracted spectrum, the two GABA

peaks (at 2.28ppm and 3.01ppm) and the residual choline and creatine peaks were identified for quantification, although only the 3.01ppm GABA peak was analysed as part of the reproducibility study.

CVs were calculated for GABA, using both the absolute values and metabolite ratios to creatine, Equation 7.1. Variance was calculated according to the F-test in Microsoft Excel (Microsoft corporation).

$$GABA(metabolite\ ratio) = \frac{GABA\ (7.4Hz)}{creatine\ (0Hz)}$$

Equation 7.1 Applied ratio for GABA metabolite ratios

7.3 Results

Following each experiment, 2D contour plots were produced and the row corresponding to the J-coupling frequency of GABA was extracted and quantified. At this frequency, peaks from GABA at both 3.01ppm and 2.28ppm were identified, as well as peaks resulting from residual choline and creatine. Representative examples of modelled spectra from experiments containing 5mM GABA and 1.2mM GABA are shown in Figure 7.1 and Figure 7.2 in the volume head coil. Corresponding spectra from the same phantoms using the surface coil are shown in Figure 7.3 (5mM GABA) and Figure 7.4 (1.2mM GABA). Figure 7.5 presents the results at 0.8mM GABA from both surface coils.

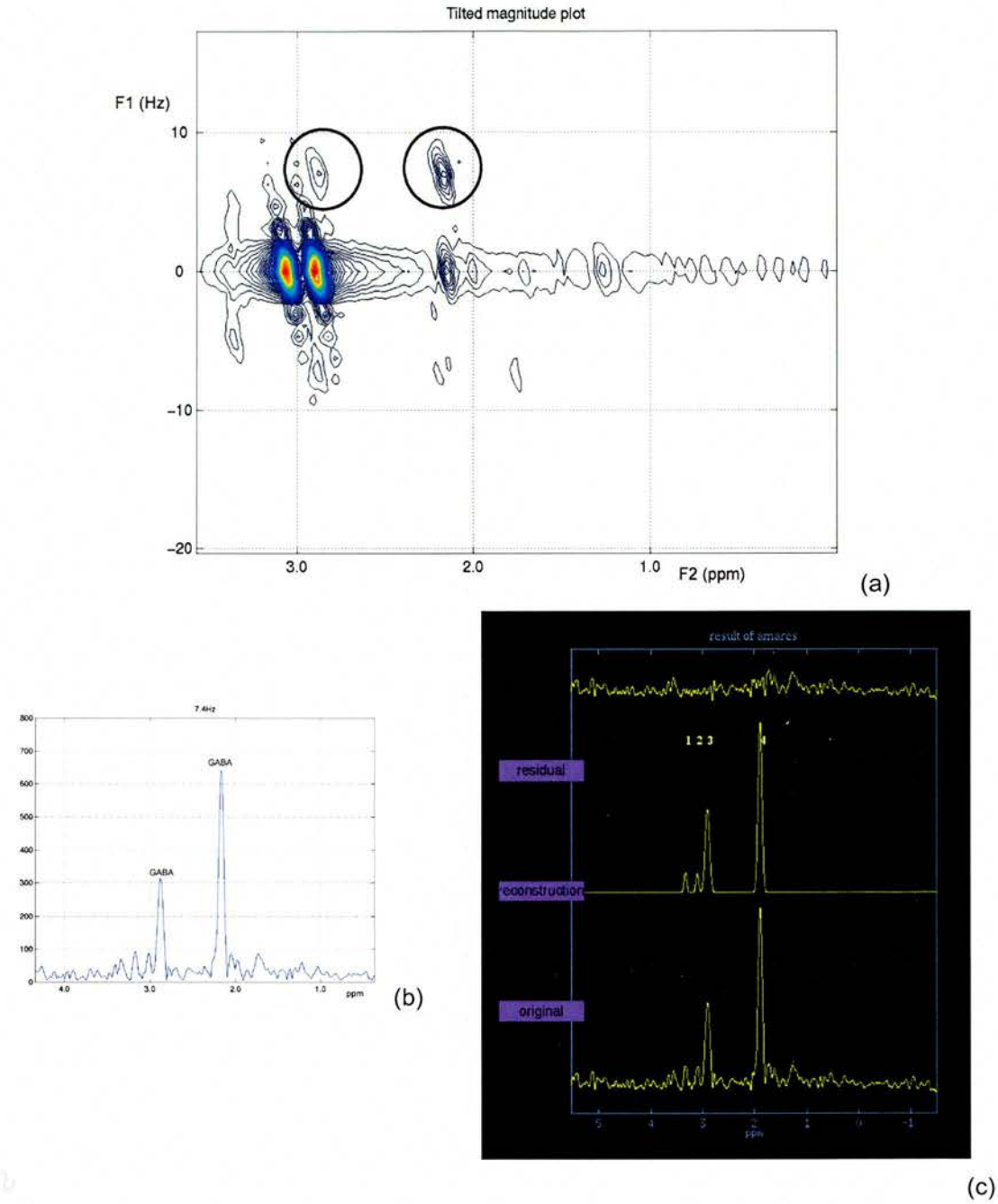

Figure 7.1 Results from the 2D experiment using a phantom containing physiological concentrations of choline and creatine, and 5mM GABA using a volume head coil. (a) 2D J-resolved spectrum with the GABA resonances marked by circular markers. The extracted spectrum at the level of the GABA J-coupling frequency is shown in (b). This spectrum was then quantified in MRUI using the associated prior knowledge file, results of which are shown in (c). Both GABA peaks (peaks 3 and 4) and the residual choline and creatine peaks (peaks 1 and 2 respectively) were quantified, and the results displayed in the table on the left-hand side of the figure (with all peaks shifted by ~0.1ppm in room temperature phantoms).

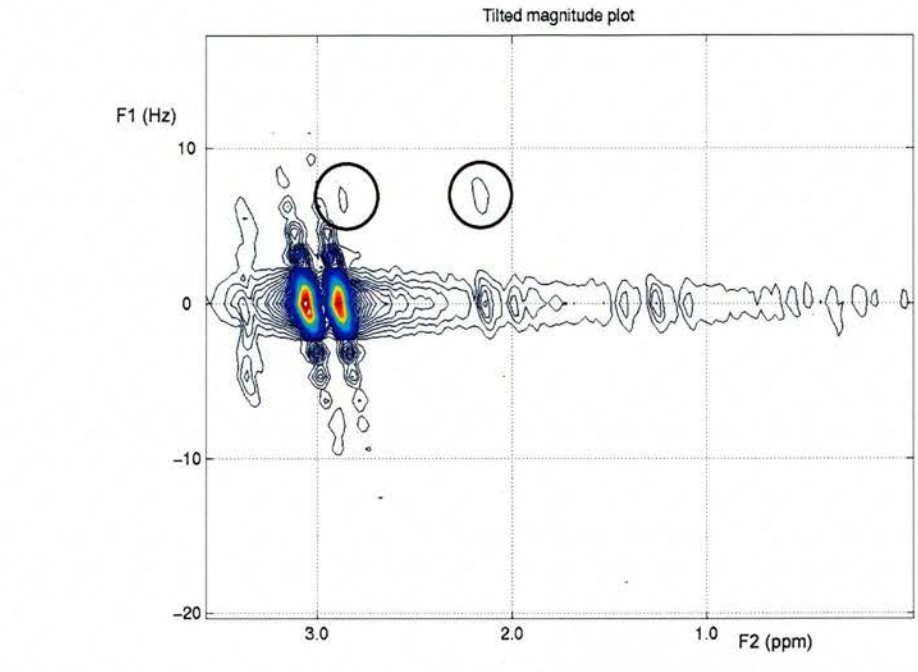

(a)

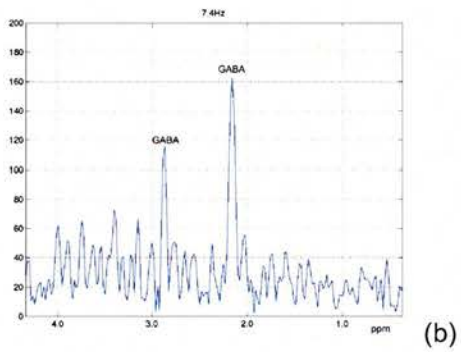

(b)

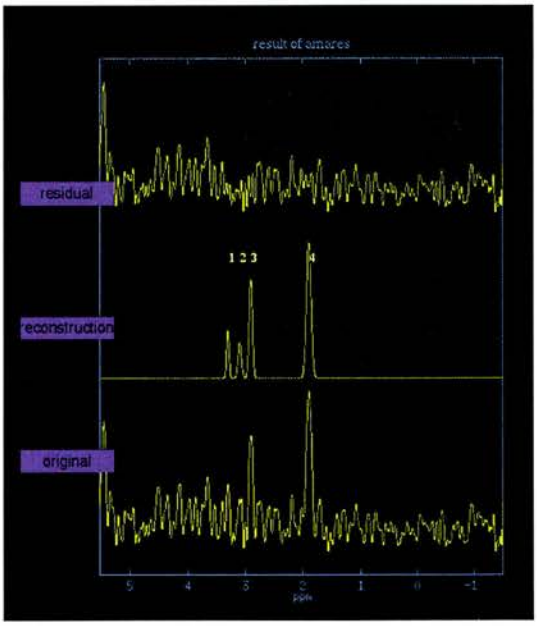

(c)

Figure 7.2 Results from the 2D experiment using a phantom containing physiological concentrations of choline and creatine and 1.2mM GABA. Again, the GABA resonances are identified within the oval markers, appearing at the 7.4Hz coupling frequency (a). The extracted spectrum (b) was quantified in the same way, using the prior knowledge files to identify and quantify the residual choline and creatine peaks, and the GABA peaks at 3.01ppm and 2.2ppm (c) (with all peaks shifted by ~0.1ppm in room temperature phantoms).

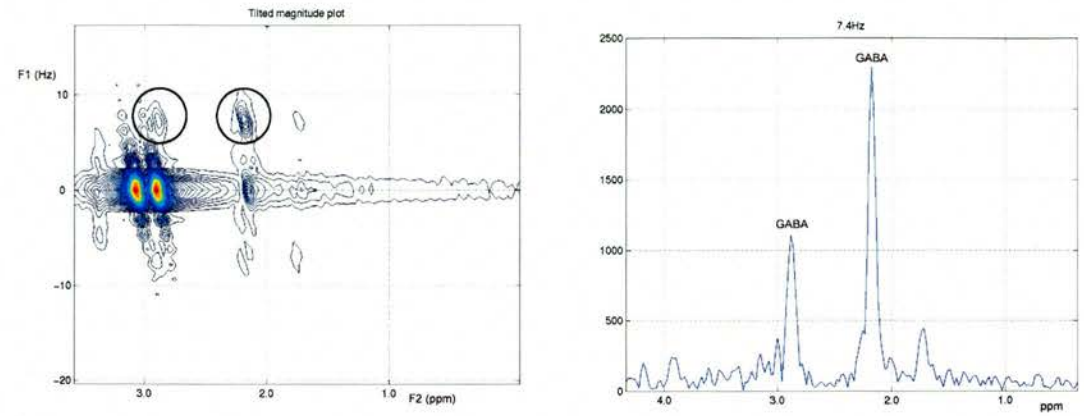

(a) (b)

Figure 7.3 Results from the 5mM phantom scanned using the 5"GP coil. Note the increase in amplitude of all metabolites due to the increased sensitively of the surface coil compared to the volume coil – in both the 2D plot (a) and extracted spectrum (b), GABA is more easily identified (with all peaks shifted by ~0.1ppm in room temperature phantoms).

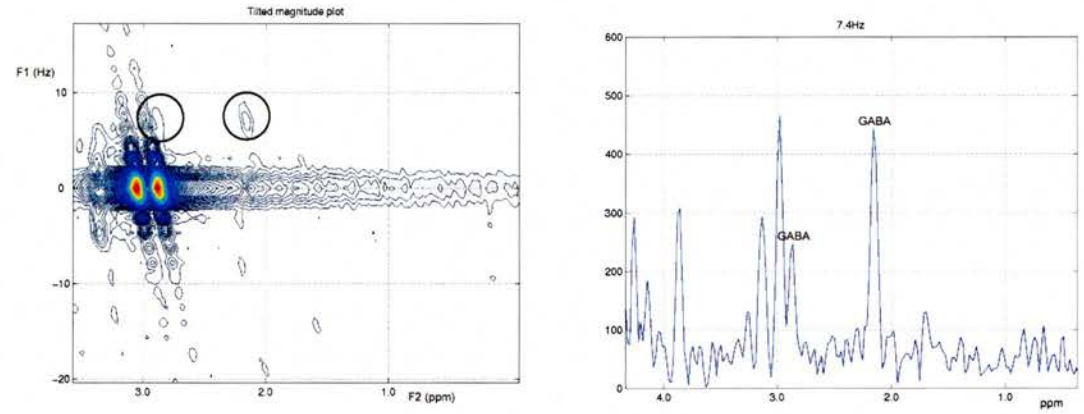

(a) (b)

Figure 7.4 Results also from the 1.2mM GABA phantom, with physiological concentrations of choline and creatine using the 5" GP coil. On the 2D plot, (a), the GABA resonances are identified within circles. With the increased sensitivity of the surface coil, even at this low concentration, GABA was still be readily identified (b) (with all peaks shifted by ~0.1ppm in room temperature phantoms).

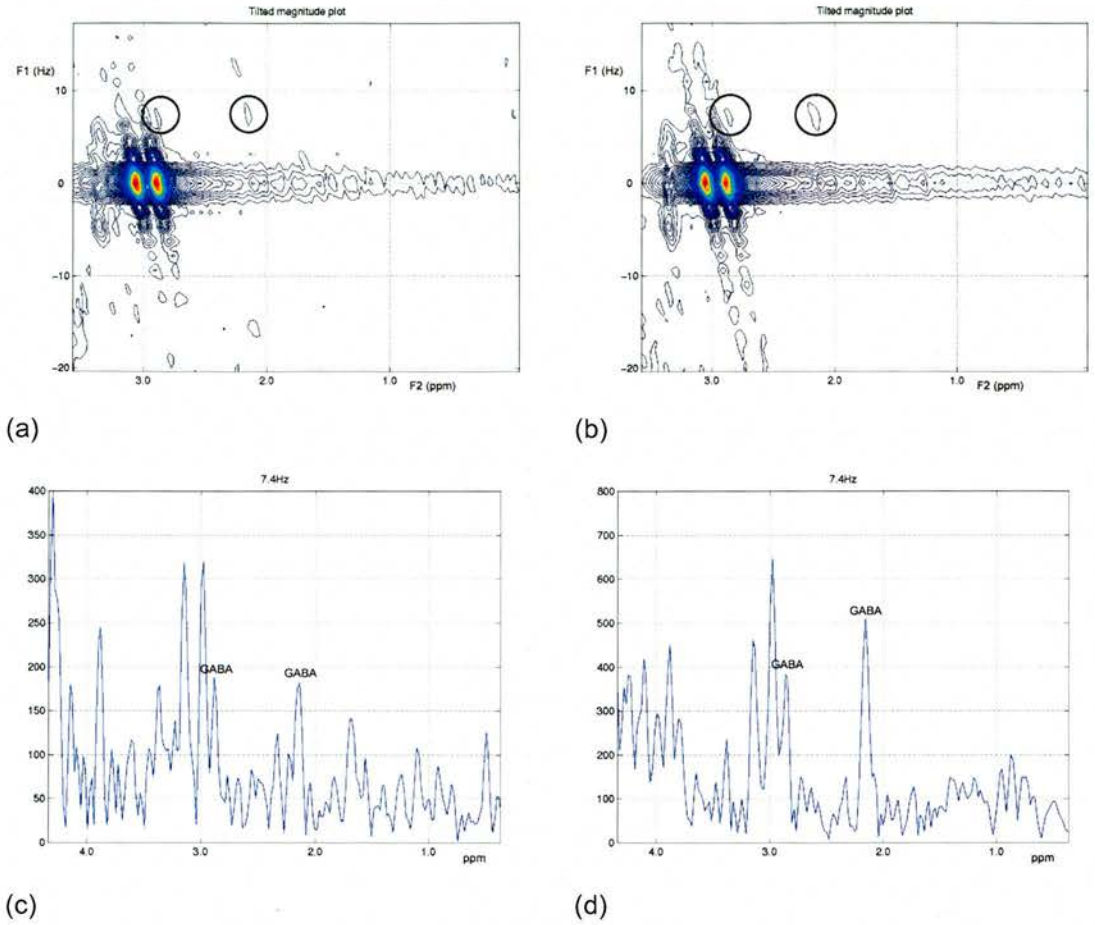

Figure 7.5 2D J-resolved spectra from a phantom containing 9mM creatine, 3mM choline and 0.8mM GABA using (a) 5" surface coil and (b) 3" surface coil. The corresponding extracted rows at the GABA J-coupling frequency are shown in (c) and (d) for the 5" and 3" surface coils respectively (with all peaks shifted by ~0.1ppm in room temperature phantoms).

The within-run experiments for each phantom were performed consecutively in the same scanning session, requiring no re-positioning of the phantom and no reselection of the VOI between each scan. The results from these experiments are shown in Figure 7.6 and listed in Table 7.3. There was no significant difference between the results obtained from both coils.

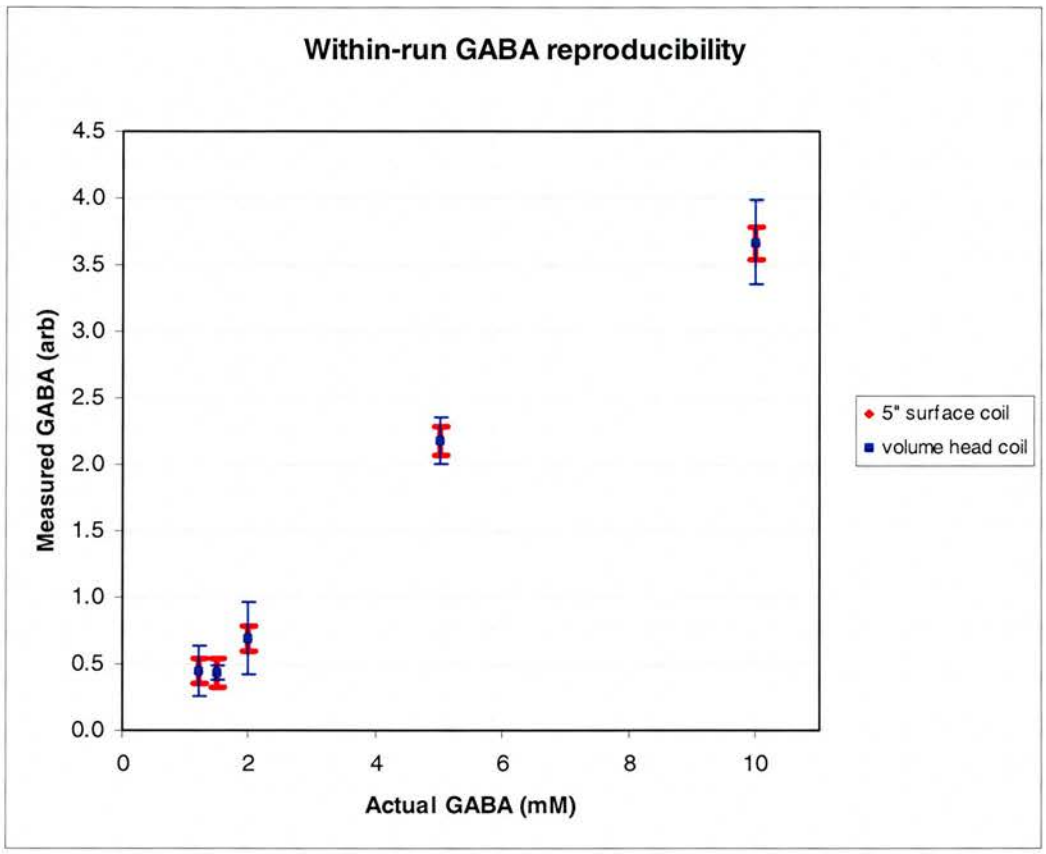

Figure 7.6 Results from the within-run reproducibility experiments in both coil arrangements. In each series, the phantoms contained GABA in concentrations varying between 10mM to 1.2mM as described in the text. The error bars in this, and all proceeding graphs, relate to the Standard Deviation of the mean.

The within-session measurements evaluate the reproducibility of data acquisition including both scanner and set-up variability. Figure 7.7 shows the within-session results across the range of GABA concentrations in each of the five phantoms. These results are summarised in Table 7.3. Analysis of variance, using the f-test, demonstrated a significant difference between the results from the two coil types at the GABA concentration of 1.5mM ($p = 0.003$) only.

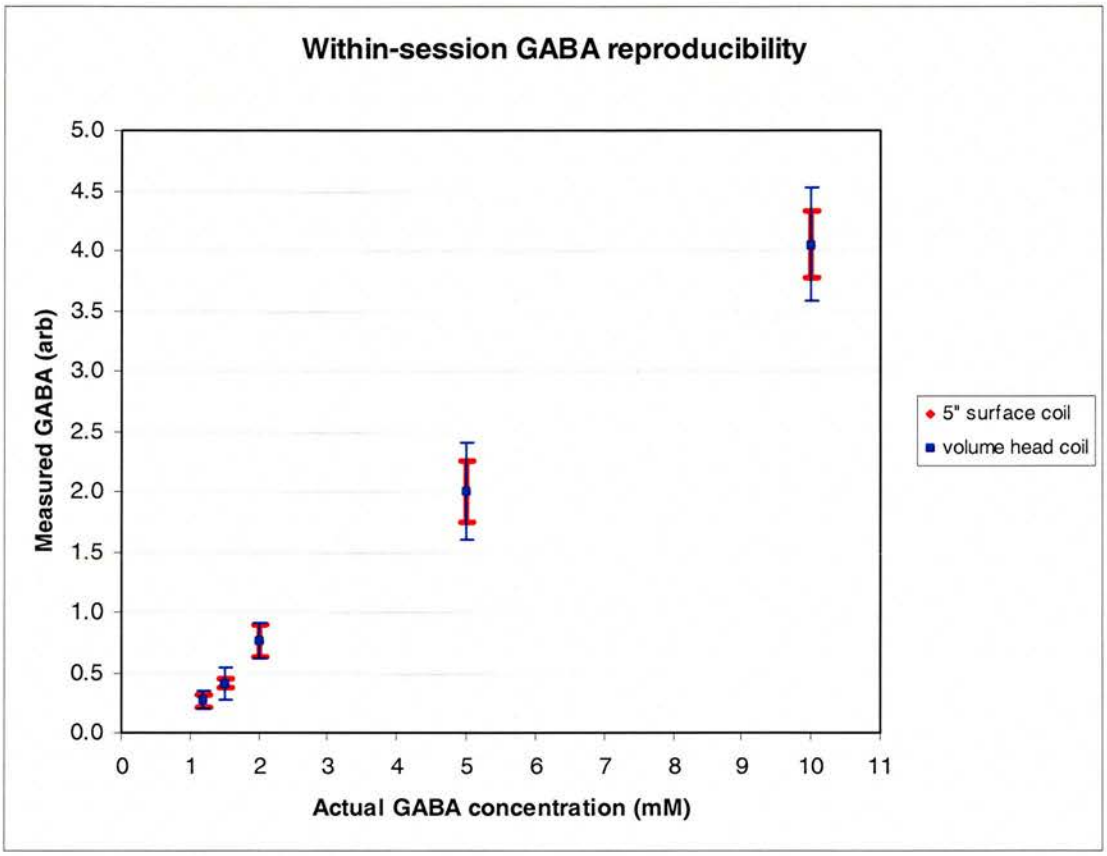

Figure 7.7 Results from the within-session reproducibility experiments in both the 5"GP and volume head coil. The results from the 5"GP are more reproducible than the volume head coil, overall, with the lowest CVs at the higher GABA concentrations.

The between-days *in-vitro* experiments most accurately reflect clinical experience, were the subjects require re-positioning on different days. The mean and SDs from the results across the full-range of GABA concentrations investigated are presented in Figure 7.8 and Table 7.3. Significant differences between the data collected from the two coils were observed at GABA concentrations of 10mM ($p = 0.05$) and 1.2mM ($p = 0.005$).

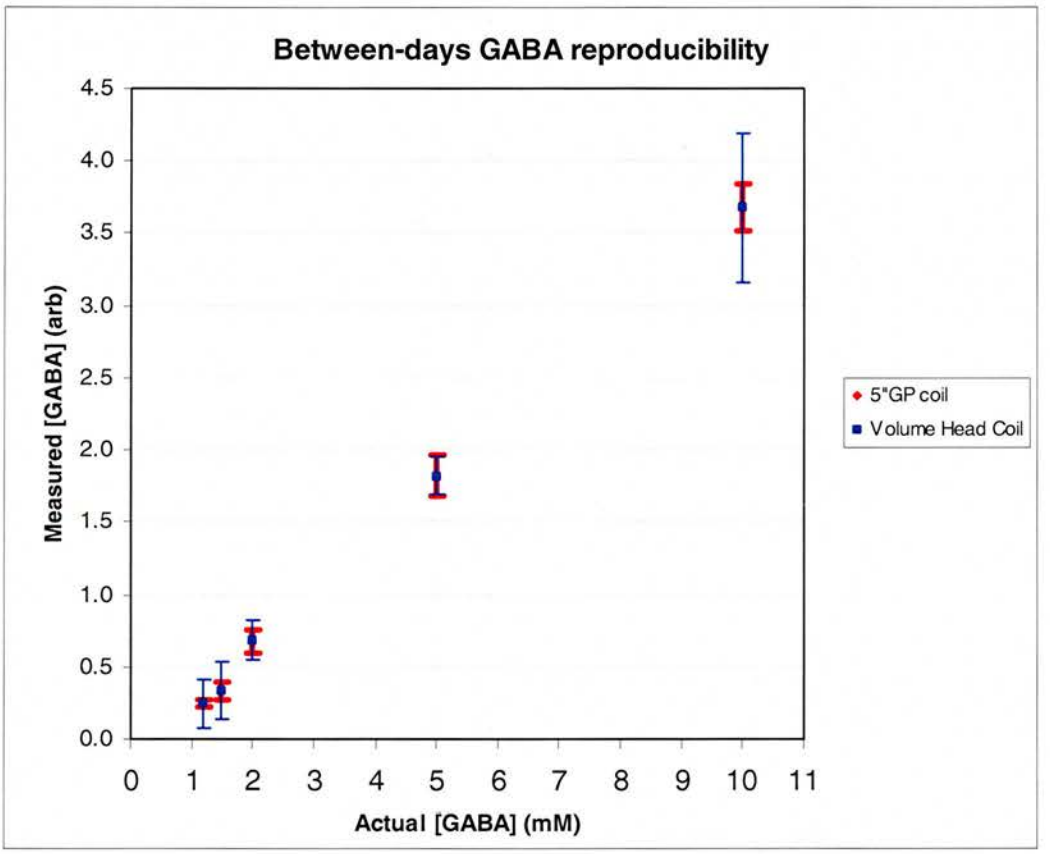

Figure 7.8 Mean and SDs of the results from the between-day reproducibility experiments in both the 5"GP and volume head coil. As will all previous results, the general trend of measured concentration with actual concentration is observed, however, the results from the 5" GP coil are generally more reproducible. More importantly for this work and potential for clinical application, this is particularly true at the lower GABA concentrations.

As described in the methods, it is not uncommon to find the results from 2D GABA measurements quoted as ratios to creatine and so to allow comparison with these, the GABA values were scaled to creatine, Table 7.4. The results from the low concentration GABA experiments in the surface coils are presented in Table 7.5.

Table 7.3 The Coefficients of Variation (CV %) of the absolute values of GABA (peak areas as calculated in MRUI) for all the within-run, within-session and between-days experiments in a volume head coil (VHC) and 5" general purpose surface coil (5"GP).

[GABA] (actual mM)	CV absolute GABA (%)					
	Within-run		Within-session		Between-days	
	VHC	5"GP	VHC	5"GP	VHC	5"GP
1.2	39.92	21.58	26.15	19.87	67.57	8.33
1.5	13.33	24.93	24.00	10.16	59.03	17.32
2	22.68	14.12	13.42	12.68	28.74	16.30
5	8.06	4.84	12.94	8.22	7.33	7.98
10	8.68	3.33	11.55	6.80	13.57	4.40

Table 7.4 CVs of the GABA ratios with respect to creatine for all the within-run, within-session and between-days experiments in a volume head coil (VHC) and 5" general purpose surface coil (5"GP).

[GABA] (actual mM)	CV GABA / Cr (%)					
	Within-run		Within-session		Between-days	
	VHC	5"GP	VHC	5"GP	VHC	5"GP
1.2	21.57	21.82	28.18	17.40	67.57	15.47
1.5	12.38	16.89	25.61	11.79	54.99	15.43
2	23.39	16.41	14.43	7.70	28.40	12.32
5	7.86	3.11	13.53	7.30	4.52	14.48
10	8.31	5.42	8.87	2.21	11.79	4.67

Table 7.5 CVs (%) of the GABA ratios with respect to creatine for all the reproducibility measurements from a phantom containing 9mM creatine, 3mM choline and 0.8mM GABA

Coil	CV GABA / Cr (%)		
	within run	within-session	between-days
5" surface coil	16.93	17.01	22.53
3" surface coil	19.28	20.56	30.21

7.4 Discussion and conclusions

Reassuringly, a clear trend of increasing measured GABA concentration with an increase in the known actual concentration is observed, Figure 7.8, with most results demonstrating a reduced CV (i.e. improved reproducibility) using the surface coil compared to the volume head coil. This is expected due to the increase in sensitivity associated with the surface coil. Rose *et al* noted a trend towards higher CV values for low concentration metabolites when using a quadrature head coil for their single voxel spectroscopy measurements (159), and Ke *et al* suggested that use of a volume head coil contributed towards the poor CV obtained in their work (24). In neither study were comparative experiments performed in both a volume and surface coil.

In the published *in-vivo* GABA-related MRS performed at 1.5T, there is considerable variation among the quoted reproducibility of the measurements. Using a 2D J-resolved sequence, Ke *et al* reported a ± 36.5% standard deviation (SD) in the mean GABA concentrations using a volume head coil to localise a 2x3x2cm^3 voxel (24). For *in-vivo* GABA measurements using a double quantum filter at 1.5T, a repeatability of 38% (± 2 SDs) in a 35cc voxel has been recorded (19). Using a spectral editing technique also at 1.5T, *in-vivo* GABA SDs of 46% and 23% for 8cc and 4cc voxels respectively, localised using a 5" surface coil, have been cited (13). More promising results were reported by Binesh *et al* investigating the reproducibility of 2D COSY where CVs for *in-vivo* GABA were less than 22% (raw volumes) (20). These results were obtained using a 3" surface coil to localise a 3 x 3 x 3cm^3 voxel in the anterior cingulate gyrus. In comparison to the published data, the initial reproducibility measurements from this work contrast very well: In the between-days experiment with a GABA concentration of 1.2mM, a CV of 8.33% (15.47% using metabolite ratios) was obtained using the 5" GP surface coil, Table 7.3.

However, further investigation of lowest concentration GABA solutions showed a dramatic reduction in the reproducibility, Table 7.5, with the value of the between-days CV in the 5" surface coil rising to 23%. This suggests that the results obtained at 1.2mM provide an over-optimistic view of the achievable reproducibility (a

hypothesis that is supported by the larger CVs calculated from the within-run and within-session measurements). Therefore, it may be that the results obtained at 0.8mM GABA reflect a more realistic idea of the obtainable reproducibility.

In translating this present work to an *in-vivo* protocol, increases in the CVs are expected due to patient motion and voxel placement in different brain regions. In addition, inhomogeneities within the brain matter, and in particular the sinuses and ventricles, will reduce the shim efficiency leading to broader linewidths than the 2Hz FWHM linewidths recorded in this work, which may also complicate GABA measurement. Application of the *in-vitro* 2D COSY work *in-vivo* saw increases in the CVs of the high concentration metabolites from < 10% to < 17% (20). Although 2D J-resolved MRS does not suffer the same theoretical signal loss as 2D COSY (21), it is likely that similar decreases in reproducibility may be recorded when measuring GABA *in-vivo.* However, with changes of the order of 50% in GABA observed in depression and epilepsy using MRS at higher field strengths (8,160), 2D J-resolved MRS may remain sufficiently reproducible to allow the routine study of these neuropsychiatric disorders at clinical field strengths.

The results from this work have shown that 2D J-resolved MRS can be used to measure *in-vitro* GABA concentrations falling within the normal physiological range of 1.3mM – 1.9mM (7) and as low as 0.8mM. CVs from between-days absolute reproducibly measurements of GABA were less than 23% at all GABA concentrations using the 5" surface coil, supporting the earlier decision to perform all *in-vivo* work using this coil. In addition, the CVs from the 5" coil suggest that 2D J-resolved MRS may yet be sufficiently reproducible to detect changes in metabolite concentrations *in-vivo*.

8 *In-vivo* 2D J-resolved MRS

8.1 Introduction

The aim of all the work thus far has been to facilitate the measurement of GABA *in-vivo,* using 2D J-resolved MRS. Therefore, having established the optimum protocol for data acquisition and post-processing, and shown that the reproducibility of the technique is sufficient to allow real, physiological changes to be measured, it was appropriate to apply the method *in-vivo.*

This chapter describes the results from the *in-vivo* experiments, specifically the application of 2D J-resolved MRS for GABA measurement, §8.2. Evaluation of the general reproducibility of the method is discussed in §8.3, and §8.4 discusses further problems associated with applying the method to *in-vivo* data. To complete the *in-vivo* work, results from acquiring 2D J-resolved spectra at 3T and applying the same post-processing principles are presented in §8.5.

8.2 *In-vivo* GABA measurement using 2D J-resolved MRS

8.2.1 Scanning and post-processing protocol

Normal, healthy volunteers were recruited for 2D J-resolved MRS and written informed consent was obtained. Each volunteer was set-up on a 5" surface coil, using a specially designed headrest for comfort and immobilisation. After acquiring a series of T_2 FSE axial images on which the spectroscopy VOI was positioned, a conventional single-voxel PRESS experiment was performed (TE = 35ms, TR = 2000ms, VOI = 3x3x3cm^3 in the occipital cortex) to ensure the acquisition of good quality spectra during the 2D sequence. The spectral linewidth was noted, and the VOI was re-positioned and / or re-sized to ensure a linewidth of less than 5Hz. In all 2D J-resolved experiments, the optimum scanning parameters were used as chosen in §6.4. These are listed in Table 8.1.

Table 8.1 Scanning parameters for *in-vivo* acquisition of 2D J-resolved spectra

Coil	5" surface coil
VOI	Not less than 15cm^3
TE_{start}	35ms
Δ TE	10ms
TR	2000ms
steps2d	66
NEX	16
t_{scan}	35:28 minutes

The raw p-files were transferred to a Sun Ultra Workstation for post-processing as described in §5.2.3. After 2D FT, the 7.45Hz rows were extracted from the 2D contour plot and converted to ascii format for quantification of any visible GABA peak.

8.2.2 Results

To date, a total of eight 2D J-resolved spectra have been acquired from four volunteers. A representative 2D J-resolved spectrum is shown in Figure 8.1 from a

healthy volunteer, using a TE_{start} = 35ms to replicate the minimum TE most commonly used in the literature. The peak at 3.01ppm, in the extracted spectrum, has been identified. Comparison with results in the literature would suggest a peak assignment of GABA and macromolecules (i.e. GABA+).

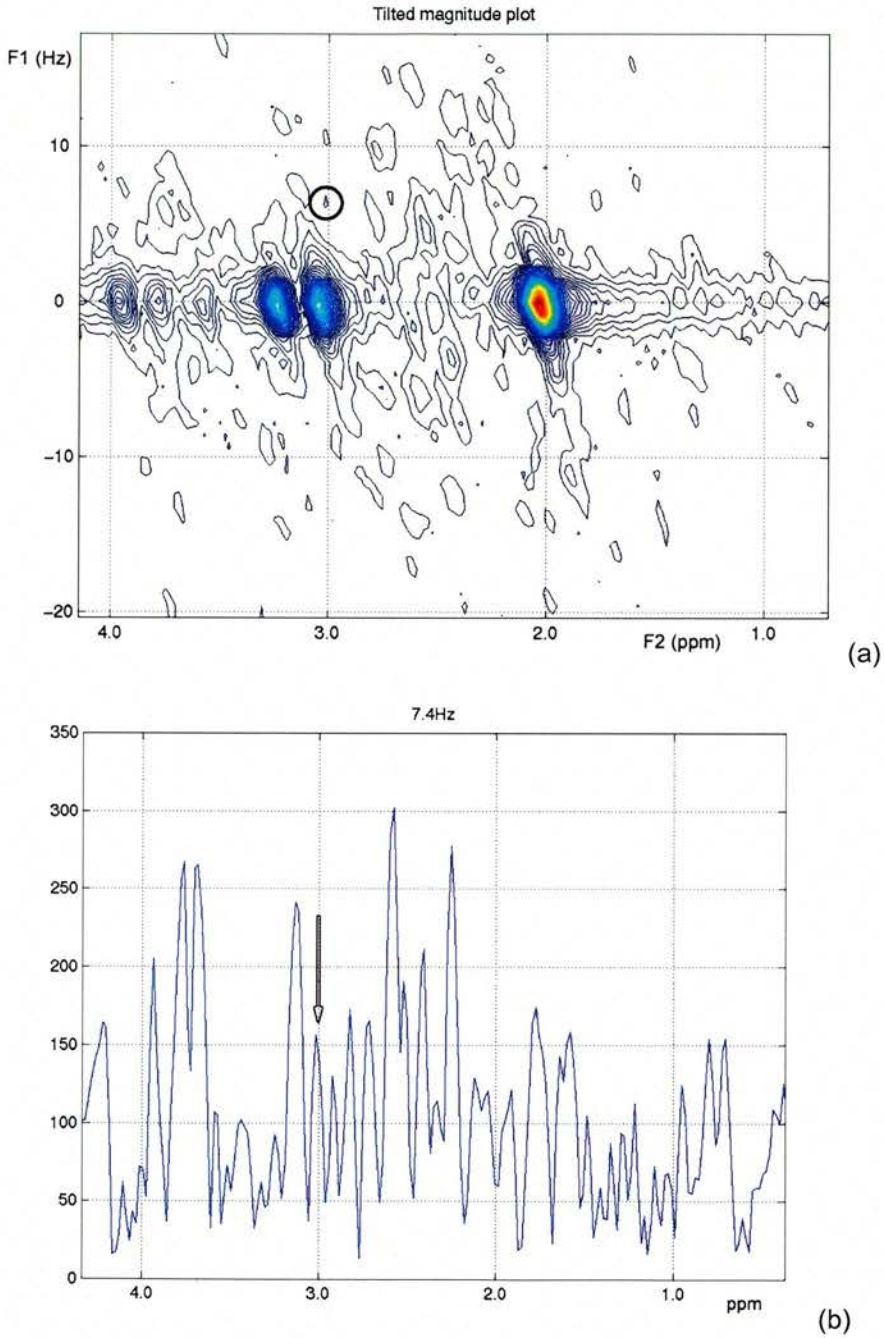

Figure 8.1 (a) 2D J-resolved spectrum and (b) extracted GABA row from a normal healthy volunteer scanned at 1.5T using the acquisition parameters listed in Table 8.1. The arrow indicates the GABA+ resonance since TE_{start} = 35ms.

8.2.3 Discussion

After all the preparatory *in-vitro* work, it was interesting to finally see the spectra resulting from the 2D J-resolved experiments *in-vivo*. It was disappointing that in no experiment, a clear and distinct GABA peak was resolved (comparable to those acquired *in-vitro*), although the results were no worse than the 2D J-resolved spectra presented in the literature (24,27). In both these examples cited, a peak assignment to GABA at 3.01ppm was made, without acknowledging any macromolecule contribution, despite both studies using a TE_{start} = 35ms. Thus, direct comparison between the published results and those presented here would suggest that *in-vivo* GABA measurement is possible. However, the final stage before applying this technique to a patient population is to determine if the *in-vivo* reproducibility is sensitive enough to allow physiological changes to be detected. This issue is addressed in the next section.

8.3 *In-vivo* reproducibility

8.3.1 Introduction

Before applying this method to a patient population, it was important to establish the reproducibility of the 3.01ppm GABA plus macromolecule peak in a normal healthy volunteer. Since in an abnormal population, the assumption of unchanging macromolecule baseline cannot be made (42,44,87), it was also vital to evaluate the results from 2D J-resolved experiments arising from a TE_{start} = 55ms.

Since 2D J-resolved MRS can be used to measure metabolites other than GABA, it was also important to gain some measure of the reproducibility of the technique - both acquisition and associated post-processing protocol - *in-vivo*. Therefore, the peaks from the commonly studied metabolites NAA, choline and creatine were quantified following 2D J-resolved MRS. At high concentrations, and free from significant overlap from other metabolites, these will provide a measure of the best achievable reproducibility using this technique *in-vivo*.

8.3.2 Scanning protocol

A measure of the "within-run" reproducibility was obtained by scanning the same volunteer three times in succession. Although a "between-days" measure may be more clinically relevant, the within-run protocol ensures that real physiological changes do not contribute to any variation. Thus, a best-case indication of *in-vivo* reproducibility was calculated. Only three experiments were performed to make the protocol more volunteer-friendly!

A single healthy volunteer was recruited for the experiment and informed consent was obtained. The volunteer was set-up on a 5" GP coil using the purpose built headrest. A 3-plane localiser was acquired, on which a 3x3x3cm^3 VOI was positioned in the occipital cortex for both 1D MRS and 2D J-resolved MRS. A 1D PRESS spectrum was acquired before 2D MRS to ensure appropriate VOI placement and the collection of good quality spectra. In addition, the voxel size and placement was chosen to ensure a 4Hz linewidth after shimming. Once satisfied that the VOI had met all these conditions, this same volume was excited in all spectroscopy experiments. Three 2D J-resolved MRS experiments were performed consecutively in the same VOI, using the acquisition parameters listed in Table 8.1. A total scanning time (including 3-plane localiser and 1D MRS) of 2.5 hours was required.

8.3.3 Post-processing

Initial post-processing was performed as was described in §5.2.3. For quantification in MRUI, a new set of prior knowledge files was created to allow quantification of the J = 0Hz NAA, choline and creatine peaks. Two 2D J-resolved spectra from each experiment were produced: One with a TE_{start} = 35ms and the second with TE_{start} = 55ms. The GABA peak at 3.01ppm was quantified from both spectra in all three experiments in MRUI, using prior knowledge from previous *in-vitro* results and guidance from existing published work.

CVs were calculated for the three main metabolites in the extracted J = 0Hz spectra and the GABA peak at 3.01ppm in the extracted J = 7.45Hz row.

8.3.4 Results

The results obtained following quantification are shown in Table 8.2. An example set of results are presented in Figure 8.2 with a TE_{start} = 35ms and the corresponding spectrum from a TE_{start} = 55ms in Figure 8.3.

Table 8.2 Within-run reproducibility results from three consecutive *in-vivo* 2D J-resolved experiments on one subject (NB All metabolite peak areas are given in arbitrary units).

TE_{start} (ms)	J (Hz)	Metabolite	Experiment			mean	SD	CV (%)
			1	2	3			
35	0	choline	2.97	2.83	3.31	3.04	0.25	8.13
35	0	creatine	2.55	2.92	2.92	2.80	0.21	7.64
35	0	NAA	6.85	6.92	7.35	7.04	0.27	3.85
35	7.4	GABA	0.10	0.12	0.07	0.10	0.03	26.03
55	7.4	GABA	0.09	0.08	0.05	0.07	0.02	28.39

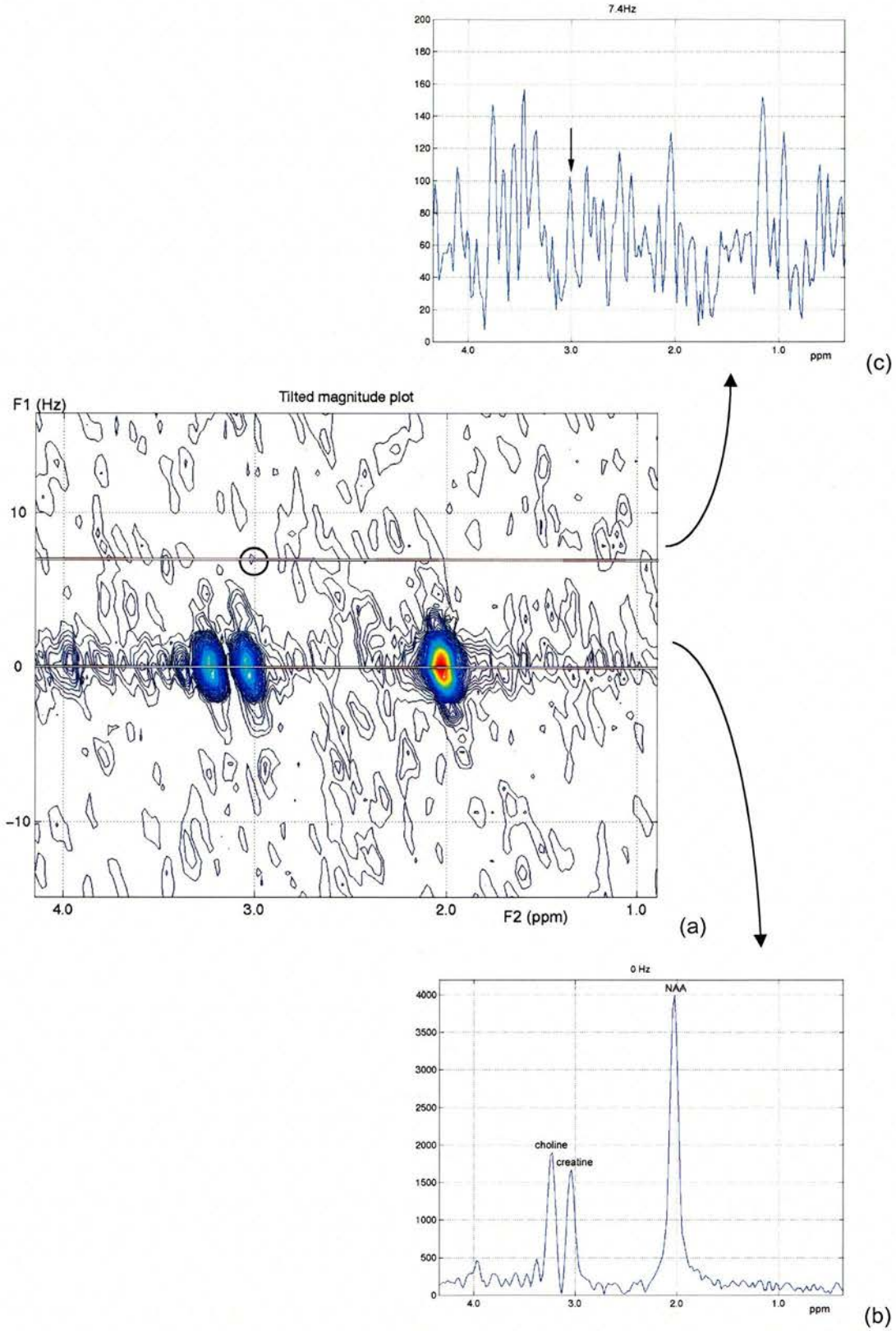

Figure 8.2 Set of *in-vivo* results from the within-run reproducibility experiments with TE_{start} = 35ms (a) 2D plot; (b) extracted J = 7.4 Hz row (c) extracted J = 0 Hz row. GABA+ is indicated by the circle and arrow in (a) and (c).

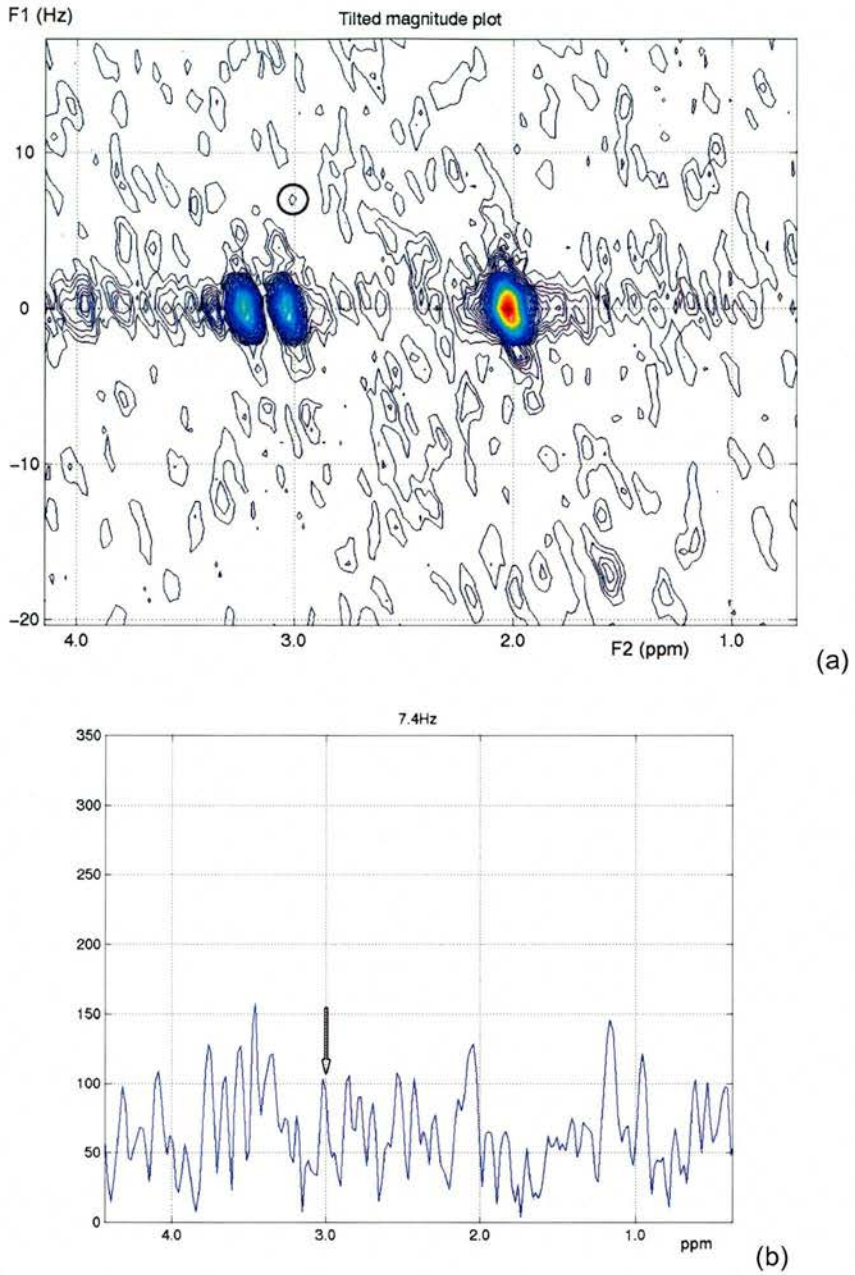

Figure 8.3 The same set of *in-vivo* results from the within-run reproducibility experiments as Figure 8.2 with TE_{start} = 55ms (a) 2D plot; (b) extracted J = 7.4 Hz row. GABA is indicated by the circle and arrow in (a) and (b).

8.3.5 Discussion and conclusion

Reassuringly, the reproducibility of the three main metabolites (that is choline, creatine and NAA) in the J = 0Hz extracted spectra were all within ± 10%. This suggests that in general, 2D J-resolved MRS is a repeatable technique when applied *in-vivo*.

The results from the 2D spectra with a TE_{start} = 35ms provided a CV for measurements of the 3.01ppm "GABA" peak of 26%. This is comparable to the *in-vitro* results presented in §7. However, as has been previously noted, this peak also contains contribution from macromolecules, so cannot be assigned only to GABA. By delaying the onset of the 2D experiment until a TE_{start} = 55ms, then the macromolecule contribution is reduced. However, the resulting peak at 3.01ppm is almost indistinguishable from the surrounding noise, as indicated in both the 2D spectrum and extracted row, Figure 8.3. As expected, the peak areas are reduced when compared to their counterparts with a TE_{start} = 35ms, Table 8.2, and there is a decrease in the reproducibility indicated by a CV of almost 28%. This suggests that the GABA plus macromolecule measurement may be the more reproducible to make, corresponding to a TE_{start} = 35ms, although in patients, changes in the macromolecule baseline cannot be ignored.

8.4 Problems with *in-vivo* acquisition of 2D J-resolved MRS

8.4.1 Introduction

The comparatively poor appearance of GABA in the *in-vivo* 2D J-resolved spectra was poorly predicted by the *in-vitro* results. This may be due to a number of reasons, including differences in linewidth and metabolite relaxation times between *in-vitro* and *in-vivo* samples. This section discusses each of these issues in turn and offers possible solutions for improvement, where applicable.

8.4.2 Signal to noise ratio

SNR is always the limiting factor when performing MRS using a clinical MRI scanner. Fundamentally, MRS is an insensitive technique, with the recorded signal arising from metabolite protons that only exist in concentrations of between 1mM and 20mM. Techniques to improve the metabolite signal include increasing the number of signal averages (§6.4) increasing the magnetic field (§8.5) or lowering the temperature (67). Clearly, in human subjects, the latter option is not possible. Additional factors that reduce the sensitivity of *in-vivo* spectra compared to *in-vitro*

signals include T_2^* relaxation, reducing the length of the detected FID, and signals arising from the many complex metabolite spin-systems other than those modelled *in-vitro*. These are inherent characteristics of the biological system under study, over which the operator has no control, and give rise to the dramatic differences in the SNR of phantom and human spectra. Despite this, it was of interest to explore the extent to which these factors affect 2D J-resolved spectra.

8.4.2.1 Relaxation effects

Throughout the thesis, it has been acknowledged that no attempt has been made to replicate *in-vivo* relaxation times. Basic spin physics theory has shown us that the rate of decay of an FID is given by $1/T_2^*$ and so has components from magnetic field inhomogeneities and spin-spin relaxation. With the phantom chemicals in free solution, the energy exchange required for T_2 relaxation is less efficient than for similar molecules confined within the anatomy of the brain, so the *in-vitro* T_2 times are longer. Since B_0 inhomogeneities will exist in all experiments, it was important to establish how the differences in relaxation times effect the end results of GABA quantification in 2D J-resolved MRS. For this purpose, the T_2 of creatine was calculated for both *in-vitro* and *in-vivo* experiments.

Using existing data from previously run 2D J-resolved experiments, a standard approach for T_2 measurement was taken (94). That is, the creatine peak area was measured over a range of TEs, whilst keeping the TR constant (as in a standard 2D J-resolved experiment), and the results fitted to Equation 8.1. Since 66 spin-echoes were collected for each single 2D J-resolved experiment, the creatine peak area was quantified for all resulting 1D spectra, and an exponential function fitted in Excel (Microsoft Corporation). This method was applied to two sets of three consecutive 2D experiments, one from a within-run phantom experiment and the other from the within-run volunteer experiment. The 3.0ppm creatine peak was chosen since it is a singlet and so does not participate in homonuclear coupling, which complicates the appearance of the spectra with changing TE.

$$S = S_0 \exp\left(\frac{-TE}{T_2}\right)$$

Equation 8.1 T_2 measurement where S = measured signal at each TE and S_0 = measured signal at the shortest TE (94).

It is possible to model T_2 relaxation using a multiexponential decay curve, to allow for the different relaxation components within the VOI, and include a correction factor to take account of noise (161). However, such forms of Equation 8.1 were not included to allow direct comparison between these results, and those previously obtained on the same scanner (162).

The results following quantification of the creatine peak in all 1D spectra from the three 2D J-resolved experiments are shown in Figure 8.4 and Figure 8.5 from the *in-vitro* and *in-vivo* experiments respectively. The T_2 times calculated from the mean results of each data set are presented in Table 8.3, with equivalent published values for comparison.

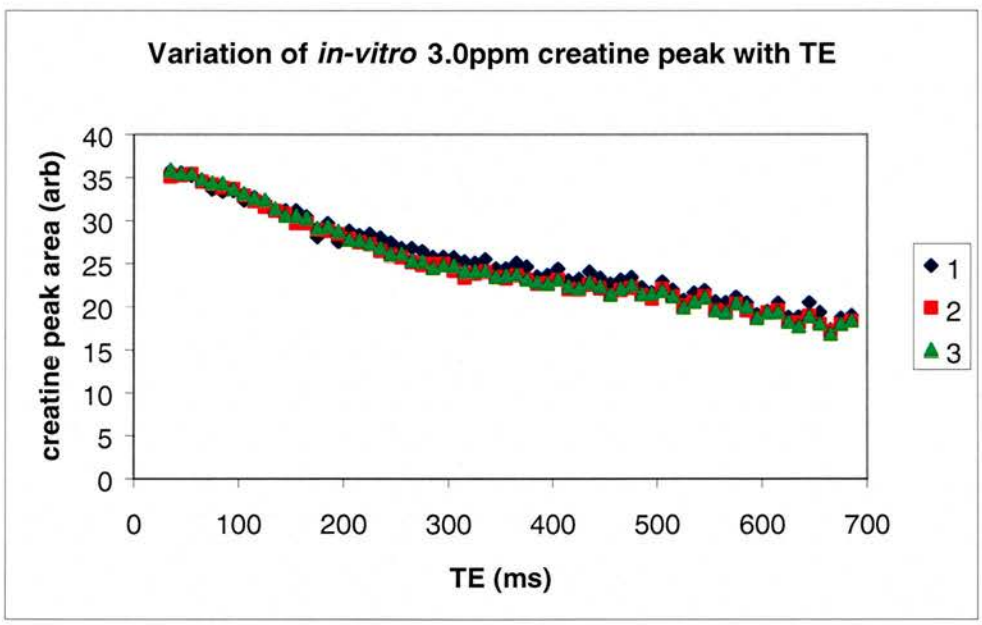

Figure 8.4 Quantification of creatine peak areas (from MRUI) for all 1D spectra comprising 2D J-resolved experiment. Acquired from 3x3x3cm^3 VOI in a phantom containing physiological concentrations of choline, creatine and GABA (3mM, 9mM and 1.2mM respectively). Data from three consecutive 2D J-resolved experiments all using a 5" surface coil.

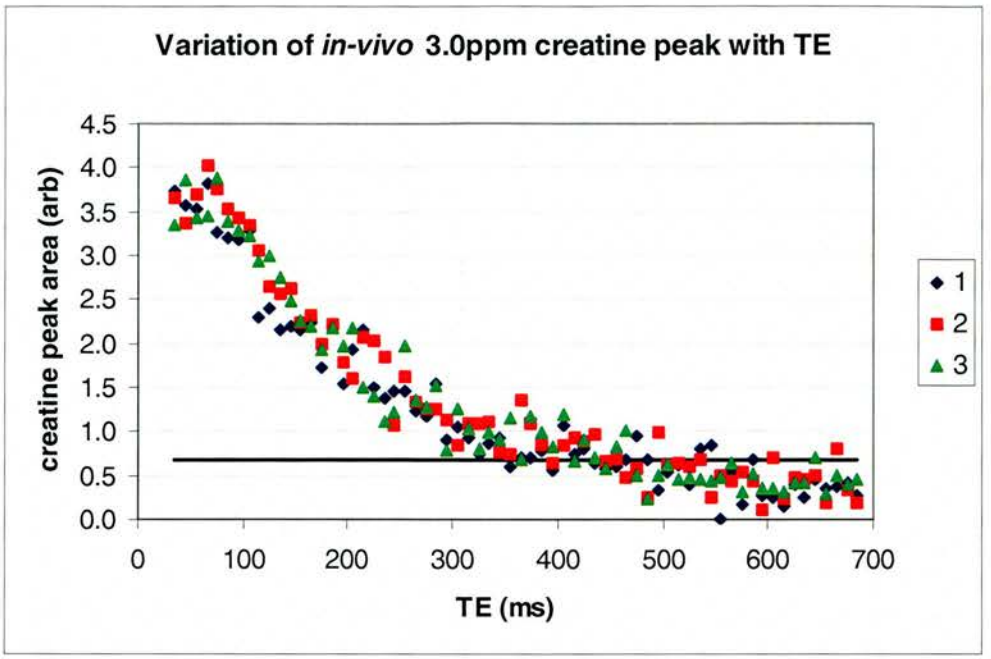

Figure 8.5 Quantification of creatine peak areas (in MRUI) for all 1D spectra comprising 2D J-resolved experiment. Acquired from 3x3x3cm^3 VOI in the occipital cortex of a healthy volunteer. Data from three 2D J-resolved experiments all using a 5" surface coil. The solid black line indicates the mean noise quantified.

Table 8.3 Comparison of results of measured creatine T_2 from this work, and published results from Soher *et al* and Bruce, S.D. In both cases, the published data was acquired on a 1.5T GE scanner, with that from Bruce on the same scanner as used for the work in this thesis

Source	creatine T_2 (secs)	
	in-vitro	*in-vivo*
Mean experimental result	0.97	0.27
Soher *et al* (94)	0.61	0.21
Bruce, S D (162)	0.87-1.00	N/A

There is very good agreement between the results from this practical work and the published data. The T_2 values calculated on the centre's MRI scanner are longer than those by Soher *et al* since Soher's phantom was doped with nickel chloride which will reduce the relaxation times. The T_2 times from both the *in-vivo* experiments are also in excellent agreement, thereby validating the in-house measurement results.

As expected, the T_2 of creatine *in-vitro* is much longer than *in-vivo*, the result of which is the acquisition of metabolite information, with a good SNR, in all 64 (or 66) spin-echoes of the 2D J-resolved experiment. This is demonstrated in Figure 8.4

with just under half of the creatine signal remaining even in phantom experiments with TEs of 665ms. From Figure 8.5 it is clear that the much shorter *in-vivo* creatine T_2 leads to quicker dephasing of the FIDs so at about TE = 485ms, all useful signal has been reduced to the level of noise. With similar patterns expected in the other metabolites, including GABA, it is small wonder that *in-vivo* measurements are so much harder to make.

8.4.2.2 Linewidth

The natural linewidth of a spectrum is determined by the T_2 relaxation of the metabolites and the inhomogeneities of the main magnetic field, B_0, Equation 8.2. Thus, the spectral lines from immobile macromolecules have much broader linewidths than those from the more highly mobile metabolites, even in the absence of magnetic field inhomogeneities. The combined effects of T_2 relaxation and B_0 inhomogeneities result in increasing linewidths of all the spectral components, reducing the spectral resolution and eventually causing all peaks to merge into an unreadable spectrum.

$$FWMH(Hz) = \frac{1}{\pi T_2 *}$$

Equation 8.2 Definition of natural linewidth of spectral lines in terms of the full width at half maximum (FWHM), where T_2* is the effective relaxation resulting from inhomogeneities of B_0 and the transverse relaxation of the metabolites, (70).

Active shimming of the magnet is essential in spectroscopy to improve the homogeneity of B_0, and to allow the very small changes in frequency associated with the metabolite resonances to be observed. By ensuring a uniformly homogeneous field across the spectroscopy volume, spectra of the narrowest linewidth and highest SNR are obtained.

Successful shimming relies on a small, well-defined VOI, in a homogenous environment. With the *in-vitro* spectra obtained in such a setting, it is clear why linewidths of 2Hz were achieved. However, with the anatomical variations that exist in a human head, and an MRI system with only 1st order shim coils, such a narrow linewidth is unachievable.

The linewidths of all *in-vivo* experiments were 4Hz, which in general spectroscopy terms, is very good. This was often achieved only after moving / resizing the VOI and / or repeated shimming of the volume. To appreciate how this 2Hz linewidth difference between the *in-vivo* and *in-vitro* work contributed to the lack of GABA measurement *in-vivo*, a series of *in-vitro* experiments with a phantom containing 1.2mM GABA was performed, with linewidths increasing from 2Hz to 5Hz, Table 8.4.

The poorer linewidths were achieved by moving the same voxel closer to the edge of the phantom. First in one dimension (i.e. positioned on the central slice but closer to the bottom of the phantom) and then in two (i.e. moving the VOI superiorly through the slices so it bordered the phantom edge on two sides). Care was taken to ensure that the entire VOI was contained within the phantom so that no signal loss could be attributed to a smaller *actual* VOI.

Four 2D J-resolved spectra were acquired and processed as described in §5, and the results from these experiments are summarised in Table 8.4.

Table 8.4 Summary of results from investigation on linewidth on measured 1.2mM GABA signal *in-vitro*

linewidth (Hz)	TE_{start} (ms)	ΔTE (ms)	TR (ms)	NEX	GABA peak area (arb)		
					3.01ppm	2.28ppm	1.89ppm
2	35	10	2000	16	0.71	0.83	0.10
3	35	10	2000	16	0.30	0.29	0.10
4	35	10	2000	16	0.19	0.24	0.05
5	35	10	2000	16	0.19	0.13	0.08

The results from quantification of all three GABA peaks show a general trend of decreasing area with increasing linewidth. Focusing in on the peak of interest, there is a dramatic reduction in the 3.01ppm GABA peak from 2Hz to 3Hz, with further reductions as the linewidth increases further.

Study of standard 1D spectra from the outer limits of the linewidths investigated show huge differences in the quality of spectra, as one would expect, Figure 8.6: With a linewidth of 2Hz and GABA at a concentration of 1.2mM GABA, only a small peak at 2.28ppm is observed. It is also clear from this spectrum, that there has been good removal of the residual water peak, leaving an undistorted baseline. This is not true in the spectrum obtained with a 5Hz linewidth, with evidence of a large residual water peak and an uneven baseline. This is probably due to a combination of poor shimming on the badly positioned VOI. Consequently, the 2.28ppm GABA peak is less obvious above the noise, and so it is no surprise that the 2D J-resolved spectra are degraded.

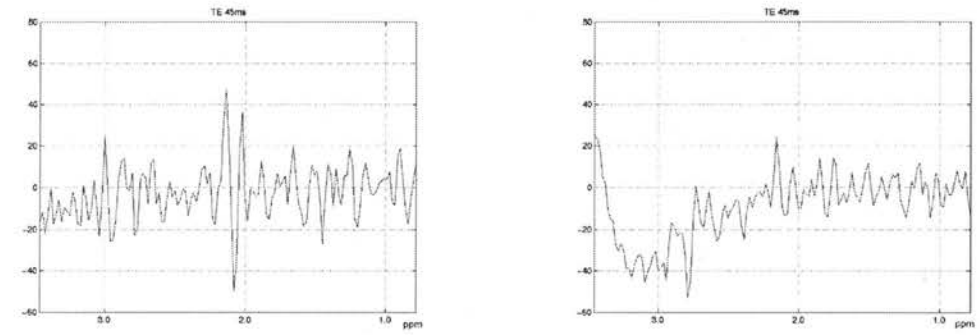

(a) (b)

Figure 8.6 Conventional 1D spectra from same phantom containing 1.2mM GABA only with a linewidth of (a) 2Hz and (b) 5Hz.

The 2D spectra and corresponding extracted GABA rows with varying linewidth are shown in Figure 8.7. The results from the *in-vitro* experiments with a 4Hz linewidth are shown to try to replicate the effects seen *in-vivo*. The spread of the residual water peak is immediately obvious in the spectra with the larger linewidth, with its presence contaminating the entire spectrum at J = 0Hz.

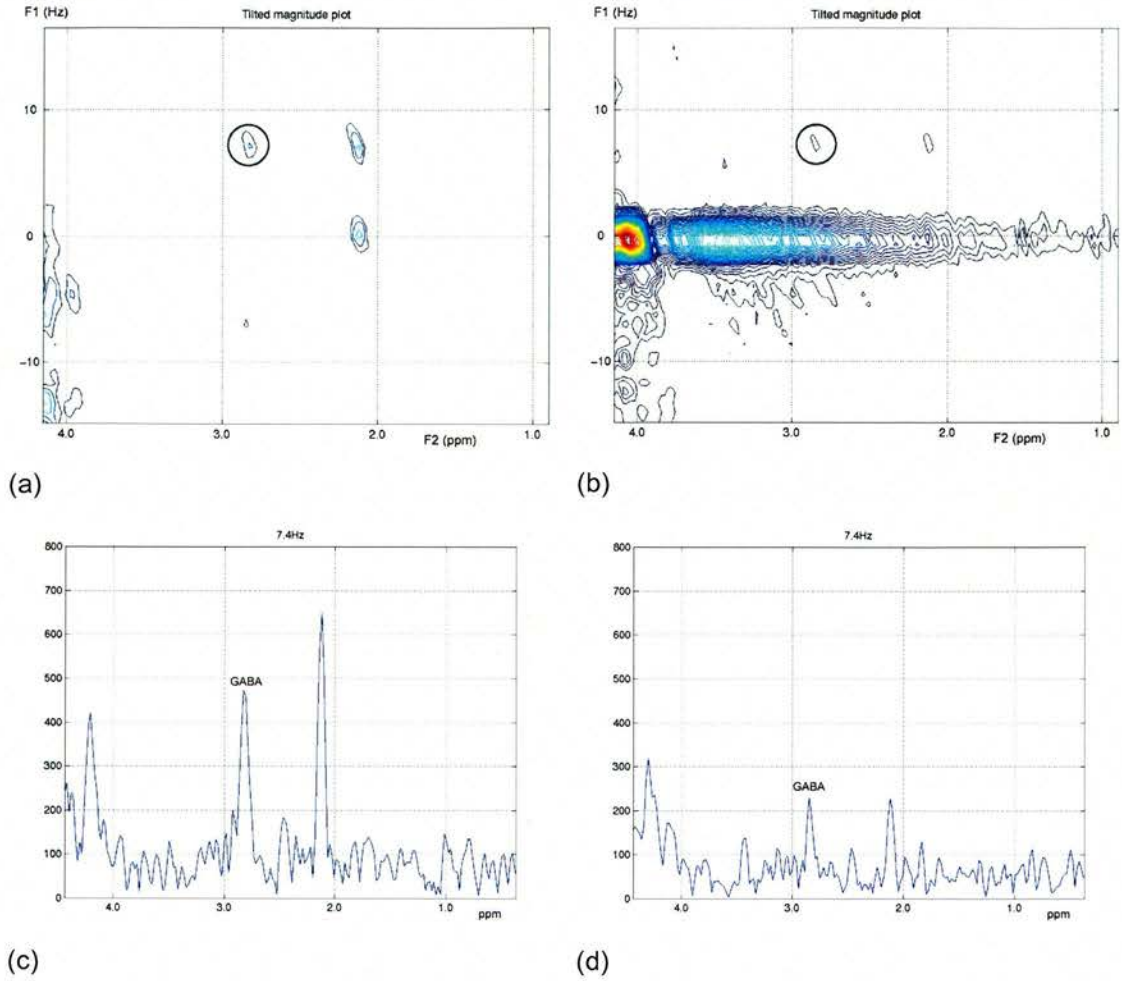

Figure 8.7 Resulting 2D J-resolved spectra and extracted GABA rows (J = 7.45Hz) from the same phantom containing 1.2mM GABA with a linewidth of 2Hz ((a) and (c) respectively) and 4Hz ((b) and (d) respectively).

In the extracted spectra, two distinct GABA peaks, corresponding to 3.01ppm and 2.28ppm are clearly seen in Figure 8.7 (c), acquired with a linewidth of 2Hz. In the equivalent spectrum at 4Hz linewidth, the 3.01ppm GABA peak is approximately a quarter of the same peak at 2Hz, Table 8.4. Thus improper voxel positioning and spectral line broadening has an extremely detrimental effect on the resulting 2D spectra and on the ability to accurately quantify the metabolites in the extracted J = 7.45Hz row. With such increases in linewidth recorded *in-vivo*, it is likely that the increase in linewidth also impaired identification of GABA.

8.5 2D J-resolved MRS at 3T

8.5.1 Introduction

The results from §8.2 do not suggest that GABA can be confidently measured *in-vivo*. With some of the most obvious limiting factors being the lack of SNR and chemical shift (F2) resolution, an obvious solution was to perform the experiment at a higher field strength.

Through the collaboration with Dr. N. Sailasuta, the author of the dedicated 2D J-resolved sequence, *in-vivo* data at 3T using this same sequence was acquired. The experiments were all performed by Dr. Sailasuta at GE Healthcare in California, and the raw p-files were sent here for processing using the methods outlined in §5.2.3.

8.5.2 Scanning protocol

All experiments were performed on a GE 3T scanner using a standard volume head coil. Three volunteers with possible elevated levels of GABA were recruited from a mood study to undergo 2D J-resolved MRS. The scan parameters used in each case are listed in Table 8.5.

Table 8.5 Acquisition parameters for 2D J-resolved in-vivo experiments performed at 3T

Scan parameters	Volunteer		
	A	B	C
TE_{start}	35	35	35
Δ TE	2.5ms	2.5ms	2.5ms
steps2d	64	128	64
NEX	4	4	16
TR	2000ms	1500ms	1500ms
coil	volume head	volume head	volume head

8.5.3 Results

The 2D spectra and corresponding extracted GABA rows are provided in Figure 8.8 to Figure 8.10. Disappointingly, in no case could the spectral assignment be made to the 3.01ppm GABA peak.

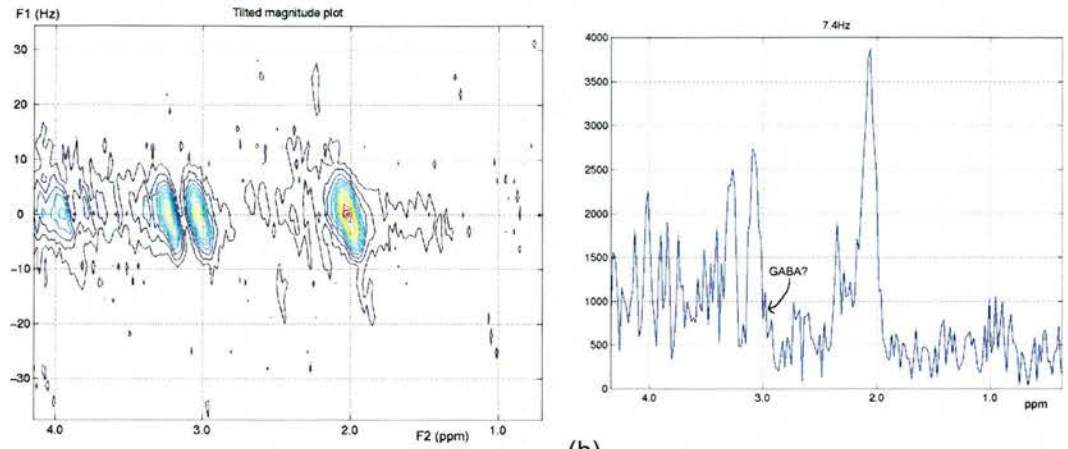

Figure 8.8 (a) 2D J-resolved spectrum from volunteer A and (b) corresponding extracted GABA row. Experiment performed at 3T – see Table 8.5 for details.

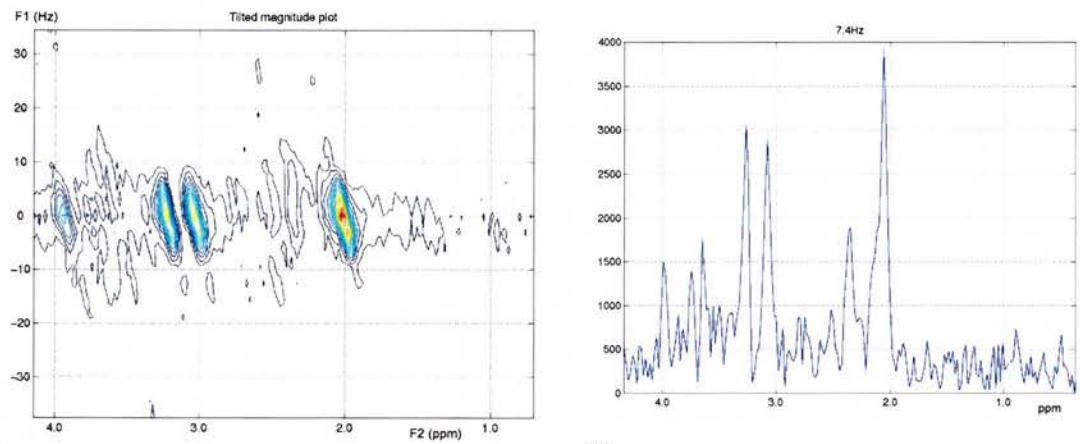

Figure 8.9 (a) 2D J-resolved spectrum from volunteer B and (b) corresponding extracted GABA row. Experiment performed at 3T – see Table 8.5 for details.

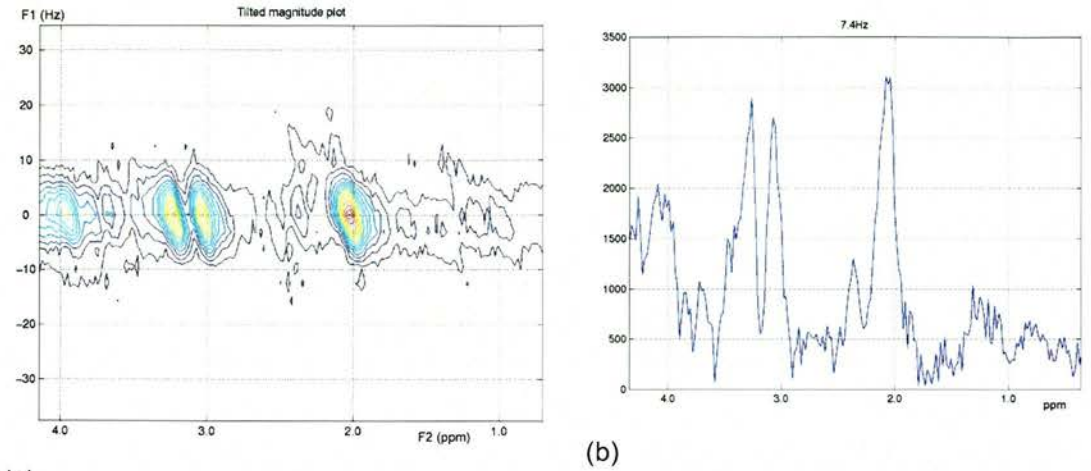

(a) (b)

Figure 8.10 (a) 2D J-resolved spectrum from volunteer C and (b) corresponding extracted GABA row. Experiment performed at 3T – see Table 8.5 for details.

8.5.4 Discussion and conclusions

The *in-vivo* results obtained at 3T are all very disappointing as in no example was the 3.01ppm GABA peak identified. This may be due to a variety of reasons specific to the protocol used, in addition to the general problems of the technique, §8.4.

In all cases, the volume head coil was used which, as shown in §6.2, has a poorer sensitivity than a surface coil. However, it is disappointing that even at 3T, with the increased SNR, GABA is undetectable.

The F1 resolution may also contribute to the lack of GABA results. Using the optimum protocol described in §6.4, an F1 resolution of 0.78Hz / frame of data is achieved after zero filling. The spectra from volunteers A and C had an F1 resolution of 3.13Hz after zero filling and with the increased number of TEs acquired for volunteer B, the F1 resolution was 1.56Hz. Consequently, the extracted spectra from volunteers A and C were at a J-coupling frequency of ~6Hz, which may be distant enough from the ideal 7.45Hz to prevent GABA detection. Although the F1 resolution was better for volunteer B, a GABA peak still remained undetected, but the quality of the spectra may have also contributed towards this. The spectra from volunteers A and B were collected under a previous software version, with the oldest acquired almost two years ago, and they are clearly much noisier than the later

spectra for volunteer C and even the spectra acquired at 1.5T. An important difference between this and the data acquired at 1.5T is the NEX: At 1.5T, a NEX = 16 was used, but at 3T only a NEX = 4 was applied. As explained in § 6.4, a NEX of eight means that all three RF pulses are phase cycled to eliminate any undesirable signals, in a total of eight combinations. Therefore, when NEX = 16 is applied, the phase cycle is repeated for a second time. A NEX = 2 indicates that only the first RF pulse is phase cycled so that the data frame consists of an average of two excitations. Thus, the NEX used in the 3T experiments (NEX = 4), implies that this phase cycling scheme has been repeated so that the final signal is averaged from four excitations. Clearly, this will have a detrimental effect of the final spectra.

The F1 bleed observed in the spectra may also indicate scanner instability, although since the system is used for GE's own research, it is hoped not! Another possibility could be patient movement during acquisition. The spectra were all acquired from patients, who may not be as used to being scanned as the volunteers recruited locally for study on the 1.5T system. Any patient movement during the scan may have given rise to phase variations in the spectra, which may have contributed to the poor spectral quality.

Without direct access to a 3T scanner on which to perform 2D J-resolved experiments, the author was unable to exactly replicate the experimental work performed at 1.5T. The 3T data presented was acquired as part of a patient study, also looking at *in-vivo* GABA levels, and the author is grateful for the opportunity to work with higher-field spectra. It is disappointing that the datasets were not of a better quality to help with the detection of GABA.

9 2D L-COSY for GABA measurement

9.1 Introduction

Although the 2D J-resolved spectra presented in the previous chapter suggested that *in-vivo* GABA measurement was possible, the results – and particularly those minimising macromolecule contributions – were not entirely convincing. Therefore, an alternative method of GABA measurement at 1.5T was investigated. Compared to spectral editing techniques, 2D methods have the advantage of acquiring information from all metabolites, and so it was desirable to attempt GABA measurement using another 2D technique. This would ensure that even if assignments to GABA resonances were not made, there was still an abundance of data pertaining to the other metabolites, allowing different measurements and comparisons to be made.

Collaborative work with Dr. M. Albert Thomas, University of California, facilitated access to a 2D Localised-COSY sequence (2D L-COSY) that had previously been applied on GE scanners at both 1.5T and 3T with encouraging results (20,21,133).

The author is grateful to Dr. Thomas for sharing his sequence, and in doing so, for allowing the practical work presented in this chapter.

As the only chapter on 2D L-COSY, the following sections describe the initial single metabolite experiments to validate the acquisition and post-processing protocols. In keeping with previous investigations of GABA measurement, preliminary results from experiments determining the threshold of GABA detection and the reproducibility of its measurement are also discussed. In addition, the first *in-vivo* results are presented.

9.2 Sequence description

9.2.1 Background

For a general description of COSY, including its basic pulse sequence, the reader is directed to §3. Localised COSY (L-COSY) was performed using the sequence shown in Figure 9.1, comprising of a series of 90° - 180° - 90° RF pulses. From the general description of a 2D sequence as provided in §2, the first excitation and refocusing pulse form the preparation period, with the mixing period comprising the second 90° pulse. The evolution and detection periods are designated t_1 and t_2 respectively. Water suppression was achieved with the application of CHESS immediately before 2D L-COSY.

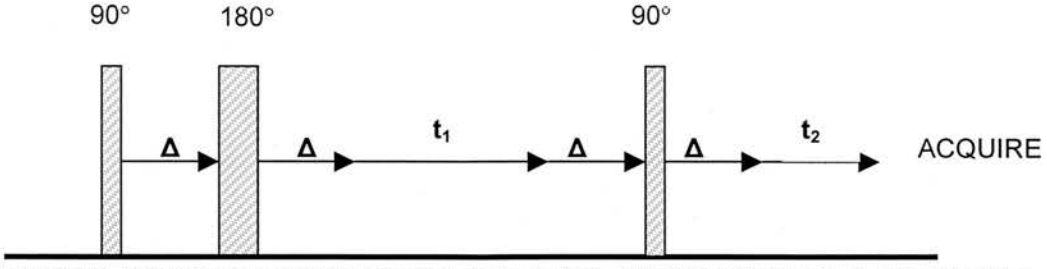

Figure 9.1 L-COSY pulse sequence as described in (21). The evolution time, t_1, is uniformly incremented to provide the required spectral width in the second dimension (F1). The detection period is denoted by t_2. Δ represent the minimum rise time of the gradients.

As with the dedicated 2D J-resolved sequence, the version of 2D L-COSY acquired for this work was also a research sequence. However, unlike the 2D J-resolved

sequence that only required manipulation of the user CVs after voxel prescription, far more user interaction was needed to run COSY. This included manual shimming to optimise the spectroscopy signal and water suppression. To aid this process, a conventional, single-voxel PRESS experiment was performed prior to COSY from which the optimisation parameters (e.g. transmitter gain) could be obtained from the automatic prescan. The manual prescan is described in more detail in the next section.

The FIDs arising from COSY acquisition contain both in-phase and anti-phase components, and so are displayed in magnitude mode, in a similar way to the 2D J-resolved data. A post-processing protocol was chosen to replicate that used by Thomas *et al*, (21,133). In contrast to the post-processing applied to raw data from 2D J-resolved FIDs, no phase correction or removal of the residual water peak occurred. The application of a shifted, skewed, squared sine-bell apodization function meant that affects from the higher intensity section of the water signal were considerably reduced. Thus further post-processing of the water peak was unnecessary.

9.2.2 Scanning protocol

All experiments were performed on a 1.5T GE Signa Horizon scanner operating in research mode and using a 5" surface coil. Prior to 2D L-COSY acquisition, a 1D PRESS experiment was performed in the defined VOI to evaluate the quality of the spectra and to provide baseline settings for the manual prescan preceding 2D L-COSY. The transmitter gain (TG) set during the automatic PRESS prescan was noted.

After loading the COSY sequence, prescription of the spectroscopy voxel and setting of the initial timing parameters was completed on the scan desktop, as with conventional 1D spectroscopy. To allow the manual prescan to be completed in the shortest possible time, both the total number of scans and NEXs were minimised during the initial sequence set-up.

Manual pre-scan involved setting the TG and receiver gains, after which the voxel was shimmed by adjusting the gradients using the slider bars on the manual prescan screen. With a magnitude display of the FID on the screen, optimisation progressed until the maximum water signal was obtained.

Once satisfied with the appearance of the water signal, the next step was to optimise the water suppression. Both the user CVs "sup" and "suppress" were set to one to activate the water suppression gradients and RF pulse respectively. Optimal suppression was achieved by changing the flip angles associated with the second and third water-suppression RF pulses. In practice, this was an iterative process achieved by viewing the FID in magnitude mode, and changing the values of the flip angles consecutively until maximum metabolite signal had been obtained.

The final part of the process was to modify the user CVs to reflect the values obtained in pre-scan optimisation (notably those of the water suppression flip angles), and to change the acquisition parameters to those more suitable for 2D L-COSY. For all initial *in-vitro* experiments, the parameters used for COSY as set *after* the pre-scan, are listed in Table 9.1, giving rise to a scan time of 25:52 minutes (excluding the pre-scan).

Table 9.1 Acquisition parameters used in 2D L-COSY

Variable	Meaning	Value
TE_{min}	Minimum echo time (ms)	30.008
TR	Repetition time (ms)	2000
specpts	number of complex points acquired per excitation	1024
specwidth	total frequency width (Hz)	2500
echomode	acquisition of a partial echo, where nearly a full echo is recorded in a shorter TE than that required for a full echo	1
dda	number of "dummy scans" acquired and discarded at the start of the sequence to achieve steady state during acquisition	4
opnex	determines phase cycling method (see §6.4 for details)	8
total_scans	total number of excitations for signal averaging	768
deltate2	t_1 increment (μs)	1600
ref_count	number of frames for water referencing	0
flip_rf02	flip angle of second water suppression pulse	as determined during manual prescan
flip_rf03	flip angle of third water suppression pulse	as determined during manual prescan

9.2.3 Post-processing protocol

The outcome of a 2D COSY experiment was a contour plot showing the correlations of J-coupled spins. As described in §3, both dimensions of the contour plot are in ppm, from which the chemical offset of both the diagonal peaks and, more significantly in terms of coupled molecules, the cross-peaks can be identified. Compared to 2D J-resolved MRS, the post-processing required to achieve this was minimal. A strategy was developed to replicate the post-processing carried out by M.A. Thomas's group to allow direct comparison between their work and the results produced here. To do this, the phase-correct and removal of the residual water peak functions were omitted from the Jresolved.c programme, used for initial post-processing of the 2D J-resolved raw data files, and so LCOSY.c performed the following:

i. Read in the raw p-file
ii. Scale the FIDs according to the pre-scan parameters (TG, receiver gains and spectroscopy voxel volume)
iii. Save the processed FIDs in a text file for further processing in Matlab (The Mathworks Inc).

In Matlab, LCOSY.m, executed the following main functions:

i. Zero-fill the raw data in both dimensions
ii. Simple sine-bell squared apodization in the F1 dimension
iii. Shifted, skewed squared sine-bell apodization in the F2 dimension to emphasise the cross-peaks in comparison to the diagonals (formulae obtained by I. Marshall from personal correspondence with M. A. Thomas)
iv. 2D Fourier Transform

Quantification of spectra extracted for specific cross-peak and diagonal peak areas was achieved in MRUI. In a similar method to the extracted J-resolved spectra, the rows of data were converted to the appropriate ascii format using GABA2DLCOSY.m for the F2 = 3.0ppm and F1 = 2.0ppm GABA peak. This cross-peak had been previously identified in published *in-vivo* data (133). The diagonal peaks from choline (F2 = 3.2ppm, F1 = 3.2ppm) and creatine (F2 = 3.0ppm, F1 = 3.0ppm) were quantified using cholcre2DLCOSY.m. Prior knowledge files were created from 2D L-COSY experiments on high concentration metabolite phantoms, thereby allowing the quantification process to be standardised.

9.3 Individual metabolite phantoms

9.3.1 Introduction

Preliminary validation of 2D L-COSY data acquisition (including the manual prescan) and post-processing protocol was performed using a series of individual phantom solutions. The resulting 2D spectra were then compared to examples provided in the literature.

9.3.2 Methods

2D L-COSY spectra were acquired using the protocol described in §9.2.2 and the raw data files were transferred to a Sun Ultra Workstation (Sun Microsystems, Mountain View, CA) for processing, §9.2.3.

Aqueous solutions of the commonly reported cerebral metabolites, at physiological concentrations, were made in 3.6 litre, glass spherical phantoms. GABA solutions were prepared at both physiological concentration (1.5mM) and at 10mM. All solutions were pH corrected to physiological pH (7.2) using a combination of sodium hydroxide and hydrochloric acid. No attempt was made to replicate physiological relaxation times.

9.3.3 Results

The 2D L-COSY spectra from the individual metabolite experiments of choline, creatine, glutamate, glutamine, myo-inositol and lactate are presented in Figure 9.2 to Figure 9.4. The corresponding results from both GABA concentrations are presented in Figure 9.5.

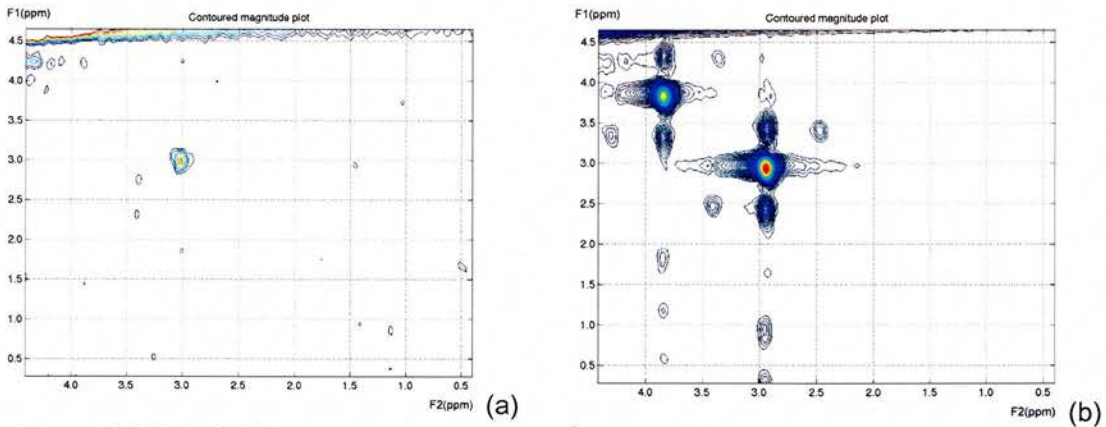

Figure 9.2 2D L-COSY spectra from a 3x3x3cm^3 VOI positioned in a phantom containing (a) 3mM choline (diagonal at F2 = F1 = 3.2ppm arising from the methyl protons). (b) 9mM creatine (diagonals at F2 = F1 = 3.0ppm and F1 = F2 = 3.9pmm; weak cross-peak at F2 = 3.9ppm, F1 = 3.0ppm). NB All cross-peaks quoted for below the diagonal (with all peaks shifted by ~0.1ppm in the room temperature phantoms).

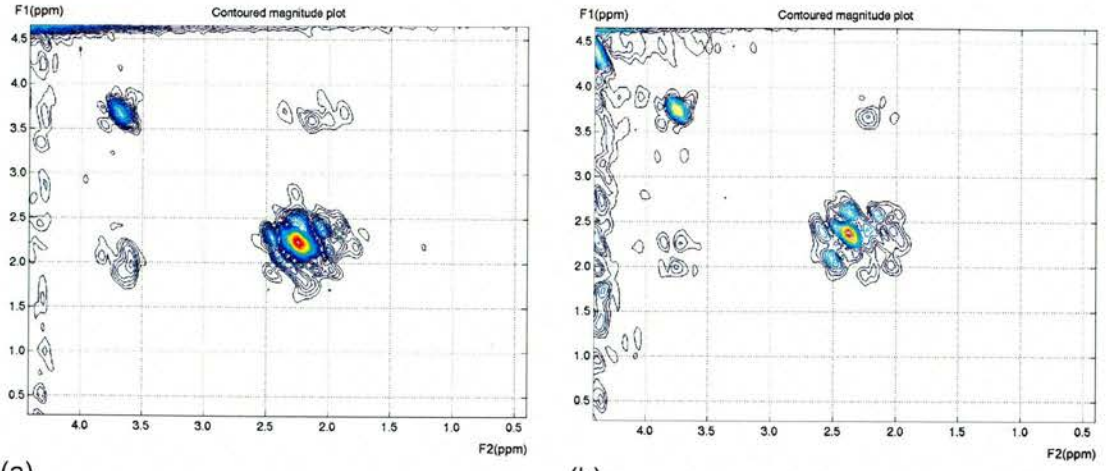

(a) (b)

Figure 9.3 2D L-COSY spectra from a 3x3x3cm^3 VOI positioned in a phantom containing (a) 12.5mM glutamate (diagonals at F2 = F1 = 2.4ppm and F2 = F1 = 3.7ppm; cross-peaks at F2 = 3.6ppm, F1 = 2.0ppm). (b) 5.8mM glutamine (diagonals at F2 = F1 = 2.5ppm and F2 = F1 = 3.8ppm; cross-peaks at F2 = 3.8ppm F1 = 2.1ppm). NB All cross-peaks quoted for below the diagonal (with all peaks shifted by ~0.1ppm in the room temperature phantoms).

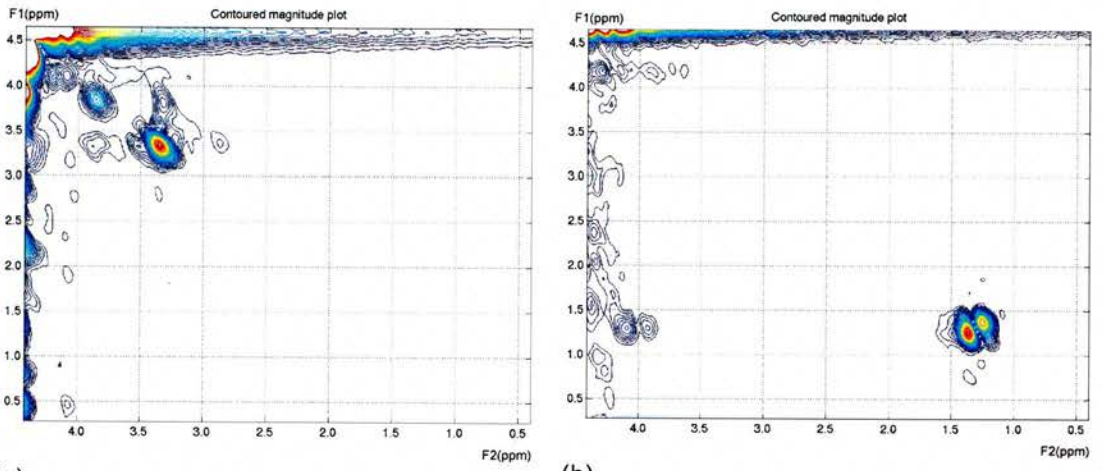

(a) (b)

Figure 9.4 (a) 8.1mM myo-inositol (diagonals at F2 = F1 = 3.5ppm and F2 = F1 = 4.0ppm; cross-peaks at F2 = 3.5ppm, F1 = 3.2ppm). (f) lactate (diagonal at F2 = F1 = 1.31ppm; cross-peak at F2 = 4.1ppm, F1 = 1.3ppm). NB All cross-peaks quoted for below the diagonal (with all peaks shifted by ~0.1ppm in the room temperature phantoms).

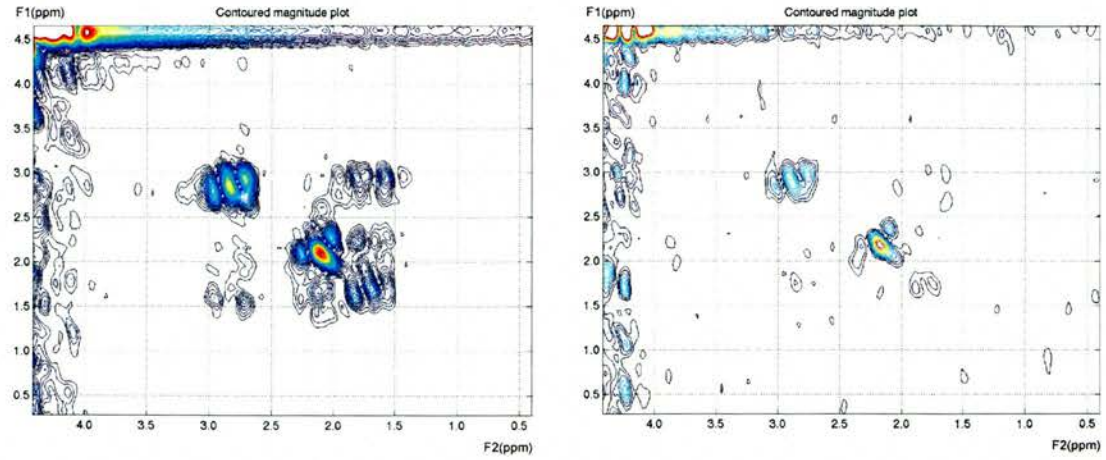

(a) (b)

Figure 9.5 2D L-COSY spectra from a 3x3x3cm^3 VOI positioned in a phantom containing GABA at (a) 10mM and (b) 1.5mM. In both spectra, the diagonals at F2 = F1 = 2.28ppm and F2 = F1 = 3.01ppm are visible. In the higher concentration phantom, the diagonals at F2 = F1 = 1.9ppm and the cross-peaks at F2 = 3.01ppm, F1 = 1.9ppm are more clearly seen. NB All cross-peaks quoted for below the diagonal (with all peaks shifted by ~0.1ppm in the room temperature phantoms).

9.3.4 Discussion and conclusions

The correlation patterns in the 2D L-COSY spectra are as predicted by the literature (20,21,124), thereby validating the technique as a whole. However, it should be noted at this point, that the quoted scan time of 25:52 minutes was rarely close to being achieved. Manual prescanning took, at best, five minutes, and at worst an extra 20 minutes - in all cases immediately following a standard single-voxel PRESS experiment. The prescan is a crucial step in the process, and will be of even greater importance *in-vivo* with the increased linewidths. However, an additional 20 minutes may not be tolerated by the subject, which brings into question the appropriateness of applying such a user-dependant method. This too, raises the issue of the reliability of the results, and specifically any reduction in reproducibility associated with the manual prescan. The results from a preliminary reproducibility study are discussed in §9.5.

9.4 GABA threshold

9.4.1 Introduction

As described in the 2D J-resolved MRS work in §4 and §5, it is important to determine the threshold of GABA measurement, to ensure that it falls within normal physiological levels. Therefore, a series of experiments were performed to establish the minimum GABA concentration detectable, *in-vitro*, using 2D L-COSY.

9.4.2 Materials and methods

Initially, all experiments were conducted following the scanning protocol described in §9.2.2 and using a 5" surface coil. 2D L-COSY spectra were acquired from a $3x3x3cm^3$ voxel centrally placed in the high signal region in the lower half of the phantom.

Seven phantoms containing physiological concentrations of choline and creatine (3mM and 9mM respectively) were made. GABA was added to three of these phantoms at higher than physiological concentrations (10mM, 5mM, 2mM), to ensure that it could be adequately detected in aqueous solution with choline and creatine. Three further phantoms were made to investigate GABA detection in normal physiological ranges (1.5mM, 1.2mM, 1.0mM, and 0.8mM). The aqueous solutions were made from dry masses of the chemicals (Sigma-Aldrich).

At the lower GABA concentrations, variations in acquisition parameters, including the use of a 3" surface coil, were investigated to aid detection of the metabolite. As discussed in §6, the SNR of the spectra can be improved by increasing the NEX and total number of scans. Since the number of FIDs acquired at different TEs is dependant on both these parameters in 2D L-COSY, Equation 9.1, both values need to be increased to ensure that a sufficient number of TEs are collected to perform COSY, at the same time as increasing the SNR. Therefore to increase the SNR and have 64 TEs for 2D Fourier Transform, NEX = 16 and total number of scans = 1024 were investigated in a scan time of 34:24 minutes.

$$number\ of\ TEs = \frac{total\ number\ of\ scans}{NEX}$$

Equation 9.1 Variation of number of TEs acquired for 2D L-COSY with the total number of scans and NEX.

Post-processing and quantification of the spectra followed the procedure described in §9.2.3.

9.4.3 Results

A summary of the results over all identifiable GABA concentrations is shown in Figure 9.6. Using the standard set-up (i.e. 5" surface coil and acquisition parameters as listed in Table 9.1), GABA was only detectable to 1.5mM. By increasing total number of scans and NEX, 1.2mM GABA was identified using the 5" surface coil. However, even with changing to the smaller surface coil and using the improved SNR acquisition parameters, cross-peaks from GABA at F2 = 3.01ppm, F1 = 1.9ppm at concentrations of neither 1.0mM nor 0.8mM were detected.

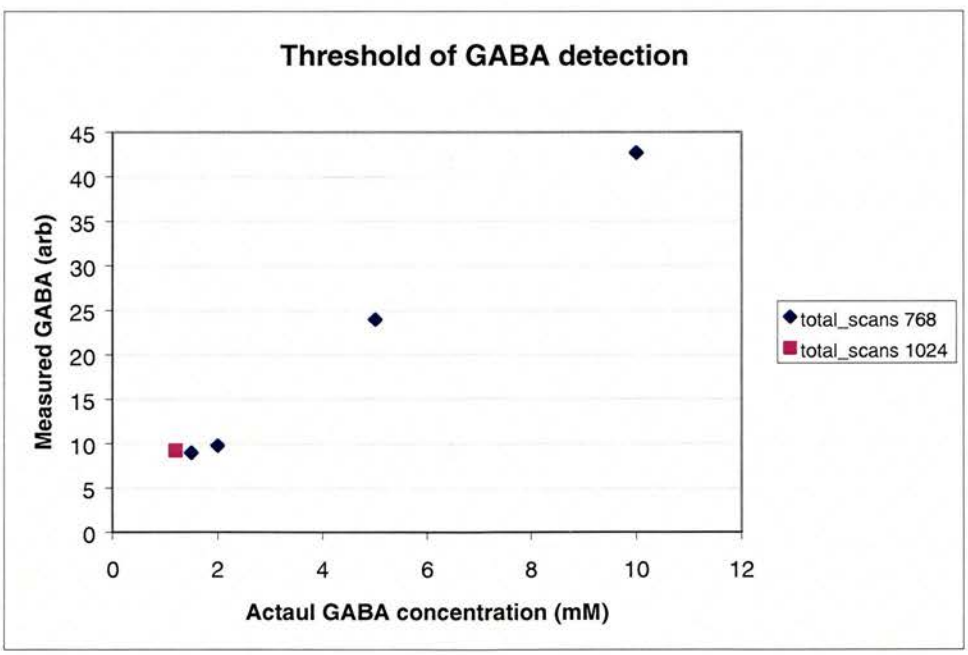

Figure 9.6 Results of *in-vitro* GABA measurement from a 3x3x3cm^3 voxel in six phantoms of decreasing GABA concentration, using a dedicated 2D L-COSY MRS sequence.

The 2D L-COSY spectrum from the phantom containing 1.2mM GABA, using the increased NEX/total number of scans, is shown in Figure 9.7 with the corresponding row containing the F2 = 3.01ppm, F1 = 1.9ppm GABA cross-peak.

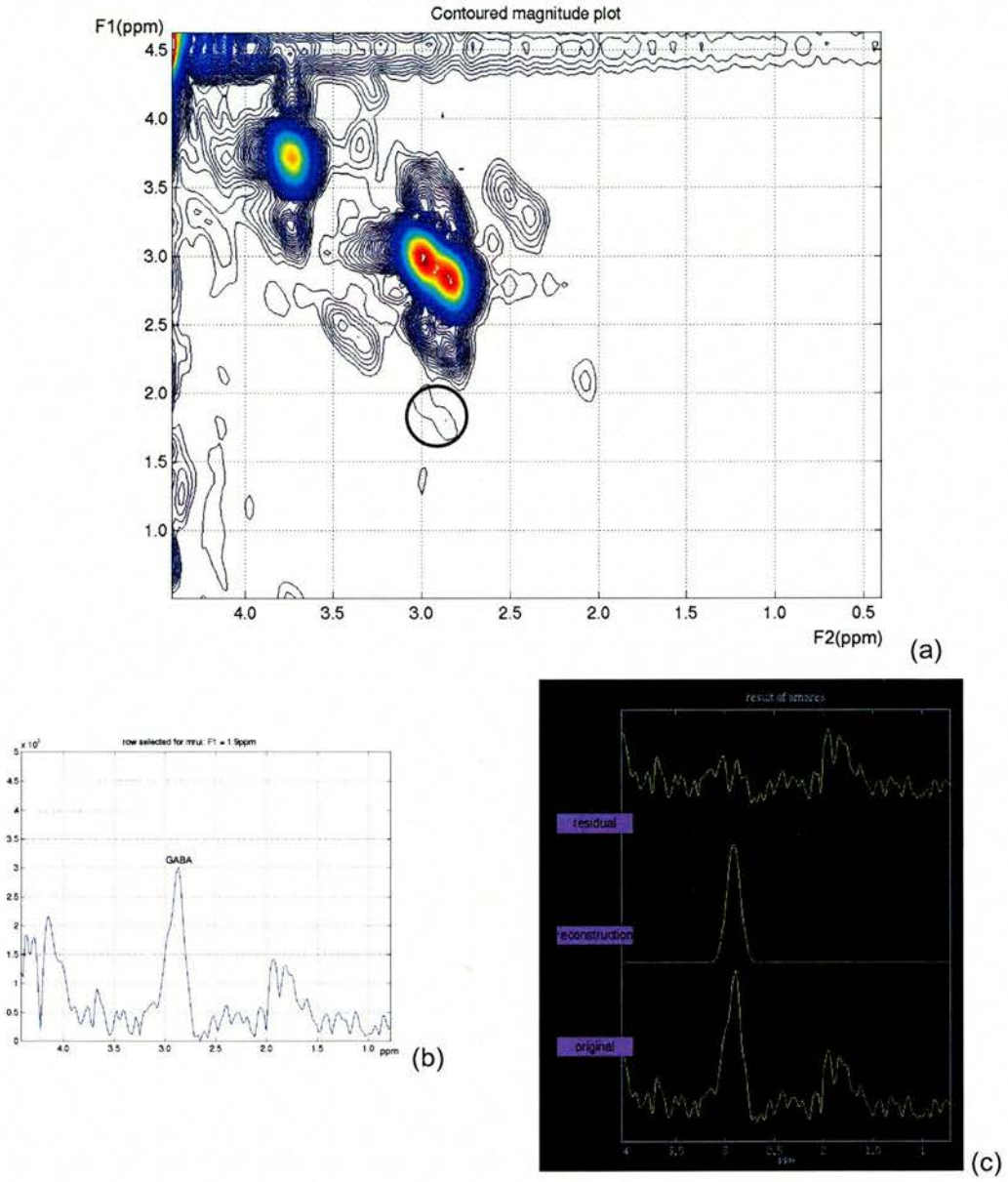

Figure 9.7 (a) 2D L-COSY spectrum from a 3x3x3cm^3 voxel in a phantom containing 3mM choline, 9mM creatine and 1.2mM GABA, using a 5" coil. The cross-peak at F2 = 3.0ppm, F1 = 1.9ppm is highlighted. (b) Extracted row from 2D contour plot showing the corresponding GABA cross-peak pre-quantification and (c) post-quantification in MRUI.

9.4.4 Discussion

These results suggest that 2D L-COSY is not as sensitive as 2D J-resolved MRS for GABA measurement. Clear peak assignments were made to GABA, *in-vitro*, at concentrations as low as 0.8mM using 2D J-resolved spectroscopy, but corresponding convincing results could not be produced using COSY. This would suggest that 2D L-COSY may only detect GABA, *in-vivo*, when present in the upper limits of the normal range of physiological concentrations (7).

However, before any conclusions can be made about the suitability of 2D L-COSY for *in-vivo* GABA measurement at 1.5T, the reliability of such results needs to be established. Results from preliminary work specifically addressing this issue are presented in the next section.

9.5 Reproducibility

9.5.1 Introduction

Although the specific application of this sequence is GABA measurement, it was also important to obtain a general measure of the reproducibility of the technique – including acquisition and post-processing. This was achieved by quantifying the diagonal peaks from choline and creatine.

In this pilot study, GABA reproducibility measurements were made in phantoms containing 5mM and at the threshold of GABA detection: 1.2mM. In each case, within-run, within-session and between-days reproducibility measurements were calculated. In addition, the results from the experiments at these GABA concentrations allowed direct comparison to the 2D J-resolved reproducibility study presented in §7.

9.5.2 Materials and methods

2D L-COSY spectra were obtained from a 5"and 3" surface coil, using a similar protocol as that given in Table 9.1. However, the NEX and total number of scans were increased to improve the SNR, as described in §9.4.2.

Two phantoms of physiological concentrations of choline and creatine (3mM and 9mM respectively), were made in two 3.6 litre glass, spherical containers. In one phantom, GABA was added at a concentration of 5mM and in the second, at 1.2mM.

As described in §7, three measures of reproducibility were taken: Within-run, within-session and between-days. In each of the three sets of measurements, five 2D L-COSY spectra were acquired, with each set performed in both phantoms. The resulting raw data files were transferred to a Sun Ultra Workstation and processed as described in §9.2.3. Coefficients of variation (CV) were calculated for all three measures of reproducibility in both phantoms.

9.5.3 Results

A summary of all the GABA measurements is given in Table 9.2, with the corresponding results from choline and creatine in Table 9.3. A representative example from the 5mM GABA phantom with results pre- and post-quantification is shown in Figure 9.8.

Table 9.2 Coefficients of Variation (CV, %) of the absolute values of GABA for all the within-run, within-session and between-days experiments in both a 5" and 3 " surface coil.

Actual GABA concentration	Within-run reproducibility (CV (%))		Within-session reproducibility (CV(%))		Between-days reproducibility (CV(%))	
	5" coil	3" coil	5" coil	3" coil	5" coil	3" coil
1.2mM	21.7	-	39.0	-	42.1	-
5mM	22.7	39.6	21.8	39.3	24.4	43.8

Table 9.3 CVs of the absolute values of choline and creatine for all the within-run, within-session and between-days experiments in both a 5" and 3 " surface coil.

Metabolite	Within-run reproducibility (CV (%))		Within-session reproducibility (CV(%))		Between-days reproducibility (CV(%))	
	5" coil	3" coil	5" coil	3" coil	5" coil	3" coil
choline	22.7	17.7	20.8	25.2	26.9	25.7
creatine	25.1	18.7	26.3	22.9	26.0	22.8

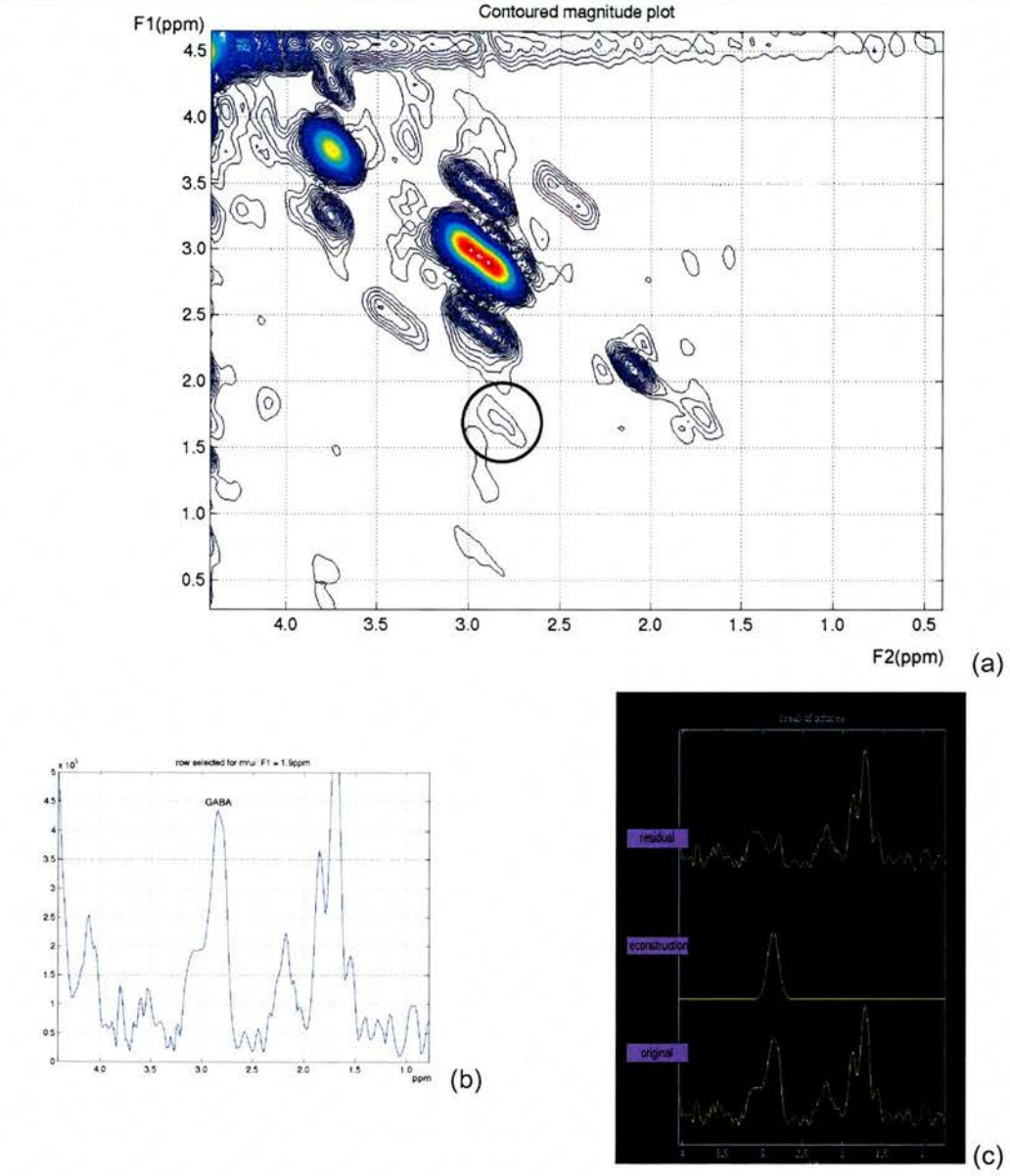

Figure 9.8 Results from the 2D experiment using a phantom containing physiological concentrations of choline and creatine, and 5mM GABA using a 5" surface coil. (a) 2D L-COSY spectrum with the F2 = 3.01ppm, F1 = 1.9ppm GABA cross-peak marked. The extracted row containing this cross-peak is given in (b) and in (c) post quantification in MRUI.

9.5.4 Discussion

It has already been noted in §7 that there is considerable variation in the published reproducibility measurements of *in-vivo* GABA at 1.5T. Even so, in comparison to some of the published data and the 2D J-resolved results presented in §7, the reproducibility measurements obtained using COSY are very disappointing.

Using the same 2D L-COSY sequence, Binesh *et al* gives a between-days CV for the choline diagonal of 2.2%, *in-vitro* (20). This is compared to 25.7% obtained locally, with both sets of measurements performed with a 3" surface coil. Since Binesh and colleagues used a standard GE spectroscopy phantom that doesn't contain GABA, evaluation of the GABA *in-vitro* results between both centres is not possible. However, *in-vivo*, Binesh cited a GABA between-days CV of 22%, again using a 3" surface coil. This is a considerable improvement on the only between-days measure obtained here, using the 5" surface coil, Table 9.2.

These comparatively poor results raise serious questions about scanner performance, operator dependency and perhaps, although less likely, the post-processing. The within-run experiments provide an indication of scanner performance, since neither the phantom nor the VOI is moved between acquisitions. Using the 5" surface coil, CVs of 22.7% and 25.1% were obtained for choline and creatine respectively, with only slightly better results when using the smaller surface coil, Table 9.3. With the equivalent results using 2D J-resolved MRS all less than 10%, §5, scanner instability cannot account for all the variation observed. Therefore, it is likely that differences in the optimisation of the signal during the manual prescan contribute significantly to the reproducibility.

With such inconsistency in five consecutive experiments, even among the high concentration metabolites, the reliability of *in-vivo* data acquisition has to be given careful consideration. In this practical work, all of the 2D L-COSY experiments were performed after a standard PRESS sequence, which incorporates automatic optimisation of the signal. *In-vitro*, it may be possible to use these pre-scan parameters for 2D L-COSY acquisition, since neither the phantom nor voxel will

have moved between one sequence and the next. *In-vivo*, this is not always the case, particularly when scanning patients. Consequently, it would be incorrect to assume zero patient / voxel movement, and so the pre-scan parameters from the PRESS sequence would not be transferable to COSY. Thus, a full prescan immediately before COSY acquisition is essential, and without automation, may not be consistent between scans.

Variation in prescan performance is evident in all measurements, in all three sets of reproducibility calculations. Results from the high concentration GABA phantom in the 5" surface coil are comparable to those from physiological concentrations of choline and creatine, with a between days CV of 24.4%. However, GABA measurement in the 3" surface coil is far worse: At 5mM, the between-days CV = 43.8%. Also in the 3" surface coil, at a concentration of 1.2mM, GABA was consistently undetectable. These appalling results are probably due to poor voxel shimming / signal optimisation. Even so, they do not bode well for *in-vivo* translation using a 3" surface coil.

In the 5" coil, GABA detection at F2 = 3.01ppm, F1 = 1.9ppm was not constant. Out of the 15 experiments performed at GABA concentrations of 1.2mM, the GABA cross-peak was identified in only eight of the resulting 2D spectra. This failure rate is far greater than that associated with 2D J-resolved MRS, which for the same GABA concentration and coil arrangement, failed to produce a clear GABA peak in only two spectra. This raises issues about the reliability of 2D L-COSY in terms of GABA detection performance, and about the decision processes involved in the interpretation of the 2D contour plots. For example, the F2 = 3.01ppm, F1 = 1.9ppm GABA cross-peak was not identified from the experiment giving rise to the 2D L-COSY spectra shown in Figure 9.9 (a): Spread of both the choline and creatine peaks obscured any evidence of GABA at this position. Study of the extracted row corresponding to F1 = 1.9ppm (Figure 9.9 (b)) showed two peaks around 3.01ppm, which from comparison with the contour plot, appeared to be from the higher concentration choline and creatine resonances. However, it is entirely possible that GABA may also have contributed to the peak area, but without a distinct and

separate contour on the 2D L-COSY plot, such assignment is very difficult. As a result, it would appear that in its current form, this approach does not have a high specificity for GABA detection.

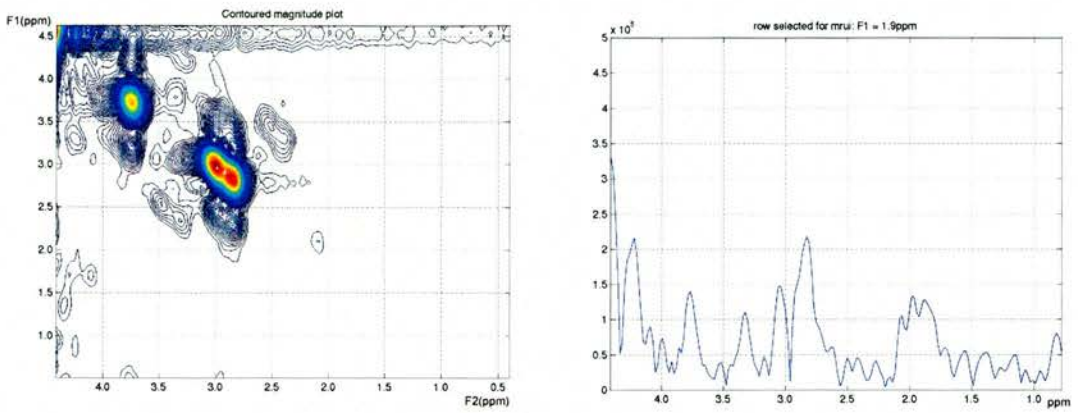

(a) (b)

Figure 9.9 Results from the 2D experiment using a phantom containing physiological concentrations of choline and creatine, and 1.2mM GABA using a 5" surface coil. (a) 2D L-COSY spectrum and (b) extracted row corresponding to F1 = 1.9ppm. No clear GABA cross-peak at F2 = 3.01ppm, F1 = 1.9ppm is visible.

In any subjective test, requiring an observer to interpret a set of results, the outcome of the test will change according to the applied decision threshold. This forms the basis of receiver operating character analysis, which describes the compromises in decision making that affect the true positive fractions (TPF) and false positive fractions (FPF) (163). (A TPF is defined as the ratio of number of true positive decisions to the number of actual positive cases; Conversely, the FPF is the ratio of the number of false positive decisions to number of actual negative cases.) In GABA detection using 2D L-COSY, a "lax" decision could be the simple criterion of the appearance of a contour at the appropriate cross-peak frequencies that gives rise to a peak in the extracted spectrum. Applying these principles to Figure 9.9 would enable a "GABA" peak to be quantified and reported on. Consequently, in this instance and in general, such relaxed criteria would increase the TPFs and FPFs. A stricter threshold requiring the "GABA" contour to be distinct from any noise or from contours arising from neighbouring metabolites, would result in the failure of GABA detection in Figure 9.9 (as reported) and consequently, a decrease in TPFs and FPFs.

Therefore, it is vital that an appropriate decision threshold is reached and adhered to, to allow consistent interpretation of the results.

Despite the poor reproducibility and inconsistent reporting of GABA cross-peak *in-vitro*, 2D L-COSY data was acquired *in-vivo*.

9.6 *In-vivo* results

9.6.1 Introduction

The aim of this work was to achieve *in-vivo* GABA measurement using 2D L-COSY. Despite the issues arising from the *in-vitro* reproducibility measurements, a protocol for quantification of GABA from 2D L-COSY spectra had been developed, and it was prudent to test this in humans. Therefore, the final section of this chapter presents the results from the *in-vivo* 2D L-COSY experiments on healthy volunteers.

9.6.2 Methods

Normal, healthy volunteers were recruited and written informed consent was obtained. Each volunteer was set-up on a 5" surface coil, in a specially designed headrest allowing immobilisation of the head.

After a series of T_2 FSE axial images, a 3x3x3cm^3 VOI was positioned in the occipital cortex, and a conventional single voxel PRESS experiment performed (TE = 35ms, TR = 2000ms). Upon acquisition of a well-resolved spectrum, free from skull-lipid contamination, 2D L-COSY was performed in the same VOI using both the scan parameters listed in Table 9.1 and those described in §9.4 to increase the SNR. The resulting raw data was processed as described in §9.2.3.

9.6.3 Results

At the time of writing, only three healthy volunteers had been scanned using the dedicated 2D L-COSY sequence. By applying the same criteria as for the *in-vitro*

data (i.e. a separate contour in the appropriate F1 / F2 intersection, distinct from any surrounding noise), in only one of the three resulting spectra could an assignment to the F2 = 3.01ppm and F1 = 1.9ppm GABA cross-peak be made, Figure 9.10 (a). The extracted spectrum corresponding to this GABA assignment is provided in Figure 9.10 (b).

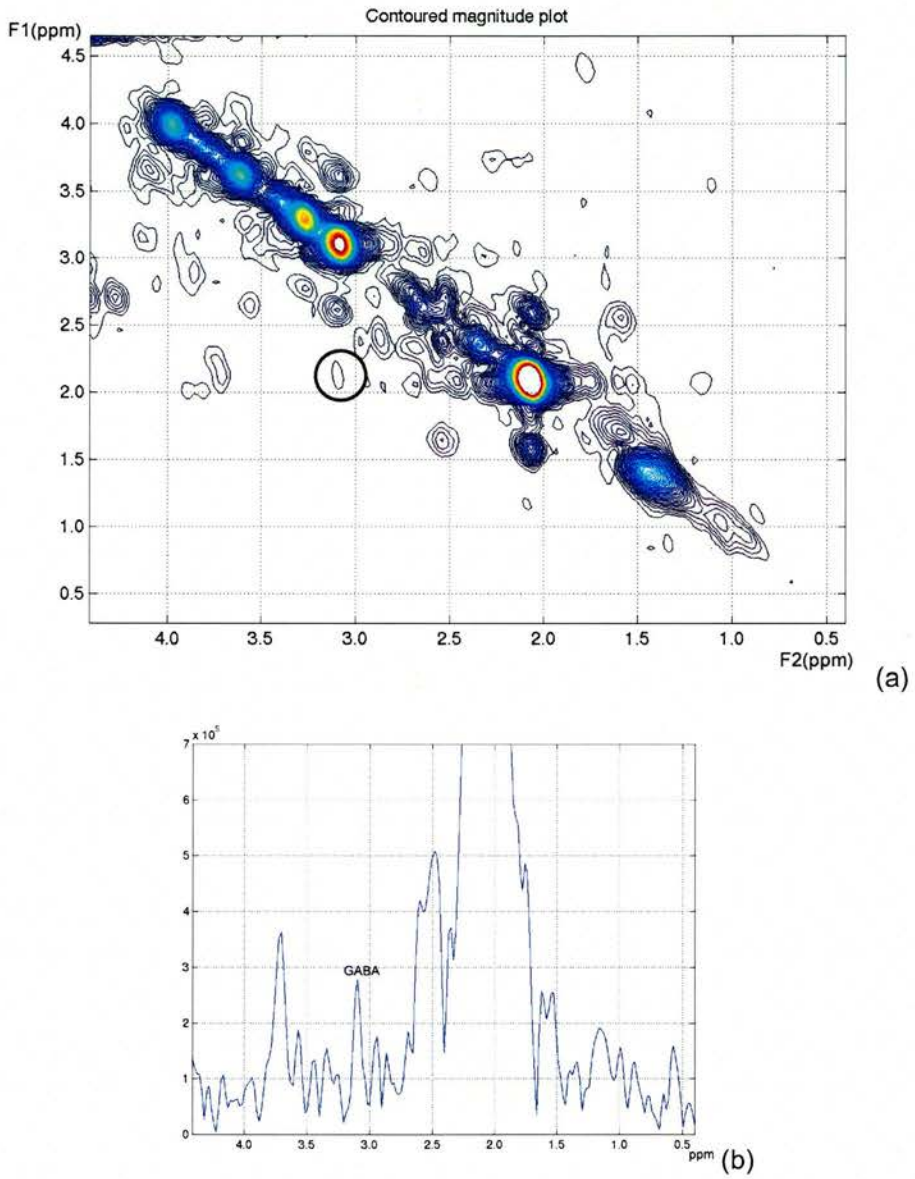

Figure 9.10 (a) 2D L-COSY spectrum from a 3x3x3cm^3 VOI placed in the occipital cortex of a normal, healthy volunteer. (b) Extracted spectrum corresponding to F1~1.9ppm from the same volunteer.

9.6.4 Discussion and conclusions

Following the disappointing *in-vitro* results, a success rate of only one in three volunteers is not surprising. In addition to the SNR problems of *in-vivo* acquisition discussed in the previous chapter, this may be due to a number of other reasons: Imperfect optimisation of the signal or voxel shimming during the manual prescan, insensitivity of the technique to the lowest concentrations of GABA and patient movement.

However, with successful GABA identification in one subject, it is hopeful that this result can be repeated. The reliability of the sequence may be improved by incorporating an automatic prescan, and this would undoubtedly reduce the overall scan time. This would also decrease the opportunity for patient movement, thereby enhancing the quality of the spectra. Investigation of the acquisition parameters, particularly the NEX and total_scans, may offer further improvements to the SNR and facilitate the detection of GABA at concentrations lower than 1.2mM.

10 Conclusions

10.1 Introduction

GABA measurement at 1.5T is very difficult due to its low concentration, complex spectrum and the overlapping of higher concentration metabolites, particularly NAA (1.9ppm), glutamate (2.35ppm) and creatine (3.0ppm). Nevertheless, the ability to measure GABA with ^{1}H MRS has become an area of increasing interest over the past decade.

Results from GABA measurement at 1.5T using a variety of techniques have been published, including difference editing, double quantum filters and 2D methods. Two-dimensional spectroscopy has the major advantage over spectral-editing methods of acquiring information about all the metabolites contained within the sample, thus providing a more complete description of the metabolic status of the individual.

The aim of this chapter is to draw together the conclusions from three years of work on 2D J-resolved and 2D L-COSY MRS. Although *in-vivo* GABA measurement was

not clinically applied as originally intended, the viability of these techniques as routine clinical tools will be assessed and suggestions made for improvements in further work.

10.2 GABA measurement using 2D J-resolved MRS comprising 64 individual PRESS sequences

Access to highly specific sequences or the skills to write and compile dedicated programmes, can be the limiting factor in applying non-standard acquisition protocols outside the research environment. The capacity to review published results from a technique of interest and then apply it on a standard MRI scanner is immensely desirable, particularly if it does not require the purchase of a dedicated sequence. For this reason, 2D J-resolved spectroscopy was performed using a conventional PRESS sequence.

As described in chapter two, one-dimensional spectroscopy using PRESS localisation is routinely applied on clinical MRI scanners, particularly when performing MRS of the brain. It is a straightforward sequence, allowing uncomplicated prescription of a spectroscopy voxel and selection of the acquisition parameters, and incorporates an automatic prescan to optimise the spectroscopy signal and suppress the water. With familiarisation of PRESS and an understanding of the general principles behind 2D J-resolved spectroscopy, the practical implementation of 2D J-resolved MRS is achievable, as shown in chapter four.

Requiring a scan time of over 2.5 hours, it was clear from the outset that 2D J-resolved spectroscopy using 64 individual PRESS sequences was never going to be clinically viable. However, from a purely scientific viewpoint, it was an interesting exercise. The resulting 2D spectra from phantoms containing aqueous solutions of single metabolites compared well to published spectra, thus confirming that accurate 2D J-resolved spectra could be produced without a dedicated sequence.

With a threshold of *in-vitro* GABA detection of 1.2mM, well within normal physiological ranges, these were encouraging results for *in-vivo* translation. However, the *in-vitro* reproducibility results from the high concentration metabolite peaks of choline, creatine and acetate (in lieu of NAA) were somewhat disappointing with coefficients of variation (CV) (defined as the percentage ratio of the standard deviation to the mean) of between 11% and 13%. As reproducibility is an important factor in the application of any new technique *in-vivo*, it was formally addressed in its own chapter at a later stage in the thesis.

For completeness, this work was taken to its logical conclusion of performing 2D J-resolved MRS, using a protocol of repeated PRESS sequences, *in-vivo*. After setting-up the volunteer in a standard volume head coil, the total scanning time including imaging and spectroscopy was almost 3.5 hours, emphatically demonstrating that the protocol could never be applied to patients. Nevertheless, it was a very worthwhile exercise, permitting a peak assignment to GABA (including a macromolecule contribution) from the resulting 2D contour plot. This brought the work to a very pleasing end, showing that 2D J-resolved MRS using 64 individual PRESS sequences allowed GABA measurement both *in-vitro* and *in-vivo*.

Aside from the academic interest of showing that 2D J-resolved MRS could be performed using a standard, manufacturer provided MRS sequence, the work was extremely useful in developing the post-processing protocol for the analysis and quantification of the all the 2D J-resolved data. Ian Marshall wrote the C program that performed the initial post-processing step, executing functions common to the processing of most spectroscopy data. This included phase correction, removal of the residual water peak and scaling of the FID according to VOI size and the pre-scan parameters. Variations of this program had been used extensively in both single-voxel and CSI analysis prior to its application in 2D J-resolved MRS, and so its operation had been well established.

The functions specific to 2D J-resolved spectroscopy, such as 2D Fourier Transform and apodization of the data were all performed in Matlab, based on a function also

written by Ian Marshall. Variations of this function, plus the programs required to convert the data to MRUI format for quantification were written by the author. This allowed the metabolite peaks in extracted rows from the 2D contour plots to be quantified using prior-knowledge files, thus standardising the whole procedure. These principles, once developed and tested for the 2D J-resolved experiments using 64 individual PRESS sequences, were used for the post-processing of data from both the dedicated 2D J-resolved and L-COSY sequences.

10.3 GABA measurement using a dedicated 2D J-resolved sequence

Collaboration with Dr. N. Sailasuta, a software engineer from GE Healthcare, permitted evaluation of a dedicated 2D J-resolved sequence. This was based on the same PRESS sequence used in the protocol described above, modified to allow the time either side of the second refocusing pulse to be uniformly incremented. Thus the raw data required for processing both dimensions of the 2D J-resolved experiment was acquired in a single pulse-sequence. Without the time to load and prescan each new sequence, the 2D J-resolved experiment that had previously taken 2.5 hours was now accomplished in 35 minutes! This clearly had more scope for clinical application.

Although the standard PRESS and dedicated 2D J-resolved sequence are fundamentally the same, a difference in the reference-data acquisition between the two necessitated a modification of the established post-processing protocol, as described in chapter five. PRESS routinely acquires water-reference spectra that were used to phase correct the data using a time domain method introduced by Ordidge and Cresshull (136). In a time-reducing effort, these water-reference, so-called "dummy scans", were no longer acquired as part of the dedicated sequence. Thus, the phase information for correction could no longer be obtained from a water-only signal. This prompted study of the various phase-correction methods in use for NMR data and the development of a frequency-domain, phase correction algorithm, written by the author. However, when tested against the adaptation of the original

phase correction function used in the post-processing of the standard PRESS sequence, the time-domain method consistently out-performed the frequency-domain method and so was implemented as standard.

Initial validation of the dedicated sequence was achieved by repeating a series of single-metabolite phantom experiments. These resulted in a set of 2D J-resolved spectra that compared favourably to those acquired using the protocol of repeated PRESS experiments and results in the published literature. Satisfied with the performance of the sequence, and that the threshold of GABA detection again fell within normal physiological levels, further practical work was performed to optimise the sequence for *in-vivo* application.

When performing any MRS experiment *in-vivo*, the aim is to acquire the maximum SNR of the metabolite(s) of interest in the shortest possible time. To do this, there are many possible variables that can be optimised, including coil arrangement, VOI size and position, acquisition parameters and modifications to the post-processing protocol. Each of these variables was investigated in turn and the results presented in chapter 6 are summarised below.

Although conventional brain imaging is performed using a volume head coil, the greater sensitivity associated with the surface coils led to an improved SNR of the quantified GABA peaks *in-vitro*. The increased sensitivity was also translated into a lower threshold of *in-vitro* GABA detection, from 1.2mM in the volume head coil to 0.8mM in both the surface coils. Results from 1D conventional MRS experiments *in-vivo* using both a volume head coil and 3" surface coil showed similar improvements in the SNR of NAA, further supporting the argument for surface coil use. Although the best improvement was seen with the 3" surface coil, the larger excitable volume associated with the 5" surface coil meant that overall, the larger surface coil was the best overall choice for *in-vivo* spectroscopy.

Another limiting factor in the overall SNR of the spectra is the size of voxel. In terms of anatomical definition and selecting specific volumes for excitation, a small

VOI is often desirable. However, in order to improve the SNR of the spectra, especially when attempting to measure signals from low concentration metabolites, a large VOI is required. A series of *in-vitro* experiments using GABA at a physiological concentration determined a minimum VOI size of $15cm^3$, after which GABA quantification broke down due to poor SNR.

As far as the 2D J-resolved sequence is concerned, there are very few parameters that can be manipulated to improve the sequence performance. Obviously, the actual RF pulse sequence and timing definitions are fixed. However, the TE range of the experiment can be optimised, as can the TR and the phase cycling and number of scans to help with signal averaging. Comparison of the available literature showed that three main timing arrangements had been used to perform 2D J-resolved MRS (23,25-27). GAMMA simulations and *in-vitro* experimental work using these different timings showed differences in SNR and F1 resolution, with both factors affecting GABA quantification. Consequently, 64 TE steps uniformly incremented at 10ms was chosen as a compromise between SNR and an F1 resolution sufficient to analyse the data at the GABA J-coupling frequency.

With the number of excitations (NEX) controlling the phase cycling scheme adopted, a NEX of 16 was chosen to improve the signal averaging by phase cycling through all three RF pulses, twice. Although the increase in NEX from 8 to 16 doubled the acquisition time, it was considered a sacrifice worth making for the associated improvement in spectral sensitivity. With *in-vivo* GABA detection so close to the threshold of detection using a 1.5T scanner, signal averaging is an important factor in determining the success of the experiment (21). A similar balance between SNR and scan time was achieved in choosing a TR = 2000ms.

In-vivo, macromolecule resonances exist at similar chemical shifts and J-coupling frequencies as the targeted GABA resonance at 3.01ppm. Conventional single-voxel experiments *in-vivo* demonstrated that by starting acquisition at TE = 55ms, an optimum balance between a reduction in macromolecule contribution and metabolite signal loss in 2D J-resolved MRS was achieved. However, since only an extra

minute was required to acquire spin-echoes from another 2 TEs (bringing the total number of TE steps to 66), the final protocol started the 2D acquisition at 35ms. This facilitated the production of two, 2D spectra: The first (TE 35ms – 665ms) with and the second (TE 55ms – 685ms) without macromolecule contributions. Consequently, the spectral changes arising from differences in *in-vivo* acquisition timings could be compared.

Before applying the optimised protocol *in-vivo*, it was tested on a phantom containing physiological concentrations of all the common cerebral metabolites. At the J-coupling frequency of GABA and at its chemical shift position, GABA was clearly identified. Processing the two TE ranges resulted in a decrease in the 3.01ppm GABA peak of approximately 10%. Changes in post-processing were also explored to demonstrate the affect of acquiring a reduced number of TE steps and zero-filling compared to the ideal number of 64. On the physiological phantom, this had a detrimental affect with considerable F1 bleed from acetate, choline and creatine, which negatively impacted on quantification of the 3.01ppm GABA resonance. The potential loss of *in-vivo* GABA signal was deemed too big a risk to justify the reduced acquisition time, so the protocol remained at 64 (+2 = 66) TE steps.

The final stage before *in-vivo* application was a formal reproducibility study of GABA measurement using 2D J-resolved MRS, chapter seven. This was a large study comprising 180 individual experiments, and was a crucial part of evaluating the performance of the technique. Phantoms were made containing physiological concentrations of choline and creatine – the metabolites with the greatest possibility of obscuring the 3.01ppm GABA resonance – and GABA at six different concentrations, covering the entire normal physiological range (164). Three measures of reproducibility were made: Within-run, within-session and between-days. From these, indications of scanner stability and errors due to re-positioning in the same scan session and over several days were obtained. The experiments were carried out in a combination of volume head coil, 5" and 3" surface coils. As the first

reproducibility study specific to 2D J-resolved MRS for GABA measurement, it has significant implications for the interpretation of *in-vivo* data.

Overall, the results were very encouraging. The CVs were all less than 10% for choline and creatine for all three measures of reproducibility. Specific to GABA measurement, a general improvement in reproducibility was seen when using the 5" surface coil instead of the volume head coil. At the lowest GABA concentration tested of 0.8mM, a CV of 22.5% was obtained following the optimised protocol. This is comparable to the only other 2D reproducibility study (20), where a CV of 22% was obtained for *in-vivo* 2D L-COSY GABA measurement. Although increases in the CVs are expected with *in-vivo* translation, these results were an encouraging point from which to start.

After all the *in-vitro* validation and optimisation of the 2D J-resolved sequence and its associated post-processing, the *in-vivo* results were disappointing, although they were comparable to those in the published literature (24,27), chapter eight. However, in the first reported 2D J-resolved experiments specifically designed to reduce the macromolecule contribution to the 3.01ppm GABA peak, the resulting GABA peaks were far from convincing. This suggested that the "GABA" peak, as identified in the literature using a starting TE of 35ms, comprised largely of macromolecules, and so prevents accurate GABA measurement. The lack of a distinct GABA-only peak *in-vivo* prevented the application of 2D J-resolved MRS to the patient population for which it was originally intended.

Results from 2D J-resolved experiments performed on a 3T scanner by Dr. Sailasuta at GE Healthcare and processed by the author failed to yield any "GABA" peak, even with a starting TE of 35ms. The failure of 2D J-resolved MRS to produce spectra even similar to those at 1.5T was attributed to the very poor quality of the spectra. However, with equally unremarkable results from an attempt to perform GABA CSI using 2D J-resolved MRS on a 4T system, as presented at the most recent scientific meeting of ISMRM (165), it would suggest an inherent SNR problem with using 2D J-resolved MRS for GABA measurement at medium fields.

10.4 GABA measurement using a dedicated 2D L-COSY sequence

As an alternative to 2D J-resolved MRS, 2D L-COSY was evaluated as a method for *in-vivo* GABA measurement at 1.5T, chapter nine. This was achieved using a dedicated sequence as provided by Dr. M.A. Thomas, from which *in-vivo* GABA results had been previously published at both 1.5T and 3T (21,133).

Correlation patterns in the 2D L-COSY spectra resulting from experiments on individual metabolite phantoms were similar to those predicted by the literature, thus validating the technique as a whole. However, it became clear in a very early stage of the experimental work that the theoretical scan time of 25 minutes could never be practically achieved due to the required manual pre-scanning. As a crucial step in the process of acquiring 2D L-COSY spectra, optimisation of the prescan parameters could take an additional 30 minutes, immediately raising questions regarding the clinical applicability of the method without an automated pre-scan.

Unlike the 2D J-resolved experiments when an *in-vitro* GABA threshold of 0.8mM was detected using a 5" surface coil, GABA was only convincingly detected in similar phantom experiments at a concentration of 1.2mM. This suggests that 2D L-COSY is not as sensitive as 2D J-resolved MRS for *in-vitro* GABA measurement, and so would only be able to detect the upper limits of normal physiological concentration when applied *in-vivo*.

Of much greater concern was the poor reproducibility of 2D L-COSY when compared to 2D J-resolved MRS and similar results in the literature. Of the high concentration metabolites, a CV of 22.7% was obtained for the within-run, *in-vitro* choline diagonal, compared to 2.2% in a corresponding reproducibility study by Binesh *et al* (20). Using 2D J-resolved MRS, CVs < 10% were acquired for choline in the J = 0Hz extracted spectrum. Such results raise questions about scanner performance and specifically to the 2D L-COSY experiments, the operator dependency on the manual pre-scan. The variation in pre-scan optimisation also contributed to the larger number of 2D L-COSY spectra where *in-vitro* GABA

detection failed as compared to 2D J-resolved MRS. With such poor results obtained in a homogeneous, motionless phantom, they do not suggest that reliable GABA measurement will be immediately forthcoming *in-vivo*. Further evidence for this view was obtained when in only one of the three volunteers scanned could the F2 = 3.01ppm, F1 = 1.9ppm GABA cross-peak be identified.

10.5 Conclusion

2D GABA measurement should only be applied routinely *in-vivo* if it has been shown that accurate and reproducible measurements can be made. *In-vitro*, 2D J-resolved MRS is a sensitive and reliable technique for GABA measurement, but these results were not reproduced *in-vivo*. In comparison, 2D L-COSY has not shown itself to be as robust or sensitive in any of the *in-vitro* or *in-vivo* experiments, but this may be due to the operator-dependant manual pre-scan. Thus, in their current form, pure GABA measurement using either of these 2D techniques at 1.5T is not suitable for routine clinical use. The absence of convincing results from the spectral editing methods reported at 1.5T (13,14,16,19,103) would also suggest that measurement of normal, physiological GABA levels on the current breed of clinical scanners is not viable. However, it may be possible to identify GABA in patients with elevated GABA concentrations (27).

10.6 Future work

In order for 2D J-resolved MRS to be successfully applied for *in-vivo* GABA measurement, a stable, high-field magnet (> 1.5T) is essential. However it is not clear to what extent the field strength needs to be increased before GABA can be reliably identified. Despite reports of GABA measurement at 1.5T (22-26), in an *in-vivo* 2D J-resolved MRS rat study at 4.7T, no spectral assignment was made to GABA (166). This is in spite of an assignment to taurine, which exists *in-vivo* at a concentration of approximately 1.5mM (7) - a comparable level to GABA. At 3T, conflicting results have been obtained using 2D L-COSY with *in-vivo* GABA assignments reported by Thomas *et al* (130) yet not by Zielger and co-workers (118). Another hardware requirement is higher order shimming to improve the linewidths of

the *in-vivo* spectra is required to improve the appearance of the 2D spectra and associated extracted rows. Application of multi-channel array coils may also improve the SNR or allow a reduction in the scanning time (167). Post-processing techniques may also improve the appearance of the spectra. Although a basic zero-order phase correction algorithm reduced t_1 noise from the main metabolites singlets as shown in chapter five, a first or higher order algorithm may further reduce any F1 bleed. Alternative apodization functions designed to suppress the dispersion of the magnitude mode spectra may lead to improvement in the F1 resolution. In addition, adaptations of other fitting programmes such as LC Model (105) or FELIX (Accelrys, San Diego, CA) may facilitate the quantification of GABA based on model solutions of the individual metabolites. However, careful consideration will need to be given to the differences between *in-vivo* and *in-vitro* data as described in chapter eight.

Similar developments may also benefit GABA detection with 2D L-COSY, although it is expected that an immediate improvement in the reliability of the sequence would be observed with the development of an automatic prescan.

Results from the literature suggest that more convincing GABA results may be possible at higher fields using 2D L-COSY (133) and spectral editing techniques (106-108,110,111). With 3T scanners becoming more commonplace in the clinical environment, there are exciting opportunities to establish the accuracy and reliability of these methods *in-vivo*.

References

1. Taylor M, Bhagwagar Z, Cowen PJ, Sharp T. GABA and mood disorders. Psychological Medicine 2003;33:387-393.
2. Chang L, Cloak CC, Ernst T. Magnetic Resonance Spectroscopy Studies of GABA in Neuropsychaitric Disorders. J Clin Psychiatry 2003;64(suppl 3):7-14.
3. Sanacora G, Mason GF, Krystal JH. Impairment of GABAergic transmission in depression: New insights from neuroimaging studies. Crit Rev Neurobiol 2000;14(1):p23-45.
4. Goddard A, Mason GF, Almai A, Rothman DL, Behar KL, Petroff OA, Charney DS, Krystal JH. Reductions in occipital cortex GABA leverls in panic disorder detected with 1H MRS. Arch Gen Psychiatry 2001;58(6):p556-561.
5. Petroff OA. Magnetic Resonance spectroscopic studies of neurotransmitters and energy metabolism in epilepsy. Epilepsa 2002;43:p40-50.
6. Mescher M. Simultaneous in vivo spectral editing and water suppression. NMR in Biomed 1998;11:p266-272.
7. Govindaraju V, Young K, Maudsley AA. Proton NMR Chemical Shifts and Coupling Constants for Brain Metabolites. NMR in Biomed 2000;13(3):129-153.
8. Sanacora G. Reduced Cortical GABA Levels in Depressed Patients Determined by Proton MRS. Arch Gen Psychiatry 1999;56:p1043-1047.
9. Epperson CN, Haga K, Mason GF, Sellers E, Gueorguieva R, Zhang W, Weiss E, Rothman DL, Krystal JH. Cortical GABA levels across the menstrual cycle in healthy women and those with premenstrual dysphoric

disorder: a proton magnetic resonance spectroscopy study. Arch Gen Psychiatry 2002;59(9):p851-858.
10. Robinson RG. The Clinical Neuropsychiatry of Stroke: Cambridge University Press; 1999.
11. Terpstra M. Direct In Vivo Measurement of Human Cerebral GABA Concentration Using MEGA-Editing at 7 Tesla. MRM 2002;47:p1009-1012.
12. Hanstock C. GABA X2 Multiplet Measured Pre-and Post-Administration of Vigabatrin in Human Brain. 2002;48:p617-623.
13. Keltner JR, Wald LL, Christensen JD, C ML, Moore CM, Cohen BM, Renshaw PF. A Technique for Detecting GABA in the Human Brain with PRESS Localization and Optimized Refocusing Spectral Editing Radiofrequency Pulses. Magn Reson Med 1996;36:458-461.
14. Mueller SG, Weber OM, Boesiger P, Wieser HG. Influence of pyridoxal 5'-phosphate alone and in combination with vigabatrin on brain GABA measured by 1H-NMR-spectrscopy. Brain Res Bull 2001;55(4):555-560.
15. Weber OM, Trabesinger AH, Duc CO, Meier D, Boesiger P. Detection of hidden metabolites by localized proton magnetic resonance spectroscopy in vivo. Technol Health Care 1997;5(6):471-491.
16. Weber OM. Effects of Vigabatrin intake on brain GABA activity as monitored by spectrally edited MRS and PET. MRI 1999;17(3):p417-425.
17. Keltner JR, Wald LL, Frederick BdB, Renshaw PF. In Vivo Detection of GABA in Human Brain Using a Localized Double-Quantum Filter Technique. Magn Reson Med 1997;37:366-371.
18. McLean MA. In Vivo GABA Measurement using a PRESS-localized double quantum filter in patients with malformations of cortical development and epilepsy. ISMRM 2002 (abstract) 2002.
19. McLean MA, Busza AL, Wald LL, Simister RJ, Barke rGJ, Williams SR. In Vivo GABA+ Measurement at 1.5T Using a PRESS Localized Double Quantum Filter. Magn Reson Med 2002;48:233-241.
20. Binesh N, Yue K, Fairbanks L, Thomas MA. Reproducibility of Localized 2D Correlated MR Spectroscopy. Magn Reson Med 2002;48:942-948.
21. Thomas MA, Yue K, Binesh N, Davanzo P, Kumar A, Siegel B, Frye M, Curran J, Lufkin, R BG, Martin P, Guze B. Localized Two-Dimensional Shift Correlated MR Spectroscopy of Human Brain. MRM 2001;46(1):p58-67.
22. Ryner LN, Sorenson JA, Thomas MA. Localized 2D J-resolved 1H MR spectroscopy: strong coupling effects in vitro and in vivo. MRI 1995;13(6):853-869.
23. Hurd RE, Gurr D, Sailasuta N. Proton Spectroscopy Without Water Suppression: The Oversampled J-resolved experiment. Magn Reson Med 1998;40:343-347.
24. Ke Y, Cohen BM, Bang JY, Yang M, Renshaw PF. Assessment of GABA concentration in human brain using two-dimensional proton magnetic resonance spectroscopy. Psychiatry Res 2000;1000(3):169-178.
25. Levy LM, Hallett M. Impaired brain GABA in focal dystonia. Annals of Neurology 2002;51(1):93-101.
26. Levy LM, Ziemann U, Chen R, Cohen LG. Rapid Modulation of GABA in Sensoimotor Cortex Induced by Acute Deafferentation. Annals of Neurology 2002;52:755-761.

27. Hwang JH, Levenson H, Sutherling W, Sailasuta N, Hurd RE, Ross BD. Detection of Elevated GABA Signals in the Human Brain at 1.5 Tesla using Phase-sensitive 2D J-Resolve H-1 Spectroscopy. ISMRM abstract 1999:1564.
28. Ross BD, Radda GK, Gadian DG, G R, M E, J F-S. Examination of a Case Suspected McArdle's Syndrome by 31P Nuclear Magnetic Resonance. N Engl J Med 1981;304(22):1338-1342.
29. Weiner MW. NMR Spectroscopy for Clinical Medicine Animal Models and Clinical Examples. Annals of The New York Academy of Sciences 1987;508:287-299.
30. Vion-Dury J, Meyerhoff DJ, Cozzone PJ, Weiner MW. What might be the impact on neurology of the analysis of brain metabolism by in vivo magnetic resonance spectroscopy? J Neurol 1994;241:354-371.
31. Bachelard H, Badar-Goffer R. NMR Spectroscopy in Neurochemistry. J Neurochem 1993;61(2):412-429.
32. Rumpel H, Lim WEH, Chang HM, Chan LL, Ho GL, Wong MC, Tan KP. Is Myo_Inositol a Measure of Glial Swelling After Stroke? A Magnetic Resonance Study. JMRI 2003;17:11-19.
33. Fulham MJ, Bizzi A, Dietz MJ, Shih HH-L, Raman R, Sobering GS, Frank JA, Dwyer AJ, Alger JR, Di Chiro G. Mapping of Brain Tumor Metabolites with Proton MR Spectroscopic Imaging: Clinical Relevance. Radiology 1992;185:675-686.
34. Valenzuela MJ. Magnetic resonance spectroscopy in AD. Neurology 2001;56:p592-598.
35. Wild JM, Macmillan CSA, Wardlaw JM, Marshall I, Cannon J, Easton VJ, Andrews PJD. 1H spectroscopic imaging of acute head injury - evidence of diffuse axonal injury. MAGMA 1999;8:109-115.
36. Bloch F, Hansen WW, Packard M. Nuclear Induction. Phys Rev 1946;69:127.
37. Purcell EM, Torrey HC, Pound RV. Resonance Absorption by Nuclear Magnetic Moments in a Solid. Phys Rev 1946;69:37.
38. Shaw TM, Elsken RH. Nuclear Magnetic Resonance Absorption in Hygroscopic Materials. J Chem Phys 1950;18:1113-1114.
39. Odeblad E, Lindstrom G. Some preliminary observations on the proton magnetic resonance in biologic samples. Acta Radiol 1955;43:469-476.
40. Behar KL, Rothman DL, Spencer DD, Petroff OA. Analysis of Macromolecule Resonances in 1H NMR Spectra of Human Brain. MRM 1994;32:294-302.
41. Mader I, Seeger U, Karitzy J, Erb M, Schick F, Klose U. Proton Magnetic Resonance Spectroscopy With Metabolite Nulling Reveals Regional Differences of Macromolecules in Normal Brain. JMRI 2002;16:538-546.
42. Graham GD, Hwang JH, Rothman DL, Prichard JW. Spectroscopic Assessment of Alterations in Macromolecule and Small-Molecule Metabolites in Human Brain After Stroke. Stroke 2001;32:2979-2802.
43. Hwang JH, Graham GD, Behar KL, Alger JR, Prichard JW, Rothman DL. Short Echo Time Proton Magnetic Resonance Spectroscopic Imaging of Macromolecule and Metabolite Signal Intensites in the Human Brain. MRM 1996;35:633-639.

44. Mader I, Seeger U, Weissert R, Klose U, Naegele T, Melms A, Grodd W. Proton MR spectroscopy with metabolite nulling reveals elevated macromolecules in acute multiple sclerosis. Brain 2001;124:953-961.
45. Moon RB, Richards JH. Determination of intracellular pH by 31P magnetic resonance. J Biol Chem 1973;248:7276-7278.
46. Hoult DI, Busby SJW, Gadian DG, Radda GK, Richards RE, Seeley PJ. Observation of tissue metabolites using 31P nuclear magnetic resonance. Nature 1974;252:285-287.
47. Dawson MJ, Gadian DG, Wilkie DR. Contraction and Recovery of Living Muscles Studied by 31P Nuclear Magnetic Resonance. J Physiol 1977;267:703-735.
48. Garlick PB, Radda GK, Seeley PJ. Studies of Acidosis in the Ischaemic Heart by Phosphorus Nuclear Magnetic Resonance. Biochem J 1979;184:547-554.
49. Ackerman JJH, Grove TH, Wong GG, Gadian DG, Radda GK. Mapping of metabolites in whole animals by 31P NMR using surface coils. Nature 1980;283:167-170.
50. Younkin DP, Delivoria-Papadopoulos M, Leonard JC, Subramanian VH, Eleff S, Leigh JS, Chance B. Unique Aspect of Human Newborn Cerebral Metabolism Evaluated with Phosphorus Nuclear Magnetic Resonance Spectroscopy. Ann Neurol 1984;16:581-586.
51. Cady EB, Dawson MJ, Hope PL, Tofts PS, Costello AMdL, Delpy DT, Reynolds EOR, Wilkie DR. Non-invasive investigation of cerebral metabolism in newborn infants by phosphorous nuclear magnetic resonance spectroscopy. Lancet 1983;14(1):1059-1062.
52. Gadian DG. NMR and its Applications to Living Systems. Oxford: Oxford University Press; 1995. 283 p.
53. Behar KL, den Hollander JA, Stromski ME, Ogino T, Shulman RG, Petroff OA, Prichard JW. High resolution 1H NMR study of cerebral hypoxia in vivo. Proc Natl Acad Sci 1983;80:4945-4948.
54. Bottomley PA, Hart HR, Edelstein WA, Schenck JF, Smith LS, Leue WM, Mueller OM, Redington RW. NMR Imaging / Spectroscopy System to study both Anatomy and Metabolism. The Lancet 1983:p273-274.
55. Bottomley PA, Hart HR, Edelstein WA, Schenck JF, Smith LS, Leue WM, Mueller OM, Redington RW. Anatomy and Metabolism of the Normal Human Brain Studied by Magnetic Resonance at 1.5T. Radiology 1984;150:441-446.
56. Bottomley PA, Foster TH, Darrow RD. Depth resolved surface coil spectroscopy (DRESS) for in vivo 1H, 31P and 13C NMR. J Magn Reson 1984;59:338-342.
57. Bottomley PA. Spatial Localization in NMR Spectroscopy in Vivo. Annals of The New York Academy of Sciences 1987;508:333-348.
58. Aue WP. Homonuclear broad band decoupling and two dimensional J-resolved NMR spectroscopy. J Chem Phys 1976;64(10):p4226-4227.
59. Maudsley AA, Hilal SK, Perman WH, Simon HE. Spatially Resolved High Resolution Spectroscopy by "Four-Dimensional" NMR. JMR 1983;51:147-152.
60. Ross B, Bluml S. Magnetic Resonance Spectroscopy of the Human Brain. New Anat 2001;265:54-84.

61. Howe FA, Maxwell RJ, Saunders DE, Brown MM, Griffiths JR. Proton Spectroscopy In Vivo. Magn Reson Quart 1993;9:31-59.
62. Burtcher IM, Holtas S. Proton MR Spectroscopy in Clinical Routine. JMRI 2001;13:560-567.
63. Ross B, Michaelis T. Clinical Applications of Magnetic Resonance Spectroscopy. Mag Reson Quart 1994;10(4):191-247.
64. Elster AD, Burdette JH. Questions and Answers in Magnetic Resonance Imaging. St Louis: Mosby; 2001. 333 p.
65. Bushberg JT, Seibert JA, Leidholt EM, Boone JM. Magnetic Resonance Imaging. The Essential Physics of Medical Imaging. Baltimore: Williams & Wilkins; 1994. p 742.
66. Westbrook C, Kaut C. MRI in Practice. Oxford: Blackwell Sciences Ltd; 1998.
67. Shaw D. Fourier Transform N.M.R. Spectroscopy. Amsterdam: Elsevier Scientific Publishing Company; 1976. 357 p.
68. Vander AJ, Sherman JH, Luciano DS. Human Physiology: the mechanisms of body function. New York: McGraw-Hill, Inc; 1994. 837 p.
69. Becker ED, Fisk CL. NMR: Physical Principles and Current Status as a Biomedical Technique. Annals of The New York Academy of Sciences 1987;508:1-9.
70. Abraham RJ, Fisher J, Loftus P. Introduction to NMR spectroscopy. Chichester: John Wiley & Sons; 1988. 271 p.
71. Claridge TDW. High-Resolution NMR Techniques in Organic Chemistry. Baldwin JE, Williams FRS, Williams RM, editors. Oxford: Elsevier Science Lts; 1999. 382 p.
72. Aue WP. Non-Invasive Localised NMR Spectroscopy in Vivo. Annals of The New York Academy of Sciences 1987;508:360-365.
73. Ordidge RJ, Mansfield P, Lohman JAB, Prime AB. Volume Selection Using Gradients and Selective Pulses. Annals of The New York Academy of Sciences 1987;508:376-385.
74. The Future of Magnetic Resonance Spectroscopy and Spectroscopic Imaging. Maudsley AA, Weiner W; 1997.
75. de Certaines JD, Bovee WMMJ, Podo F. Magnetic Resonance Spectroscopy in Biology and Medicine. Oxford: Pergamon Press; 1992. 689 p.
76. Freeman R. Spin Choreography Basic Steps in High Resolution NMR. Oxford: Oxford University Press; 1998. 391 p.
77. Cavanagh J, Fairbrother WJ, Palmer III AG, Skelton NJ. Protein NMR Spectroscopy Principles and Practice. San Diego: Academic Press, Inc; 1996. 587 p.
78. Stryer L. Biochemistry: W.H. Freeman and Company; 1988.
79. Roberts E. GABA and nervous system function - a perspective. Biochem Pharm 1974;23:p2637-2649.
80. Petty F, Kramer GL, Dunnam D, Rush AJ. Plasma Gaba in Mood Disorders. Psychpharm Bull 1990;26(2):157-161.
81. Morris P, Mayberg H, Bolla K, Wong D, Dannals R, Starkstein S, Robinson RG. A preliminary study of cortical S2 serotonin receptors and cognitive performance following stroke. J Neuropsychiatry Clin Neurosci 1993;5(4):395-400.

82. Mayberg H, Parikh R, Morris P, Robinson RG. Spontaneous remission of post-stroke depression and temporal changes in cortical S2-serotonin receptors. J Neuropsychiatry Clin Neurosci 1991;3(1):80-83.
83. Mayberg H, Robinson RG, Wong D, Parikh R, Bolduc P, Starkstein S, Price T, Dannals R, Links J, Wilson A. PET imaging of cortical S2 serotonin receptors after stroke: lateralized changes and relationship to depression. Am J Psychiatry 1988;145(8):937-943.
84. Hoing A, Bartlett JR, Bouras N, Bridges PK. Amino acid levels in depression: a preliminary investigation. J Psychiatr Res 1988;22(3):159-164.
85. Perry EK, Gibson PH, Blessed G, Perry RH, Tomlinson NE. Neurotransmitter enzyme abnormalities in senile dementia. J Neuro Sci 1977;34:247-265.
86. Hofmann L, Slotboom J, Boesch C, Kreis R. Characterization of the Macromolecule Baseline in Localized 1H-MR Spectra of Human Brain. Magn Reson Med 2001;46:855-863.
87. Howe FA, McLean MA, Saunders DE, Bell BA, Griffiths JR. Metabolite nulling in short echo time on vivo 1H MRS of human brain tumors. ISMRM 1995 (abstract) 1995:1705.
88. Petroff OA, Mattson RH, Behar KL, Hyder F, Rothman DL. Vigabatrin increases human brain homocarnosine and improves seizure control. Ann Neurol 1998;44(6):948-952.
89. Yongbi NM, Payne GS, Leach MO. Quantification of signal selection efficiency, extra volume suppression and contamination for ISIS, STEAM and PRESS localized 1H NMR spectroscopy using and EEC localization test object. Phys Med Biol 1995;40:1293-1303.
90. de Graaf RA, Rothman DL. In Vivo Detection and Quantification of Scalar Coupled 1H NMR Resonances. Concepts Magn Reson 2001;13(1):32-76.
91. Thompson RB. Sources of Variability in the Response of Coupled Spins to the PRESS Sequence and Their Potential to Impact on Metabolite Quantification. MRM 1999;41:p1162-1169.
92. Ebel A, Maudsley AA. Comparison of Methods for Reduction of Lipid Contamination for In Vivo Proton MR Spectroscopic Imaging of the Brain. Magn Reson Med 2001;46:706-712.
93. McKnight TR. An Automated Technique for the Quantitative Assessment of 3D-MRSI Data from Patients with Glioma. JMRI 2001;13:p167-177.
94. Soher BJ. Quantitative Proton MR Spectroscopy Imaging of the Human Brain. MRM 1996;35:p356-363.
95. Michaelis T. Absolute Concentrations of Metabolites in the Adult Human Brain in Vivo: Quantification of Localized Proton MR Spectra. Radiology 1993;187:219-227.
96. de Graaf RA. Two-dimensional NMR. In Vivo NMR Spectroscopy: Principles and Techniques: John Wiley and Sons, Ltd; 1998.
97. de Graaf RA. In vivo NMR spectroscopy Principles and Techniques. Chichester: John Wiley & Sons Ltd; 1998. 508 p.
98. Rothman DL, Petroff OA, Behar KL, Mattson RH. Localized 1H measurements of GABA in human brain in vivo. Proc Natl Acad Sci 1993;90:5662-5666.

99. Barrere B, Peres M, Gillet B, Mergui S, Beloeil J-C, Seylaz J. 2D COSY 1H NMR: a new tool for studying in situ brain metabolism in the living animal. FEBS Letters 1990;264(2):198-202.
100. Hetherington HP, Newcomer BR, Pan JW. Measurements of Human Cerebral GABA at 4.1T Using Numerically Optimized Editing Pulses. Magn Reson Med 1998;39:6-10.
101. Freeman R. A Handbook of Nuclear Magnetic Resonance. New York: Longman Scientific and Technical; 1988. 312 p.
102. Knuttel A, Kimmich R. Double-Quantum Filtered Volume Selective NMR Specroscopy. Magn Reson Med 1989;10:404-410.
103. Simister RJ, McLean MA, Barker GJ, Duncan JS. A Proton Magnetic Resonance Spectroscopy Study of Metabolites in the Occipital Lobes in Epilepsy. Epilepsa 2003;44(4):550-558.
104. Simister RJ, McLean MA, Barker GJ, Duncan JS. Proton MRS reveals frontal lobe metabolite abnormalities in idiopathic generalized epilepsy. Neurology 2003;61:897-902.
105. Provencher SW. Estimation of Metabolite Concentrations from Localized in Vivo Proton NMR Spectra. MRM 1993;30:p672-679.
106. Shen J. In Vivo GABA Editing Using a Novel Doubly Selective Multiple Quantum Filter. MRM 2002;47:p447-454.
107. Lei H, Peeling J. Simultaneous spectral editing for gamma-aminobutyric acid and taurine using double quantum coherence transfer. J Magn Reson 2000;143:95-100.
108. Shungu DC, Palmer III AG, Ramasamy R. GABAssale: Selective Homonuclear MQC Transfer Schemes for Unambiguous in vivo GABA Detection with Full Signal Recovery and Complete Water Suppression in a Single Scan. 2002; Honolulu, Hawaii, USA.
109. Choi I-Y, Lee S-P, Shen J. Single-shot Localized Multiple Quantum Spectroscopy of GABA in the Human Brain In Vivo with Two Double-Band Pulses for Enhanced Selectivity. 2004; Kyoto, Japan. p 685.
110. Choi IY, Lee S-P, Merkle H, Shen J. Simultaneous detection of multiple quantum filtered GABA and single quantum creatine in the human brain in vivo using a single shot, two-echo acquisition scheme. 2004; Kyoto, Japan. p 308.
111. Choi IY, Lee S-P, Merkle H, Shen J. In Vivo Detection of Gray and White Matter Difference of GABA concentration in the Human Brain using Chemical Shift Imaging of GABA. 2004; Kyoto, Japan. p 109.
112. Shen J. In Vivo Chemical Shift Imaging of GABA in the Human Brain. Magn Reson Med 1999;41:p35-42.
113. Claridge TDW. Chapter 5 Correlations through the chemical bond I: Homonuclear shift correlation. High-Resolution NMR Techniques in Organic Chemistry. First ed. Volume 19, Tetrahedron Organic Chemistry Series. Oxford: Pergamon, Elsevier Science Ltd; 1999. p 147-220.
114. Cohen Y, Chang L-H, Litt L, James TL. Spatially Localized COSY Spectra from a Surface Coil Using Phase-Encoding Magnetic Field Gradients. J Magn Reson 1989;85:203-208.

115. Kumar A, Hosur RV, Chandrasekhar K. A Superior Pulse Scheme for Homonuclear Two-Dimensional Correlated Spectroscopy. J Magn Reson 1984;60:143-148.
116. Behar KL, Ogino T. Assignment of resonance in the 1H spectrum of rat brain by two-dimensional shift correlated and J-resolved NMR spectroscopy. MRM 1991;17(2):285-303.
117. Pierard C, Peres M, Satabin P, Guezennec CY, Lagarde D. Effects of GABA-transaminase inhibition on brain metabolism and amino-acid compartmentation: an in vivo study by 2D 1H-NMR spectroscopy coupled with microdialysis. Exp Brain Res 1999;127:321-327.
118. Brereton M. Localized Two-Dimensional Shift Correlated Spectroscopy in Humans at 2 Tesla. MRM 1994;32(2):p251-257.
119. McKinnon GC, Bosiger P. Localized Double-Quantum Filter and Correlation Spectroscopy Experiments. Magn Reson Med 1988;6:334-343.
120. Blackband SJ, McGovern KA, Mc Lennan IJ. Spatially Localized Two-Dimensional Spectroscopy. SLO-COSY and SLO-NOESY. JMR 1988;79:184-189.
121. Ziegler A, Gillet B, Beloeil J-C, Macher J-P, Decorps M, Nedelec J-F. Localized 2D correlation spectroscopy in human brain at 3 T. MAGMA 2002;14(1):45-49.
122. Claridge TDW. Chapter 7 Separating shifts and coupling constants: J-resolved spectroscopy. High-Resolution NMR Techniques in Organic Chemistry. First ed. Volume 19, Tetrahedron Organic Chemistry Series. Oxford: Pergamon, Elsevier Science Ltd; 1999. p 259-275.
123. Ryner LN, Sorenson JA, Thomas MA. 3D Localized 2D NMR Spectroscopy on an MRI Scanner. JMR B 1995;107:126-137.
124. Thomas MA, Ryner LN, Mehta MP, Turski PA, Sorenson JA. Localized 2D J-resolved 1H MR Spectroscopy of Human Brain Tumors in vivo. JMRI 1996;6:453-549.
125. Ernst T. Coupling effects in Volume Selective 1H Spectroscopy of Major Brain Metabolites. MRM 1991;21:p82-96.
126. Kumar A. Two-Dimensional Spin-Echo NMR Spectroscopy: A General Method for Calculation of Spectra. JMR 1978;30:p227-249.
127. Wang ZJ, Bergqvist C, Hunter JV, Jin D, Wang DJ, Wehrli S, Zimmerman RA. In vivo Measurement of Brain Metabolites Using Two-Dimensional Double-Quantum MR Spectroscopy-Exploration of GABA Levels in a Ketogenic Diet. Magn Reson Med 2003;49:615-619.
128. Wang ZJ, Bergqvist C, Hunter JV, Tavelli B, Cao Q, Scherzer M, Jin D, Wang DJ, Wehrli S, Zimmerman RA, Detre JA. In Vivo Measurement of Brain GABA in Ketogenic Diet Using Two-Dimensional Double-Quantum MR Spectroscopy. 2002; Hawaii.
129. Sotak CH, Freeman DM, Hurd RE. The Unequivocal Determination of in Vivo Lactic Acid Using Two-Dimensional Double Coherence-Transfer Spectroscopy. J Magn Reson 1988;78:335-361.
130. Hurd RE, Freeman DM. Metabolite specific proton magnetic resonance imaging. Proc Natl Acad Sci 1989;86:4402-4406.
131. Crozier S, Brereton IM, Rose SE, Field J, Shannon GF, Doddrell DM. Application of Volume-Selected, Two-Dimensional Multiple-Quantum

Editing in Vivo to Oberserve Cerebral Metabolites. Magn Reson Med 1990;16:496-502.
132. Choi IY, Branch CA, Shen J. Two-Dimensional Multiple Quantum Spectroscopy of GABA. 2002; Honolulu, Hawaii, USA.
133. Thomas MA, Hattori N, Umeda M, Sawada T, Naruse S. Evaluation of 2D L-COSY and JPRESS Using a 3T MRI Scanner: From Phantoms to Human Brain in vivo. In: Haga K, editor; 2004. p copy of paper submitted for review.
134. Smith SA, Levante TO, Meier BH, Ernst RR. Computer Simulations in Magnetic Resonance. An Object-Orientated Programing Approach. JMR Series A 1994;106:75-105.
135. Marshall I, Haga K, Lymer K. Theoretical and Experimental studies of 2D J-resolved Spectroscopy of GABA. 2004; Kyoto, Japan. p 2302.
136. Ordidge RJ, Cresshull ID. The Correction of Transient B0 Field Shifts following the Application ofPulsed Gradients by Phase Correction in the Time Domain. JMR 1986;69:p151-155.
137. van den Boogaart A, Ala-Korpela M, Jokisaari J, Griffiths JR. Time and Frequency Domain Analysis of NMR Data Compared: An Application to 1D 1H Spectra of Lipoproteins. Magn Reson Med 1994;31:347-358.
138. Pijnappel WWF, van den Boogaart A, de Beer D, van Ormondt R. SVD-based quantification of magnetic resonance signals. J Magn Reson 1992;97:122-134.
139. Wild JM. Proton Magnetic Resonance Spectroscopic Imaging of the Human Brain. Edinburgh: University of Edinburgh; 1998. 288 p.
140. Jacobs MA. Quantitative Proton MR Spectroscopic Imaging of Normal Human Cerebellum and Brain Stem. MRM 2001;46:p699-705.
141. Marshall I, Wardlaw JM, Cannon J, Slattery J, Sellar RJ. Reproducibility of metabolite peak areas in 1H MRS of brain. Magn Reson Imaging 1996;14:281-292.
142. Schirmer T, Auer DP. On the reliability of quantitative clinical magnetic resonance spectroscopy of the human brain. NMR in Biomed 2000;13(1):p28-36.
143. Hoch JC, Stern AS. NMR Data Processing. New York: Wiley -Liss; 1996. 196 p.
144. Riddle WR, Gibbs SJ, Willcott MR. Removing effects of edy currents in proton MR spectroscopy. Med Phys 1992;19(2):501-509.
145. Maudsley AA, Wu Z, Meyerhoff DJ, Weiner MW. Automated Processing for Proton Spectroscopic Imaging Using Water Reference Deconvolution. Magn Reson Med 1994;31:589-595.
146. Roebuck JR, Hearshen DO, O'Donnell M, Raidy T. Correction of Phase Effects Produced by Eddy Currents in Solvent Suppressed 1H-CSI. Magn Reson Med 1993;30:277-282.
147. Webb PG, Sailasuta N, Kohler SJ, Raidy T, Moats RA, Hurd RE. Automated Singel-Voxel Proton MRS: Technical Development and Mulitsite Verification. Magn Reson Med 1994;31:365-373.
148. Klose U. In Vivo Proton Spectroscopy in Presence of Eddy Currents. Magn Reson Med 1990;14:26-30.

149. Siegel MM. The Use of the modified simplex method for automatic phase correction in Fourier Transform Nuclear Magnetic Resoance Spectroscopy. Analytica Chimica Acta 1981;133:103-108.
150. Ernst RR, Anderson WA. Application of Fourier transform spectrscopy to magnetic resonance. Rev Sci Instrum 1966;37:93-102.
151. Chen C-n, Kan L-s. An iterative phase correction program of nuclear magnetic resonance (NMR) spectra. Computer Methods and Programs in Biomedicine 1988;26:81-84.
152. Balacoo G. A New Criterion for Automatic Phase Correction of HIgh-Resolution NMR Spectra Which Does Not Require Isolated or Symmetrical Lines. J Magn Reson 1994;110:19-25.
153. Hoffman RE, Delaglio F, Levy GC. Phase Correction of Two-Dimensional NMR Spectra Using DISPA. J Magn Reson 1992;98:231-237.
154. Wardlaw JM, F SD, Marshall I. Letter to the Editor: Re: Serial Precision of Metabolite Peak Area Ratios and Water References Metabolite Peak Areas in Proton MR Spectroscopy of the Human Brain Simmons et al 1996, vol. 16, pages 319-330 1998. Magn Reson Imaging 1998;17(3):483-486.
155. Haase A, Hanicke W, Frahm J. The Influence of Experimental Parameters in Surface-Coil NMR. J Magn Reson 1984;56:401-412.
156. Lymer K, Haga K, Marshall I, Wardlaw JM. 2D J-resolved GABA measurement Without Macromolecule Contamination. 2003 15th January 2003; Manchester.
157. Brooks WM, Friedman SD, Stidley CA. Reproducibility of 1H-MRS In Vivo. MRM 1999;41:193-197.
158. Marshall I, Carpenter T, Haga K. Spectroscopy QA - is it worthwhile? ; 2003 1st July 2003; Royal Marsden Hospital Education and Conference Centre, London.
159. Rose SE, de Zubicaray GI, Wang D, Galloway GJ, Chalk JB, Eagle SC, Semple J, Doddrell DM. A 1H MRS study of probable Alzheimer's Disease and Normal Aging: Implications for longitudinal monitoring dementai progression. MRI 1999;17:291-299.
160. Petroff OA, Hyder F, Rothman DL, Mattson RH. Homocarnosine and seizure control in juvenile myoclonic epilepsy and complex partial seizures. Neurology 2001;56:709-715.
161. Tofts P. Quantitative MRI of the Brain: Measuring changes caused by disease. Chichester: Wiley; 2003. 633 p.
162. Bruce SD. Accurate Quantification of the Proton NMR Spectra of Human Brain Metabolites. Edinburgh: Napier University; University of Edinburgh; 2002. 290 p.
163. Metz CE. Basic Priniciples of ROC Analysis. Sem Nucl Med 1978;8(4):283-298.
164. Lymer K, Haga K, Marshall I, Wardlaw JM. Reproducibility of in-vitro GABA measurements using 2D J-resolved MRS. 2004; Kyoto, Japan.
165. Jensen JE, Frederic BD, Wang L, Brown J, Renshaw PF. In vivo two-dimensional J-resolved GABA spectroscopic imaging at 4.0T. 2004; Kyoto, Japan. p 2301.
166. Dreher W, Leibfritz D. On the Use of Two-Dimensional-J NMR Measurements for in Vivo Proton MRS:Measurment of Homonuclear

Decoupled Spectra without the need for Short Echo Times. MRM 1995;34:p331-337.

167. Binesh N, Thomas MA. 2D spectroscopy using multi-channel array coil. 2004; Kyoto, Japan. p 2303.

Appendix: List of Abstracts

Lymer, K., Marshall, I., A comparison of automatic phase correction algorithms for GABA measurement using 2D J-resolved MRS, In: Book of Abstracts: 10th Annual Meeting of the British Chapter of ISMRM, Edinburgh 2004:P14

Haga, K., **Lymer, K.**, Wardlaw, J., Thomas, A., Marshall, I., Detection of GABA at 1.5T: Comparison of 2D JPRESS and 2D L-COSY, In: Book of Abstracts: 10th Annual Meeting of the British Chapter of ISMRM, Edinburgh 2004:L22

Lymer, K., Haga, K., Marshall, I., Wardlaw, J., Reproducibility of *in-vitro* GABA measurements using 2D J-resolved MRS, In: Book of abstracts: 12th Annual Meeting of International Society for Magnetic Resonance in Medicine, Berkeley, CA: ISMRM 2004: 686

Marshall, I., Haga, K., **Lymer, K.**, Theoretical and Experimental Studies of 2D J-Resolved Spectroscopy of GABA, In: Book of abstracts: 12th Annual Meeting of International Society for Magnetic Resonance in Medicine, Berkeley, CA: ISMRM 2004: 2302

Lymer, K., Haga, K., Marshall, I., Wardlaw, J.M., 2D J-resolved GABA measurement without macromolecule contamination, 13th Annual NMR Symposium, Manchester, UK (2003)